MAGNETIC PROPERTIES OF A TWO-DIMENSIONAL HEISENBERG ANTIFERROMAGNET: $Cu(HCOO)_2 \cdot 4H_2O$

by

Kazuo Yamagata

CONTENTS

CONTENTS (continued)

List of Tables and Figures

Abstract

Magnetic properties of a two-dimensional antiferromagnet, $Cu(HCOO)_2 \cdot 4H_2O$, were studied both experimentally and theoretically with special interests in its magnetization process. The magnetization measurement up to 20 kOe was done at 4.2K for single crystals of $Cu(HCOO)_2 \cdot 4H_2O$ and the proton nmr of the deuterated salt, $Cu(HCOO)_2 \cdot 4D_2O$, was also studied at 4.2K. It was found that some experimental results such as a magnetization jump observed at 5.3 kOe when an external field is parallel to the b-axis can not be explained by the two-sublattice model used by Seehra and Castner. The four-sublattice theory in which the inter- and intralayer exchange interactions, the symmetric and antisymmetric anisotropies and the Zeeman energies are taken into account was applied to this compound and the experimental results were satisfactorily explained.

The intra- and interlayer exchange fields, H_{ex} and h_{ex}, were obtained as 1.5×10^6 and 4.0×10 Oe, respectively. Thus the small ratio of h_{ex}/H_{ex}, 2.7×10^{-5}, guarantees the two-dimensionality of the crystal.

The magnetization curve of a similar compound, copper formate bis-urea dihydrate, $Cu(HCOO)_2 \cdot 2(NH_2)_2CO \cdot 2H_2O$, was studied at 4.2K. The results indicate that the interlayer coupling of this crystal is about 1/20 of that in $Cu(HCOO)_2 \cdot 4H_2O$ while the intralayer exchange is of the same order in both crystals.

Acknowledgements

The author would like to express his sincere thanks to Professor Muneyuki Date, under whose continual guidance this work was done, for his valuable suggestion and encouragement. Also, the author wishes to express his sincere thanks to Professor Taiichiro Haseda, to Professor Mitsuhiro Motokawa and to Professor Motohiro Matsuura for their helpful discussion and comments. The author is much indebted to Emeritus Professor Teinosuke Kanda and to Professor Ojiro Nagai both of Kobe University for their hearty support throughout the course of the study and kind help in preparing the manuscript.

§ 1. Introduction

Many theoretical and experimental investigations have been dedicated to simple magnetic model systems.[1] Two-dimensional(hereafter referred to 2d) Heisenberg antiferromagnets are particularly interesting because their properties are sensitive to the anisotropy and the interlayer coupling. In this paper, magnetic properties of a nearly 2d Heisenberg $S=\frac{1}{2}$ antiferromagnet $Cu(HCOO)_2 \cdot 4H_2O$ and those of a similar compound copper formate bis-urea dihydrate, $Cu(HCOO)_2 \cdot 2(NH_2)_2CO \cdot 2H_2O$, are studied with special interests in the magnetic structure, the anisotropy and the interlayer coupling.

The two-dimensionality in $Cu(HCOO)_2 \cdot 4H_2O$(CuFTH) was first suggested by Kobayashi and Haseda,[2] who investigated various exchange paths in this crystal considering the layer structure[3] parallel to the c-plane. The Néel temperature T_N(17K[4]) is much lower than the Weiss temperature (175K[5]) and the magnetic susceptibility has a broad maximum at about 65K.[2] The peak of the specific heat at T_N is anomalously small.[6,7] Therefore, the compound seems to be a quasi 2d Heisenberg antiferromagnet. Short range order effects are observed in electron spin resonance,[8,9] in proton resonance[10,11,12] and in neutron diffraction experiment.[13]

Magnetic properties below T_N also have been studied by many researchers. Kobayashi and Haseda(KH)[2] found the induced weak ferromagnetism in the L_1L_2-plane. Van der Leeden et al.[14] did the proton nmr experiment and concluded the $P_{2c}2_1/a$ symmetry for the magnetic structure. Dupas and Renard[15] suggested the necessity of the

4-sublattice model with spin easy axis nearly along the a-axis. These investigations are followed by the AFMR experiment and the analysis by Seehra and Castner(SC).[16] Their analysis is the first systematic study of the microscopic magnetic properties below T_N, although their treatment is limited within the 2-sublattice model because of the complexity in calculating the AFMR frequencies for the 4-sublattice model. Accordingly, a weak interlayer exchange interaction could not be taken into account. By using the hamiltonian which consists of the isotropic exchange, the symmetric and antisymmetric anisotropies and the anisotropic Zeeman interaction, they found that the spin easy axis is the a"-direction close to the a-axis and explained the 90° rotation of the antiferromagnetic axis caused by the external field parallel to the c-axis. However, they could not explain the jump of the magnetization observed when the external field is parallel to the b-axis. Ajiro and Terata[10] pointed out that the jump may be explained by a structure change from the 4-sublattice state to the 2-sublattice state induced by the external field. Their hamiltonian contains the interlayer exchange but the symmetric anisotropy and the anisotropic part of the Zeeman energies are dropped out.

Ideally speaking, it is clear that one should consider the anisotropic Zeeman energy, the symmetric and antisymmetric exchange interactions both for the intra- and interlayer couplings based on the 4-sublattice model to understand whole magnetic properties such as the magnetization process and AFMR. However, it is very tedious for this compound so that many researchers have partly explained various magnetic properties by truncating the whole hamiltonian. Recently, we succeeded to analyze

the magnetization process without truncating the important hamiltonian terms. The results show that the treatment can explain all important magnetization process satisfactorily compared with the previous work. The extended magnetization and nmr measurements were also performed to ensure the treatment.

Following the introduction, a summary of the crystal structure and the magnetic properties is given in §2. The general hamiltonian and the derivation of the magnetization curves are presented in §3. In §4, experimentals including the performance of the moving-sample magnetometer are shown. Results of the magnetization measurements up to 20 kOe at 4.2K are compared with the consequences of the theory in §5, where the intra- and interlayer exchanges, the symmetric and antisymmetric anisotropies and the anisotropic components of the g-tensor are estimated consistently. Results of the nmr experiments up to 60MHz at 4.2K are discussed in §6, where the angular dependence of the resonance field was studied mostly for the deuterated crystal $Cu(HCOO)_2 \cdot 4D_2O$(CuFTD). In §7, we deal with the magnetic properties of the similar crystal, $Cu(HCOO)_2 \cdot 2(NH_2)_2CO \cdot 2H_2O$(CuFUH), whose intralayer coupling is nearly equal to that in CuFTH[17] while the interlayer spacing of the former is larger by about 30% than that of the latter.[18]

§ 2. Crystal Structure and Magnetic Properties

Unit cell of CuFTH crystal[3] is shown in Fig. 1. The unit cell contains two chemical units. At room temperature protons of water molecules migrate around oxygen atoms due to the hindered rotation.[19] Ordering of the protons takes place at -38.9°C.[19] Symmetry of the crystal is lower below this temperature.[20,21] However, no apparent changes of atomic position were deteced by X-ray diffraction.[22] Results of recent neutron diffraction studies[23,24] support the conclusions of the earlier works. No further structure changes were detected down to 12K by specific heat measurement.[25]

Copper ions are coordinated octahedrally by two water-oxygens and four $HCOO^-$-oxygens. The octahedrons are elongated by about 20% along the H_2O-Cu^{2+} directions which are denoted by Z_1 for the corner ion and Z_2 for the base-center ion in Fig. 2. Consequently, g-value of copper ions is expected to be approximately 2.1 in the plane perpendicular to Z_i(i=1,2) and 2.4 along Z_i. The axes Z_1 and Z_2 make an angle of 41° in the L_1L_2-plane, where L_1 is a bisector of two Z_i's and L_2 is the b-axis. A paramagnetic resonance experiment[26] has revealed that the principal axes of the effective g-tensor of exchange narrowed line are L_1, L_2 and L_3 perpendicular to L_1 and L_2. The effective g-values are $g(L_1)$= 2.362, $g(L_2)$=2.116, $g(L_3)$=2.071.[27]

The absolute value $|J|$($J<0$) of the magnetic interaction between ions in the ab-plane was estimated from the round peak of the susceptibility as about 36K.[28] The interlayer exhange J' was first

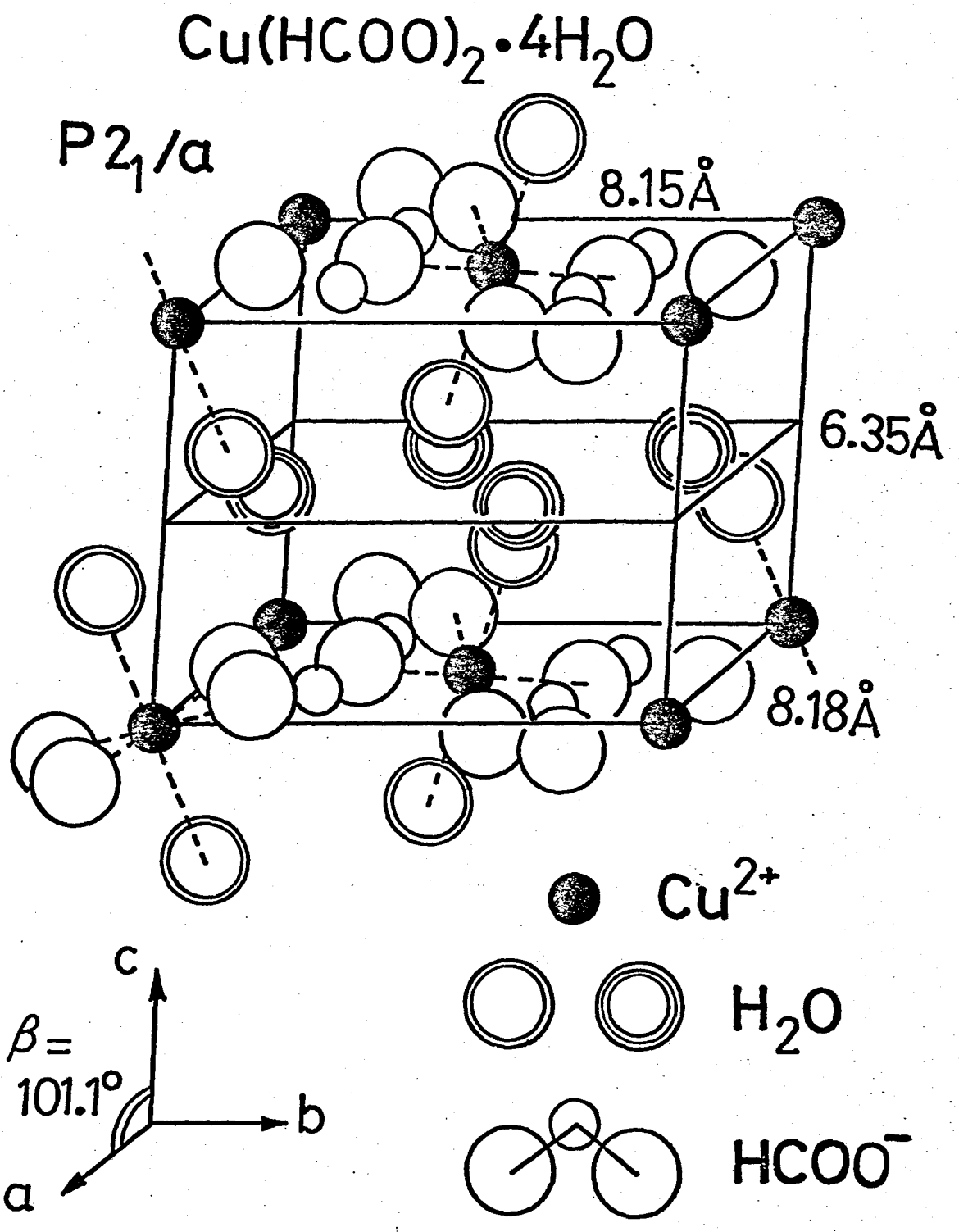

Fig. 1 Crystal structure of $Cu(HCOO)_2 \cdot 4H_2O$. Cu^{2+} ions linked by $HCOO^-$ groups from 2-dimensional networks parallel to the c-plane and H_2O molecules are sandwitched between them. The double or triple circles for H_2O indicate whether they are linked to Cu^{2+} or not.

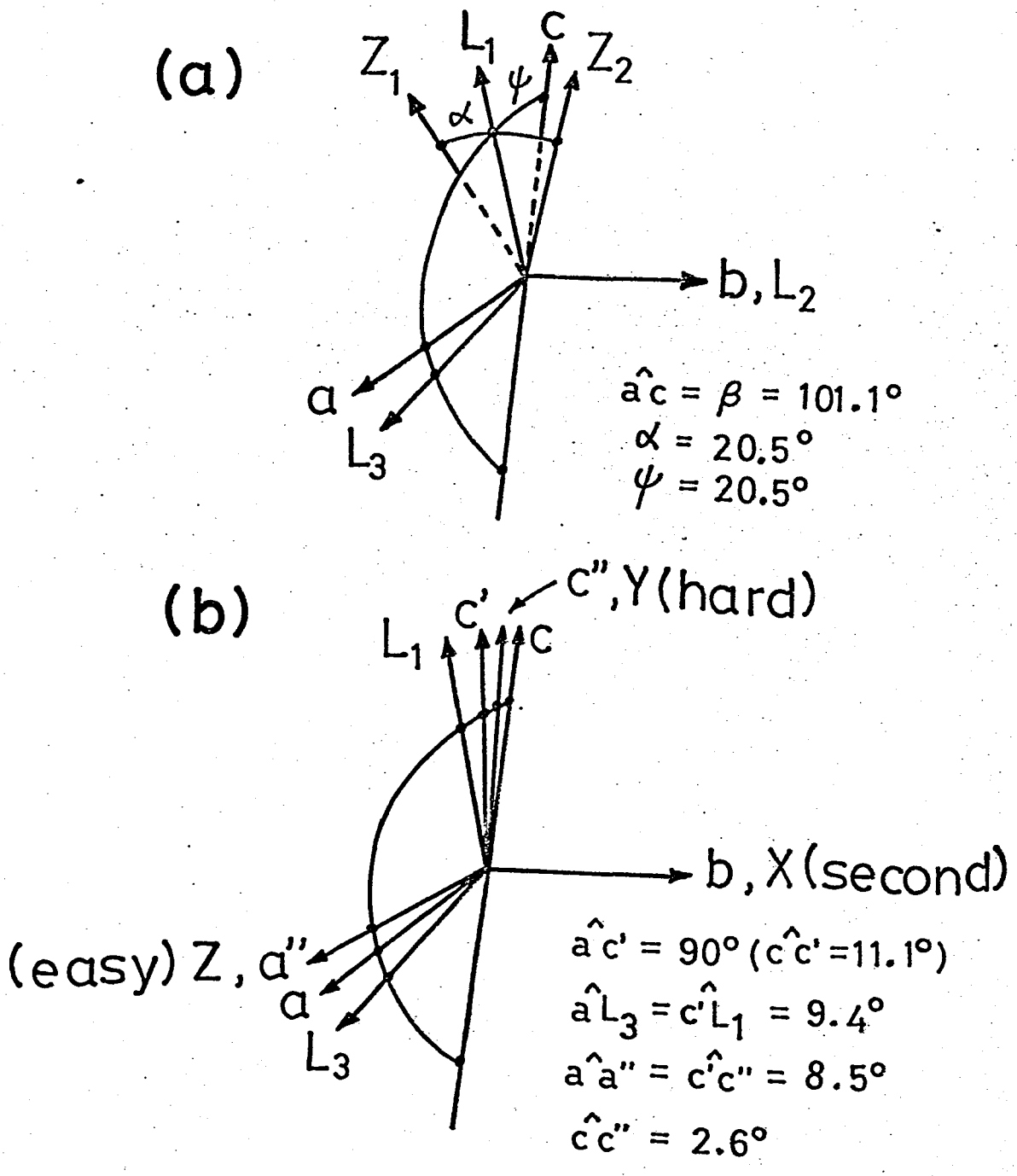

Fig. 2 (a) Relation between H_2O-Cu^{2+} directions(Z_1 and Z_2) and the principal axes of amalgamated g-tensor(L_1, L_2 and L_3).[26,27]

(b) Relation between the antiferromagnetic principal axes (a", b(L_2) and c")[16] and other axes. The notations X, Y and Z are used for calculations in §3.

inferred by KH considering possible exchange paths to be about 0.1K. This implies $|J'/J| \simeq 10^{-3}$. Ajiro and Terata[10] have suggested from the analysis of the magnetization jump that the interlayer exchange field is about 200 Oe($J'/J \simeq 10^{-4}$) and antiferromagnetic. This value is larger than the newly estimated value, 40 Oe, as will be given in §3 and §5.

Magnetization process was first studied by KH under an external magnetic field $\vec{H}$ up to 9 kOe parallel to L_1, L_2 and L_3. Their data are extended up to 20 kOe by the present author[29] and are shown in Fig. 3. It is noticed that the spontaneous ferromagnetic moment was not observed at zero external field. The low field susceptibility for L_1 and L_2 is much larger than that of L_3. For $\vec{H}//L_2$, abrupt increase of the magnetization was observed at about 5 kOe above which the magnetization gradually becomes flat as for L_1. The "saturated" value is about 3% of total copper moments.

Crystal structure and magnetic properties of the deuterated crystal CuFTD seem to be quite similar to those of light water crystal CuFTH. For example, two crystals have the same value of T_N[30] and exhibit the same angular dependence of proton resonance for the $HCOO^-$ proton.[11,14,15,20] In this paper, the $HCOO^-$ proton position of the paraelectric state of CuFTH crystal[19] is used for calculating the dipole field for the antiferroelectric state of CuFTD crystal, because the proton position of the latter case is not known.

Magnetic structure was first studied by van der Leeden et al[14] by using proton resonance of the deuterated crystal, CuFTD. They determined the magnetic space group $P_{2c}2_1/a$ and proposed a magnetic structure of

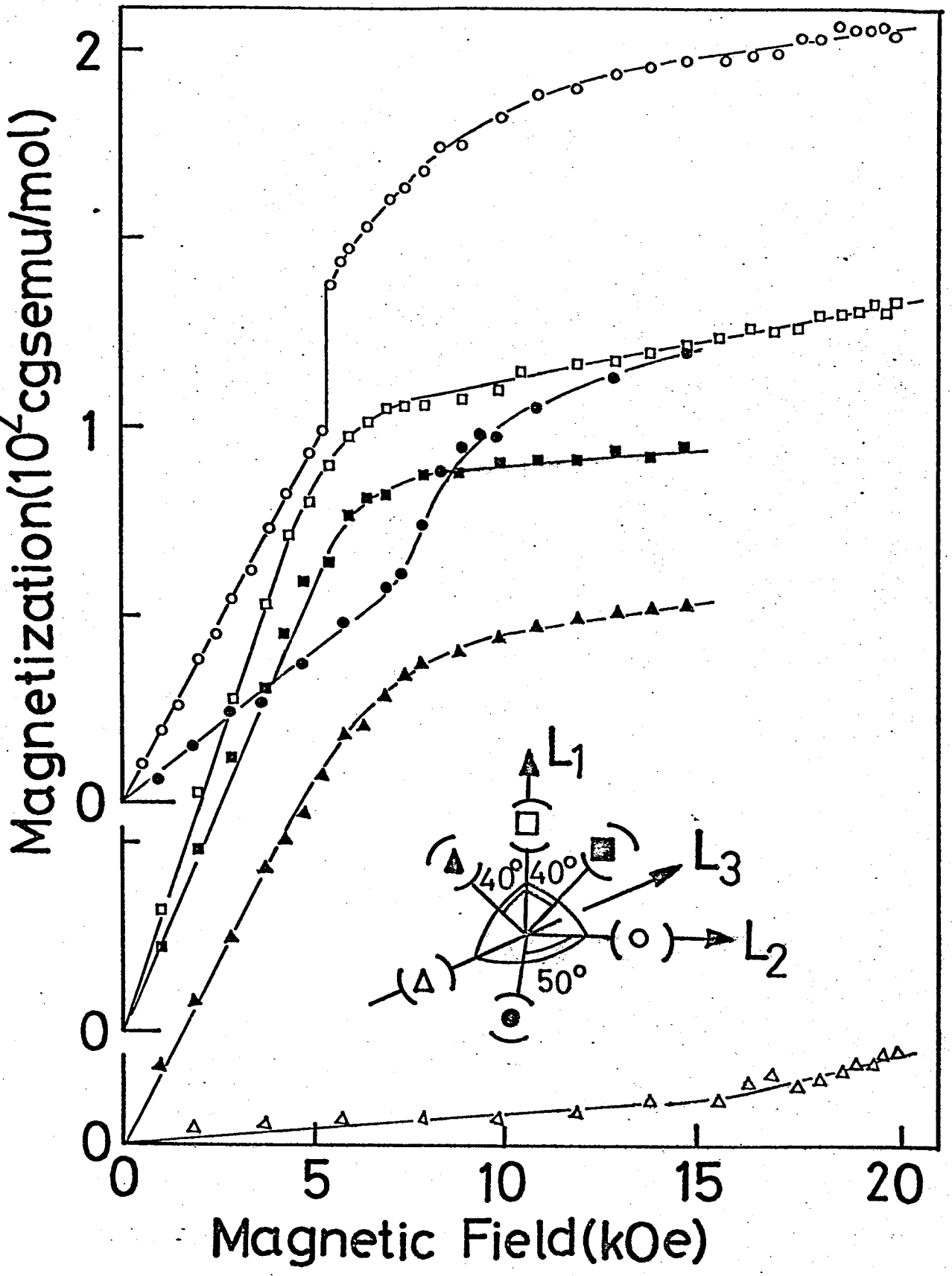

Fig. 3 Magnetization parallel to the external field for various field directions in a single crystal of $Cu(HCOO)_2 \cdot 4H_2O$ at 4.2K.

2-sublattice antiferromagnet. Although their magnetic group was correct, the proposed 2-sublattice magnetic structure was incorrect. Dupas and Renard[15] studied the proton resonance again and proposed a 4-sublattice magnetic structure whose magnetic unit cell consists of two crystal cells. Their proposal of the magnetic structure is correct except for the fact that the spin easy direction a" in Fig. 4(a) was not found precisely. It is noted that the reported thermal average of spin at zero external field is only 53% of $S=\frac{1}{2}$ even in the temperature range $0.1 \sim 0.2T_N$. Ajiro and Terata[10] also studied the proton nmr and suggested a field-induced structure change from the 4-sublattice state to the 2-sublattice state. This conclusion is correct as will be seen later in §5. However, other two results that the spin easy axis in the 4-sublattice structure is parallel to the c-direction and that the weak ferromagnetism is due to the Dzyaloshinsky-Moriya(DM) interaction are inadequate.[11,16,29,31,32]

Antiferromagnetic resonance experiments and the analysis by SC may be the remaining subject of this section. However, as this problem has been already considered in §1, a short summary of the results will be given below. The antiferromagnetic principal axes are a", b and c" given in Fig. 2(b). The easy axis is the a"-direction and the second or the intermediate axis is the b-direction. The antiferromagnetic axis moves widely by applying the external magnetic field. This movement was mainly attributed to the tilting in the g-tensors of two copper ions in the unit cell. These conclusions agree well with those of the present paper as is seen in the analysis of the magnetization curve in §5.

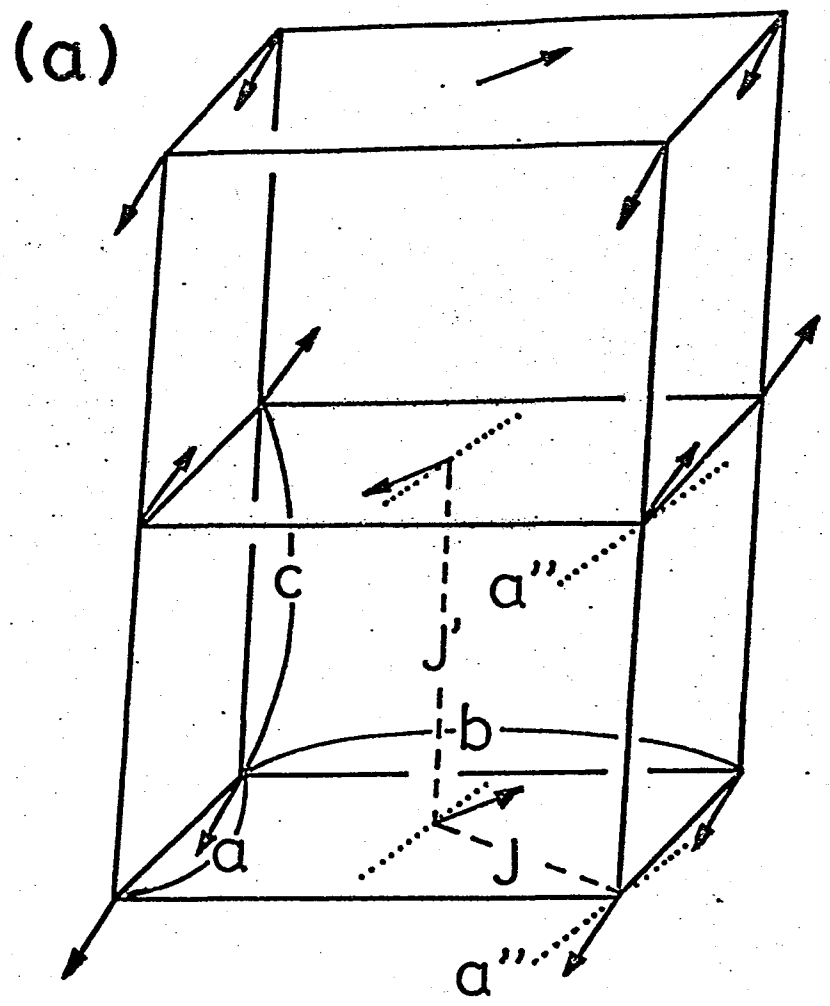

Fig. 4(a) Spin structure of $Cu(HCOO)_2 \cdot 4D_2O$ at zero external field. The magnetic unit cell consists of two crystal cells adjoining along the c-direction. The antiferromagnetic easy axis a'' is close to the a-axis in the ac-plane. The canting(0.4°) to b allowed by crystal symmetry occurs between spins in the 2-dimensional ab-plane keeping the adjacent-plane spins antiparallel.

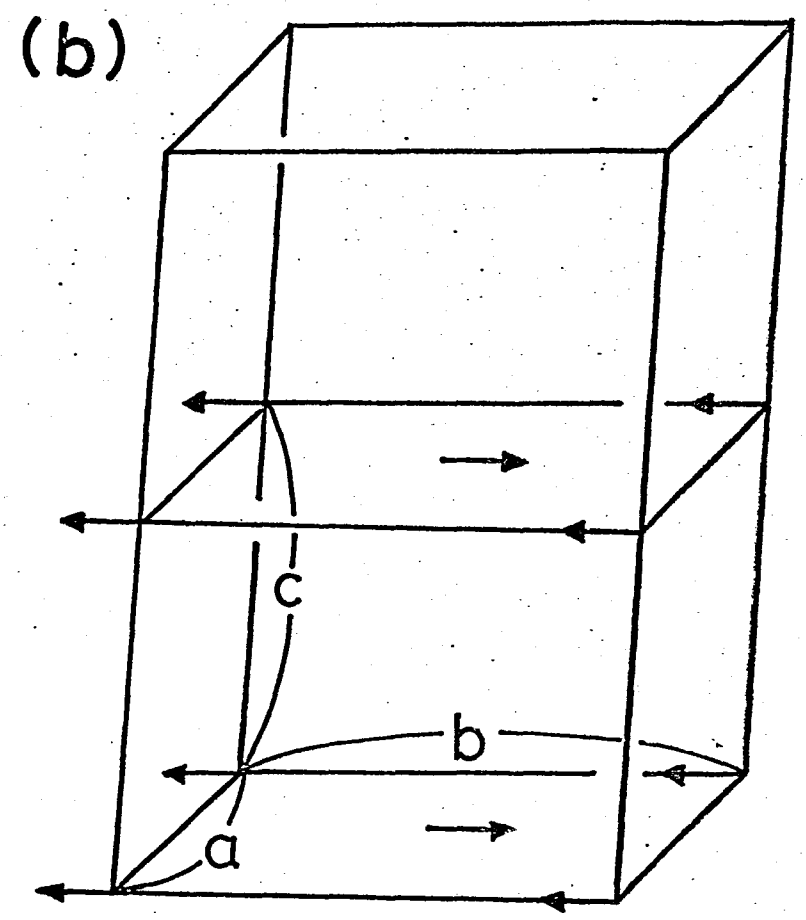

Fig. 4(b) Spin structure in the high-field 2-sublattice state. Spins in the neighboring planes are parallel. The antiferromagnetic axis depends on the field direction. For example, it is parallel to the b-axis as shown in the figure for $\vec{H}$ in the ac-plane.*) For details see Fig. 24.

*) For simplicity, small canting ($gH/4H_{ex}$ along $\vec{H}$ plus 0.4° to a" and -0.1° to c") is not shown in this figure.

§ 3. Magnetization Process Based on the 4-sublattice Model

In this section, we deal with the molecular field theory of the magnetization process at T=0. The 2-sublattice hamiltonian introduced by Seehra and Castner is extended to the 4-sublattice case. A weak isotropic interlayer coupling is newly taken into account. Equations of torque balance are derived from the hamiltonian and are solved. The 4-sublattice treatment developed by Joenk[33] for $CuCl_2 \cdot 2H_2O$ is not directly applicable to the present case, because roles of various anisotropy terms in these two cases are different.

3.1 Hamiltonian and equilibrium conditions

3.1.1 Torque equations and free energy

We consider four sublattices, 1, 2, 3 and 4. The sublattices 1 and 2 represent, as is shown in Fig. 5, the corner and the base-center ions of one layer and 3 and 4 represent the corresponding ions of another layer. The coordinate system XYZ shown in Fig. 2(b) is used after SC. The axes X, Y and Z are parallel to the second easy axis b, the hard axis c'' and the easy axis a'', respectively. The hamiltonian H consists of three parts, namely two intralayer parts H_{12} and H_{34} and the interlayer hamiltonian H_{int},

$$H = H_{12} + H_{34} + H_{int} \quad . \tag{3-1}$$

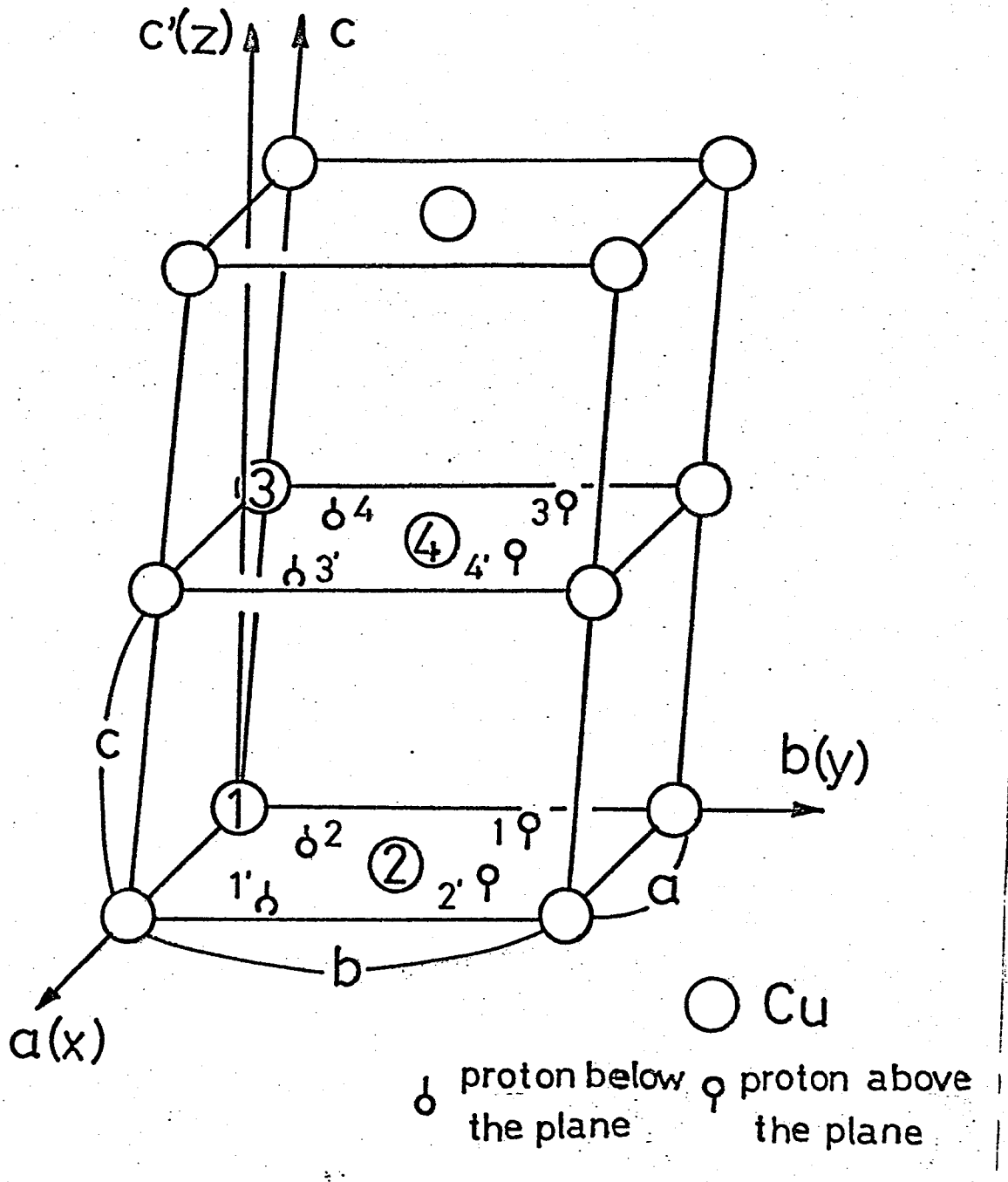

Fig. 5 Four independent copper ions and eight $HCOO^-$-protons in the magnetic unit cell. The positional parameters of proton-1 are 0.207, 0.692, 0.071 in the oblique abc coordinate system. The coordinates xyz are used for calculating the dipole field in §6.

As the present treatment is based on the molecular field approximation, the following reduced form is used: for example, the isotropic exchange and Zeeman energies in H_{12} are given by

$$-2J \sum_{<i,j>} \vec{S}_i \cdot \vec{S}_j - \mu_B \Big(\sum_i \vec{H} \cdot \tilde{g}_1 \cdot \vec{S}_i + \sum_j \vec{H} \cdot \tilde{g}_2 \cdot \vec{S}_j \Big)$$

$$= \left(\frac{1}{2}N\right) \{ 2z|J| \vec{S}_1 \cdot \vec{S}_2 - \mu_B \vec{H} \cdot (\tilde{g}_1 \cdot \vec{S}_1 + \tilde{g}_2 \cdot \vec{S}_2) \} \quad , \tag{3-2}$$

where the summation $\sum_{<i,j>}$ is taken for all nearest neighbor pairs. N and z represent the total number of spins in 1 and 2 sites and the nearest neighbor spin number, respectively. Therefore, the total intralayer hamiltonian per ½N which is written as H_{12} hereafter is given as follows:

$$\begin{aligned} H_{12} = \; & I \vec{S}_1 \cdot \vec{S}_2 + K S_{1Z} S_{2Z} + K'(S_{1X} S_{2X} - S_{1Y} S_{2Y}) \\ & + A(S_{1Y} S_{2Z} + S_{1Z} S_{2Y}) - D_Y(S_{1Z} S_{2X} - S_{1X} S_{2Z}) \\ & - D_Z(S_{1X} S_{2Y} - S_{1Y} S_{2X}) - \mu_B \vec{H} \cdot (\tilde{g}_1 \cdot \vec{S}_1 + \tilde{g}_2 \cdot \vec{S}_2) \end{aligned} \tag{3-3a}$$

with

$$I = 2z|J| \quad , \quad J < 0 \quad , \quad z = 4 \quad . \tag{3-3b}$$

The first and the last terms of eq. (3-3a) are, of course, the isotropic intralayer exchange and the Zeeman interaction treated in eq. (3-2). The K-, K'- and A-terms are due to the symmetric anisotropic exchange and D_Y- and D_Z-terms stand for the antisymmetric anisotropic exchange or the Dzyaloshinsky-Moriya interaction. This hamiltonian H_{12} which contains

the most general bilinear intralayer exchange interaction allowed by monoclinic symmetry for $S=\frac{1}{2}$ case is first introduced by SC. H_{34} is obtained from eq. (3-3a) by changing 1 and 2 to 3 and 4, respectively. The g-tensors $\tilde{g}_1(=\tilde{g}_3)$ and $\tilde{g}_2(=\tilde{g}_4)$ are given by

$$\tilde{g}_1,\ \tilde{g}_2 = \begin{pmatrix} g_{XX} & \pm g_{XY} & \pm g_{ZX} \\ \pm g_{XY} & g_{YY} & g_{YZ} \\ \pm g_{ZX} & g_{YZ} & g_{ZZ} \end{pmatrix} , \tag{3-3c}$$

where + and - correspond to $\tilde{g}_1$ and $\tilde{g}_2$, respectively. The interlayer interaction H_{int} is given by

$$H_{int} = I'(\vec{S}_1 \cdot \vec{S}_3 + \vec{S}_2 \cdot \vec{S}_4) , \tag{3-4a}$$

$$I' = 2z'|J'| , \quad J' < 0 , \quad z' = 2 . \tag{3-4b}$$

The equations of motion are given by

$$\frac{\hbar}{i}\frac{d\vec{S}_i}{dt} = [H, \vec{S}_i] \quad (i=1,2,3,4) .$$

For example, dS_{1X}/dt is given as

$$\begin{aligned} \hbar dS_{1X}/dt = {} & I(S_{1Y}S_{2Z} - S_{1Z}S_{2Y}) + KS_{1Y}S_{2Z} + K'S_{1Z}S_{2Y} \\ & + A(S_{1Y}S_{2Z} - S_{1Z}S_{2Z}) - D_Y S_{1Y}S_{2X} - D_Z S_{1Z}S_{2X} \\ & - \mu_B\{(H_X g_{ZX} + H_Y g_{YZ} + H_Z g_{ZZ})S_{1Y} - (H_X g_{XY} + H_Y g_{YY} + H_Z g_{YZ})S_{1Z}\} \\ & + I'(S_{1Y}S_{3Z} - S_{1Z}S_{3Y}) . \end{aligned} \tag{3-5}$$

We take thermal average of these equations with the notation $< >$. Quantities $<S_{i\alpha}S_{j\beta}>(i,j=1,2,3,4)$ are replaced by $<S_{i\alpha}><S_{j\beta}>$, where α and β stand for one of X, Y and Z. For simplicity, normalized vector components X_i, Y_i and Z_i are introduced as

$$<S_{iX}> = <S_i>X_i \quad ,$$

$$<S_{iY}> = <S_i>Y_i \quad ,$$

$$<S_{iZ}> = <S_i>Z_i \qquad (i=1,2,3,4) \quad . \tag{3-6}$$

Usually, one can assume $<S_1> = <S_2> = <S_3> = <S_4> \equiv <S>$. Following SC the simplified notations given by

$$I<S>/2\mu_B = H_{ex} \ , \quad K<S>/2\mu_B = H_K \ , \quad K'<S>/2\mu_B = H_{K'} \ ,$$

$$A<S>/2\mu_B = H_A \ , \quad D_Y<S>/2\mu_B = h_{DM} \ , \quad D_Z<S>/2\mu_B = H_{DM} \ ,$$

$$I'<S>/2\mu_B = h_{ex} \ , \tag{3-7}$$

are used. Then eq. (3-5) is written as

$$\begin{aligned} |\gamma|^{-1}dX_1/dt = {} & H_{ex}(Y_1Z_2 - Z_1Y_2) + H_KY_1Z_2 + H_{K'}Z_1Y_2 \\ & + H_A(Y_1Y_2 - Z_1Z_2) - h_{DM}Y_1X_2 - H_{DM}Z_1X_2 \\ & - \{(H_Xg_{ZX}/2 + H_Yg_{YZ}/2 + H_Zg_{ZZ}/2)Y_1 \\ & \quad - (H_Xg_{XY}/2 + H_Yg_{YY}/2 + H_Zg_{YZ}/2)Z_1\} \\ & + h_{ex}(Y_1Z_3 - Z_1Y_3) \quad , \end{aligned}$$

where

$$|\gamma| = 2\mu_B/\hbar \quad .$$

The equilibrium condition is given by

$$dX_i/dt = dY_i/dt = dZ_i/dt = 0 \quad (i=1,2,3,4) \quad . \tag{3-8}$$

Of these 12 equations, $dX_1/dt = 0$ and $dX_2/dt = 0$ are given as follows:

$$\begin{aligned} & H_{ex}(Y_1Z_2 - Z_1Y_2) + H_K Y_1 Z_2 + H_{K'} Z_1 Y_2 + H_A(Y_1Y_2 - Z_1Z_2) \\ & \quad - h_{DM} Y_1 X_2 - H_{DM} Z_1 X_2 \\ & \quad - \{(H_X g_{ZX}/2 + H_Y g_{YZ}/2 + H_Z g_{ZZ}/2) Y_1 \\ & \qquad - (H_X g_{XY}/2 + H_Y g_{YY}/2 + H_Z g_{YZ}/2) Z_1\} \\ & \quad + h_{ex}(Y_1Z_3 - Z_1Y_3) = 0 \quad , \end{aligned} \tag{3-9a}$$

$$\begin{aligned} & H_{ex}(Z_1Y_2 - Y_1Z_2) + H_K Z_1 Y_2 + H_{K'} Y_1 Z_2 + H_A(Y_1Y_2 - Z_1Z_2) \\ & \quad + h_{DM} X_1 Y_2 + H_{DM} X_1 Z_2 \\ & \quad - \{(-H_X g_{ZX}/2 + H_Y g_{YZ}/2 + H_Z g_{ZZ}/2) Y_2 \\ & \qquad - (-H_X g_{XY}/2 + H_Y g_{YY}/2 + H_Z g_{YZ}/2) Z_2\} \\ & \quad + h_{ex}(Y_2Z_4 - Z_2Y_4) = 0 \quad . \end{aligned} \tag{3-9b}$$

The free energy in unit of magnetic field, f_{tot}, is defined as follows:

$$\begin{aligned} f_{tot} &\equiv \langle H \rangle / 2\mu_B \langle S \rangle \\ &= f_{12} + f_{34} + f_{int} \quad , \end{aligned} \tag{3-10a}$$

where

$$f_{12} = H_{ex}(X_1X_2 + Y_1Y_2 + Z_1Z_2) + H_K Z_1Z_2 + H_{K'}(X_1X_2 - Y_1Y_2)$$

$$+ H_A(Y_1Z_2 + Z_1Y_2) - h_{DM}(Z_1X_2 - X_1Z_2) - H_{DM}(X_1Y_2 - Y_1X_2)$$

$$- \frac{1}{2}\{(H_X g_{XX}+H_Y g_{XY}+H_Z g_{ZX})X_1 + (H_X g_{XX}-H_Y g_{XY}-H_Z g_{ZX})X_2$$

$$+ (H_X g_{XY}+H_Y g_{YY}+H_Z g_{YZ})Y_1 + (-H_X g_{XY}+H_Y g_{YY}+H_Z g_{YZ})Y_2$$

$$+ (H_X g_{ZX}+H_Y g_{YZ}+H_Z g_{ZZ})Z_1 + (-H_X g_{ZX}+H_Y g_{YZ}+H_Z g_{ZZ})Z_2\} \qquad (3\text{-}10b)$$

and f_{34} is obtained by changing 1 and 2 to 3 and 4. The term f_{int} is given by

$$f_{int} = h_{ex}(X_1X_3 + Y_1Y_3 + Z_1Z_3 + X_2X_4 + Y_2Y_4 + Z_2Z_4) \quad . \qquad (3\text{-}10c)$$

3.1.2 Simplification of the torque equations and the free energy

We derive the following 6 pairs of equations by adding and subtracting eqs. (3-8):

$$dR_1/dt \pm dR_2/dt = 0 \quad , \quad dR_3/dt \pm dR_4/dt = 0 \quad , \qquad (3\text{-}11)$$

where R stands for X, Y and Z. An example of these pairs obtained from eq. (3-9a) for X_1 and eq. (3-9b) for X_2 is as follows:

$$H_K(Y_1Z_2+Z_1Y_2) + H_{K'}(Y_1Z_2+Z_1Y_2) + 2\,H_A(Y_1Y_2-Z_1Z_2)$$

$$+ h_{DM}(X_1Y_2-Y_1X_2) + H_{DM}(X_1Z_2-Z_1X_2)$$

$$- \{H_X(g_{ZX}/2)(Y_1-Y_2) + H_Y(g_{YZ}/2)(Y_1+Y_2) + H_Z(g_{ZZ}/2)(Y_1+Y_2)$$

$$- H_X(g_{XY}/2)(Z_1-Z_2) - H_Y(g_{YY}/2)(Z_1+Z_2) - H_Z(g_{YZ}/2)(Z_1+Z_2)\}$$

$$+ h_{ex}(Y_1Z_3-Z_1Y_3+Y_2Z_4-Z_2Y_4) = 0 \quad , \tag{3-12a}$$

$$2H_{ex}(Y_1Z_2-Z_1Y_2) + H_K(Y_1Z_2-Z_1Y_2) + H_{K'}(Z_1Y_2 - Y_1Z_2)$$

$$- h_{DM}(Y_1X_2+X_1Y_2) - H_{DM}(Z_1X_2+X_1Z_2)$$

$$- \{H_X(g_{ZX}/2)(Y_1+Y_2) + H_Y(g_{YZ}/2)(Y_1-Y_2) + H_Z(g_{ZZ}/2)(Y_1-Y_2)$$

$$- H_X(g_{XY}/2)(Z_1+Z_2) - H_Y(g_{YY}/2)(Z_1-Z_2) - H_Z(g_{YZ}/2)(Z_1-Z_2)\}$$

$$+ h_{ex}(Y_1Z_3-Z_1Y_3-Y_2Z_4+Z_2Y_4) = 0 \quad . \tag{3-12b}$$

By using new vectors (l,m,n), (l',m',n'), (L,M,N) and (L',M',N') given by

$$l = \frac{1}{2}(X_1+X_2) \ , \quad m = \frac{1}{2}(Y_1+Y_2) \ , \quad n = \frac{1}{2}(Z_1+Z_2) \ ;$$

$$l' = \frac{1}{2}(X_3+X_4) \ , \quad m' = \frac{1}{2}(Y_3+Y_4) \ , \quad n' = \frac{1}{2}(Z_3+Z_4) \ ;$$

$$L = \frac{1}{2}(X_1-X_2) \ , \quad M = \frac{1}{2}(Y_1-Y_2) \ , \quad N = \frac{1}{2}(Z_1-Z_2) \ ;$$

$$L' = \frac{1}{2}(X_3-X_4) \ , \quad M' = \frac{1}{2}(Y_3-Y_4) \ , \quad N' = \frac{1}{2}(Z_3-Z_4) \ , \tag{3-13}$$

eqs. (3-12a) and (3-12b) are rewritten as

$$2(H_K+H_{K'})(mn-MN) + 2H_A(m^2-M^2-n^2+N^2)$$

$$+ 2h_{DM}(-1M+Lm) + 2H_{DM}(-1N+Ln)$$

$$- \{H_X g_{ZX} M + (H_Y g_{YZ}+H_Z g_{ZZ})m - H_X g_{XY} N - (H_Y g_{YY}+H_Z g_{YZ})n\}$$

$$+ 2h_{ex}(mn'+MN'-nm'-NM') = 0 \quad , \tag{3-14a}$$

$$2(2H_{ex}+H_K-H_{K'})(-mN+Mn) - 2h_{DM}(1m-LM) - 2H_{DM}(1n-LN)$$

$$- \{H_X g_{ZX} m + (H_Y g_{YZ}+H_Z g_{ZZ})M - H_X g_{XY} n - (H_Y g_{YY}+H_Z g_{YZ})N\}$$

$$+ 2h_{ex}(mN'+Mn'-nM'-Nm') = 0 \quad . \tag{3-14b}$$

Equations (3-14a) and (3-14b) are the equilibrium condition of the vector components 1 and L, respectively. Later on, after a simplification, (3-14a) and similar equations derived from eq. (3-11) are used to determine the direction of the antiferromagnetic axes, (L,M,N) and (L',M',N').*) Equation (3-14b) and similar equations are used to determine the direction and the magnitude of the canting, (1,m,n) and (1',m',n').

Before discussing the simplification, nature of the terms in eqs. (3-14a) and (3-14b) is considered. The first and the second terms of (3-14a) represent the time derivative of 1 due to the anisotropy fields arising from the symmetric anisotropic exchanges. The third and the

---

*) Hereafter, (L,M,N) and (L',M',N') are referred to the major components of the spins and (1,m,n) and (1',m',n') are referred to the minor components.

fourth terms are due to the DM-interaction. These terms indicate that the DM-interaction works as an effective anisotropy for the major components. The origin is that the energy of the system is low when the antiferromagnetic axis is close to the plane perpendicular to the DM-vector. The fifth term with { } gives the effects of the Zeeman interaction. In the brackets, terms with M or N are due to the tilting of g-tensors. Terms with m or n are due to the interaction between the external field and the minor components. The last term comes from the interlayer exchange. It is noted that the interaction is divided into two parts, namely interactions between minor components and those between major components. Next, eq. (3-14b) is considered. The first term implies that torques arising from the isotropic and the symmetric anisotropic exchanges and acting on m originate the change of L. The second and the third are due to the DM-interaction. The spin canting in a DM-type weak ferromagnet is derived by combining these terms and the first term. The fourth term with { } represents the Zeeman interaction, where terms with M and N are the origin of the spin canting by the external field, in other words, that by the perpendicular susceptibility. Terms with m or n indicate the antisymmetric motion of the spins in a tilted-g system. The last is the interlayer exchange term. Its nature is similar to that of the intralayer exchange term.

To simplify these equations, we neglect terms of two types. In eq. (3-14a), terms arising from the anisotropy and the interlayer exchange fields acting on the minor components, namely those indicated by underlines(———), are neglected. Hereafter, they are referred to the type-one neglected terms. Anisotropies in the Zeeman interaction of the minor

components are also neglected. They are referred to type-two. Terms with broken underlines(-----) and deviation of $H_Z g_{ZZ} m$ and $H_Y g_{YY} n$(····· terms) from their isotropic parts $H_Z gm$*) and $H_Y gn$ belong to it, where g is given by

$$g \equiv \{ \frac{1}{3}(g_{XX}^2 + g_{YY}^2 + g_{ZZ}^2) \}^{\frac{1}{2}} . \qquad (3\text{-}15)$$

The order of magnitude of these terms are shown in Appendix A. We have done calculations including the type-two terms. The result indicates that they introduce small corrections to the expression of the perpendicular susceptibility and the effective canting fields. Therefore, they are neglected for simplicity. For the terms of type-one, complex quantitative examinations are desirable. We discuss this problem in Appendix A. The result shows that these terms are negligible up to 10^4 Oe except for two special cases. The exceptions are the bending points of the magnetization curve for $\vec{H}$//Y and Z. Next, in eq. (3-14b), terms other than the isotropic exchange, canting fields acting on the major component and the isotropic part of the Zeeman interaction are neglected. Namely, the neglected terms are the anisotropic symmetric exchange, canting fields acting on the minor components, anisotropic Zeeman terms and h_{ex}-terms. Similar to the case of (3-14a), nature of the neglected terms is indicated by three kinds of underlines.

The resulting simplified form of eq. (3-14a) and (3-14b) are as

---

*) $H_Z g_{ZZ} m$ can be rewritten as $H_Z\{g+(g_{ZZ}-g)\}m = H_Z gm + H_Z(g_{ZZ}-g)m$.

follows:*)

$$-2(H_K+H_{K'})MN - 2H_A(M^2-N^2) - 2h_{DM}(lM-Lm) + 2H_{DM}(nL-Nl)$$

$$- (H_X g_{ZX} M + H_Z gm - H_X g_{XY} N - H_Y gn) + 2h_{ex}(MN'-NM') = 0 \ , \qquad (3\text{-}16a)$$

$$4H_{ex}(-mN+Mn) + 2h_{DM}LM + 2H_{DM}NL - (H_Z gM - H_Y gN) = 0 \ . \qquad (3\text{-}16b)$$

Similarly, the free energies f_{12} and f_{int} given by eqs. (3-10b) and (3-10c) are truncated as

$$f_{12} = -H_{ex} + 2H_{ex}(l^2+m^2+n^2) - H_K N^2 - H_{K'}(L^2-M^2) - 2H_A MN$$

$$+ 2h_{DM}(nL-Nl) + 2H_{DM}(lM-Lm)$$

$$- (H_X gl + H_Y gm + H_Z gn + H_Y g_{XY} L$$

$$+ H_Z g_{ZX} L + H_X g_{XY} M + H_X g_{ZX} N) \ , \qquad (3\text{-}17a)$$

$$f_{int} = 2h_{ex}(LL' + MM' + MN') \ . \qquad (3\text{-}17b)$$

3.1.3 Equations for determining the antiferromagnetic axes

The equations obtained from $dR_i/dt - dR_j/dt = 0$, for example eq. (3-16b), are solved by using the conditions $lL+mM+nN = 0$**) and

---

*) Remaining pairs obtained from (3-11) are shown in Appendix B.

**) This condition arises from $|\langle\vec{S}_1\rangle| = |\langle\vec{S}_2\rangle|$.

$l'L'+m'M'+n'N' = 0$. The solutions are

$$l = (1/4H_{ex})\{ 2h_{DM}N - 2H_{DM}M + H_X g(M^2 + N^2) - H_Y gLM - H_Z gNL \} , \quad (3\text{-}18a)$$

$$m = (1/4H_{ex})\{ 2H_{DM}L + H_Y g(N^2 + L^2) - H_Z gMN - H_X gLM \} , \quad (3\text{-}18b)$$

$$n = (1/4H_{ex})\{ -2h_{DM}L + H_Z g(L^2 + M^2) - H_Y gMN - H_X gLN \} , \quad (3\text{-}18c)$$

and similar equations for l', m' and n'. Substituting them in equations $dR_i/dt+dR_j/dt = 0$, six equations for (L,M,N) and (L',M',N') are deduced. An example corresponding to eq. (3-16a) is given by

$$\begin{aligned} &-2(H_K+H_{K'}+h_{DM}^2/H_{ex}-H_{DM}^2/H_{ex})MN - 2(H_A-H_{DM}h_{DM}/2H_{ex})(M^2-N^2) \\ &- (g_{ZX} + h_{DM}g/2H_{ex})H_X M + (g_{XY} - H_{DM}g/2H_{ex})H_X N \\ &+ (g^2/4H_{ex})\{ -H_Z{}^2MN + H_Y{}^2MN - H_X H_Y NL \\ &\qquad + H_X H_Z LM + H_Y H_Z(M^2-N^2) \} \\ &+ 2h_{ex}(MN' - NM') = 0 \quad . \end{aligned} \quad (3\text{-}19)$$

Similarly, f_{12} given by eq. (3-17a) is rewritten as

$$
\begin{aligned}
f_{12} = {} & \underline{-H_{ex}} - \underline{(H_{DM}^2/2H_{ex})} - \underline{\tfrac{1}{2}(h_{DM}^2/2H_{ex})} \\
& -(H_K - H_{DM}^2/2H_{ex} + \tfrac{1}{2}h_{DM}^2/2H_{ex})N^2 \\
& -(H_{K'} + \tfrac{1}{2}h_{DM}^2/2H_{ex})(L^2-M^2) - 2(H_A - H_{DM}h_{DM}/2H_{ex})MN \\
& -[\{(g_{XY} + gH_{DM}/2H_{ex})H_Y + (g_{ZX} - gh_{DM}/2H_{ex})H_Z\}L \\
& \quad + (g_{XY} - gH_{DM}/2H_{ex})H_X M + (g_{ZX} + gh_{DM}/2H_{ex})H_X N\ ] \\
& -(g^2/8H_{ex})\{H_X^2(M^2+N^2) + H_Y^2(N^2+L^2) + H_Z^2(L^2+M^2) \\
& \qquad -2H_XH_YLM - 2H_XH_ZLN - 2H_YH_ZMN\} \quad . \qquad (3\text{-}20)
\end{aligned}
$$

The first three terms with underlines are isotropic, so that can be neglected. As X, Y and Z are the antiferromagnetic principal axes, the cross term $-2(H_A-H_{DM}h_{DM}/2H_{ex})MN$ should always be zero. Therefore, we have

$$H_A = H_{DM}h_{DM}/2H_{ex} \quad . \qquad (3\text{-}21)$$

For simplicity, the following notations are introduced:

$$
\begin{aligned}
& H_K - H_{DM}^2/2H_{ex} + \tfrac{1}{2}h_{DM}^2/2H_{ex} = H_K^* \ , \quad H_{K'} + \tfrac{1}{2}h_{DM}^2/2H_{ex} = H_{K'}^* \ , \\
& g_{XY} - H_{DM}g/2H_{ex} = g_{XY}^* \ , \quad g_{XY} + H_{DM}g/2H_{ex} = g_{XY}^{**} \ , \\
& g_{ZX} + h_{DM}g/2H_{ex} = g_{ZX}^* \ , \quad g_{ZX} - h_{DM}g/2H_{ex} = g_{ZX}^{**} \ . \qquad (3\text{-}22)
\end{aligned}
$$

Then, the equations for (L,M,N) and (L',M',N') are given by

$$-2(H_K^* + H_{K'}^*)MN - g_{ZX}^* H_X M + g_{XY}^* H_X N$$
$$+ (g^2/4H_{ex}) \{ -H_Y^2 MN + H_Z^2 MN - H_X H_Y NL$$
$$+ H_X H_Z LM + H_Y H_Z (M^2 - N^2) \}$$
$$+ 2h_{ex}(MN' - NM') = 0 \quad , \tag{3-23a}$$

$$2(H_K^* - H_{K'}^*)NL + g_{ZX}^* H_X L - (g_{XY}^{**} H_Y + g_{ZX}^{**} H_Z)N$$
$$+ (g^2/4H_{ex}) \{ H_X^2 NL - H_Z^2 NL + H_X H_Y MN$$
$$+ H_X H_Z (N^2 - L^2) - H_Y H_Z LM \}$$
$$+ 2h_{ex}(NL' - LN') = 0 \quad , \tag{3-23b}$$

$$4H_{K'}^* ML - g_{XY}^* H_X L + (g_{XY}^{**} H_Y + g_{ZX}^{**} H_Z)M$$
$$+ (g^2/4H_{ex}) \{ -H_X^2 LM + H_Y^2 LM + H_X H_Y (L^2 - M^2)$$
$$- H_X H_Z MN + H_Y H_Z NL \}$$
$$+ 2h_{ex}(LM' - ML') = 0 \tag{3-23c}$$

and similar equations which are obtained by interchanging L, M, N and L', M', N'. Hereafter, we call the latter as associated equations. The anisotropy part f of the free energy f_{tot} is given by

$$f = - H_K^*(N^2+N'^2) - H_{K'}^* \{(L^2-M^2) + (L'^2-M'^2)\}$$

$$- \{g_{XY}^* H_X(M+M') + g_{ZX}^* H_X(N+N') + (g_{XY}^{**} H_Y + g_{ZX}^{**} H_Z)(L+L')\}$$

$$- (g^2/8H_{ex}) [H_X^2\{(M^2+N^2) + (M'^2+N'^2)\}$$

$$+ H_Y^2\{(L^2+N^2) + (L'^2+N'^2)\}$$

$$+ H_Z^2\{(L^2+M^2) + (L'^2+M'^2)\} - 2H_X H_Y(LM+L'M')$$

$$- 2H_Y H_Z(MN+M'N') - 2H_Z H_X(NL+N'L')]$$

$$+ 2h_{ex}(LL'+MM'+NN') \quad . \tag{3-24}$$

Equations (3-23a) ∿ (3-23c) and (3-24) are fundamental equations by which the magnetization process of CuFTH is examined. In general, we first solve eqs. (3-23a) ∿ (3-23c) and the associated equations*) under the condition:

$$L^2 + M^2 + N^2 = 1 \quad , \qquad L'^2 + M'^2 + N'^2 = 1 \quad . \tag{3-25}$$

Next, by inserting LMN and L'M'N' of the solutions to (3-24) and comparing the resulting f's, the lowest-energy equilibrium state is found. Equation (3-23a) and similar equations are not analytically solvable for $\vec{H}//X$ in the 4-sublattice state. For this case, (3-24) is examined numerically by using a computer and the lowest-energy state is found.

---

*) Of these six equations four are independent. However, we write all equations for a while because the adequate set should be selected in each case later.

Equation (3-24) indicates that the free energy of the 4-sublattice system can be regarded as the free energy of a fictitious 2-spin system when the directions of the antiferromagnetic axes of two layers, (L,M,N) and (L',M',N'), are supposed as fictitious spins. The first and the second terms of (3-24) represent the effective one-ion type anisotropy. The third term is the effective Zeeman interaction, where the fictitious g-tensor is given by

$$\begin{pmatrix} 0 & g_{XY}^{*} & g_{ZX}^{*} \\ g_{XY}^{**} & 0 & 0 \\ g_{ZX}^{**} & 0 & 0 \end{pmatrix} .$$

The fourth term is due to the perpendicular susceptibility of the real system and, by this term, (L,M,N) and (L',M',N') are inclined to be perpendicular to the external field. We may consider this effect as the field dependence of the effective one-ion type anisotropy. The last term is the exchange interaction of the fictitious system. As these terms are of the same order of magnitude in CuFTH, we must deal with a 2-sublattice model in which the one-ion anisotropy and the Zeeman interaction are comparable to the exchange interaction.

3.2 Two special cases: H=0 and h_{ex}=0

Before examining the 4-sublattice model or the fictitious 2-spin system in general, two special cases, the H=0 and the h_{ex}=0 cases, are considered. Study of them is useful for the analysis of the general case and the examination of the results by SC. The latter h_{ex}=0 case corresponds to the 2-sublattice model or the fictitious 1-spin system when the primed fictitious spin is disregarded.

3.2.1 H=0

(a) $H=h_{ex}=0$

By neglecting the primed fictitious spin, the free energy is written as

$$f = - H_K^* N^2 - H_{K'}^* (L^2-M^2). \tag{3-26}$$

The equilibrium condition is given by

$$-2(H_K^* + H_{K'}^*)MN = 0 \quad , \tag{3-27a}$$

$$2(H_K^* - H_{K'}^*)NL = 0 \quad , \tag{3-27b}$$

$$4H_{K'}^* ML = 0 \quad . \tag{3-27c}$$

The solutions are obtained as

$$L = \pm 1 \ , \quad M = 0 \ , \quad N = 0 \ ; \tag{3-28a}$$

$$L = 0 \ , \quad M = \pm 1 \ , \quad N = 0 \ ; \tag{3-28b}$$

$$L = 0 \ , \quad M = 0 \ , \quad N = \pm 1 \ . \tag{3-28c}$$

The corresponding free energies are

$$f = - H_{K'}^{*} \qquad \text{for } L = \pm 1 \ , \tag{3-29a}$$

$$= + H_{K'}^{*} \qquad \text{for } M = \pm 1 \ , \tag{3-29b}$$

$$= - H_{K}^{*} \qquad \text{for } N = \pm 1 \ . \tag{3-29c}$$

When $H_K^* > H_{K'}^* > 0$, $N=\pm 1$ gives the lowest state. In the 4-sublattice case the solution $N=\pm 1$, $N'=\pm 1$ gives the lowest state.

(b) $H=0$, $h_{ex} > 0$

For this case the free energy f is given by

$$f = - H_K^* (N^2+N'^2) - H_{K'}^* \{ (L^2-M^2) + (L'^2-M'^2) \}$$

$$+ 2h_{ex}(LL' + MM' + NN') \ . \tag{3-30}$$

The torque equations for H=0 are

$$-2(H_K^* + H_{K'}^*)MN + 2h_{ex}(MN' - NM') = 0 \quad , \tag{3-31a}$$

$$2(H_K^* - H_{K'}^*)NL + 2h_{ex}(NL' - LN') = 0 \quad , \tag{3-31b}$$

$$4H_{K'}^*ML + 2h_{ex}(LM' - ML') = 0 \tag{3-31c}$$

and the associated equations obtained by interchanging L, M, N and L', M', N'. These equations have 36 solutions which can be grouped to (i) ∿ (ix). Detailed list of the solutions is given in Appendix C and Fig. 6 shows the characteristics of each groups schematically. The free energies are obtained as

$$\text{(i)}\ f = -H_{K'}^* - 2h_{ex}\ , \qquad \text{(ii)}\ f = -H_K^* + 2h_{ex}\ ,$$

$$\text{(iii)}\ f = -H_K^* - H_{K'}^*\ , \qquad \text{(iv)}\ f = -2H_{K'}^* + 2h_{ex}\ ,$$

$$\text{(v)}\ f = 2H_{K'}^* - 2h_{ex}\ , \qquad \text{(vi)}\ f = 0\ ,$$

$$\text{(vii)}\ f = -2H_K^* - 2h_{ex}\ , \qquad \text{(viii)}\ f = 2H_{K'}^* + 2h_{ex}\ ,$$

$$\text{(ix)}\ f = -H_K^* + H_{K'}^*\ . \tag{3-32}$$

The lowest-energy state is the (vii)-state.

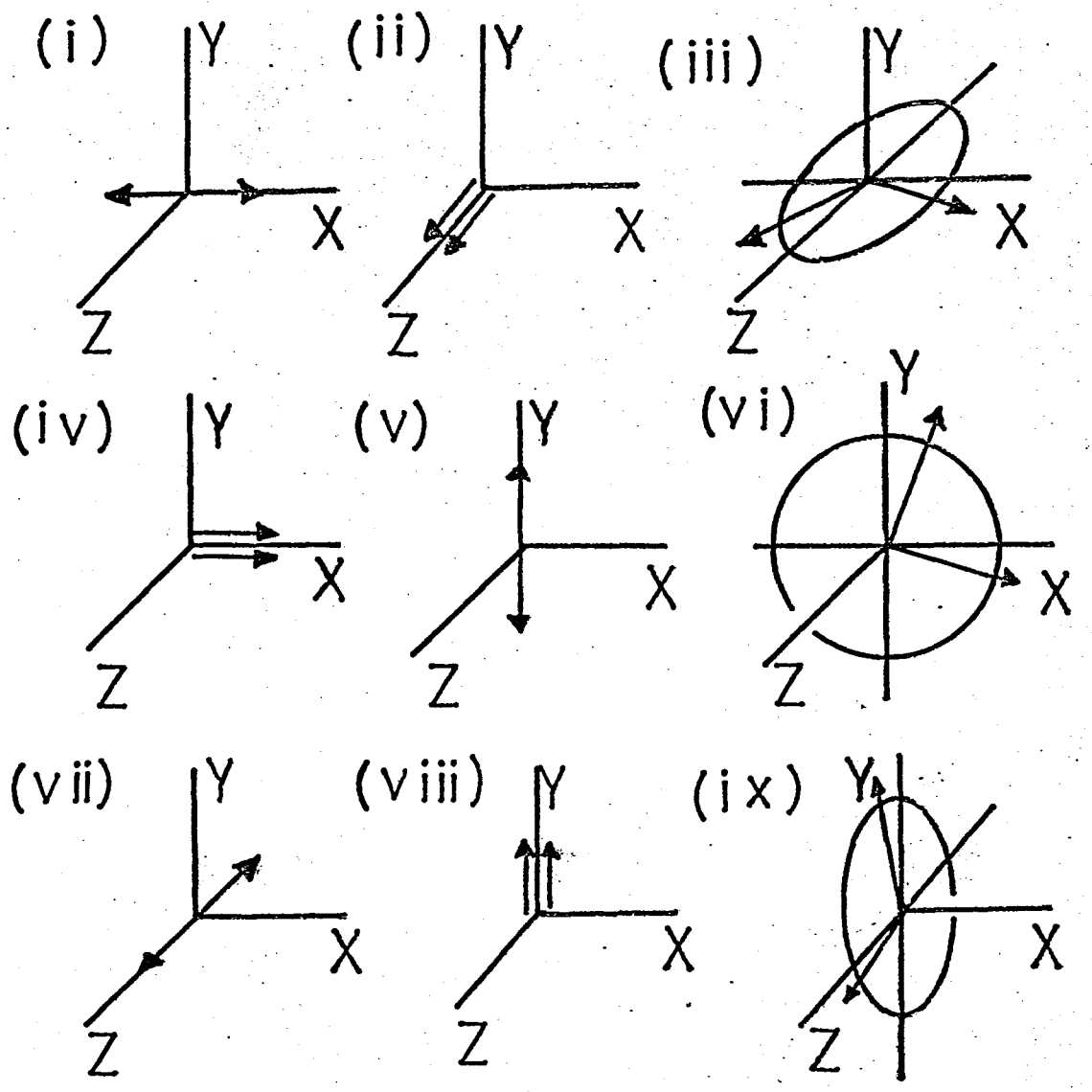

Fig. 6 Nine stable and unstable equilibrium configurations for the H=0 and $h_{ex} > 0$ case. The arrow marks in the figure represent the directions of the fictitious spins.

3.2.2 $h_{ex}=0$, $H\neq 0$

Three cases, $\vec{H}//Y$, Z and X, are considered.*)

(a) $\vec{H}//Y$

The free energy and the equilibrium conditions are given by

$$f = -(H_K^* + g^2H_Y^2/8H_{ex})N^2 - (H_{K'}^* + g^2H_Y^2/8H_{ex})L^2 + H_{K'}^*M^2 - g_{XY}^{**}H_YL \tag{3-33}$$

and

$$-2(H_K^* + H_{K'}^*)MN - (g^2/4H_{ex})H_Y^2MN = 0 , \tag{3-34a}$$

$$2(H_K^* - H_{K'}^*)NL - g_{XY}^{**}H_YN = 0 , \tag{3-34b}$$

$$4H_{K'}^*ML + g_{XY}^{**}H_YM + (g^2/4H_{ex})H_Y^2LM = 0 , \tag{3-34c}$$

respectively.

Equations (3-34a) ∿ (3-34b) have four solutions:

(i) $L = \mathrm{sign}(g_{XY}^{**})\cdot 1$, $M=N=0$

$$f = -(H_{K'}^* + g^2H_Y^2/8H_{ex}) - |g_{XY}^{**}|H_Y . \tag{3-35a}$$

---

*) H_Y, H_Z and H_X can be assumed to be positive with no loss of generality.

(i') $L = -\mathrm{sign}(g_{XY}^{**}) \cdot 1$, $M=N=0$.

$$f = -(H_{K'}^{*} + g^2 H_Y^2/8H_{ex}) + |g_{XY}^{**}|H_Y \quad . \tag{3-35a'}$$

Hereafter, we disregard this solution because f for (i') is always larger than that for (i).

(ii) $L = g_{XY}^{**}H_Y/2(H_K^{*} - H_{K'}^{*})$,

$M = 0$ for $H_Y \leqq 2(H_K^{*} - H_{K'}^{*})/|g_{XY}^{**}|$.

$$f = -(H_K^{*} + g^2 H_Y^2/8H_{ex}) - (g_{XY}^{**}H_Y)^2/4(H_K^{*} - H_{K'}^{*}) \quad . \tag{3-35b}$$

(iii) $L = -g_{XY}^{**}H_Y/2(2H_{K'}^{*} + g^2 H_Y^2/8H_{ex})$,

$N = 0$ for $H_Y \leqq 2(2H_{K'}^{*} + g^2 H_Y^2)/|g_{XY}^{**}|$.

$$f = H_{K'}^{*} + \frac{1}{4}(g_{XY}^{**}H_Y)^2/(2H_{K'}^{*} + g^2 H_Y^2/8H_{ex}) \quad . \tag{3-35c}$$

This solution can be also neglected because two terms in the right hand side of eq. (3-35c) is positive and, in eq. (3-35a), two terms are negative. Configurations (i) and (ii) are shown in Fig. 7(a) and their free energies are compared graphically in Fig. 7(b), where H_{BY} is defined as

$$H_{BY} = 2(H_K^{*} - H_{K'}^{*})/|g_{XY}^{**}| \quad . \tag{3-36}$$

If $H_Y \leqq H_{BY}$, (ii) is lower, otherwise (i) is lower. We see later that H_{BY} corresponds to the sharp bend of the magnetization curve for $\vec{H}//Y(c'')$.

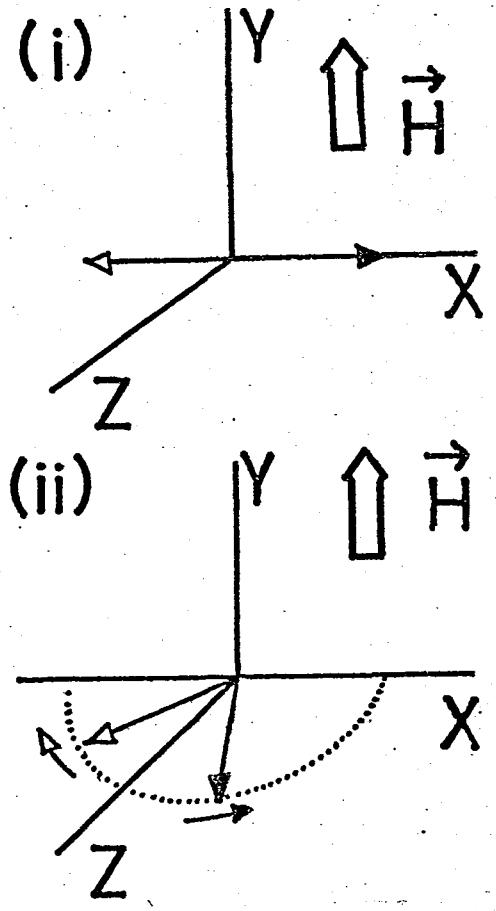

Fig. 7(a) Two equilibrium configurations for the $h_{ex}=0$ and $H_Y \neq 0$ case. The arrow marks ⟶ and ⟹ correspond to $g_{XY}^{**} > 0$ and $g_{XY}^{**} < 0$, respectively.

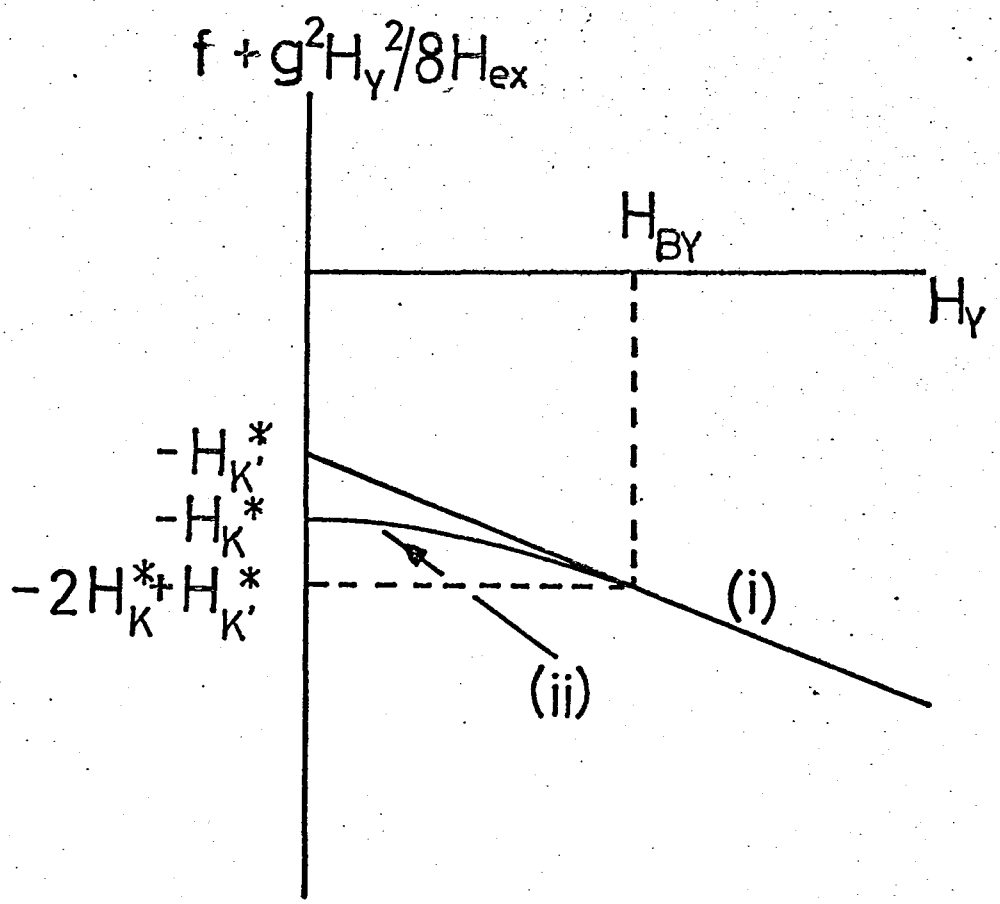

Fig. 7(b) Free energy values for two low-energy equilibrium configurations of the $h_{ex}=0$ and $H_Y \neq 0$ case. For simplicity we draw $f+(g^2H_Y^2/8H_{ex})$ instead of f itself, because $-(g^2H_Y^2/8H_{ex})$ is common in two cases.

The magnetization per ion, $\vec{M}$, is calculated by the equation

$$M_X = \frac{1}{2}\mu_B\langle S\rangle \{ g(l+l') + g_{XY}(M+M') + g_{ZX}(N+N') \}, \tag{3-37a}$$

$$M_Y = \frac{1}{2}\mu_B\langle S\rangle \{ g(m+m') + g_{XY}(L+L') \}, \tag{3-37b}$$

$$M_Z = \frac{1}{2}\mu_B\langle S\rangle \{ g(n+n') + g_{ZX}(L+L') \}. \tag{3-37c}$$

l, m, n, l', m' and n' are given in eqs. (3-18a) ∿ (3-18c) and similar equations. By substituting (3-35a) and (3-35b) in (3-37a) ∿ (3-37c), the magnetization are obtained as

$$M_X = \pm \mu_B\langle S\rangle g_{ZX}^* \{ 1 - (g_{XY}^{**}H_Y)^2/4(H_K - H_{K'}^*)^2 \}^{\frac{1}{2}} \quad \text{for} \quad H_Y \leqq H_{BY} \tag{3-38a}$$

$$= 0 \qquad \text{for} \quad H_Y > H_{BY}, \tag{3-38b}$$

$$M_Y = \mu_B\langle S\rangle \{ (g_{XY}^{**})^2/2(H_K^* - H_{K'}^*) + g^2/4H_{ex} \} H_Y \qquad \text{for} \quad H_Y \leqq H_{BY} \tag{3-39a}$$

$$= \mu_B\langle S\rangle (|g_{XY}^{**}| + g^2H_Y/4H_{ex}) \qquad \text{for} \quad H_Y \geqq H_{BY}, \tag{3-39b}$$

and

$$M_Z = \mu_B\langle S\rangle g_{XY}^{**}g_{ZX}^{**}H_Y/2(H_K^* - H_{K'}^*) \qquad \text{for} \quad H_Y \leqq H_{BY} \tag{3-40a}$$

$$= \mu_B\langle S\rangle \mathrm{sign}(g_{XY}^{**})g_{ZX}^{**} \qquad \text{for} \quad H_Y > H_{BY} \tag{3-40b}$$

The double sign ± for M_X arising from the two possiblities of the sign for N in case (ii) indicates that for $\vec{H}//Y$ both are allowed. The magnetization is not, in general, parallel to the external field because M_X, $M_Z \neq 0$. The magnetization parallel to the external field, M_Y has a sharp bending at H_{BY}. Finite M_X should be observed at zero external field unless $g_{ZX}^*=0$, because $M_X=\pm\mu_B\langle S\rangle g_{ZX}^*$, $M_Y=M_Z=0$ for $H_Y=0$. These conclusions are consistent with the results obtained by SC for the 2-sublattice model.

(b) $\vec{H}//Z$

The magnetization process is similar to the $\vec{H}//Y$ case but the calculations are complex, because the vector (L,M,N) is always perpendicular to the external field for $\vec{H}//Y$ but is not for the present case. The free energy and the equilibrium conditions are given as

$$f = - H_K^* N^2 - (H_{K'}^* + g^2 H_Z^2/8H_{ex}) L^2 + (H_{K'}^* - g^2 H_Z^2/8H_{ex}) M^2 - g_{ZX}^{**} H_Z L \quad (3\text{-}41)$$

and

$$- 2(H_K^* + H_{K'}^*) MN = 0 \quad , \quad (3\text{-}42a)$$

$$2(H_K^* - H_{K'}^*) NL - g_{ZX}^{**} H_Z N - (g^2/4H_{ex}) H_Z^2 NL = 0 \quad , \quad (3\text{-}42b)$$

$$4H_{K'}^* ML + g_{ZX}^{**} H_Z M = 0 \quad . \quad (3\text{-}42c)$$

Comparison between the f-values of solutions of these equations is not simple, because one of the f's is not a linear nor a quadratic function of H_Z. Therefore, calculations are shown in Appendix D and only the results are given below.

The bending field for $\vec{H}//Z$, H_{BZ}, is given as the positive solution of a self consistent equation:

$$H_{BZ} = 2(H_K^* - H_{K'}^* - g^2 H_{BZ}^2/8H_{ex})/|g_{ZX}^{**}| \quad . \quad (3\text{-}43)$$

The magnetization parallel to the external field is given by

$$M_Z = \mu_B \langle S \rangle \{ (g_{ZX}^{**})^2 (H_K^* - H_{K'}^*) / 2 (H_K^* - H_{K'}^* - g^2 H_Z^2 / 8H_{ex})^2 \} H_Z$$

$$\text{for} \quad H_Z \leqq H_{BZ}$$

$$= \mu_B \langle S \rangle (|g_{ZX}^{**}| + g^2 H_Z / 8H_{ex}) \quad \text{for} \quad H_Z > H_{BZ} \ . \tag{3-44}$$

Other components are calculated as

$$M_Y = \mu_B \langle S \rangle g_{XY}^{**} g_{ZX}^{**} H_Z / 2 (H_K^* - H_{K'}^* - g^2 H_Z^2 / 8H_{ex})$$

$$\text{for} \quad H_Z \leqq H_{BZ}$$

$$= \mu_B \langle S \rangle g_{XY}^{**} \text{sign}(g_{ZX}^{**}) \quad \text{for} \quad H_Z > H_{BZ} \tag{3-45}$$

and

$$M_X = \mu_B \langle S \rangle \left[\pm g_{ZX}^{**} \{ 1 - g_{ZX}^{**2} H_Z^2 / 4 (H_K^* - H_{K'}^* - g^2 H_Z^2 / 8H_{ex})^2 \}^{\frac{1}{2}} \right.$$

$$\mp (g_{ZZ}^2 H_Z / 4H_{ex}) \{ 1 - g_{ZX}^{**2} H_Z^2 / 4 (H_K^* - H_{K'}^* - g^2 H_Z^2 / 8H_{ex})^2 \}^{\frac{1}{2}}$$

$$\left. \times \{ g_{ZX}^{**} H_Z / 2 (H_K^* - H_{K'}^* - g^2 H_Z^2 / 8H_{ex}) \} \right]$$

$$\text{for} \quad H_Z \leqq H_{BZ}$$

$$= 0 \quad \text{for} \quad H_Z > H_{BZ} \ . \tag{3-46}$$

(c) $\vec{H}//X$

SC have suggested the existence of the magnetization jump for this case but we show here that their conclusion seems not to be good.

The free energy is given by

$$f = -(H_K^* + g^2H_X^2/8H_{ex})N^2 - H_{K'}^*L^2 + (H_{K'}^* - g^2H_X^2/8H_{ex})M^2 - g_{XY}^*H_XM - g_{ZX}^*H_XN \quad . \tag{3-47}$$

The equilibrium condition is written as follows:

$$-2(H_K^* + H_{K'}^*)MN - g_{ZX}^*H_XM + g_{XY}^*H_XN = 0 \quad , \tag{3-48a}$$

$$2(H_K^* - H_{K'}^*)NL + g_{ZX}^*H_XL + g^2H_X^2NL/4H_{ex} = 0 \quad , \tag{3-48b}$$

$$4H_{K'}^*ML - g_{XY}^*H_XL - g^2H_X^2ML/4H_{ex} = 0 \quad . \tag{3-48c}$$

At first L=0 is assumed as was done by SC. This point is reconsidered later. Equations (3-48b) and (3-48c) are satisfied automatically. By using (3-48a) and $M^2+N^2=1$, the following fourth order equation is obtained for M:

$$4(H_K^* + H_{K'}^*)^2M^4 - 4(H_K^* + H_{K'}^*)g_{XY}^*H_XM^3$$

$$+ \{(g_{XY}^*H_X)^2 + (g_{ZX}^*H_X)^2 - 4(H_K^* + H_{K'}^*)^2\}M^2$$

$$+ 4(H_K^* + H_{K'}^*)g_{XY}H_XM - (g_{XY}^*H_X)^2 = 0 \quad . \tag{3-49}$$

The magnetization is given by

$$M_X = \mu_B\langle S\rangle(g_{XY}^*M + g_{ZX}^*N + g^2H_X/4H_{ex}) \ ,$$

$$M_Y = 0 \ , \quad M_Z = 0 \ , \tag{3-50}$$

where the direction cosine N is given by

$$N = \text{sign}(g_{ZX}^*)\cdot(1 - M^2)^{\frac{1}{2}} \quad . \tag{3-51}$$

The sign for N is adjusted so as to minimize the free energy.

As the fourth order equation (3-49) is not physically transparent, we consider graphically how the equilibrium position changes as a function of H_X. By writing $M=\sin\theta$ and $N=\cos\theta$, the free energy is rewritten as

$$f = - H_K^*\cos^2\theta + H_{K'}^*\sin^2\theta - g^2H_X^2/8H_{ex}$$

$$- g_{XY}^*H_X\sin\theta - g_{ZX}^*H_X\cos\theta \quad . \tag{3-52}$$

The equilibrium condition is given by

$$(H_K^* + H_{K'}^*)\sin2\theta + (g_{XY}^{*2} + g_{ZX}^{*2})^{\frac{1}{2}}H_X\sin(\theta - \Delta) = 0 \ , \tag{3-53a}$$

where Δ is determined as

$$\sin\Delta = g_{XY}^*/(g_{XY}^{*2} + g_{ZX}^{*2})^{\frac{1}{2}} \quad , \qquad \cos\Delta = g_{ZX}^*/(g_{XY}^{*2} + g_{ZX}^{*2})^{\frac{1}{2}} \quad . \tag{3-53b}$$

Of course, eq. (3-53a) is equivalent to eq. (3-48a).

Figure 8(a) shows the first term and the negative of the second term of eq. (3-53a) for the $g_{XY}^* < 0$ and $g_{ZX}^* > 0$ case. In the figure, one of the abbreviated notations defined by

$$H_{K+}^* = H_K^* + H_{K'}^* \quad , \qquad H_{K-}^* = H_K^* - H_{K'}^* \tag{3-54}$$

is used following SC. The figure indicates that eq. (3-53a) has 4 or 2 solutions depending on the field strength. Next, we consider the free energy. Fig. (b) shows two θ-dependent terms of f;

$$\text{(i)} \quad -\frac{1}{2}(H_K^* + H_{K'}^*)\cos 2\theta \quad ,$$

and

$$\text{(ii)} \quad -(g_{XY}^{*2} + g_{ZX}^{*2})^{\frac{1}{2}} H_X \cos(\theta - \Delta) \quad .$$

Unless $H_X = 0$, we obtain a stable minimum in the fourth quadrant and, in the low field region, a meta-stable minimum in the third quadrant. Figure (c) shows how the extrema change with the external field. The situation is similar for every pairs of the signs of g_{XY}^* and g_{ZX}^*. Thus we can conclude that the 2-sublattice model never accompanies an instability of the antiferromagnetic axis, in other words, never gives the magnetization jump. The essence of the SC's explanation is to identify the disappearance of the meta-stable state to the magnetization

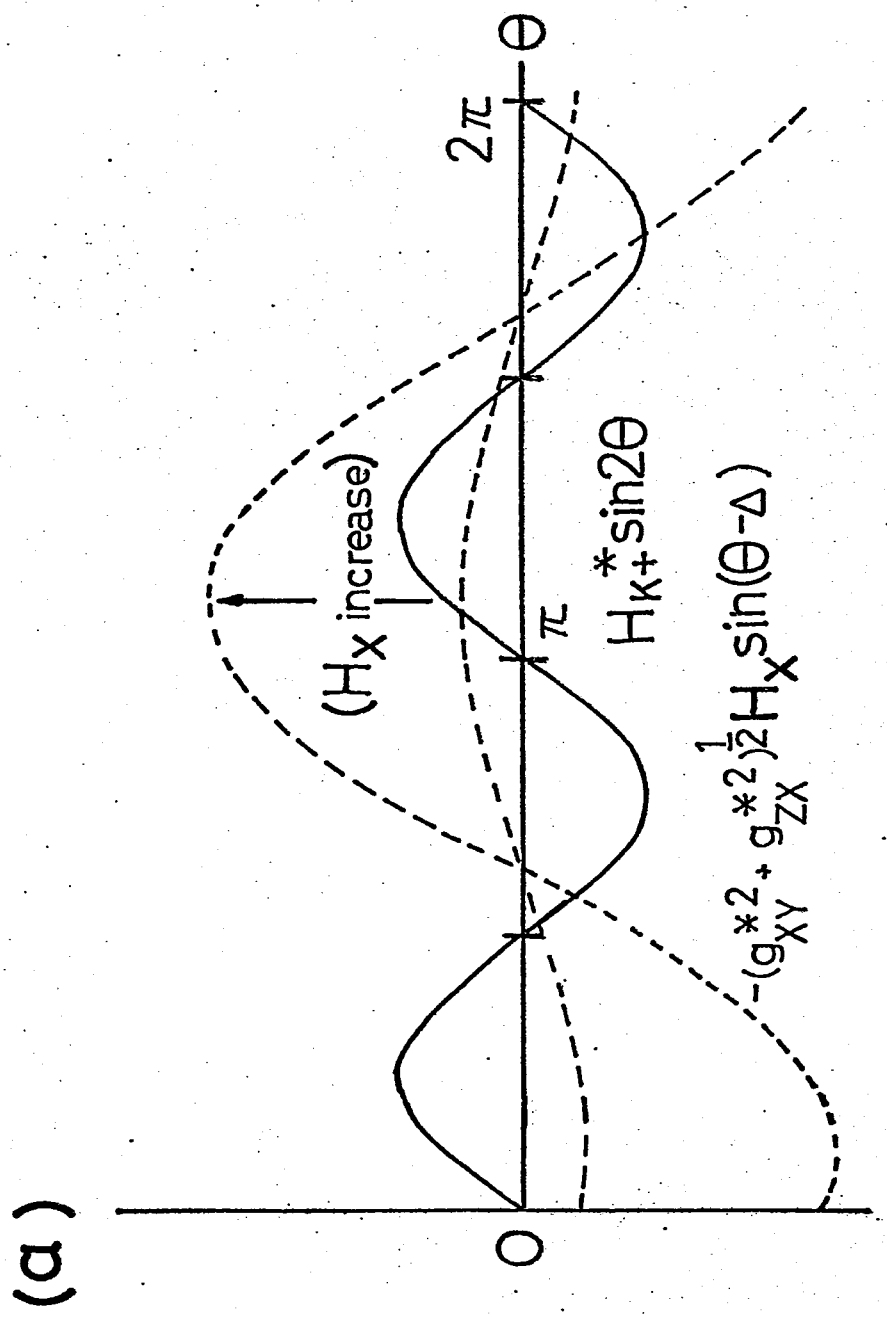

Fig. 8(a) Graphical solution for eq. (3-53a). The solutions are θ's of two or four intersections of solid and dotted curves.

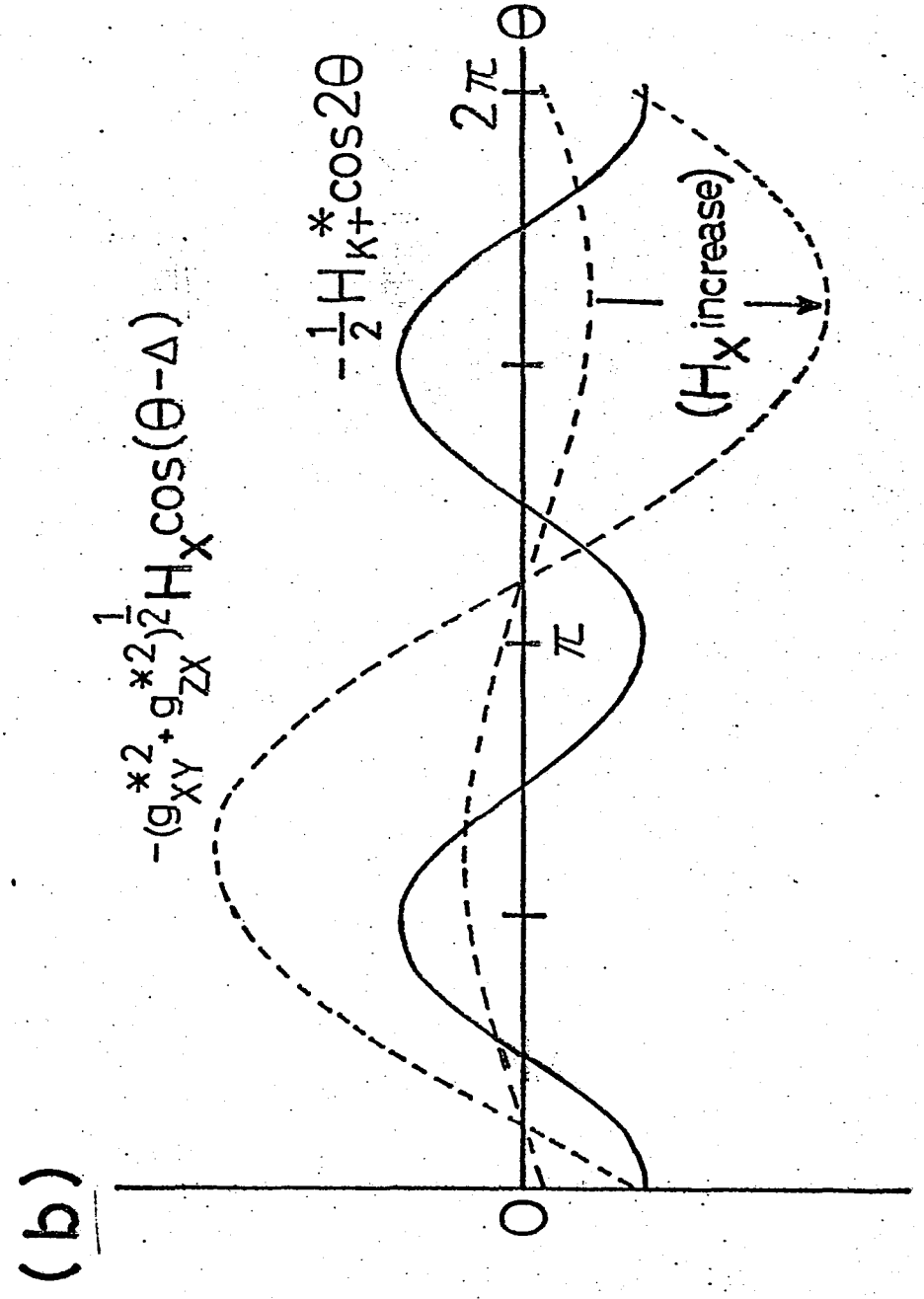

Fig. 8(b) Two angular-dependent terms of the free energy. Minimum point of the sum of solid and dotted curves corresponds to the free energy minimum.

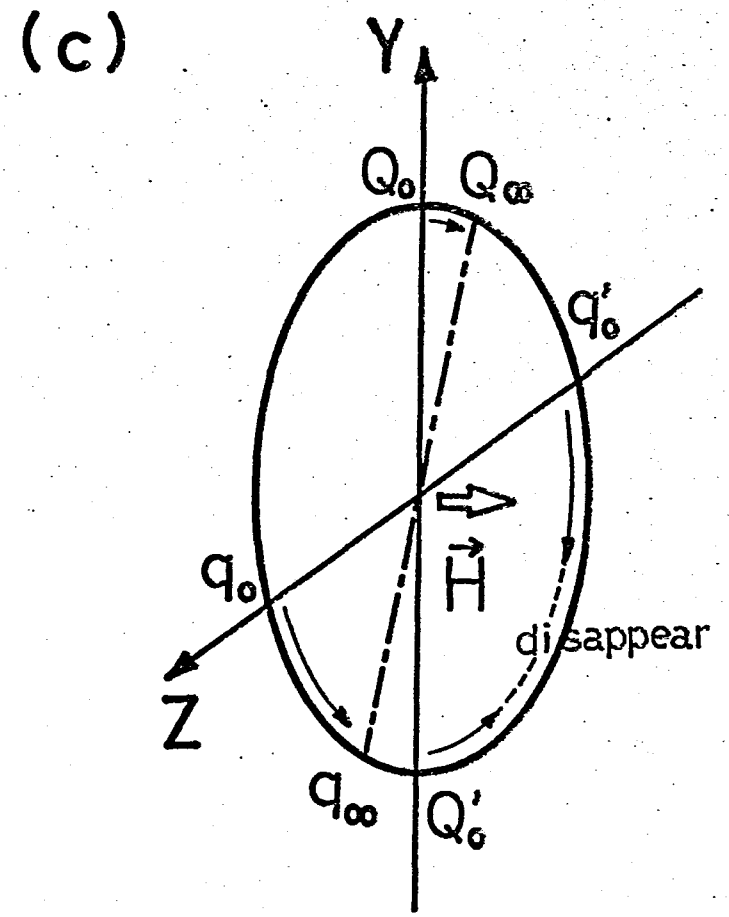

Fig. 8(c) Field dependence of the free energy extrema. Q_0 and Q_0' are the maximum points for $H_X=0$ and q_0 and q_0' the minimum points for $H_X=0$. Q_∞ and q_∞ are the maximum and the minimum points for $H_X=\infty$ respectively.

jump. Of course, it is not correct.

The assumption L=0 is reconsidered. Equations (3-48a) ∿ (3-48c) have two L≠0 type solutions. However, they are neglected by the following reasons: These solutions reduce to L=±1 when H_X=0 and, by increasing H_X, moves continuously to the third quadrant of the ZY-plane, namely they connect saddle points and the confluence point. These properties of L≠0 solutions suggest that the minimum is on the L=0 plane.

Examples of the magnetization curves are included in Fig. 11(b) of the next subsection.*) Open circles and open triangles correspond to the g_{ZX}*=0 and g_{ZX}*≠0 cases, respectively. The contribution of $\chi_\perp$ is neglected for simplicity. It is noticed that for $H_X = 0(\vec{H}=0)$ we have from (3-50) and (3-51)

$$M_X = \mu_B \langle S \rangle |g_{ZX}^*| \ . \tag{3-55a}$$

For $H_X \to \infty$, one obtains $\theta \to \Delta$ (See (3-53a).) so that

$$M_X \to \mu_B \langle S \rangle (g_{XY}^* \sin\Delta + g_{ZX}^* \cos\Delta)$$

$$= \mu_B \langle S \rangle (g_{XY}^{*2} + g_{ZX}^{*2})^{\frac{1}{2}} \ . \tag{3-55b}$$

A term arising from $\chi_\perp$ is neglected for simplicity.

---

*) These magnetization curves are obtained numerically as special(h_{ex}=0) cases of the 4-sublattice model instead of solving eq. (3-49) directly. Two methods are equivalent.

3.3 Magnetization process

The magnetization process of the 4-sublattice system or the fictitous 2-spin system is considered. The interlayer exchange field h_{ex} is assumed to be positive and three cases, $\vec{H}//Y$, Z and X are examined. The result is applied to CuFTH in §5.

3.3.1 $\vec{H}//Y$

The free energy is written as

$$f = -(H_K^* + g^2H_Y^2/8H_{ex})(N^2 + N'^2) - (H_{K'}^* + g^2H_Y^2/8H_{ex})(L^2 + L'^2)$$
$$+ H_{K'}^*(M^2 + M'^2) - g_{XY}^{**}H_Y(L + L') + 2h_{ex}(LL' + MM' + NN') \quad . \qquad (3\text{-}56)$$

The equilibrium condition is given by

$$-2(H_K^* + H_{K'}^*)MN - (g^2H_Y^2/4H_{ex})MN + 2h_{ex}(MN' - NM') = 0 \ , \qquad (3\text{-}57a)$$

$$2(H_K^* - H_{K'}^*)NL - g_{XY}^{**}H_YN + 2h_{ex}(NL' - LN') = 0 \ , \qquad (3\text{-}57b)$$

$$4H_{K'}^*ML + g_{XY}^{**}H_YM + (g^2H_Y^2/4H_{ex})LM + 2h_{ex}(LM' - ML') = 0 \ , \qquad (3\text{-}57c)$$

and the associated equations obtained by interchanging L, M, N and L', M', N'. An equivalent problem has been considered by Gorter and coworkers[34] under the assumption M=M'=0. In this paper the relation M=M'=0 is not assumed but derived.

First we notice from eq. (3-56) that f is low when $MM' \leqq 0$ and $NN' \leqq 0$. As f does not depend on the signs of M and N themselves, the followings can be assumed with no loss of generality:

$$N \geqq 0 , \quad M \geqq 0 , \quad N' \equiv -N'' \leqq 0 , \quad M' \equiv -M'' \leqq 0 . \tag{3-58}$$

Then the free energy is written as follows:

$$f = - (H_K^* + g^2 H_Y^{\,2}/8H_{ex})(N^2 + N''^2) - (H_{K'}^* + g^2 H_Y^{\,2}/8H_{ex})(L^2 + L''^2)$$
$$+ H_{K'}^*(M^2 + M''^2) - g_{XY}^{**} H_Y (L + L') + 2h_{ex}(LL' - MM'' - NN'') . \tag{3-59}$$

The following derivative of f is considered:

$$(\partial/\partial M) f(L,M,L'',M'') = 2(H_K^* + g^2 H_Y^{\,2}/8H_{ex})M/N + 2H_{K'}^* M$$
$$+ 2h_{ex} N''M/N - 2h_{ex} M'' , \tag{3-60}$$

where N is not independent of L and M. The condition $(\partial f/\partial M)=0$ yields

$$M = M'' \cdot 2h_{ex}/\{2(H_K^* + g^2 H_Y^{\,2}/8H_{ex})(1/N) + 2h_{ex}(N''/N) + 2H_{K'}^*\}$$
$$\leqq M'' \cdot h_{ex}/H_{K+}^* . \tag{3-61}$$

A similar equation can be derived for M'' because M and M'' are equivalent in eq. (3-59). As the factor h_{ex}/H_{K+}^* is estimated as about 1/6 in this crystal(See §3.3.3.), the two equations conflict each other unless M=M''=0. Thus, the relation is proved. The spin configuration which satisfies M=M''=0 is shown in Fig. 9(a).

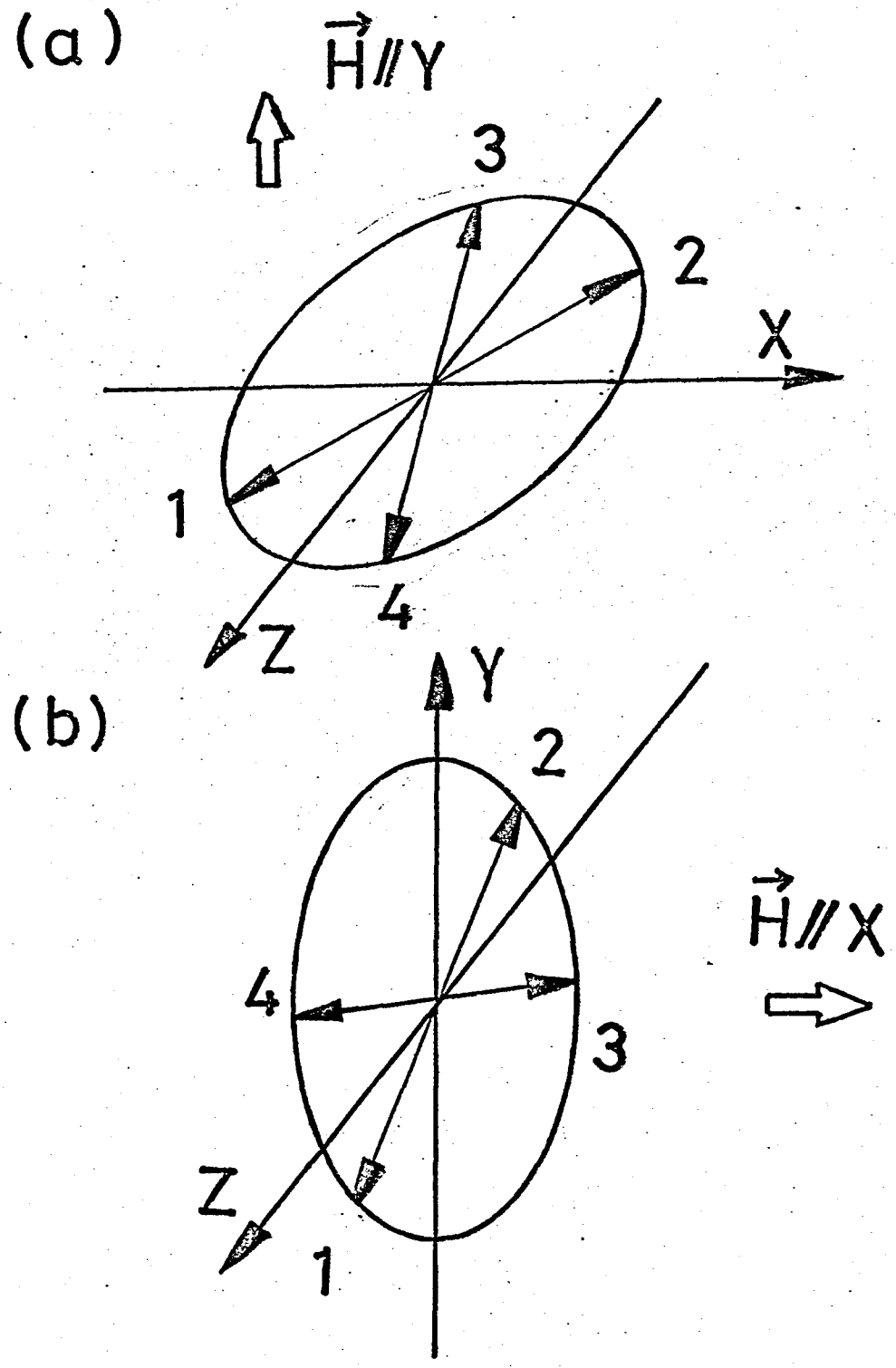

Fig. 9 Spin configurations for $\vec{H}$//Y(Fig. a) and $\vec{H}$//X(Fig. b). Only the negative g_{XY}** cases are shown for simplicity.

By using the condition M=M'=0, the expression of the free energy is rewritten as

$$f = -(H_K^* + g^2H_Y^2/8H_{ex})(N^2 + N'^2) - (H_{K'}^* + g^2H_Y^2/8H_{ex})(L^2 + L'^2)$$
$$- g_{XY}^{**}H_Y(L + L') + 2h_{ex}(LL' + NN') \quad . \tag{3-62}$$

The equilibrium condition is given by

$$2(H_K^* - H_{K'}^*)NL - g_{XY}^{**}H_YN + 2h_{ex}(NL' - LN') = 0 \quad , \tag{3-63a}$$

$$2(H_K^* - H_{K'}^*)N'L' - g_{XY}^{**}H_YN' + 2h_{ex}(N'L - L'N) = 0 \quad . \tag{3-63b}$$

In the followings we show L=L', N=-N'. Instead of f itself, a modified form f* is introduced as

$$f^* \equiv \{f + 2H_{K'}^* + (g^2H_Y^2/4H_{ex})\}/(H_K^* - H_{K'}^*) \quad . \tag{3-64}$$

From eq. (3-62) we have

$$f^* = -(N^2 + N'^2) - x(L + L') + h(LL' + NN') \quad , \tag{3-65}$$

where

$$x \equiv g_{XY}^{**}H_Y/(H_K^* - H_{K'}^*) \quad , \qquad h \equiv 2h_{ex}/(H_K^* - H_{K'}^*) \quad . \tag{3-66}$$

From the definition h is positive and x can be assumed as positive with no loss of generality. Following the method given by Gorter and co-workers,[34] extrema of f* are found.*) Configurations corresponding to four important extrema are shown in Fig. 10. Their f*'s are given as

$$\text{(i)}\quad f^*_{\mathrm{I}} = -2x + h\ , \tag{3-67a}$$

$$\text{(ii)}\quad f^*_{\mathrm{II}} = -2 - h - x^2/2(1+h) \qquad \text{for} \quad x \leqq 2(1+h)\ , \tag{3-67b}$$

$$\text{(iii)}\quad f^*_{\mathrm{III}} = -2 + h - x^2/2 \qquad \text{for} \quad x \leqq 2\ , \tag{3-67c}$$

$$\text{(iv)}\quad f^*_{\mathrm{IV}} = \tfrac{1}{4}x^2 - (1-h)^{\frac{1}{2}}x - 1 \qquad \text{for} \quad x \leqq 2(1-h)^{\frac{1}{2}}\ . \tag{3-67d}$$

By comparing f*'s, the relation $f^*_{\mathrm{III}}, f^*_{\mathrm{IV}} > f^*_{\mathrm{II}}$ is deduced. The resulting allowed configurations (i) and (ii) satisfy the required condition L'=L, N=-N'.

Under the condition L'=L, N=-N', f is written as

$$f = -2(H_K^* + g^2H_Y^2/8H_{ex})N^2 - 2(H_{K'}^* + g^2H_Y^2/8H_{ex})L^2 - 2g_{XY}^{**}H_YL + 2h_{ex}(L^2 - N^2)\ . \tag{3-68}$$

The equilibrium condition is given by

$$2(H_K^* - H_{K'}^* + 2h_{ex})NL - g_{XY}^{**}H_YN = 0\ . \tag{3-69}$$

) For details of the calculations and for the comparison of f's of the extrema, see appendix E.

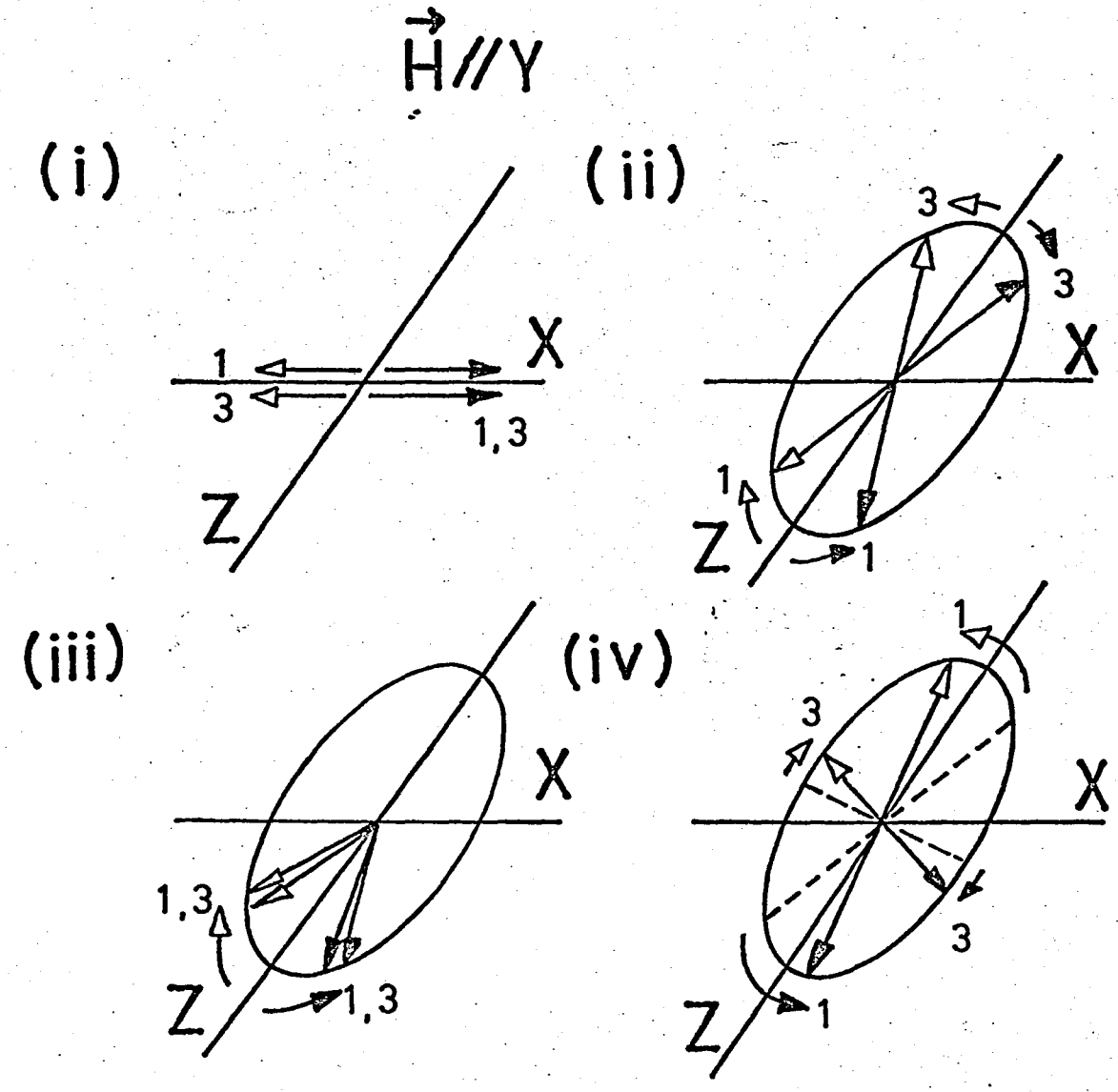

Fig. 10 Spin configurations corresponding to four non-trivial extrema of $\vec{H}//Y$ case. Spin-2 which is nearly antiparallel to 1 and spin-4 nearly antiparallel to 3 are not shown for simplicity. The arrows ⟶ and ⟶ correspond to $g_{XY}^{**} > 0$ and $g_{XY}^{**} < 0$, respectively.

The free energy and the equilibrium condition can be transformed into eqs. (3-33) and (3-34b) respectively,*) when $H_K^* + h_{ex}$ and $H_{K'}^* - h_{ex}$ are converted to H_K^* and $H_{K'}^*$. Therefore, following the results of the former case, we obtain

$$M_Y = \mu_B \langle S \rangle \{ g_{XY}^{**2}/2(H_K^* - H_{K'}^* + 2h_{ex}) + g^2/4H_{ex} \} H_Y \quad \text{for} \quad H_Y \leqq H_{BY} \tag{3-70a}$$

$$= \mu_B \langle S \rangle (|g_{XY}^{**}| + g^2 H_Y/4H_{ex}) \quad \text{for} \quad H_Y > H_{BY} \tag{3-70b}$$

where

$$H_{BY} = 2(H_K^* - H_{K'}^* + 2h_{ex})/|g_{XY}^{**}| \ . \tag{3-71}$$

We use eqs. (3-70a) and (3-70b) in the analysis of the magnetization curve for $\vec{H}//Y(b)$. Components perpendicular to the external field are given by

$$M_Z = \mu_B \langle S \rangle g_{ZX}^{**} g_{XY}^{**} H_Y/2(H_K^* - H_{K'}^* + 2h_{ex}) \quad \text{for} \quad H_Y \leqq H_{BY}$$

$$= \mu_B \langle S \rangle \mathrm{sign}(g_{XY}^{**}) g_{ZX}^{**} \quad \text{for} \quad H_Y > H_{BY} \tag{3-72}$$

$$M_X = 0 \ . \tag{3-73}$$

M_Z is smaller than M_Y by a factor g_{ZX}^{**}/g_{XY}^{**}. The last conclusion $M_X=0$ is an important result of the four-sublattice model.

---

*) In comparing eqs. (3-68) and (3-33) we may make M=0 in the latter equation, because the low-energy states of (3-33) satisfies the condition.

3.3.2 $\vec{H}//Z$

For this case, rigorous treatments are not done because the calculations seem to be very complex. As an alternative, we assume that the similarity between the $\vec{H}//Y$ cases of $h_{ex}=0$ and $h_{ex}\neq 0$ can be extended to the $\vec{H}//Z$ cases.

Then the magnetization parallel to the external field is given by

$$M_Z = \mu_B \langle S \rangle (g_{ZX}^{**})^2 (H_K^* - H_{K'}^* + 2h_{ex}) H_Z / 2 (H_K^* - H_{K'}^* - g^2 H_Z^2 / 8H_{ex} + 2h_{ex})^2$$

$$\text{for } H_Z \leq H_{BZ} \tag{3-74a}$$

$$= \mu_B \langle S \rangle (|g_{ZX}^{**}| + g^2 H_Z / 4H_{ex}) \qquad \text{for } H_Z > H_{BZ} \ , \tag{3-74b}$$

where H_{BZ} is determined by a self-consistent equation

$$H_{BZ} = 2(H_K^* - H_{K'}^* - g^2 H_{BZ}^2 / 8H_{ex} + 2h_{ex}) / |g_{ZX}^{**}| \ . \tag{3-75}$$

In §5.2.2 these results are applied to CuFTH.

3.3.3 $\vec{H}//X$

It is noticed that the magnetization jump appears when $\vec{H}$ is applied parallel to X(b). The free energy for $\vec{H}//X$ is given by

$$f = -(H_K^*+g^2H_X^2/8H_{ex})(N^2+N'^2) - H_{K'}^*(L^2+L'^2)$$
$$+ (H_{K'}^*-g^2H_X^2/8H_{ex})(M^2+M'^2) - \{g_{XY}^*H_X(M+M')+g_{ZX}^*H_X(N+N')\}$$
$$+ 2h_{ex}(LL'+MM'+NN') \quad . \tag{3-76}$$

The method given in 3.3.1 is not applicable for the present case. However, there are two evidences for L=L'=0; (1) If $g_{ZX}^*=0$, the rigorous method works giving L=L'=0. (2) Qaulitative considerations using an equation similar to eq. (3-61) of 3.3.1 suggests L=L'=0 provided $h_{ex} < H_K^*-H_{K'}^*+g^2H_X^2/8H_{ex}$. To insure L=L'=0 directly for the case of CuFTH, f is examined by using a computer. Various sets of magnetic parameters including the case corresponding to CuFTH are considered. Intervals of latitudes θ, θ' and longitudes ϕ, ϕ' (See Fig. 11(a).) in the computation are both 6°. Nine values of H_X are considered. Small terms arising from the perpendicular susceptibility which favors L=L'=0 are neglected for simplicity. The results clearly indicate L=L'=0. An example is given in Table I.

By inserting L=L'=0, the free energy is simplified to

$$f = -H_K^*(N^2+N'^2) + H_{K'}^*(M^2+M'^2) - \{g_{XY}^*H_X(M+M')+g_{ZX}^*H_X(N+N')\}$$
$$+ 2h_{ex}(MM'+NN') - g^2H_X^2/4H_{ex} \quad . \tag{3-77}$$

Table I Field dependence of equilibrium latitudes θ, θ' and longitudes ϕ, ϕ' for $\vec{H}//X$. For the definition of angles, see Fig. 11(a). The results given below are obtained by using the magnetic parameters corresponding to the case of $Cu(HCOO)_2 \cdot 4H_2O$. The parameters are listed in the lower part of the table. The signs for g_{XY}^* and g_{ZX}^* are taken as negative and positive, respectively.

$\lvert g_{ZX}^* \rvert H_X/H_K^*$	θ , ϕ	θ' , ϕ'
0.0	0 -	180 -
0.1	6 270	174 270
0.2	12 270	162 270
0.3	24 270	156 270
0.4	30 270	144 270
0.5	42 270	48 270
0.6	54 270	54 270
0.7	60 270	60 270
0.8	60 270	60 270
$2h_{ex}/H_K^* = 0.5$, $H_{K'}^*/H_K^* = 0.4$, $\lvert g_{ZX}^*/g_{XY}^* \rvert = 0.2$		

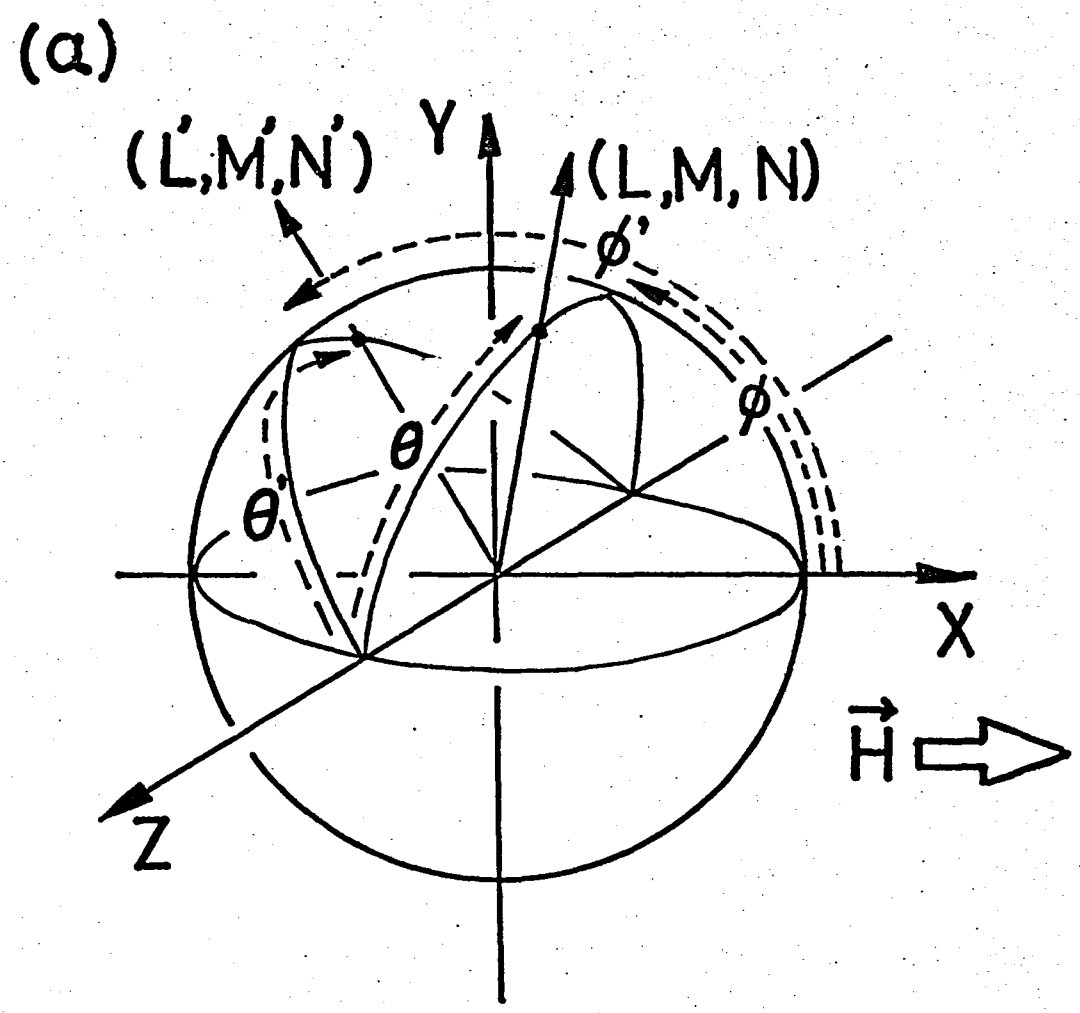

Fig. 11(a) Definition of latitudes θ, θ' and longitudes ϕ, ϕ'.

The equilibrium condition is given by

$$-2(H_K^* + H_{K'}^*)MN - g_{ZX}^* H_X M + g_{XY}^* H_X N$$

$$-2h_{ex}(MN' - NM') = 0 \qquad (3\text{-}78)$$

and an equation obtained by interchanging M, N, and M', N'. Analytical solution of these equations still seems to be difficult. Therefore, the numerical examination of f is done again by using a computer. The minimum of f** defined by

$$f^{**} \equiv f + (g^2 H_X^2/4H_{ex}) - 2H_{K'}^* \qquad (3\text{-}79)$$

is considered. By using eq. (3-77) and the condition $M^2+N^2=1$, f** is transformed into

$$f^{**} = -(H_K^* + H_{K'}^*)(N^2 + N'^2) - \{g_{XY}^* H_X(M + M') + g_{ZX}^* H_X(N + N')\}$$

$$+ 2h_{ex}(MM' + NN') \ . \qquad (3\text{-}80)$$

In the numerical analysis of eq. (3-80), intervals of θ and θ' are both 2° and 50 or more points of H_X are considered. Several combinations of parameters are considered so as to visualize some typical cases and to reproduce the magnetization curve of CuFTH. The magnetization is calculated by using

$$M_X = \mu_B \langle S \rangle \{g_{XY}^* \tfrac{1}{2}(M+M') + g_{ZX}^* \tfrac{1}{2}(N+N') + g^2 H_X/4H_{ex}\} \ ,$$

$$M_Y = M_Z = 0 \ . \qquad (3\text{-}81)$$

Figure 11(b) shows the resulting magnetization curves*) for several typical cases, where $\chi_\perp$ term in eq. (3-73) is dropped for simplicity giving

$$M_X = \mu_B \langle S \rangle \{ g_{XY}^* \tfrac{1}{2}(M+M') + g_{ZX}^* \tfrac{1}{2}(N+N') \} \quad . \tag{3-82}$$

Figure (c) represents θ and θ' as a function of the field for a speical case where the parameters take the values close to those of CuFTH. Figure (d) is the corresponding magnetization curve. The theoretical curve**) is clearly consistent with the experimental result. Details of the adjustment of the parameters are given in §5.2.3.

The high field state seems to correspond to the $\theta=\theta'$ type extremum of the free energy (3-77) ($M=M'$ and $N=N'$ are consistent with (3-78) and the associated equation.). If it is true, the magnetization curve in this region strictly coincides with that of the $h_{ex}=0$ case. We assume this to be true.

---

*) The magnetization curves can be assigned by two parameters, $|g_{ZX}^*/g_{XY}^*|$ and $2h_{ex}/H_{K+}^*$, when the magnetization and the field are normalized by $\mu_B \langle S \rangle [(g_{XY}^*)^2 + (g_{ZX}^*)^2]^{1/2}$ (See (3-55b).) and $H_{K+}^*/|g_{XY}^*|$, respectively. The latter scaling property can be seen by dividing f** of (3-80) by H_{K+}^* and rewriting the second term as $H_X/(H_{K+}^*/g_{XY}^*)(M+M') + (g_{ZX}^*/g_{XY}^*)H_X/(H_{K+}^*/g_{XY}^*)(N+N')$.

**) The jumping occurs $H_X \simeq 2h_{ex}/|g_{ZX}^*|$ whereas the jumping field for the mechanism suggested by Ajiro and Terata[10] is $2h_{ex}/|g_{XY}^*|$ which results in an over-estimation of h_{ex} by a factor $|g_{XY}^*/g_{ZX}^*|$. In CuFTH and CuFUH, this factor amounts to about 5 and 10, respectively.

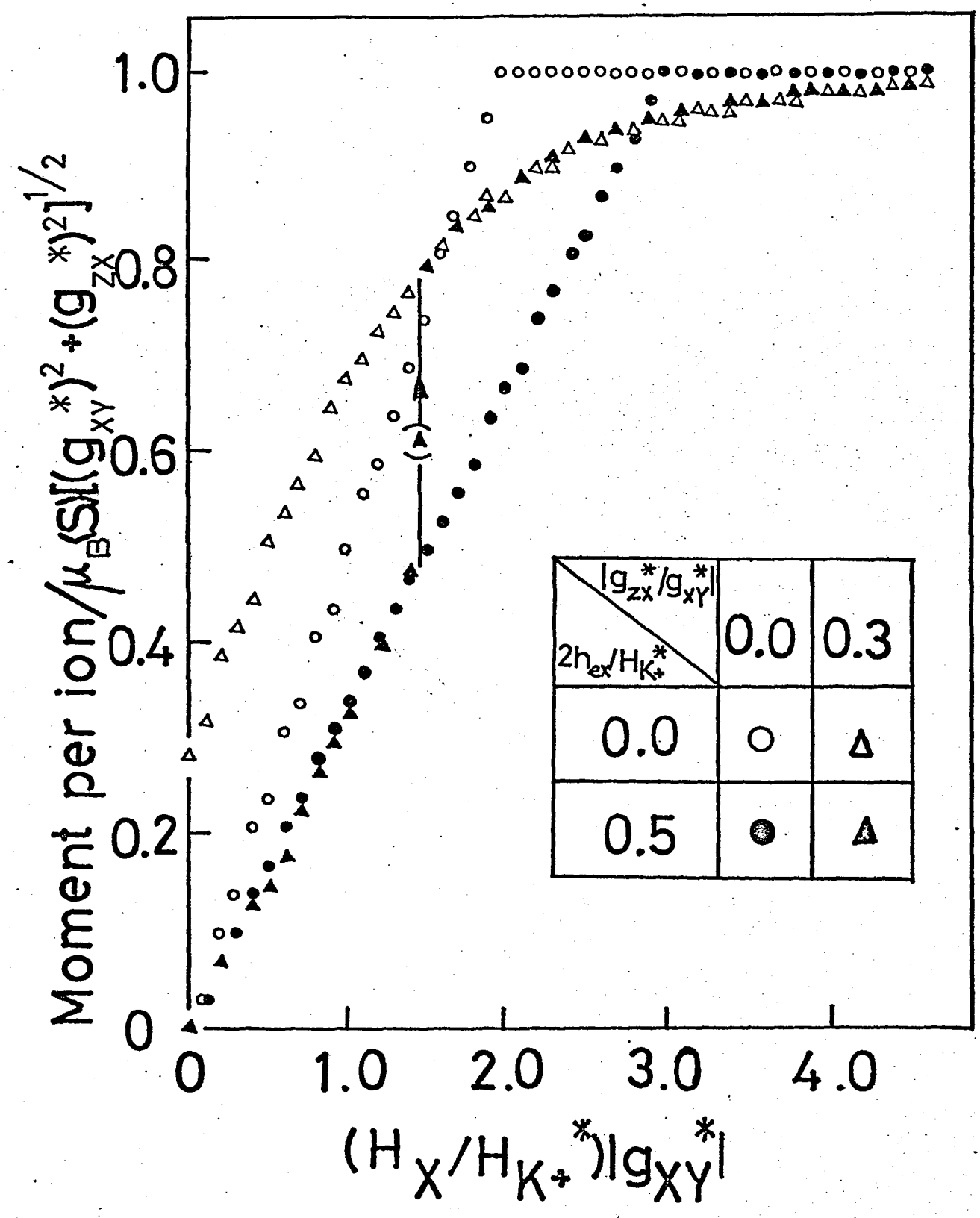

Fig. 11(b) Theoretical magnetization curves for $\vec{H}$//X. Curves corresponding to four typical combinations of parameters are given.

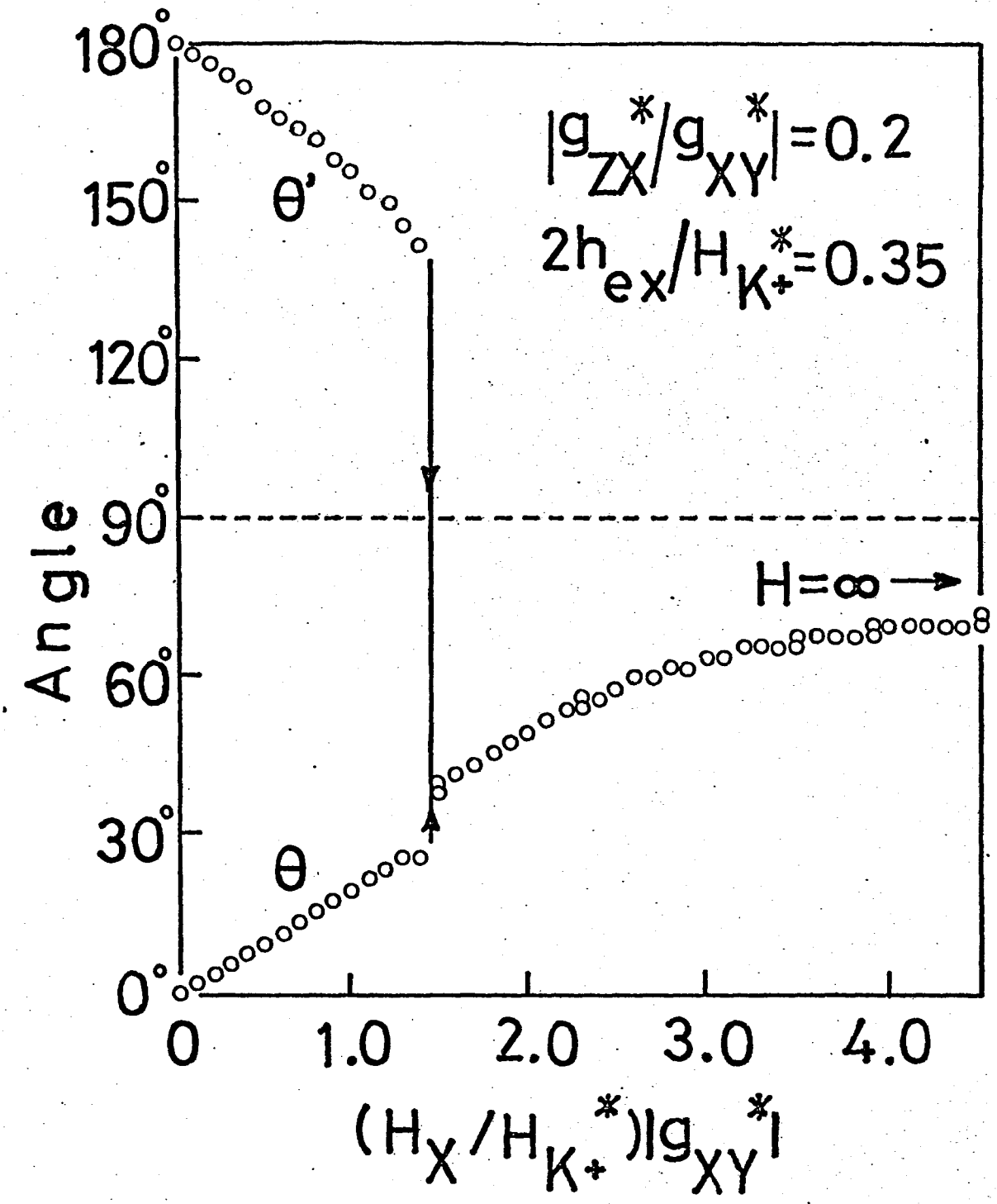

Fig. 11(c) Theoretical field dependence of spin directions. The listed parameters are chosen so as to reproduce the magnetization curve of CuFTH approximately.

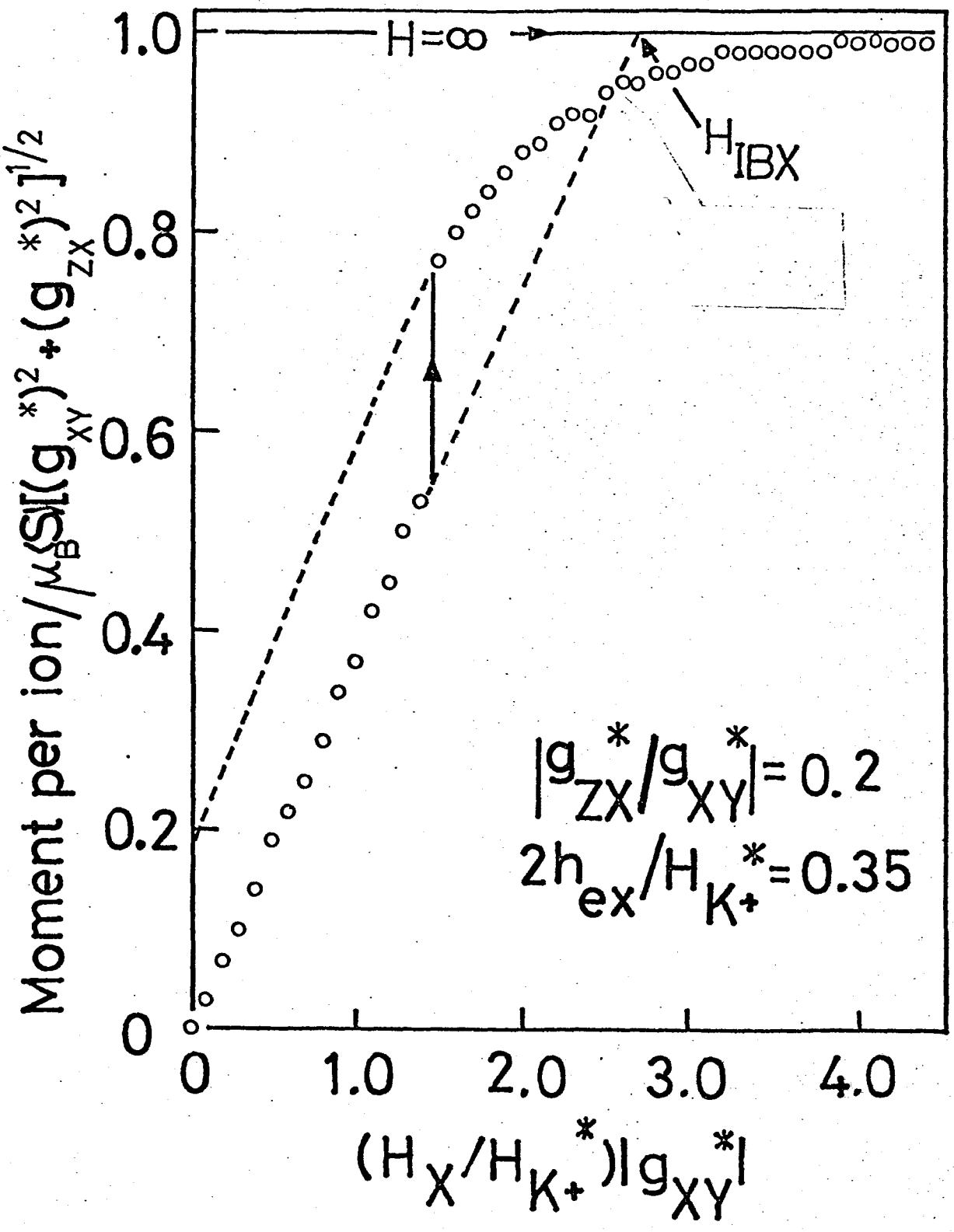

Fig. 11(d) Theoretical magnetization curve corresponding to Fig. (c). For the broken lines and H_{IBX} see §5.2.3.

3.4 Spin rotation in the high-field state

In order to analyze the angular dependence of the nmr spectra in the high field 2-sublattice state(See §6.3.2.), the spin direction is studied as a function of the field direction. As the rigorous treatment of this problem is difficult, we simplify the calculation by neglecting terms arising from anisotropy and perpendicular susceptibility. Then, the equilibrium condition is written as

$$-g_{ZX}{}^{*}H_X M + g_{XY}{}^{*}H_X N = 0 \ , \tag{3-83a}$$

$$g_{ZX}{}^{*}H_X L - (g_{XY}{}^{**}H_Y + g_{ZX}{}^{**}H_Z)N = 0 \ , \tag{3-83b}$$

$$-g_{XY}{}^{*}H_X L + (g_{XY}{}^{**}H_Y + g_{ZX}{}^{**}H_Z)M = 0 \ . \tag{3-83c}$$

The corresponding f is given by

$$f/2 = -g_{XY}{}^{*}H_X M - g_{ZX}{}^{*}H_X N - (g_{XY}{}^{**}H_Y + g_{ZX}{}^{**}H_Z)L \ , \tag{3-84}$$

where a constant term coming from h_{ex} is neglected.

If the field direction is not parallel to a special direction satisfying $g_{XY}{}^{**}H_Y+g_{ZX}{}^{**}H_Z=0$, the solution is given by

$$L = (g_{XY}{}^{**}H_Y + g_{ZX}{}^{**}H_Z)/G \ , \tag{3-85a}$$

$$M = g_{XY}{}^{*}H_X/G \ , \tag{3-85b}$$

$$N = g_{ZX}{}^{*}H_X/G \ , \tag{3-85c}$$

where G is defined by the following equation:

$$G \equiv \{(g_{XY}{}^{**}H_Y + g_{ZX}{}^{**}H_Z)^2 + (g_{XY}{}^{*}H_X)^2 + (g_{ZX}{}^{*}H_X)^2\}^{\frac{1}{2}} . \tag{3-86}$$

When the external field is in the YZ-plane(H_X=0), eqs. (3-85a) ∿ (3-85c) are simplified to

$$L = 1 \cdot \mathrm{sign}(g_{XY}{}^{**}H_Y + g_{ZX}{}^{**}H_Z), \quad M=0, \quad N=0, \tag{3-87}$$

where the sign of L is determined by using energy-minimum condition. For the case $\vec{H}//X(H_Y=H_Z=0)$ we have

$$M = g_{XY}{}^{*}\mathrm{sign}(H_X)/(g_{ZX}{}^{*2} + g_{XY}{}^{*2})^{\frac{1}{2}} , \tag{3-88a}$$

$$N = g_{ZX}{}^{*}\mathrm{sign}(H_X)/(g_{ZX}{}^{*2} + g_{XY}{}^{*2})^{\frac{1}{2}} , \tag{3-88b}$$

if $g_{ZX}{}^{*}$, $g_{XY}{}^{*} \neq 0$.

For the sake of later use, we consider the spin rotation when the field direction is rotated in the plane shown in Fig. 12(a). For this case eqs. (3-85a) ∿ (3-85c) can be rewritten as

$$L = \sin\omega(g_{XY}{}^{**}\sin\delta + g_{ZX}{}^{**}\cos\delta)/G' , \tag{3-89a}$$

$$M = \cos\omega g_{XY}{}^{*}/G' , \tag{3-89b}$$

$$N = \cos\omega g_{ZX}{}^{*}/G' , \tag{3-89c}$$

where G' is given by

$$G' = \{(g_{XY}{}^{**}\sin\delta + g_{ZX}{}^{**}\cos\delta)^2\sin^2\omega + (g_{XY}{}^{*2} + g_{ZX}{}^{*2})\cos^2\omega\}^{\frac{1}{2}} . \tag{3-90}$$

To make clear the physical meaning of the result, a simple example is considered. Let $g_{ZX}{}^{*}=g_{ZX}{}^{**}=0$, $\delta=\pi/2$, then eqs. (3-89a) ~ (3-89c) are reduced to

$$L = \sin\omega g_{XY}{}^{**}/(g_{XY}{}^{**2}\sin^2\omega + g_{XY}{}^{*2}\cos^2\omega)^{\frac{1}{2}} , \tag{3-91a}$$

$$M = \cos\omega g_{XY}{}^{**}/(g_{XY}{}^{**2}\sin^2\omega + g_{XY}{}^{*2}\cos^2\omega)^{\frac{1}{2}} , \tag{3-91b}$$

$$N = 0 . \tag{3-91c}$$

When the weak ferromagnetism is pure g-tilting type: $g_{XY}{}^{**}=g_{XY}{}^{*}$, eqs. (3-91a) and (3-91b) result in

$$\cos(\Omega + \omega) = 0 , \tag{3-92}$$

where Ω is defined, as is shown in Fig. 12(b), by

$$L = \cos\Omega, \qquad M = \sin\Omega . \tag{3-93}$$

When the weak ferromagnetism is pure Dzyaloshinsky-Moriya type: $g_{XY}{}^{**}=-g_{XY}{}^{*}$, we have

$$\cos(\Omega - \omega) = 0 . \tag{3-94}$$

Eqs. (3-92) and (3-94) indicate that the sense of the forced spin-rotation in the g-tilting type weak ferromagnet and that in the DM-type weak ferromagnet are different. Namely, in the latter case, the spin rotates with the external field but, in the former case, the spin rotates in the opposite direction. These conclusions are applied to the discussion of the experimental results in §5 and 6.

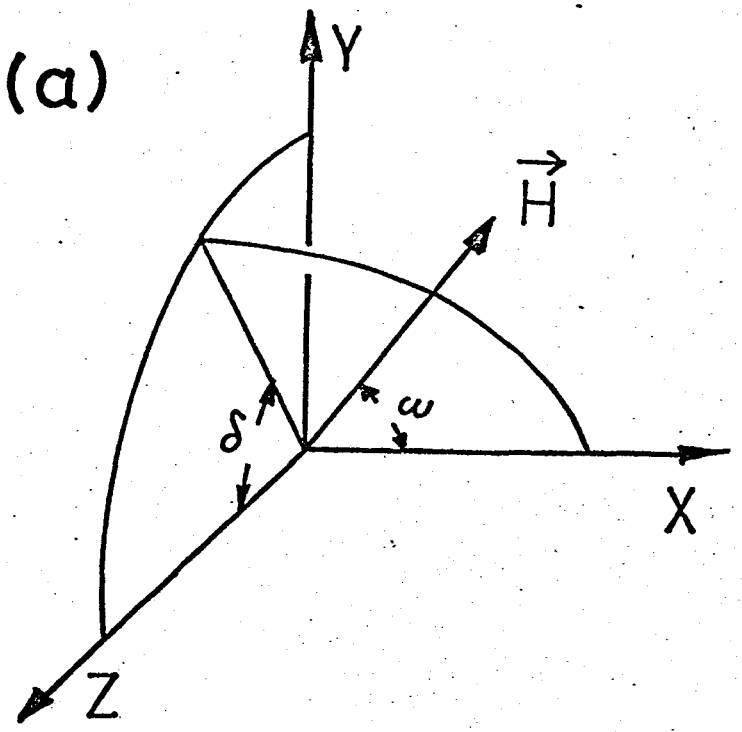

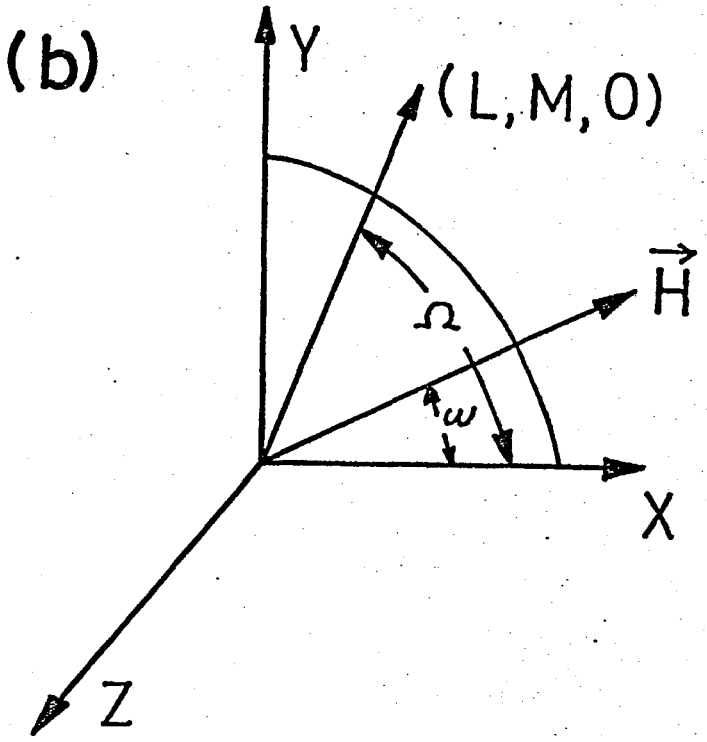

Fig. 12(a) Definition of the angles δ and ω.

(b) That of Ω.

§ 4. Experimental Procedure

4.1 Preparation of crystals

To obtain high purity specimens, commercially obtained copper formate tetrahydrate was purified by recrystallizations. The light-water single crystals were obtained by slow cooling of the solution of purified materials. A part of the purified materials was deuterated and the D_2O single crystals were grown from the heavy-water solution of the deuterated polycrystals. Three D_2O single crystals with dimensions of about 1cm·1cm·1cm and several H_2O crystals were used for experiments. The crystals were stored in liquid paraffine to prevent efflorescence.

4.2 Measurement of magnetization

The measurement of magnetization was done by using a moving-sample magnetometer specially designed and constructed for the present experiment. The outline of the apparatus is shown in Fig. 13. The characteristic of the apparatus is its convenience in measuring the angular dependence of the magnetization curve. To obtain accuracy of the order of 1% throughout the change of the field direction performed by the rotation of the sample and the interchange of the sample itself,*) a small fraction of the space between pair coils is used for the sample. The volume between the coils is about $20cm^3$

---

*) This means the change in the sample shape.

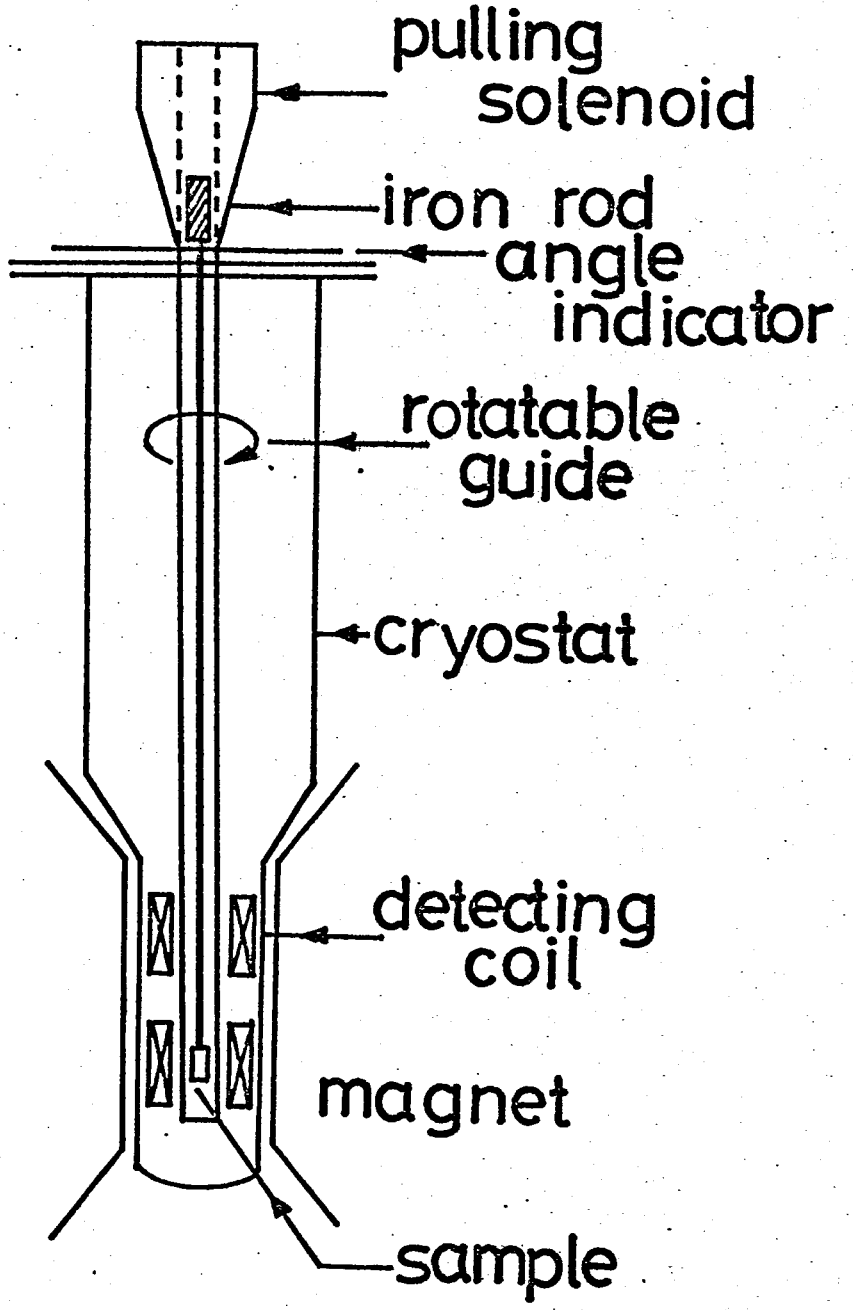

Fig. 13 The moving-sample magnetometer for studying the angular dependence of the magnetization curve.

and the sample volume is about $0.7cm^3$. As a result, (1) the signal to noise ratio and (2) the accuracy in the blank subtraction are not so good as an ordinary moving-sample magnetometer. The signal was amplified and integrated by using operational-amplifier circuits. The integrated voltage was read by using a digital voltmeter and about ten readings were averaged by hand calculations.

Figure 14 shows the average of voltmeter readings as a function of the field direction for a test sample made of the manganese Tutton salt. The results guarantee the accuracy of the apparatus in the angular dependence measurement.

Axes of the crystal were determined by using the crystal habits given in Fig. 15. The crystal was polished to near cylindrical form to fit the sample case. The estimated overall error of the sample cutting and setting is ±3°. The X-ray test of a sample indicates that the accuracy is within the estimated value. Comparison of the result of the magnetization measurement with the published data[2,17] also supports the estimation.

4.3 Proton resonance

Schematic view of sample setting for nmr measurement is shown in Fig. 16. Sample crystals were polished to near cylindrical form convenient to fit closely in a glass tube on which the sample coil is wound. Error of sample setting is larger than that of magnetization measurement. Error of axis in polishing the crystal is not more than ±5°. Error of setting the crystals in each runs is estimated within ±3°.

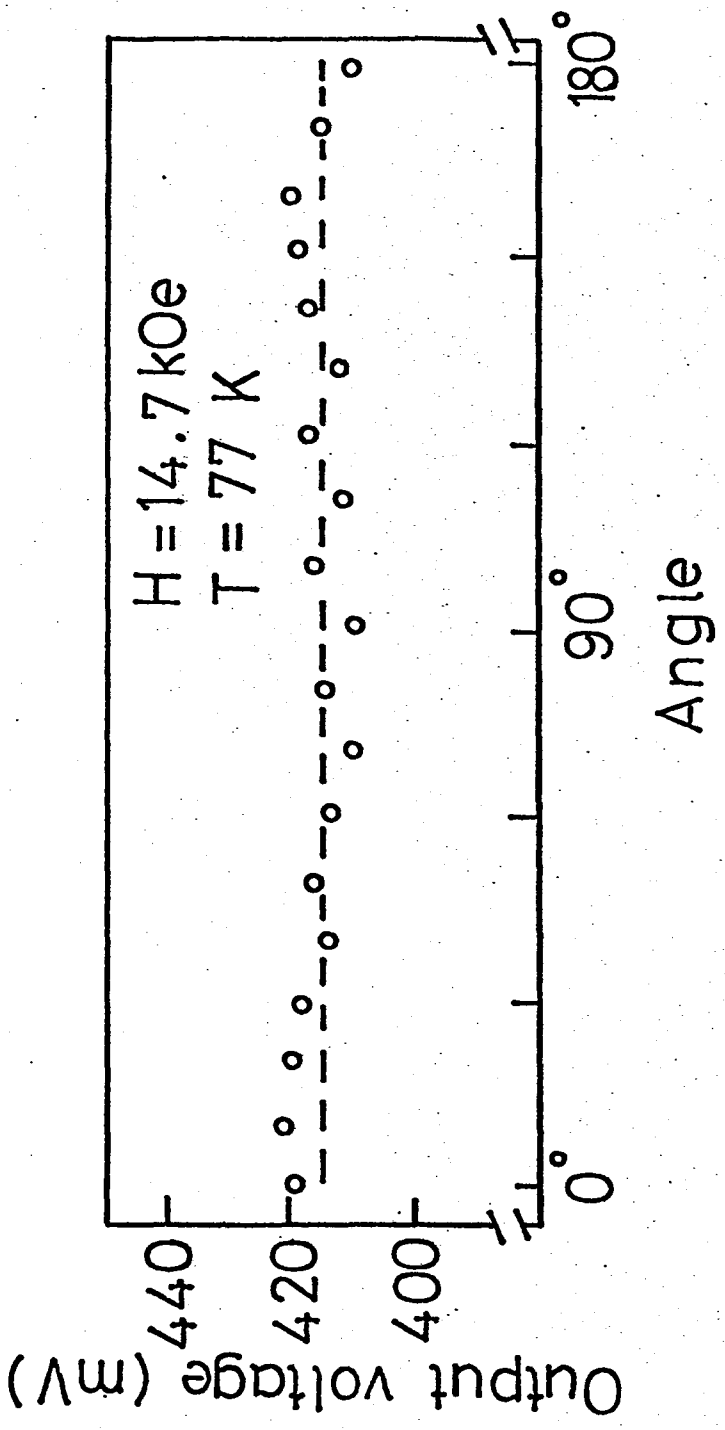

Fig. 14 Voltmeter readings for various field directions. The test sample is made of the manganese Tutton salt.

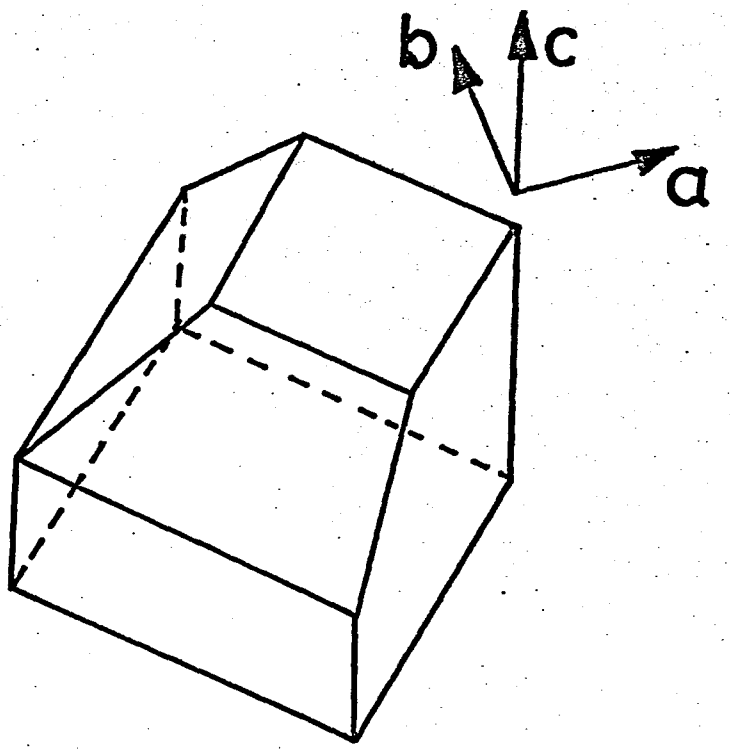

Fig. 15 Crystal habit of $Cu(HCOO)_2 \cdot 4H_2O$ and $4D_2O$ crystals.

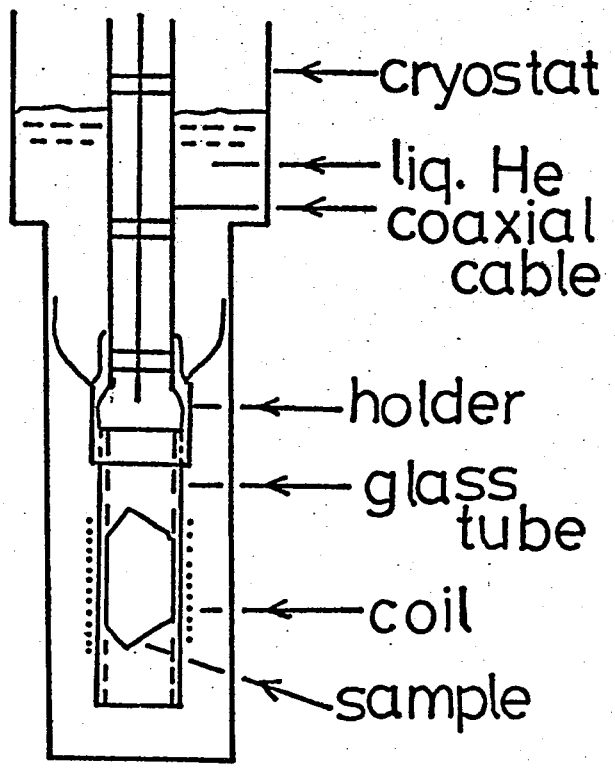

Fig. 16 Sample setting for nmr measurement.

The nmr signals were obtained by using a Pound-Knight spectrometer operating from 1.2 to 60MHz at liquid helium temperature range. First derivatives of absorption signals were obtained by sweeping magnetic field. Resonance signals coming from free protons of residual liquid paraffine were used as a marker of magnetic field. The amplitude of field modulation was 10 Oe peak to peak. Although this value of modulation is large compared with those used in ordinary proton resonance experiments, it was selected for good signal to noise ratio. As a result, detailed knowledge of line shape and line width was not obtained.

Two examples of the recorder trace are given in Fig. 17.

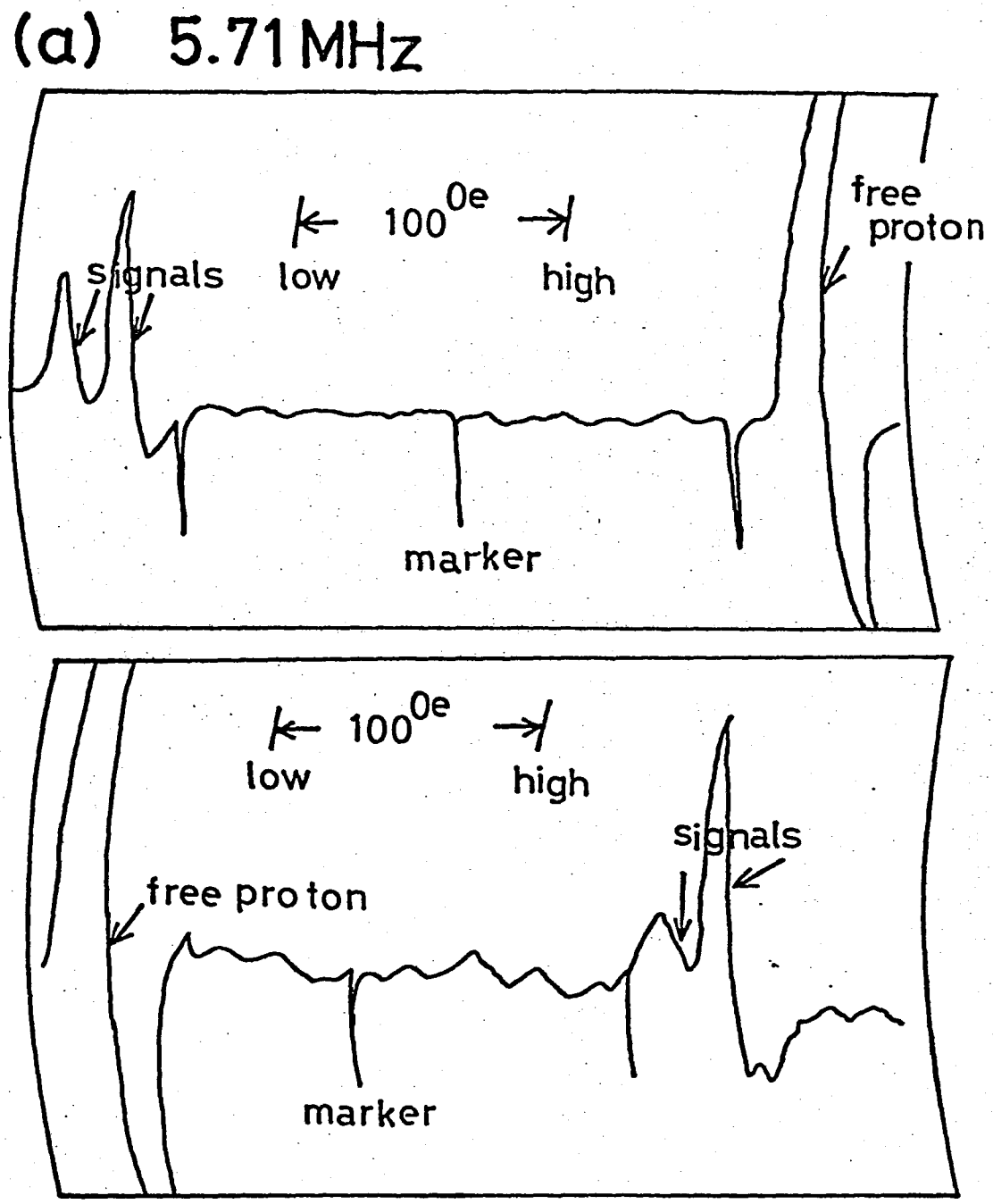

Fig. 17 Two examples of the proton nmr signals for the D_2O crystal at 4.2k. (a) Signals for $\vec{H}$ apart from the -c-axis by 20° to the a-axis in the ac-plane. The upper and the lower figures correspond to the spectra below and above the free proton line, respectively.

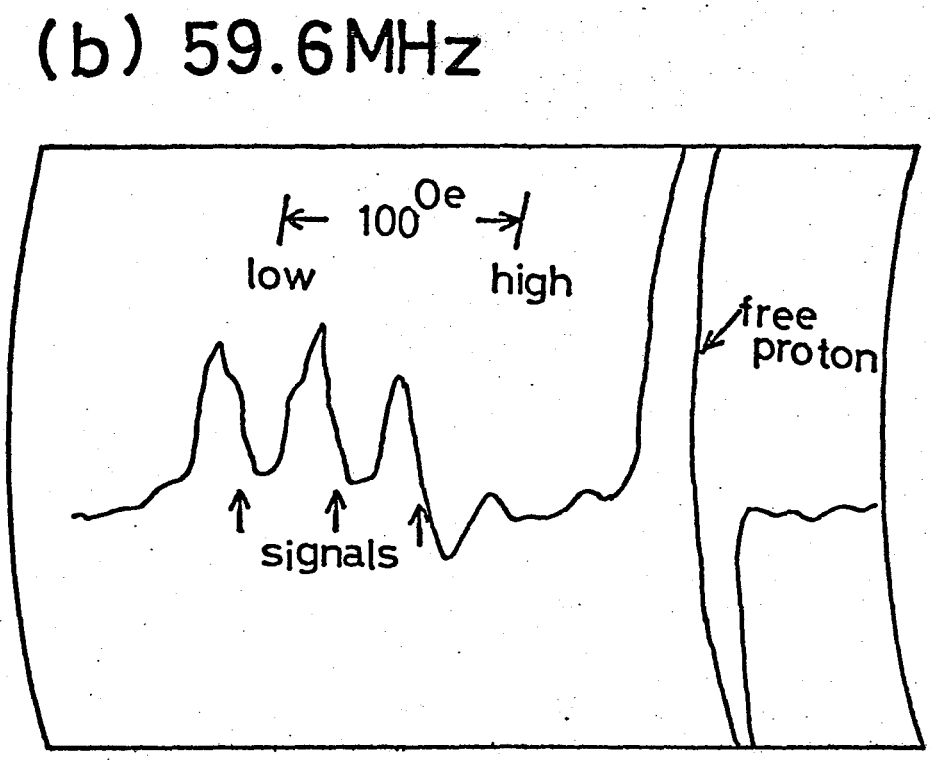

Fig. 17 (b) Signals for $\vec{H}$ apart from the -c-axis by 10° to the a-axis in the ac-plane.

§ 5. Analysis of the Magnetization Curves

In this section, results of the magnetization measurements are presented and analyzed by using the theory of the magnetization process developed in §3. Subsection 5.1 consists of the description of the experimental results and their qualitative considerations. The quantitative examination is done in §5.2.

5.1 Experimental results

The magnetization measurements were done in three planes, L_1L_2, L_2L_3 and L_1L_3. Figures 18 and 19 represnt the results. Most features of the earlier work(KH)[2] are reproduced as was discussed in §2. However, a noteworthy difference can be pointed out between the results of two experiments. It is the fact that, in the earlier work, the magnetization curves for $\vec{H}//L_1$ and L_2 coincide with each other at high field region but they do not in the present work. Namely, the magnetization curve for the L_2-axis saturates slower than that for the L_1-axis and the "saturated" magnetization is about 20% larger than that for L_1. These facts indicate, as we shall see later, that the magnetization process for two axes are considerably different from each other and that two mechanisms of weak ferromagnetism, the Dzyaloshinsky-Moriya (DM) and the tilted g-tensor mechanisms, should be taken into account at the same time.

The weak ferromagnetism(wf) was attributed in some papers[2,10,15] to the Dzyaloshinsky-Moriya interaction but in others[16,31] to the tilting of

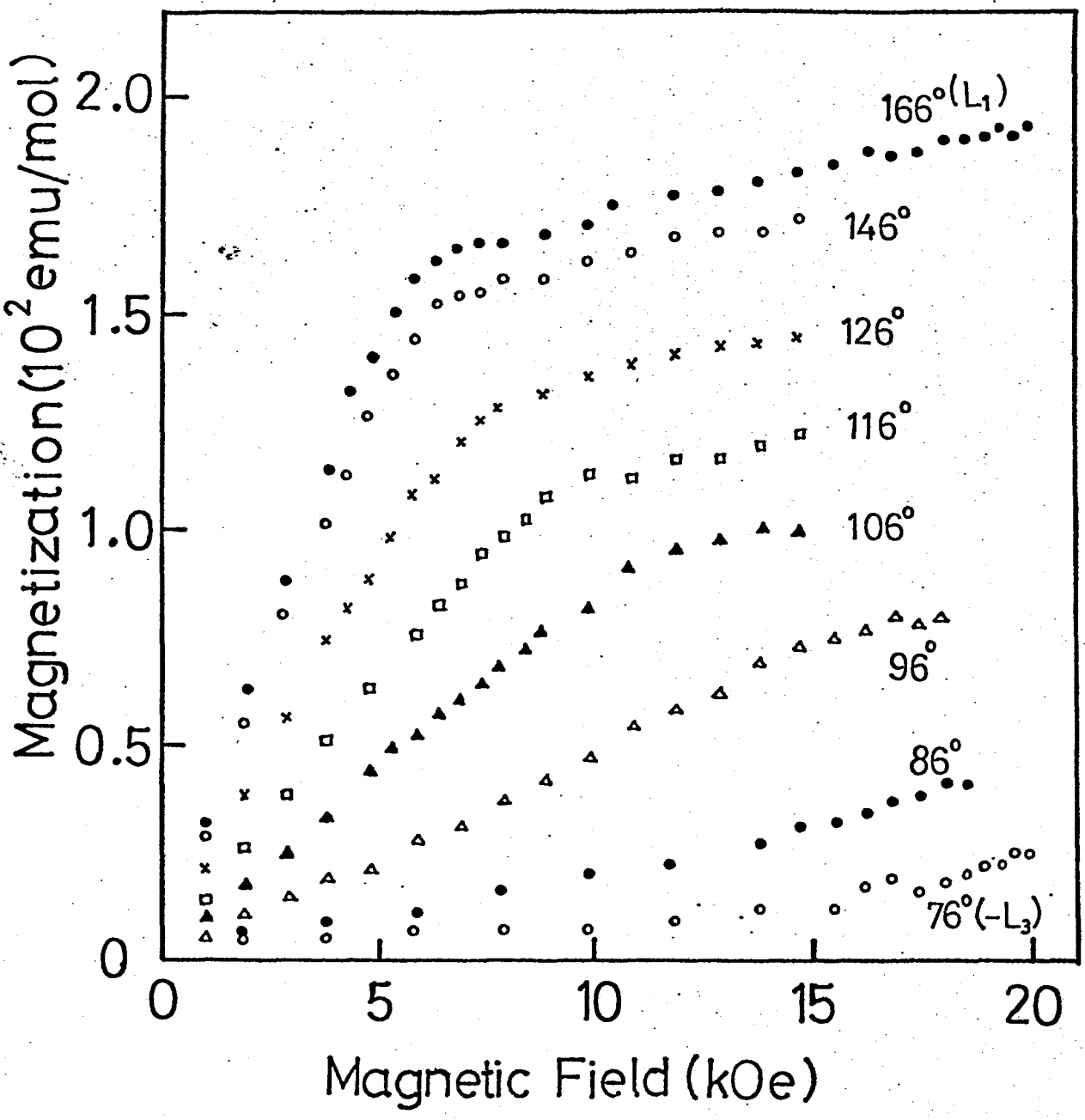

Fig. 18 (a) Magnetization curves in the L_1L_3-plane for a single crystal of $Cu(HCOO)_2 \cdot 4H_2O$ at 4.2K.

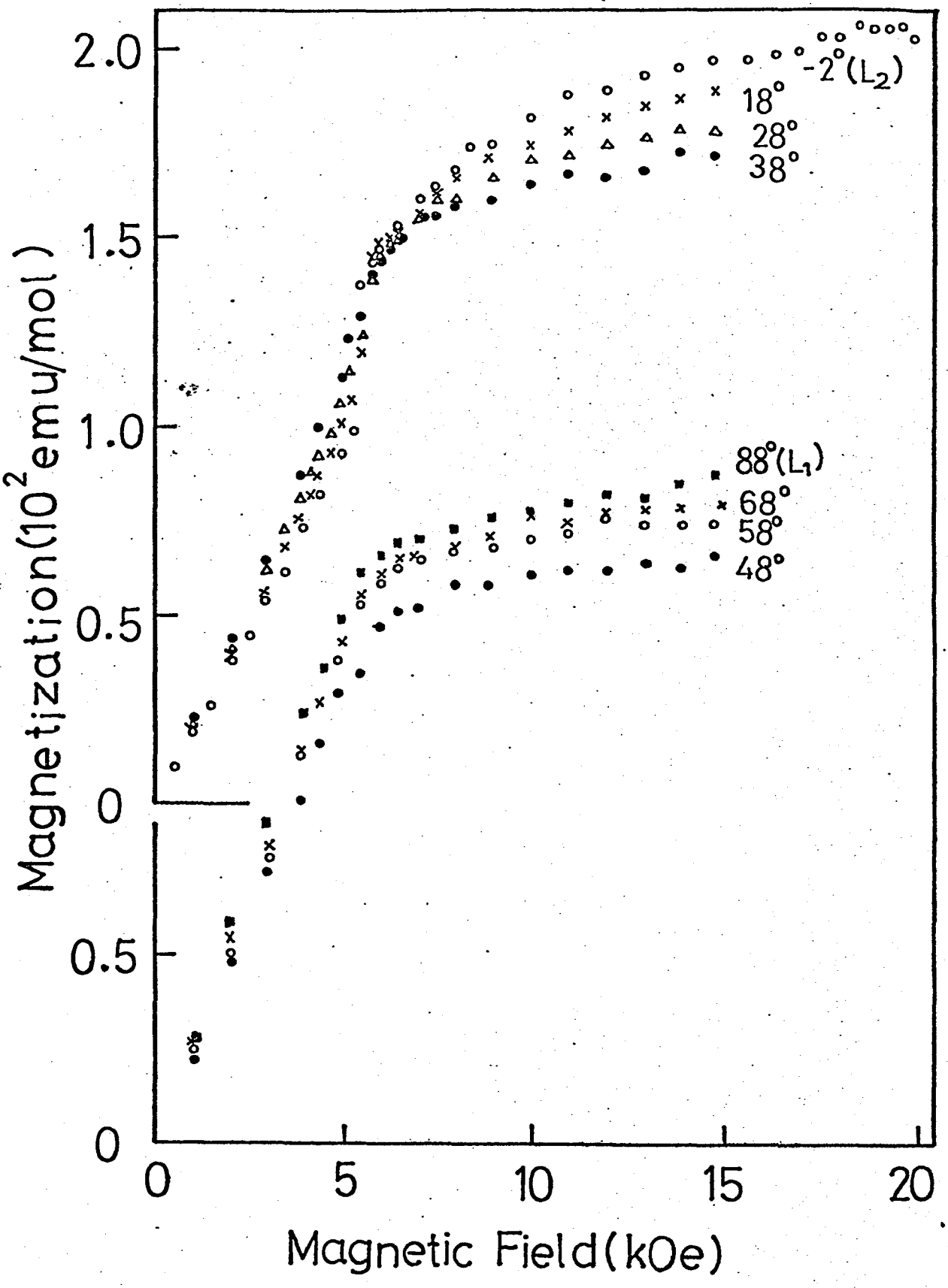

Fig. 18 (b) Magnetization curves in the L_1L_2-plane.

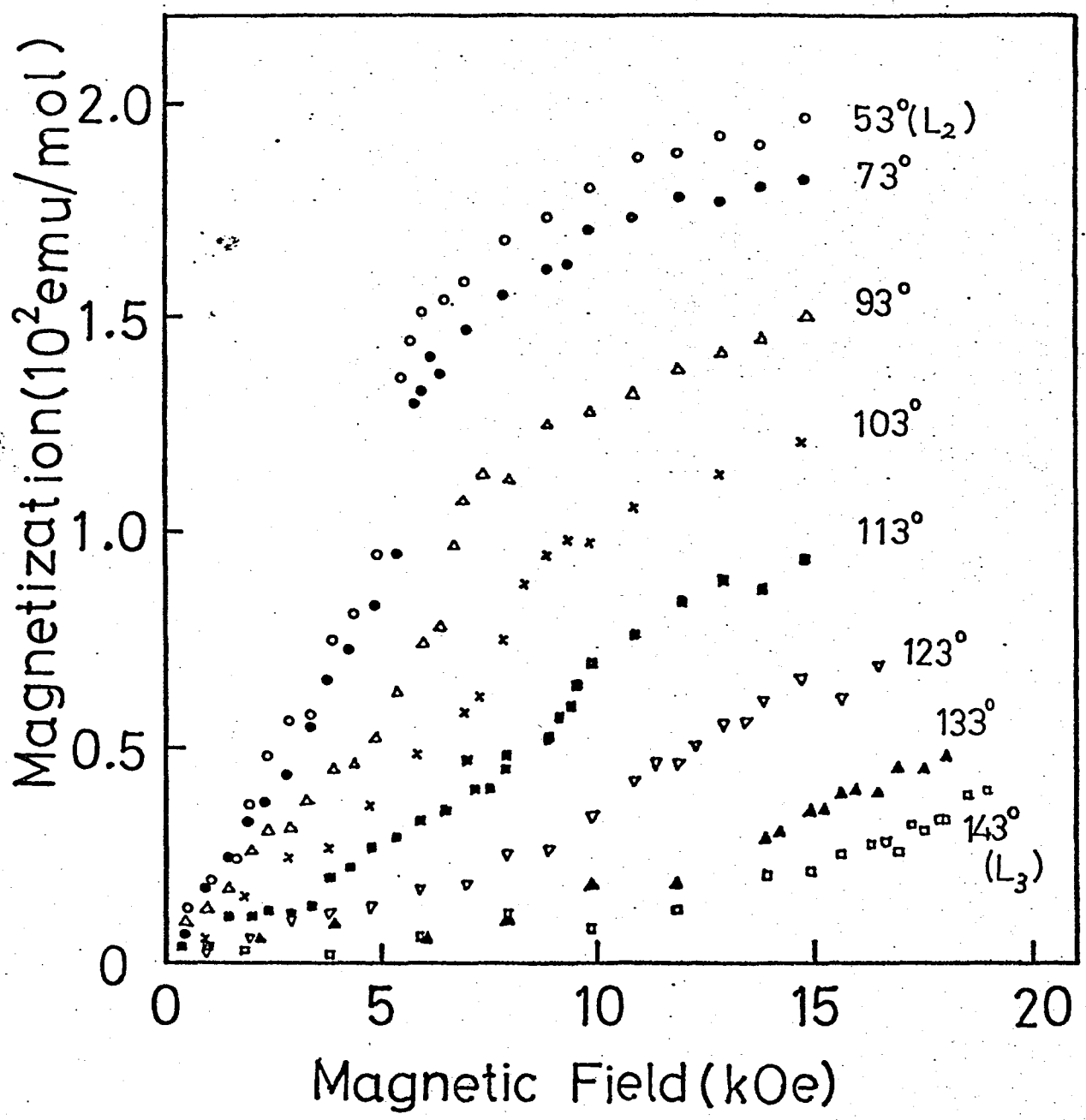

Fig. 18 (c) Magnetization curves in the L_2L_3-plane.

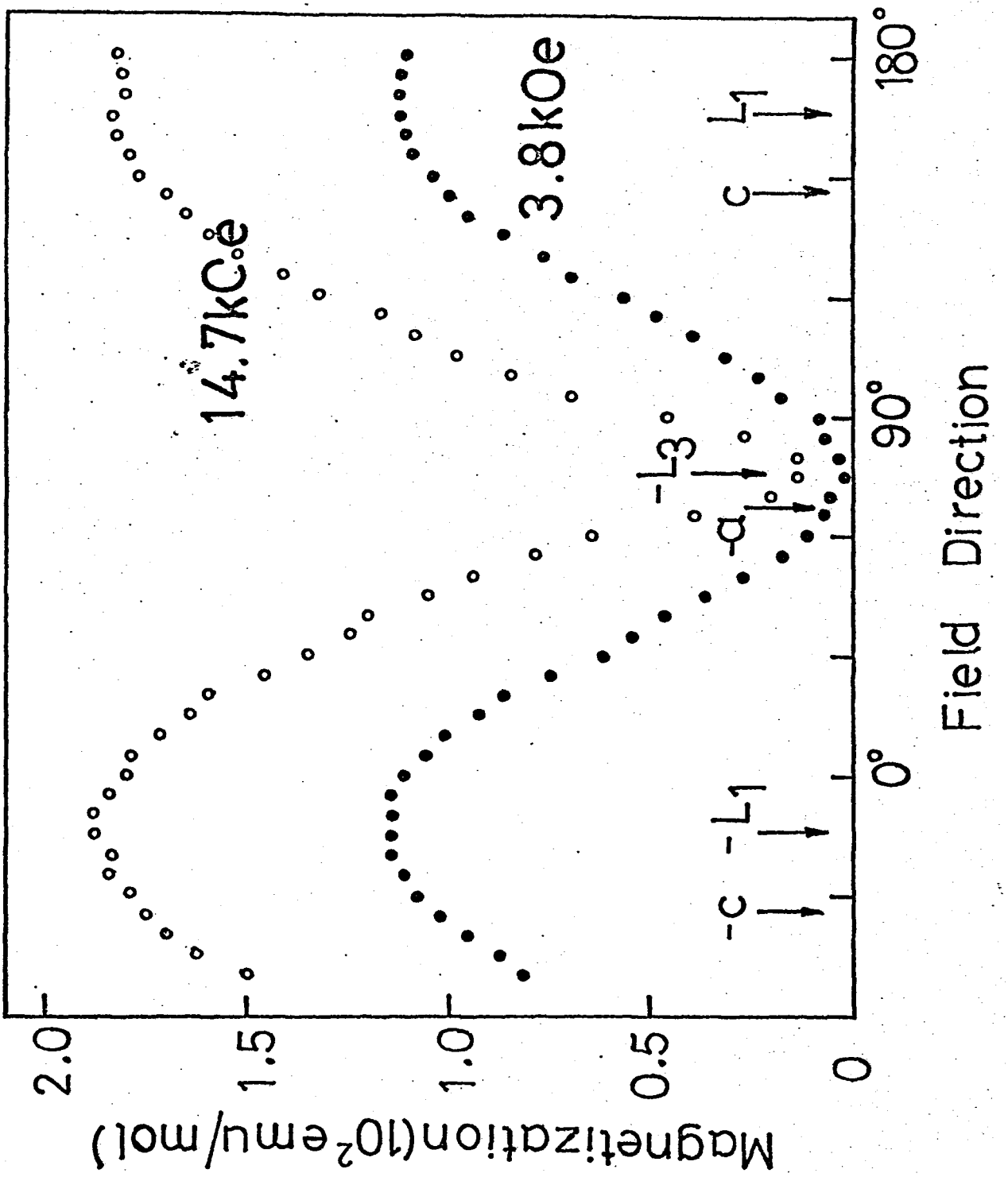

Fig. 19 Angular dependence of magnetization in $Cu(HCOO)_2 \cdot 4H_2O$ single crystals at 4.2K. (a) Results in the L_1L_3-plane.

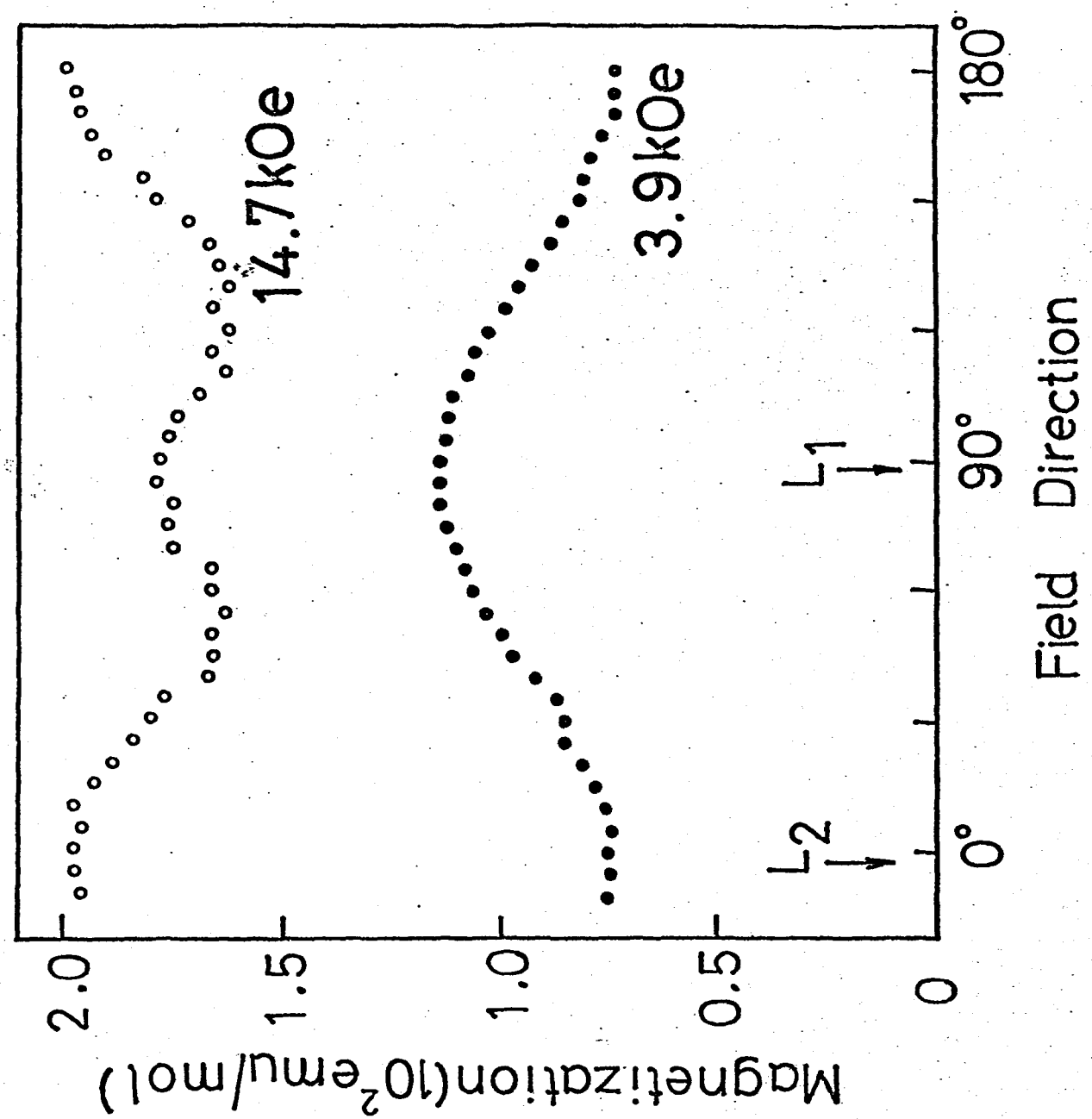

Fig. 19 (b) Results in the L_1L_2-plane.

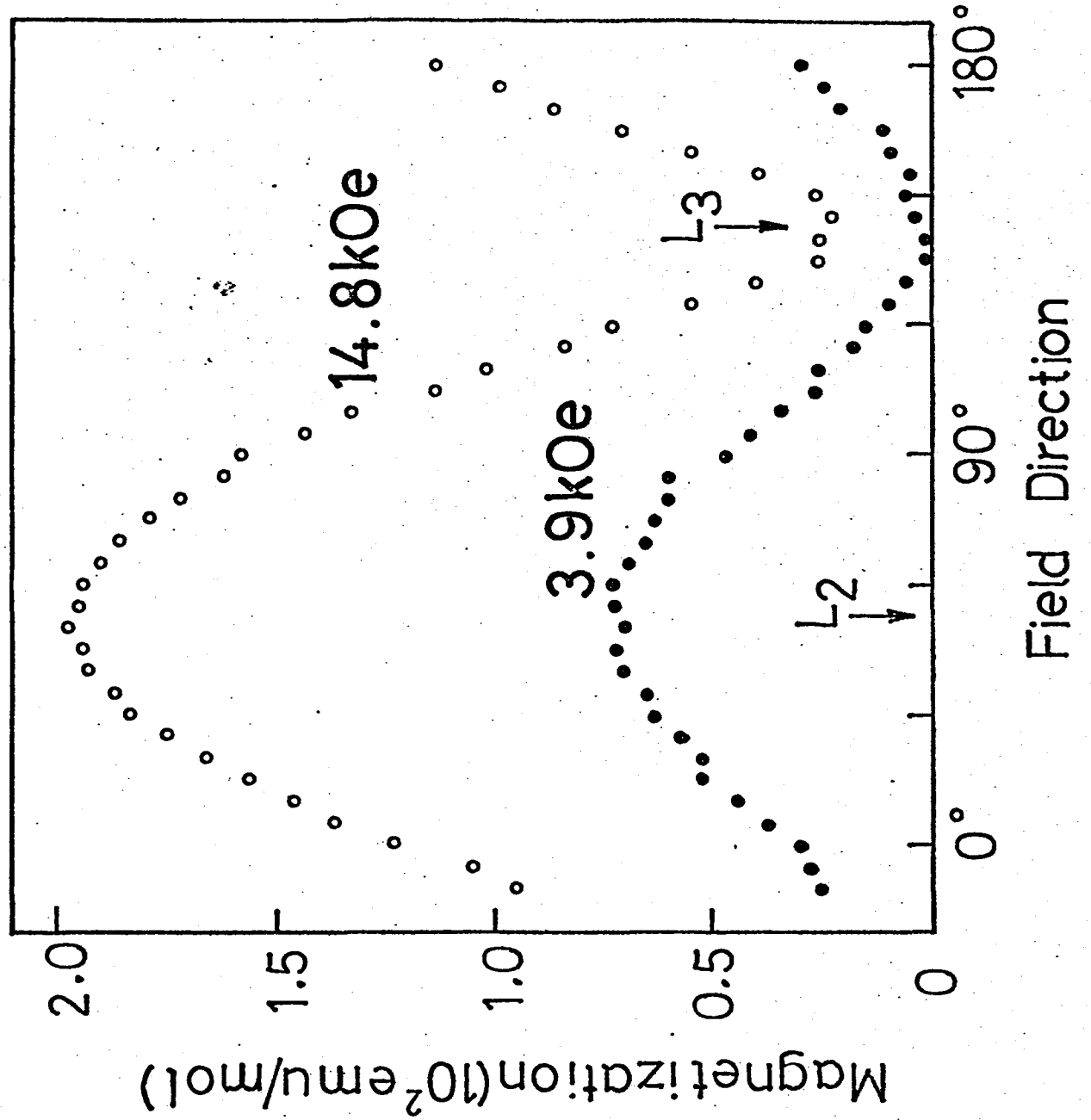

Fig. 19 (c) Results in the L_2L_3-plane.

g-tensors of two copper ions in the unit cell. The present result suggests the latter is the case except for a relatively small contribution from the DM-mechanism. The reason is as follows: If the wf is due to the DM-interaction, differential susceptibility after the saturation of the induced wf should be always $\chi_\perp$ for $\vec{H}$ in the L_1L_2-plane. On the other hand, if the wf is due to the g-tilting mechanism, the susceptibility should be $\chi_\perp$ for $\vec{H}//L_1$ and L_2 and be considerably smaller for $\vec{H}$ along intermediate directions(See §3.4.). The experimental result (solid squares in Fig. 3 or the dip in the 14.7kOe curve in Fig. 19(b)) supports the latter mechanism.

The absolute value $|J|$ of the intraplane exchange constant estimated from $\chi_\perp$ by using molecular field approximation is 50K. The result is considerably larger than the value, 36K, obtained from the temperature of the susceptibility maximum.[28),*)]

A jump of magnetization is observed in the L_2L_3-plane. Angular dependence of the jumping point is given in Fig. 20(a). The result indicates that the jump corresponds to the phase boundary observed in a proton resonance experiment(decrease of the number of lines).[35)] As one rotates the field direction from L_2 to L_1, the jump gradually changes to the bend at about the same field. Angular dependence of the bending field in the L_1L_3-plane is also given in the figure. In the angular dependence of proton resonance, abrupt decrease of

---

*) The Weiss temperature of 150K[2)] or 175K[5)] implies $|J| = 75 \sim 88$K. These values are larger than the value estimated from the susceptibility maximum. The discrepancy may be due to the deficient accuracy of the determination of the Weiss constant.

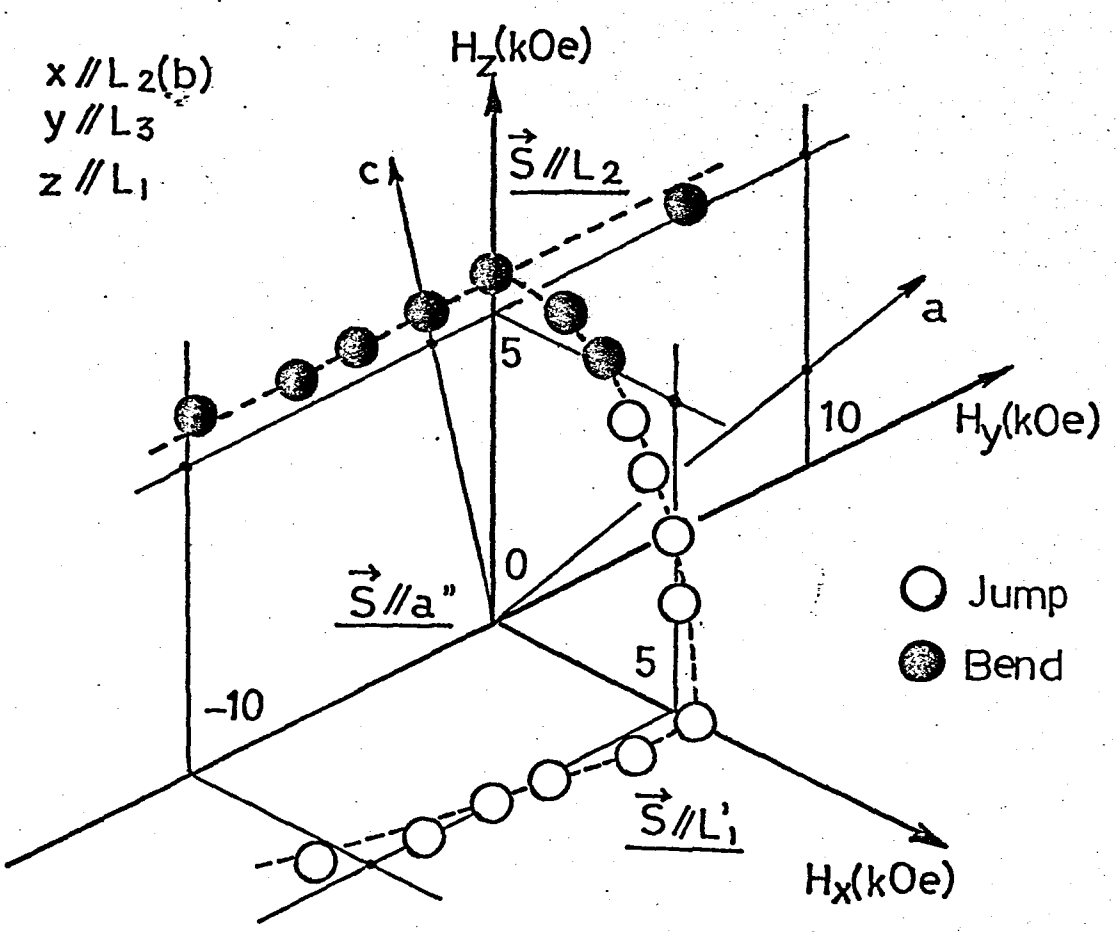

Fig. 20 (a) Phase boundary of $Cu(HCOO)_2 \cdot 4H_2O$ determined from the magnetization curve at 4.2K.

separation is observed on the bend-type boundary(See §6 or top of Fig. 1 of ref. 31). Angular dependence of the proton resonance anomalies obtained from the nmr result of the present paper is given in Fig. 20(b).

The phase outside the boundary is a 2-sublattice state,[16,31,32] but that inside the boundaries has not yet identified.[10,14,15,16] We consider the nature of the latter. One sees that the easy axis lies near the L_3-axis, since the observed susceptibility along L_3 is remarkably smaller than $\chi_\perp$. The result is consistent with the conclusion of ref. 15 and 16. The magnetic structures which are compatible both with the appearance of wf and the proton resonance results are a 4-sublattice structure with hidden canting and a 2-sublattice one with domains of wf. The former is consistent with the observation, since the magnetization curve along L_2 is reproduced theoretically only for the 4-sublattice structure with a" easy axis[16] having a weak (10^{-2}K) coupling between neighboring layers(See §3.). On the contrary, one has to assume a very unnatural behavior of the domains for the 2-sublattice structure as was discussed by Seehra and Castner.[16] In conclusion, the phase boundary corresponds to a transition from a low field 4-sublattice state to a high field 2-sublattice state.

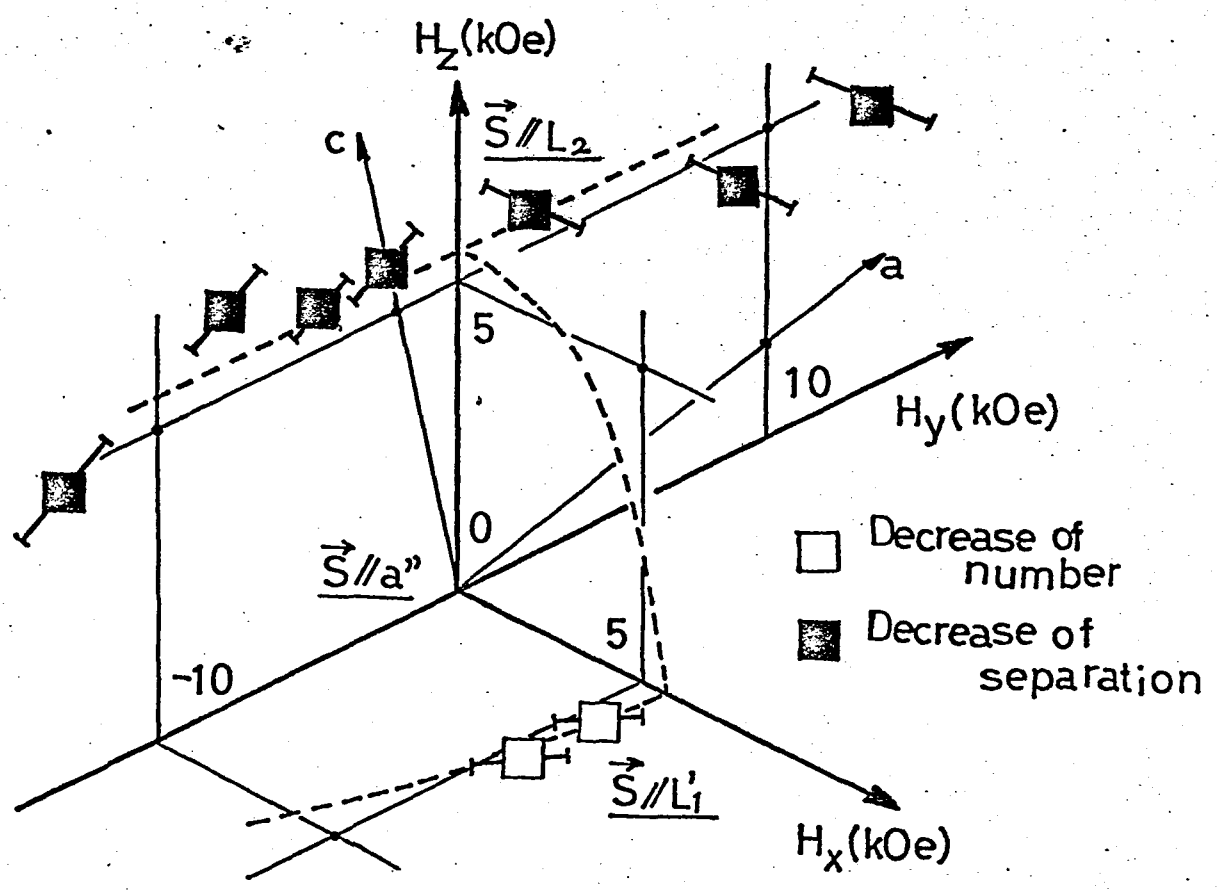

Fig. 20 (b) Anomalies observed on the phase boundary in the proton nmr of $Cu(HCOO)_2 \cdot 4D_2O$.

5.2 Analysis of the results

Three cases, $\vec{H}$//Y(c"), Z(a") and X(b) are considered. The magnetization curve for $\vec{H}$//X(b) is given in Fig. 18(b) and (c). But the magnetization curves strictly corresponding to H//Y(c") and Z(a") are not found in Fig. 18 because, in the present experiment, the measurements were done with 10° step in the fourth quadrant of the L_1L_3-plane. However, the angle between the Y-direction and the direction indicated by the notation 146° in Fig. 18(a) is only 2.1° so that the 146° data can be practically regarded as the c" data. For the a" direction, the angular dependence of the magnetization given in Fig. 19(a) is helpful. One sees that the magnetization for $\vec{H}$//a" is 10∿15% smaller than that for the 96° direction of Fig. 18(a).

The diamagnetic susceptibility of CuFTH is estimated from the ionic susceptibilities.[36] The estimated value, 82×10^{-6} emu/mol, amounts to about 4% of the perpendicular susceptibility of this crystal. The correction due to the diamagnetic susceptibility is therefore small but is taken into account in the followings.

5.2.1 $\vec{H}$//Y(c")

The experiments clearly show the linear increase of the magnetization and the bending predicted by the theory (See eqs. (3-70a,b).). Comparing the experimental value of the high field susceptibility and the last term of eq. (3-70b), we have

$$\mu_B \langle S \rangle g^2/4H_{ex} = 0.37 \times 10^{-26} \text{ emu/ion} . \qquad (5\text{-}1)$$

As g, the average of g_{XX}, g_{YY} and g_{ZZ} defined by (3-15), is 2.19, H_{ex} is estimated as

$$H_{ex}/(\langle S \rangle/S) = 1.50 \times 10^6 \text{ Oe} , \qquad (5\text{-}2)^{*)}$$

which yields $|J|$ of 50K mentioned in the preceding subsection when $\langle S \rangle/S = 1$ is assumed. Next, we can estimate $\mu_B \langle S \rangle |g_{XY}^{**}|$ from the high field line extrapolated to H=0 (See (3-70b).). The experimental result gives

$$\mu_B \langle S \rangle |g_{XY}^{**}| = 0.23 \times 10^{-21} \text{ emu/ion} , \qquad (5\text{-}3)$$

which yields

$$|g_{XY}^{**}| \langle S \rangle/S = 5.0 \times 10^{-2} . \qquad (5\text{-}4)$$

The bending field is 5.6 kOe so that one obtains from (3-71)

$$2(H_K^* - H_{K'}^* + 2h_{ex})/|g_{XY}^{**}| = 5.6 \times 10^3 \text{ Oe} . \qquad (5\text{-}5)$$

---

*) The accuracy for the estimation of H_{ex}, ±15%, is poorer than that for other parameters (several %), because the perpendicular susceptibility of this crystal is obtained from the experimental results in a rather narrow range of the field by subtracting the blank susceptibility of the sample holder and binding materials, which amounts to about 30% of the susceptibility of the sample and fluctuates about 50% from experiment to experiment.

Using the value of $|g_{XY}^{**}|\langle S\rangle/S$ given above, we have

$$(H_K^* - H_{K'}^* + 2h_{ex})\langle S\rangle/S = 1.4 \times 10^2 \text{ Oe} . \qquad (5\text{-}6)$$

The theoretical magnetization curve obtained by using these parameters is shown in Fig. 21. The calculation agrees well with the experimental results except for the inconsistence around the bending point. The calculation can be improved, in principle, by using the original rigorous equations such as (3-14a) and (3-14b) instead of the simplified forms as (3-16a) and (3-16b). However, it is not done in this paper.

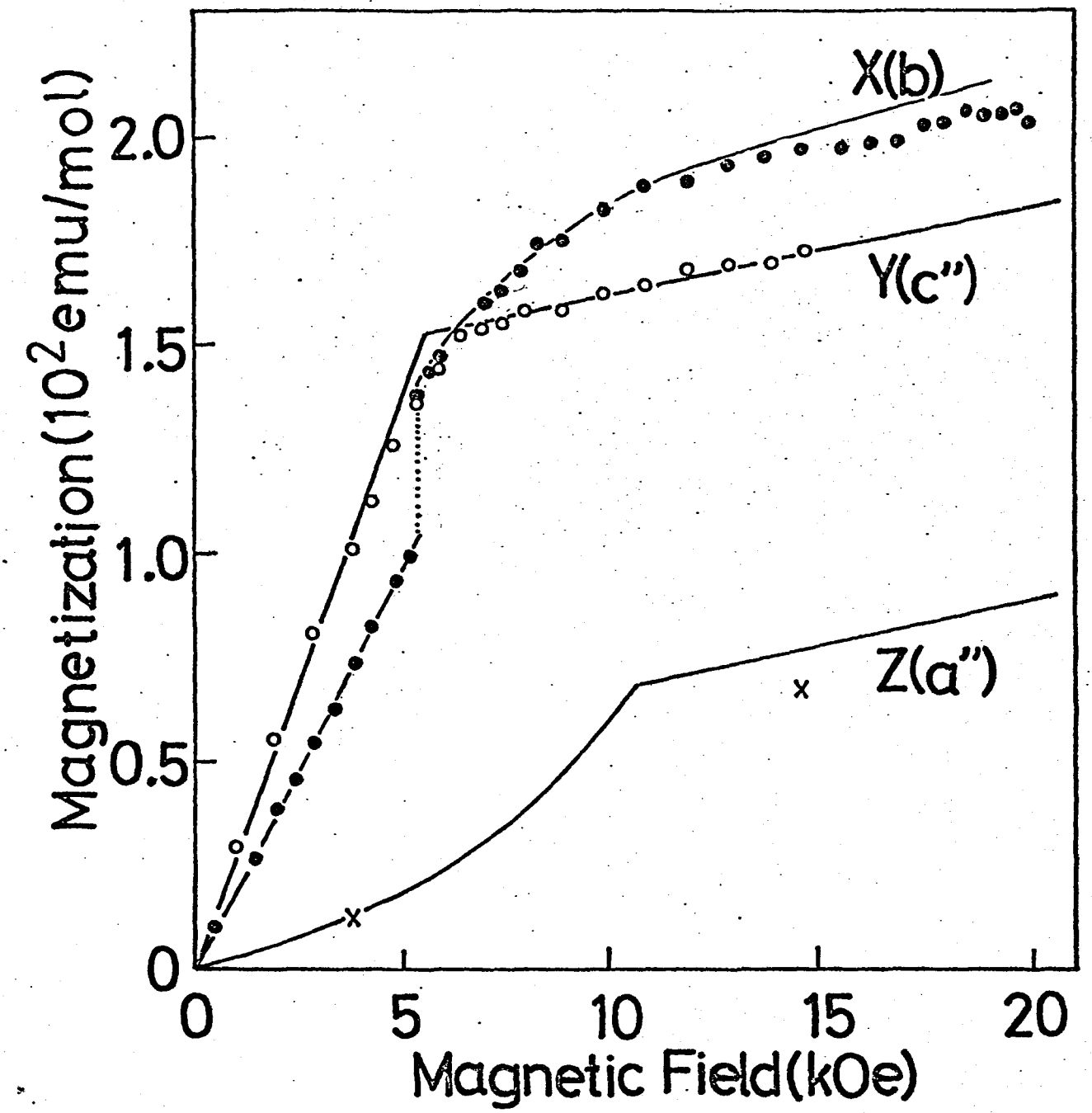

Fig. 21 Calculated magnetization curves for three principal axes and the experimental results.

5.2.2 $\vec{H}//Z(a'')$

In order to calculate the magnetization curve for $\vec{H}//a''$ by using (3-74a,b), the value of g_{ZX}^{**} is necessary. It is estimated from the relation

$$g_{ZX}^{**}/g_{XY}^{**} = -\tan(\text{angle between } a'' \text{ and } L_3 \text{ or that between } c'' \text{ and } L_1)^{*)}$$

$$= -\tan(-17.9^\circ) = 0.3230 \ . \qquad (5\text{-}7)$$

By using the value of $|g_{XY}^{**}|\langle S\rangle/S$ given in eq. (5-4), $|g_{ZX}^{**}|$ is estimated as

$$|g_{ZX}^{**}|\langle S\rangle/S = 1.6 \times 10^{-2} \ . \qquad (5\text{-}8)$$

The calculated magnetization curve is given in Fig. 21, where the bending field H_{BZ} is calculated by using (3-75) as

$$H_{BZ} = 1.06 \times 10^4 \text{ Oe} \ . \qquad (5\text{-}9)$$

---

*) We use the simplification used in §3.4 in the high field 2-sublattice state. When the field is in the ac-plane the magnetization parallel to the external field is found from eq. (3-84) to be proportional to

$$|g_{XY}^{**}\sin\theta + g_{ZX}^{**}\cos\theta| \ ,$$

where θ is the angle of the external field from the a''-axis measured toward the c''-axis. A constant term arising from the perpendicular susceptibility is neglected. The minimum of this quantity is obtained when θ satisfies the relation:

$$\tan\theta = -g_{ZX}^{**}/g_{XY}^{**} \ .$$

The direction of minimum magnetization is the L_3-axis.

Two experimental points in the figure are taken from the angular dependence. Detailed experiments on the similar compound CuFUH indicate that two experimental points (×) in Fig. 21 can be interpolated by a monotonic smooth curve. Therefore, the calculation seems to be plausible except for the sharp bending at about 11 kOe(H_{BZ}) which may arise from the simplification of the calculation.

5.2.3 $\vec{H}//X(b)$

In this case, the parameters determining the magnetization curve are g_{XY}^* , g_{ZX}^*, H_{K+}^* and h_{ex}. At first, their roles are considered qualitatively. We notice from (3-55a,b) that the "saturation" magnetization and the extrapolation of the magnetization curve after the jump to H=0(See the left broken line in Fig. 11(d).) are proportional to $(g_{XY}^{*2} + g_{ZX}^{*2})^{\frac{1}{2}}$ and $|g_{ZX}^*|$, respectively. The experimental result indicates that $|g_{ZX}^*|$ is 1/5 ∿ 1/3 of $|g_{XY}^*|$. Therefore, the height of the magnetization curve is mostly determined by $|g_{XY}^*|$ and the shape of the magnetization curve is modified by the ratio $|g_{ZX}^*/g_{XY}^*|$. On the other hand, as has been pointed out in §3.3.3(foot note of page 60), the external field, the abscissa of the magnetization curve, can be scaled by $H_{K+}^*/|g_{XY}^*|$. Consequently, the ratio $2h_{ex}/H_{K+}^*$(The factor 2 is added for convenience.) can be considered the second quantity which determines the shape of the magnetization curve.

Before determining the parameters precisely, we examine the order of magnitude of them. By using the height of the magnetization curve, $|g_{XY}^*|$ is estimated to be about 0.06. The computed curves given in Fig. 11(b) indicate that the magnetization saturates at a field satisfying

$$(H_X/H_{K+}^*)\,|g_{XY}^*| \simeq 4 \ . \qquad (5\text{-}10)$$

The experimental results show that the corresponding field in CuFTH is about 15kOe. Therefore, H_{K+}^* is calculated as about 230 Oe. Equation (5-6) indicates that $2h_{ex}$ is less than 140 Oe so that $2h_{ex}/H_{K+}^*$ is estimated to be at most about 0.5. The theoretical curves also indicate that, when

$|g_{ZX}^*/g_{XY}^*|$ and $2h_{ex}/H_{K+}^*$ have the values mentioned above, the linear part of the theoretical, in other words, computed magnetization curve before the jump practically coincides with the line corresponding to $g_{ZX}^*=0$. For $g_{ZX}^*=0$, analogously to eq. (3-71), the bending field is given by

$$H_{IBX} \equiv 2(H_{K+}^* + 2h_{ex})/|g_{XY}^*| \ , \tag{5-11}$$

where the suffix I(imaginary) indicates that the bending does not occur in real $g_{ZX}^* \neq 0$ systems.

The fine adjustment of $|g_{ZX}^*/g_{XY}^*|$ and $2h_{ex}/H_{K+}^*$ is done in Appendix F by comparing the details of the shape of the experimental and the computed magnetization curves. The result shows

$$|g_{ZX}^*/g_{XY}^*| = 0.20 \ . \tag{5-12a}$$

and

$$2h_{ex}/H_{K+}^* = 0.35 \ . \tag{5-12b}$$

The accuracy of the estimation is about 10%.

Using the perpendicular susceptibility given in §5.3.1, we obtain for the "saturation" magnetization

$$\mu_B \langle S \rangle (g_{XY}^{*2} + g_{ZX}^{*2})^{\frac{1}{2}} = 0.28 \times 10^{-21} \text{ emu/ion} \ , \tag{5-13}$$

which yields

$$(g_{XY}^{*2} + g_{ZX}^{*2})^{\frac{1}{2}} (\langle S \rangle / S) = 6.0 \times 10^{-2} \ . \tag{5-14}$$

By using the ratio of two g's given in eq. (5-12a), g_{XY}^* and g_{ZX}^* are calculated as

$$|g_{XY}^*|(\langle S\rangle/S) = 5.9 \times 10^{-2} , \tag{5-15}$$

$$|g_{ZX}^*|(\langle S\rangle/S) = 1.2 \times 10^{-2} . \tag{5-16}$$

The initial susceptibility minus the high field susceptibility is estimated from the experimental results as

$$0.28 \times 10^{-25} \text{ emu/ion} . \tag{5-17}$$

Dividing the "saturation" magnetization by it one obtains

$$H_{XIB} = 10.0 \text{ kOe} , \tag{5-18}$$

because the height divided by the tangent gives the abscissa. Using the ratio of $2h_{ex}$ to H_{K+}^*, $|g_{XY}^*|(\langle S\rangle/S)$ given in eq. (5-15) and eq. (5-11) we have

$$H_{K+}^*(\langle S\rangle/S) = 0.22 \times 10^3 \text{ Oe} . \tag{5-19}$$

$$h_{ex}(\langle S\rangle/S) = 40 \text{ Oe} . \tag{5-20}$$

The calculated magnetization curve is given in Fig. 21. The agreement between the calculation and the experiment is good.

5.2.4 Magnetic parameters

The left column of Table II represents the parameters obtained in the preceding subsections, where H_{K-}* is determined from eqs. (5-6) and (5-20). The signs of g-components are determined in the proton resonance experiments in the next section.

The right column of Table II represents the parameters obtained by using the definitions of these parameters given in §3. The spin canting l_0 at zero external field is estimated from (3-18a) as

$$l_0 = h_{DM}/2H_{ex} = 6.4 \times 10^{-3} \text{ radian}(0.4°) \ . \qquad (5\text{-}21)$$

Table II Magnetic parameters of $Cu(HCOO)_2 \cdot 4H_2O$ determined from the analysis of the magnetization curve. The left half of the table shows the parameters determined directly from the analysis and the right half shows the parameters derived from them.

$H_{ex}/(\langle S\rangle/S)$	1.50×10^{6} Oe	$H_K{}^*\langle S\rangle/S$	1.4×10^{2} Oe
$H_{K+}{}^*\langle S\rangle/S$	2.2×10^{2} Oe	$H_{K'}{}^*\langle S\rangle/S$	8.9×10 Oe
$H_{K-}{}^*\langle S\rangle/S$	6.0×10 Oe	$g_{XY}\langle S\rangle/S$	-5.5×10^{-2}
$h_{ex}\langle S\rangle/S$	4.0×10 Oe	$g_{ZX}\langle S\rangle/S$	-2.2×10^{-3}
$g_{XY}{}^{**}\langle S\rangle/S$	-5.0×10^{-2}	H_{DM}	6.2×10^{3} Oe
$g_{ZX}{}^{**}\langle S\rangle/S$	-1.6×10^{-2}	h_{DM}	1.9×10^{4} Oe
$g_{XY}{}^{*}\langle S\rangle/S$	-5.9×10^{-2}	$H_A\langle S\rangle/S$	3.9×10 Oe
$g_{ZX}{}^{*}\langle S\rangle/S$	1.2×10^{-2}	l_0	6.4×10^{-3}

§6. Analysis of The Results of Proton Resonance

6.1 Experimental results

6.1.1 Angular dependence

Experiments were carried out in the ac-, L_3b- and bc'-planes by rotating single crystals. Examples of the angular dependence of resonance point are shown in Fig. 22. As the frequency dependence below 5MHz and the temperature dependence at liquid helium temperature range are small,[14,15,37] they are not discussed in this paper.

6.1.2 Phase boundary

The shift of resonance field ΔH given by

$$\Delta H = H^r - H^f \tag{6-1}$$

is considered, where H^r is the observed resonance field and H^f is the resonance field of a free proton. The shift is of cource coming from the internal field $\vec{H}^i$ due to the magnetic moment of copper ions. The internal field(about 0.3kOe) is considerably smaller than H^f of the present experiments(1.3kOe for 5.7MHz). For this case, the shift is given by

$$\Delta H = - H^i_{//} - \frac{1}{2}(H^i_{\perp})^2/H^f + \cdots , \tag{6-2}$$

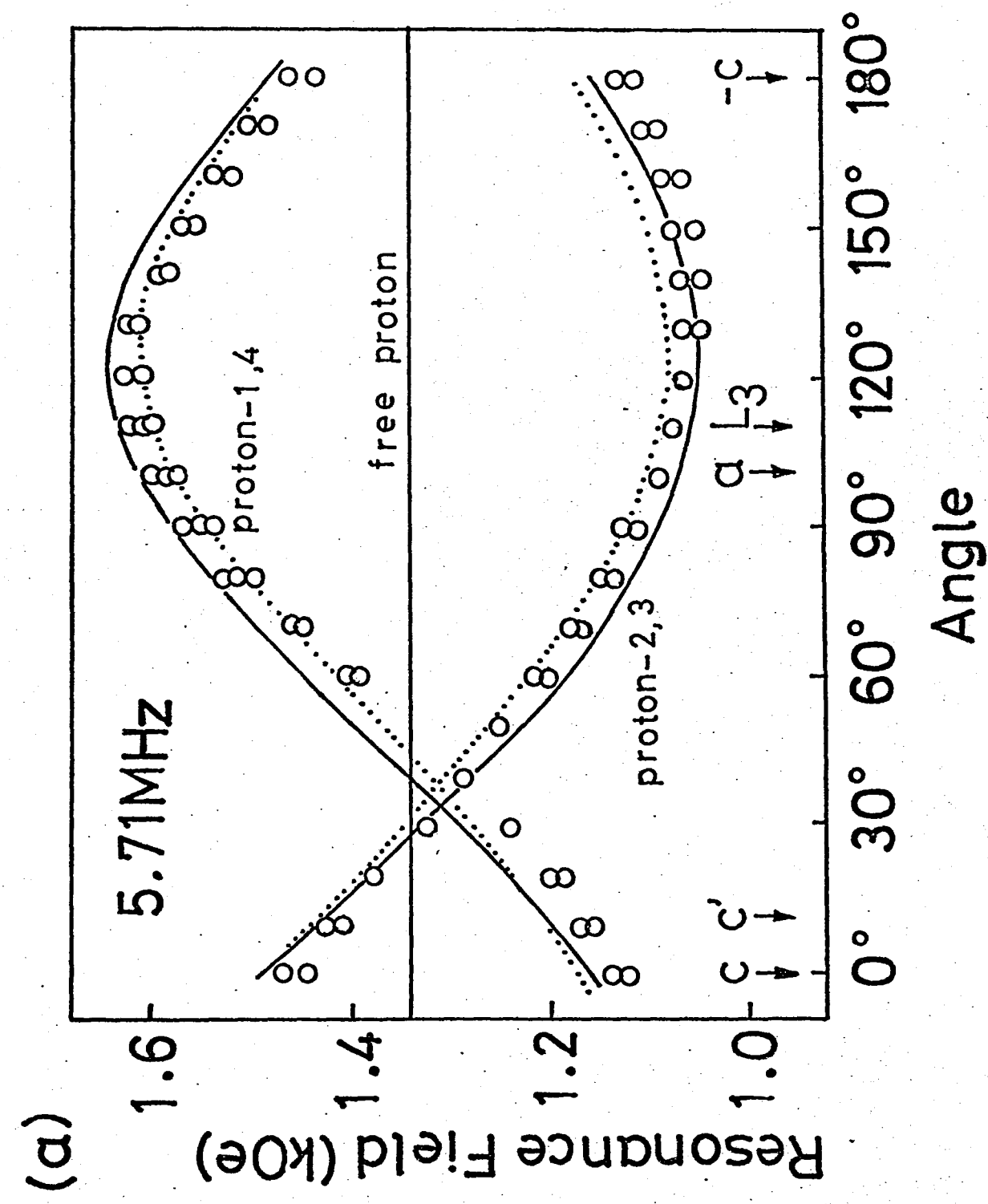

Fig. 22 (a)-(d) Angular dependence of resonance points in the ac-plane for protons of $Cu(HCOO)_2 \cdot 4D_2O$ at 4.2K. (a')-(d') Angular dependence in the L_3b-plane. (a")-(b") Angular dependence in the bc'-plane. For the lines representing calculated resonance points, see text.

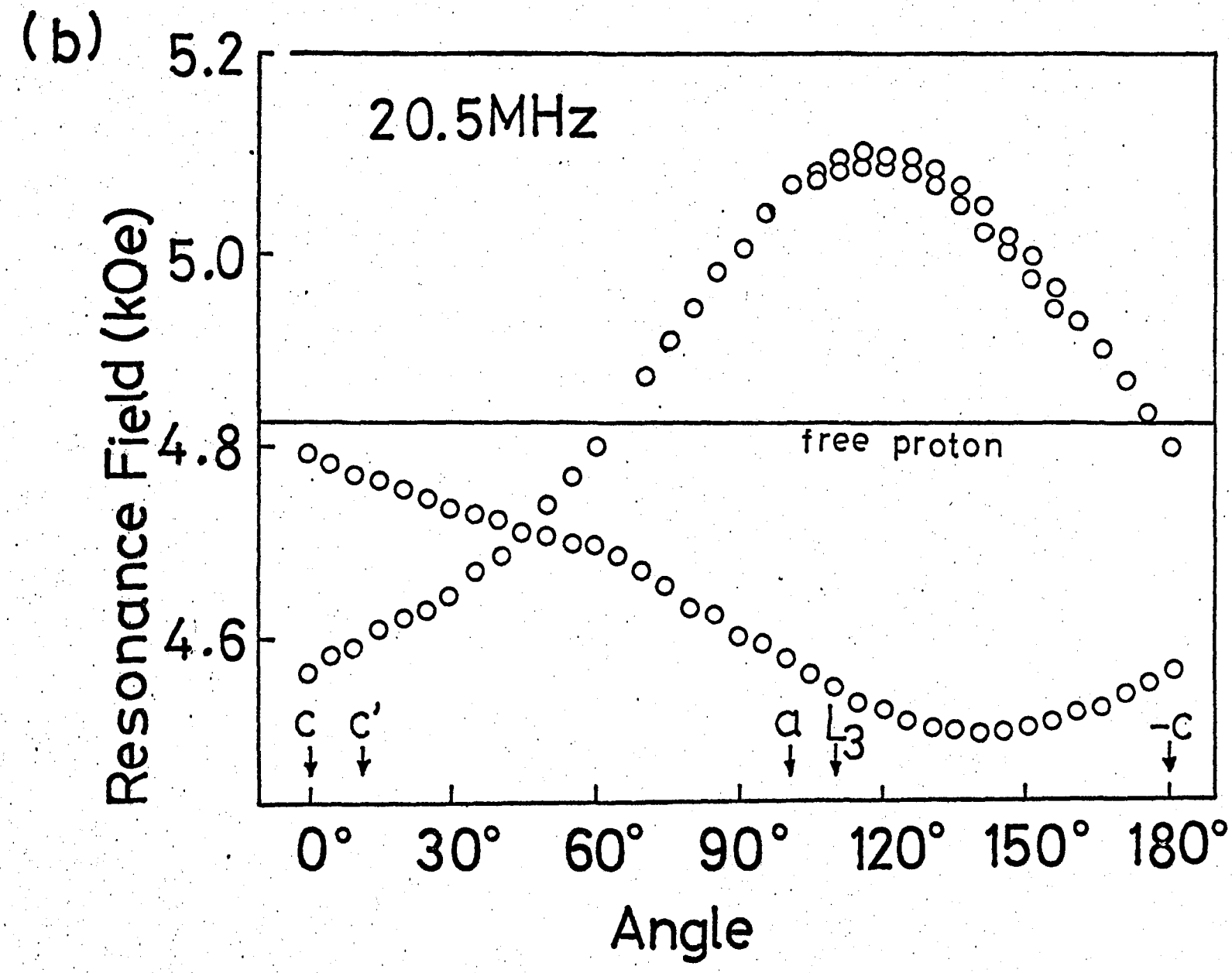
(b)
20.5MHz
free proton
Resonance Field (kOe)
5.2
5.0
4.8
4.6
c
c'
a
L3
-c
0°
30°
60°
90°
120°
150°
180°
Angle

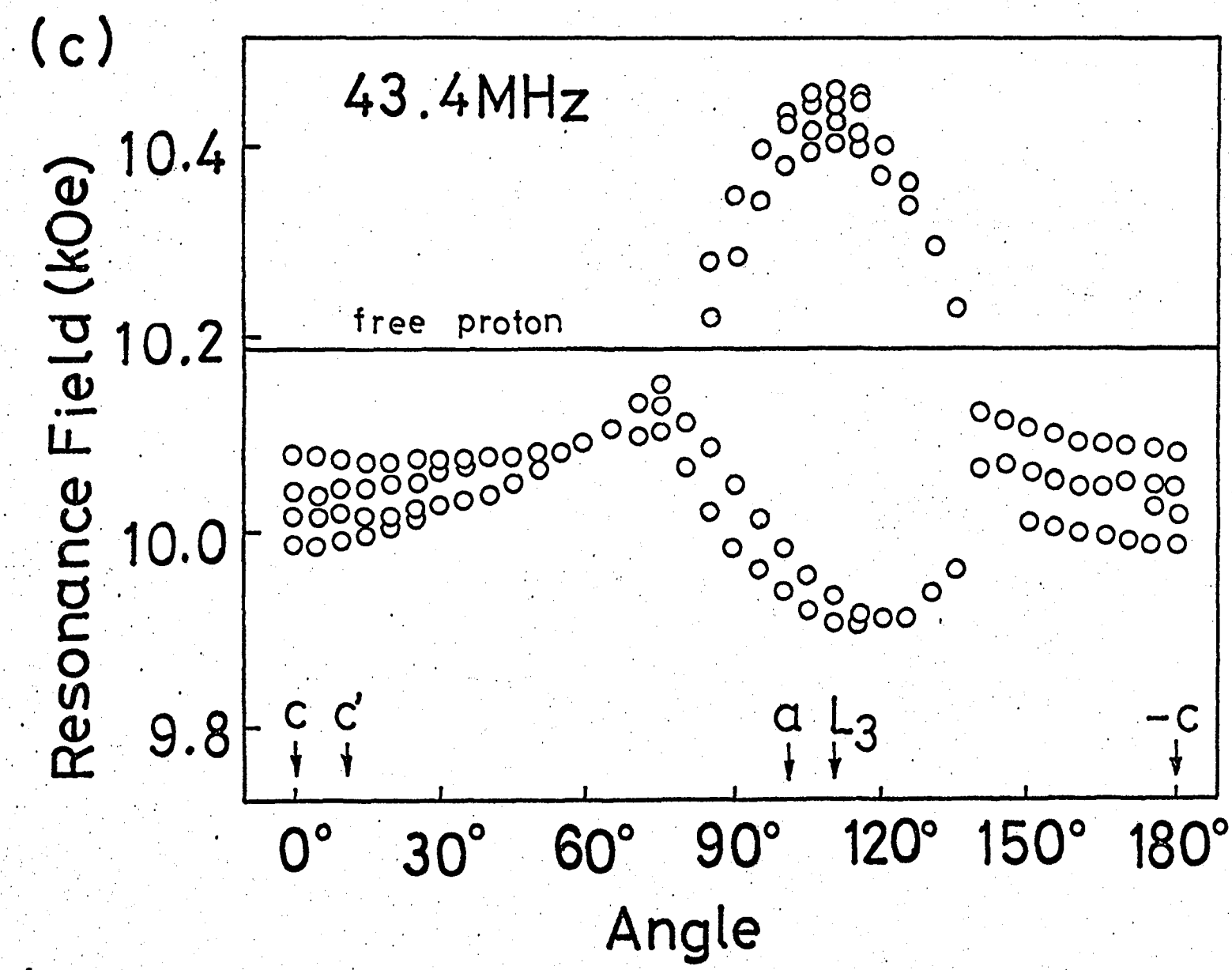
(c)
43.4MHz
free proton
Resonance Field (kOe)
10.4
10.2
10.0
9.8
c
c'
a
L3
-c
0°
30°
60°
90°
120°
150°
180°
Angle

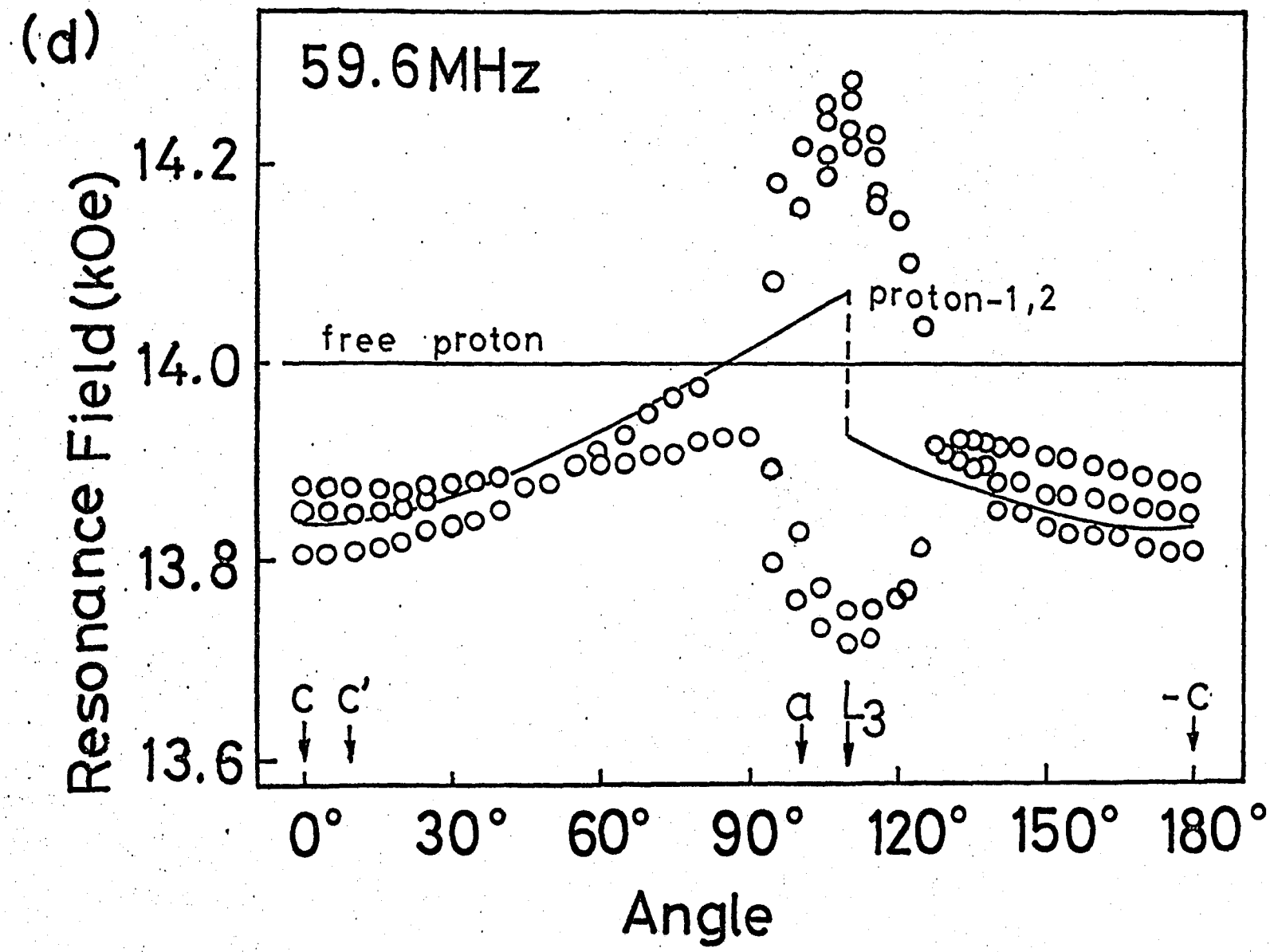
(d)
59.6MHz
Resonance Field (kOe)
14.2
14.0
13.8
13.6
free proton
proton-1,2
c
c'
a
L3
-c
0°
30°
60°
90°
120°
150°
180°
Angle

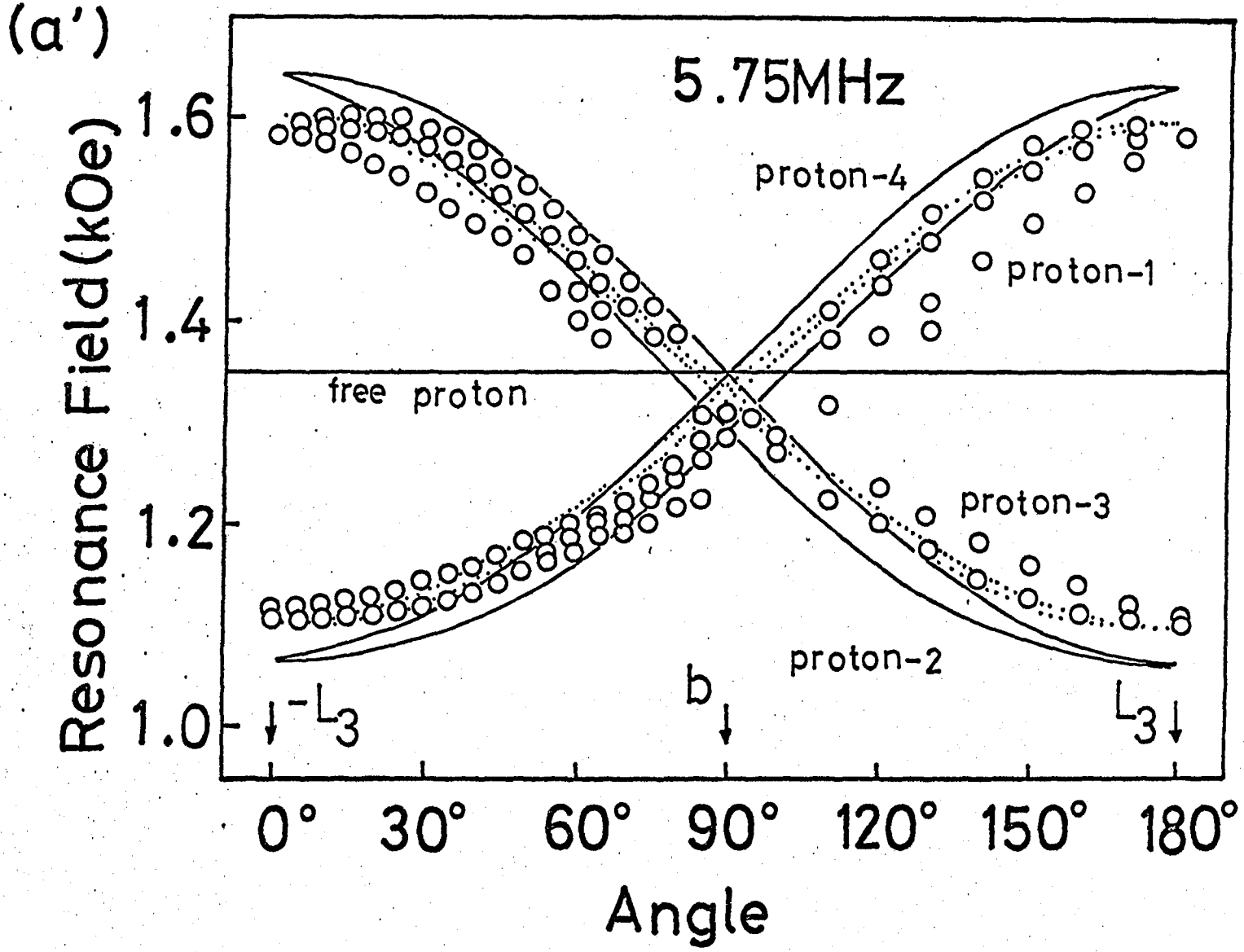
(a')
5.75MHz
Resonance Field(kOe)
1.6
1.4
1.2
1.0
proton-4
proton-1
free proton
proton-3
proton-2
$-L_3$
b
L_3
0°
30°
60°
90°
120°
150°
180°
Angle

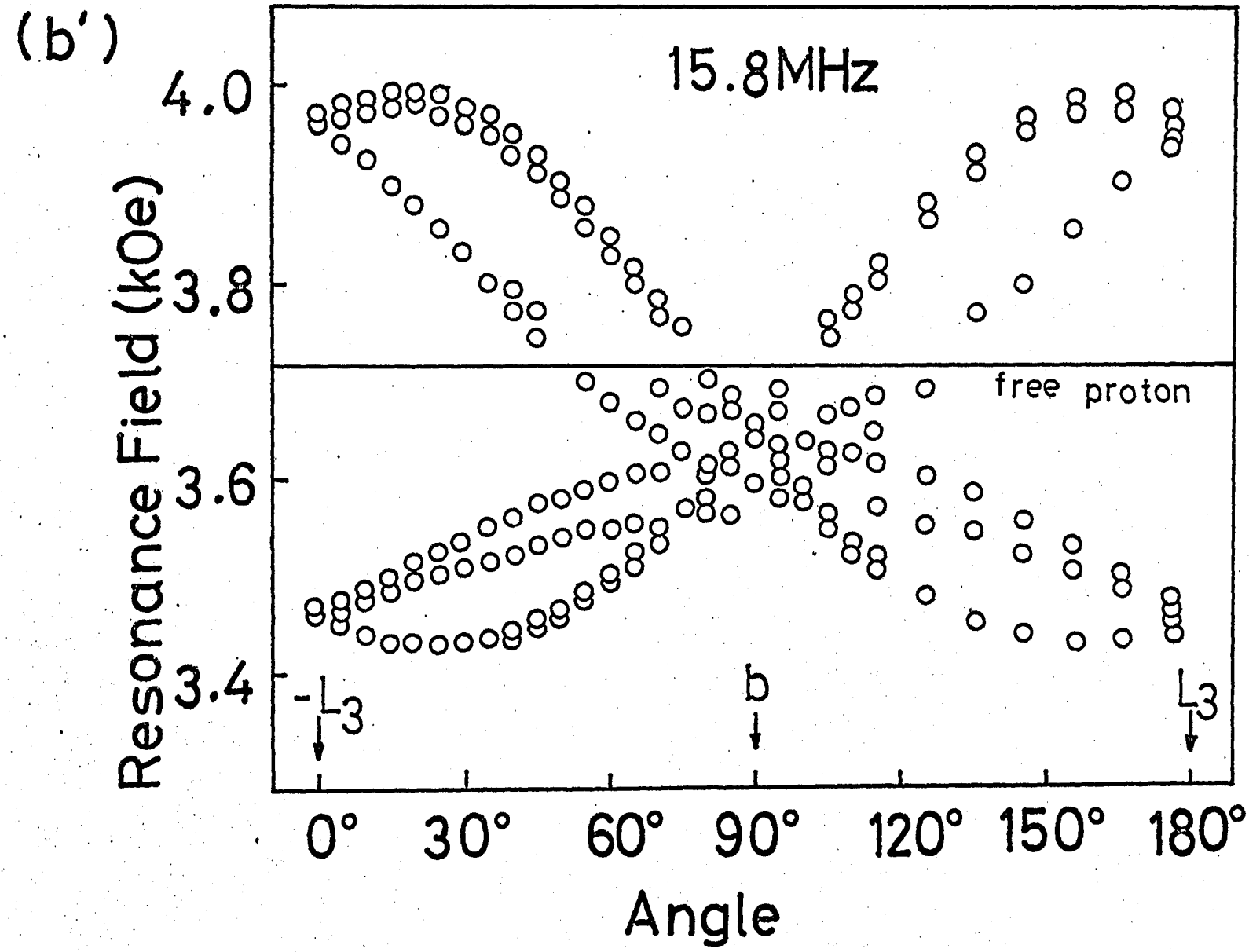
(b')
15.8MHz
free proton
Resonance Field (kOe)
4.0
3.8
3.6
3.4
-L3
b
L3
0°
30°
60°
90°
120°
150°
180°
Angle

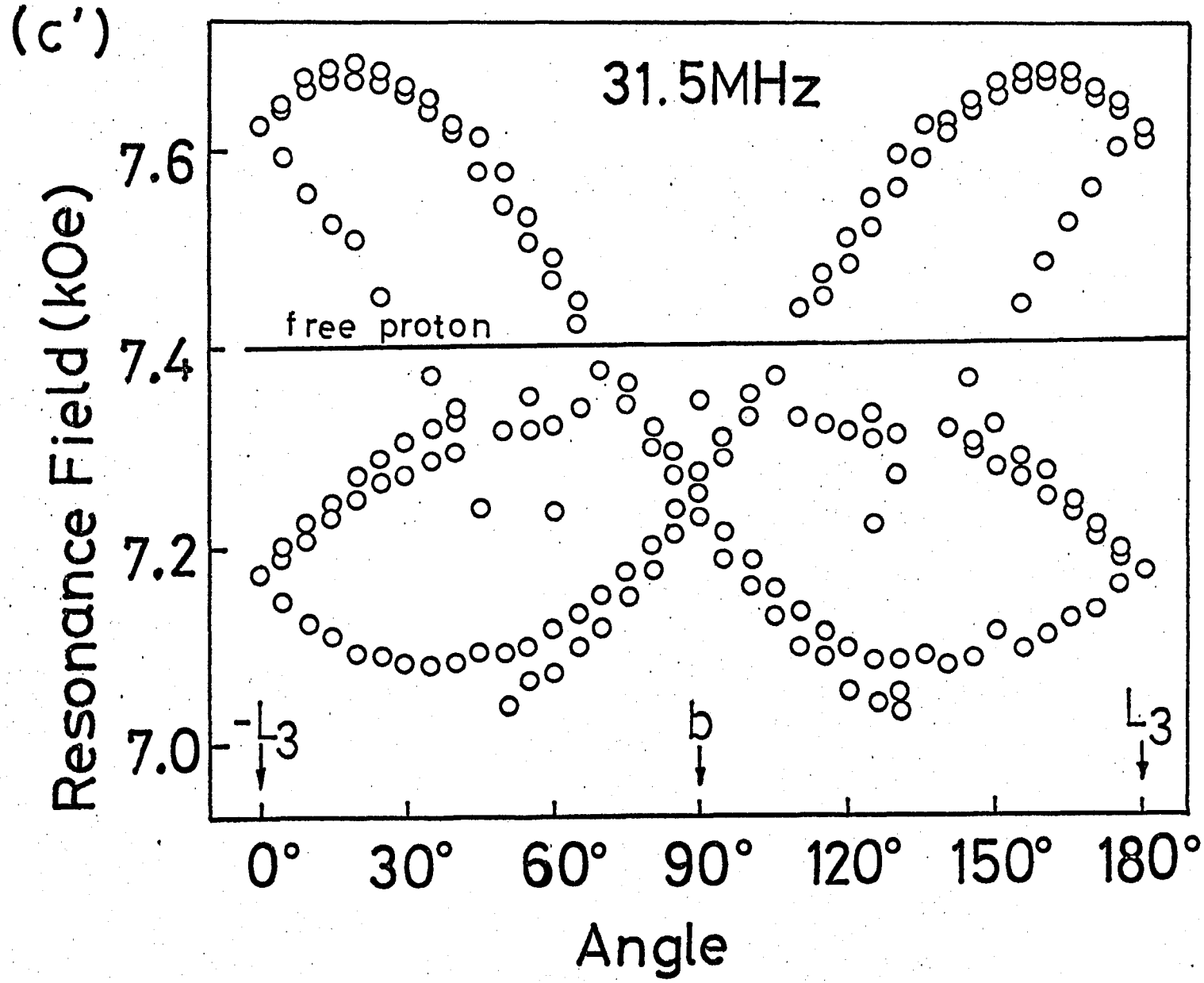
(c')
31.5MHz
free proton
Resonance Field (kOe)
7.6
7.4
7.2
7.0
-L3
b
L3
0°
30°
60°
90°
120°
150°
180°
Angle

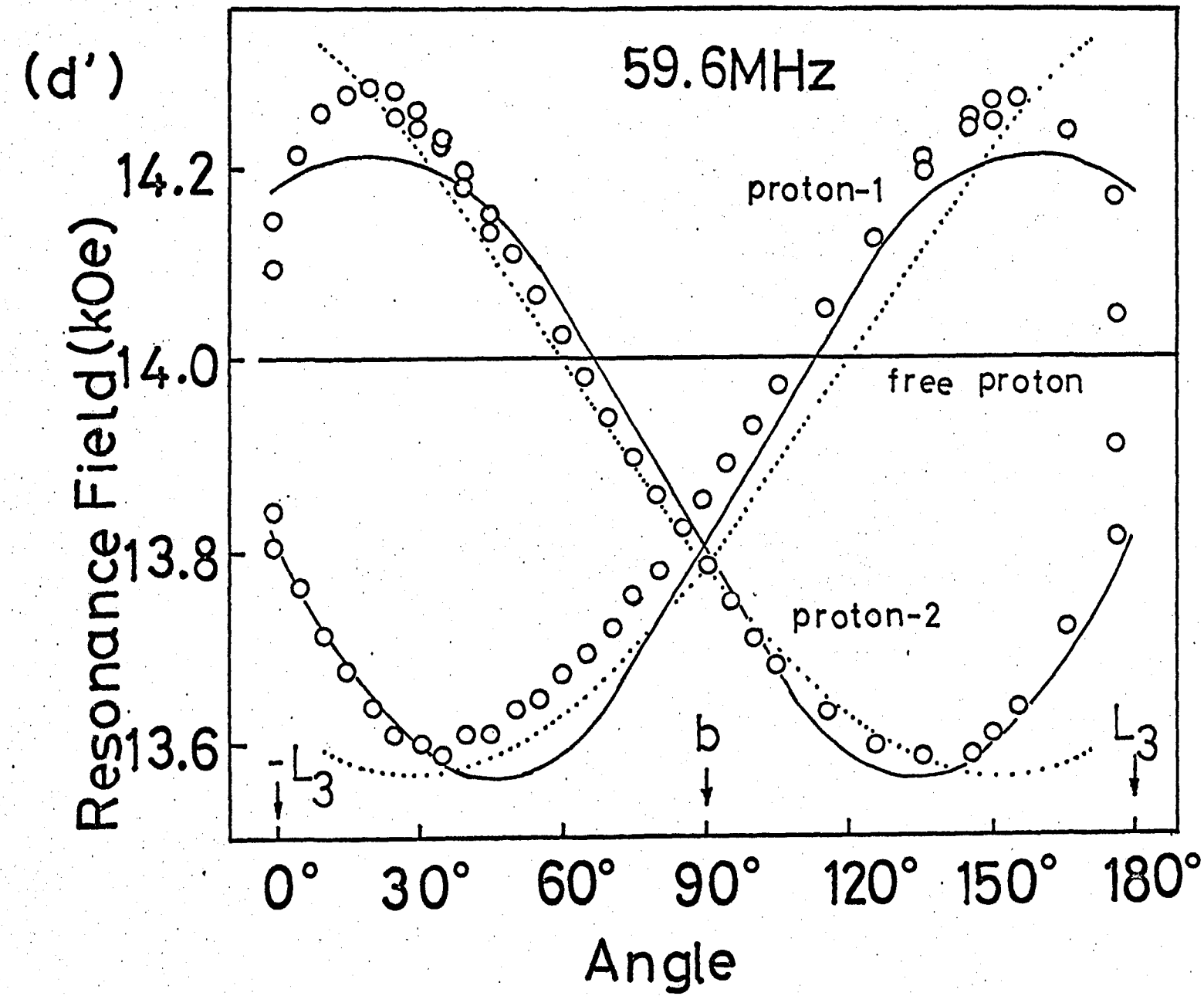
(d')
59.6MHz
Resonance Field (kOe)
14.2
14.0
13.8
13.6
proton-1
free proton
proton-2
-L3
b
L3
0°
30°
60°
90°
120°
150°
180°
Angle

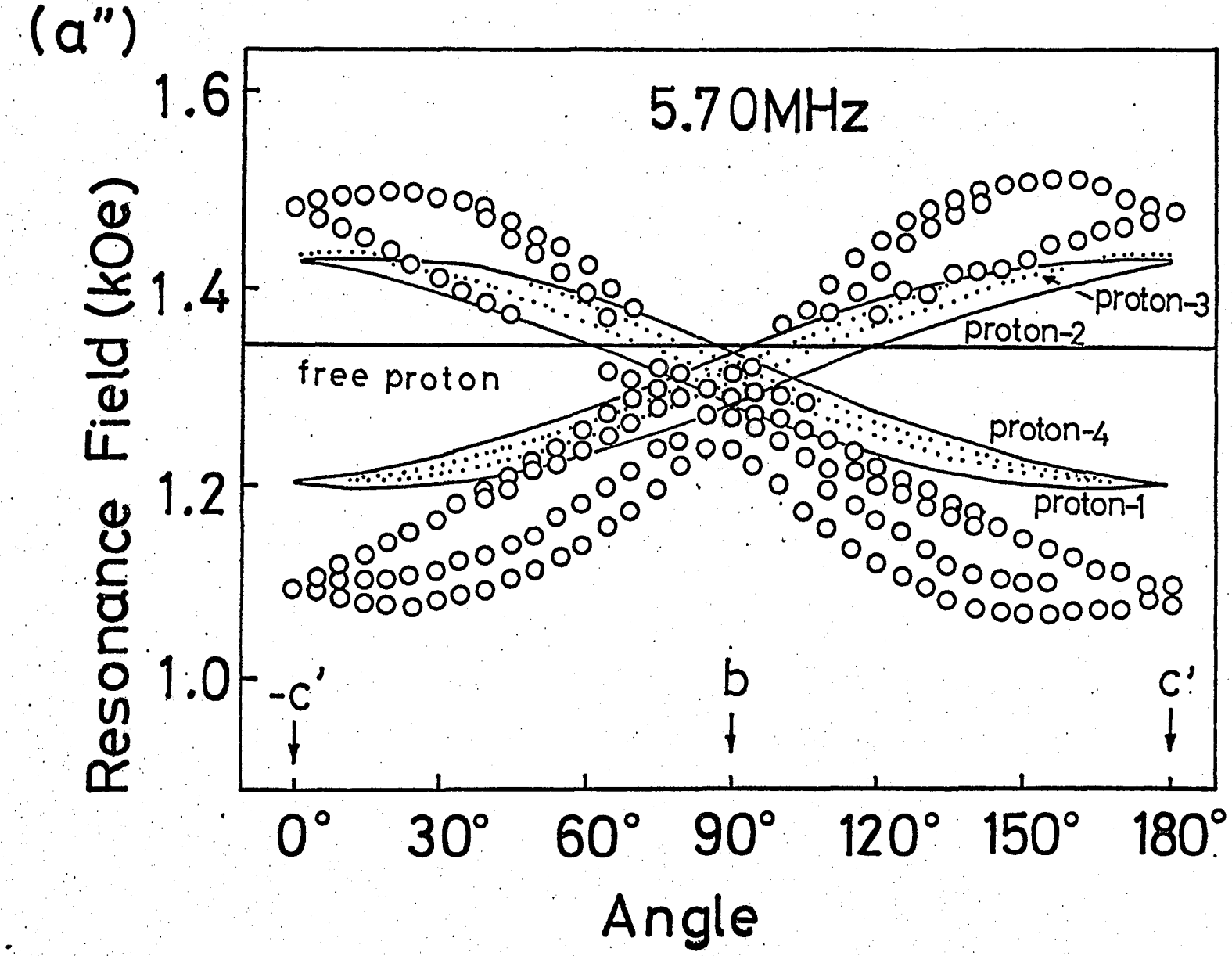
(a")
5.70MHz
Resonance Field (kOe)
1.6
1.4
1.2
1.0
free proton
proton-3
proton-2
proton-4
proton-1
-c'
b
c'
0°
30°
60°
90°
120°
150°
180°
Angle

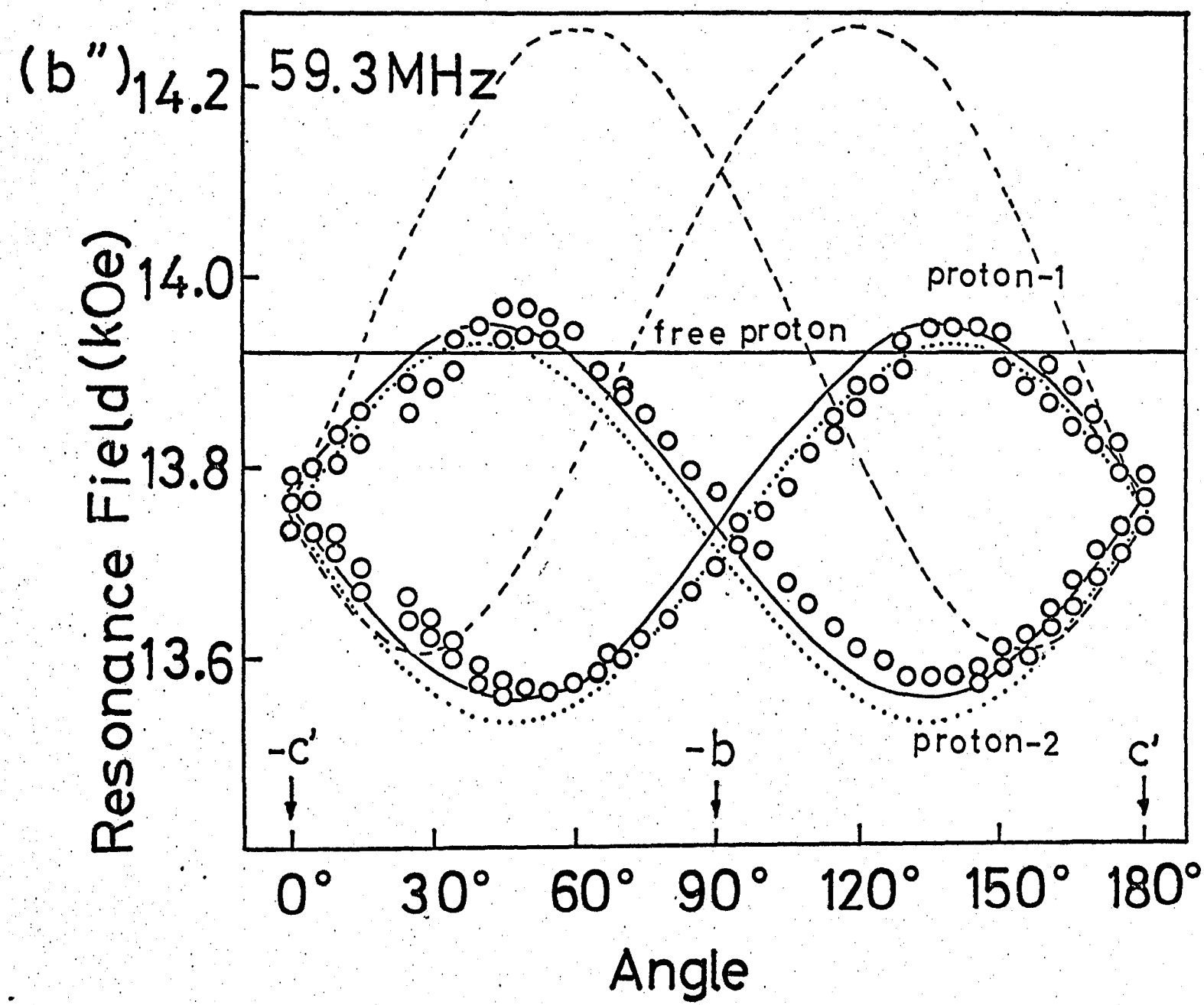
(b")
59.3MHz
14.2
14.0
13.8
13.6
Resonance Field (kOe)
free proton
proton-1
proton-2
-c'
-b
c'
0°
30°
60°
90°
120°
150°
180°
Angle

where // and $\perp$ are used for components parallel and perpendicular to the external field respectively.

Above about 15MHz ΔH is practically given by the first term of eq. (6-2). Therefore, if the internal field(or the magnetic structure) is not influenced by the external field, the angular dependence of ΔH is a sine curve for every frequency and the shift plotted versus frequency is flat for every field direction.

Frequency dependence of ΔH is shown in Fig. 23 for three typical directions, L_1, L_3 and B. The direction B is a bisector of b and L_3. It is selected instead of b because the frequency dependence for b is accidentaly insensitive to the change of magnetic structure. The frequency dependence given in Fig. 23(a) and (b) indicates that the magnetic structure changes with the external field for $\vec{H}//L_1$ but it does not for $\vec{H}//L_3$ up to 14kOe. In the former case, the structure becomes independent of the field intensity above about 6kOe. Field dependence of the magnetic structure for $\vec{H}//B$ is analogous to that for $\vec{H}//L_1$. Similar boundary(change of separation or change of number) is seen in the angular dependence given in Fig. 22. The transition occurs at a field much lower than the estimated[16] spin flop field(22kOe).

Fig. 20(b) shows a profile of the boundary. Dotted lines in the figure represent the phase boundary determined from a jump or a bend of the magnetization curve. Boundaries in two experiments are due to the same origin. The result in the L_3b-plane is consistent with a recent work by Dupas and Renard.[35]

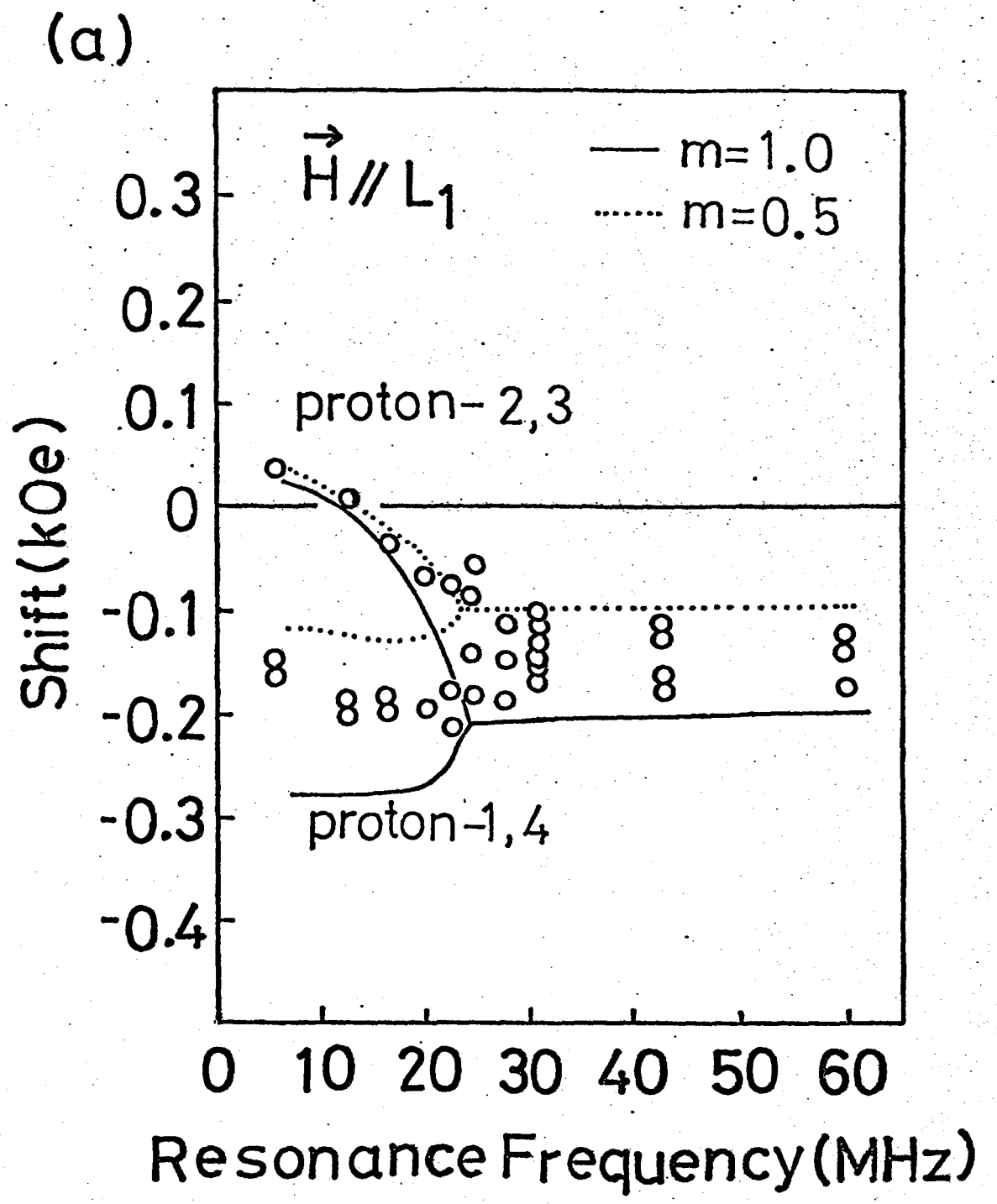

Fig. 23 Frequency dependence of the nmr shift. Three field-directions, L_1, L_3 and B, are considered. The direction B corresponding to fig. (c) of p. 113 is a bisector of b and L_3. For the lines representing calculated shift, see text.

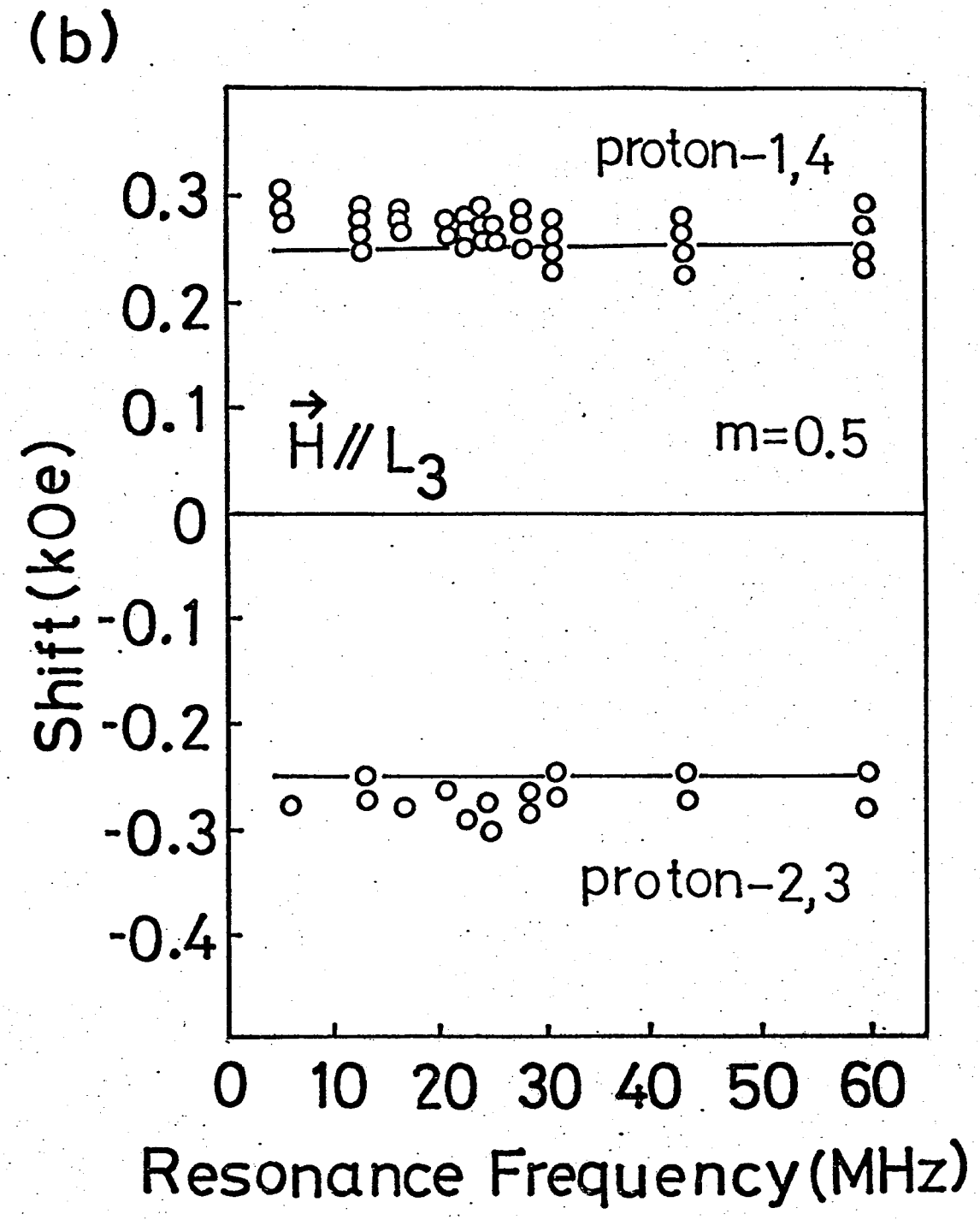
(b)
proton-1,4
0.3
0.2
0.1
0
-0.1
-0.2
-0.3
-0.4
$\vec{H} // L_3$
m=0.5
proton-2,3
Shift (kOe)
0 10 20 30 40 50 60
Resonance Frequency (MHz)

(c)

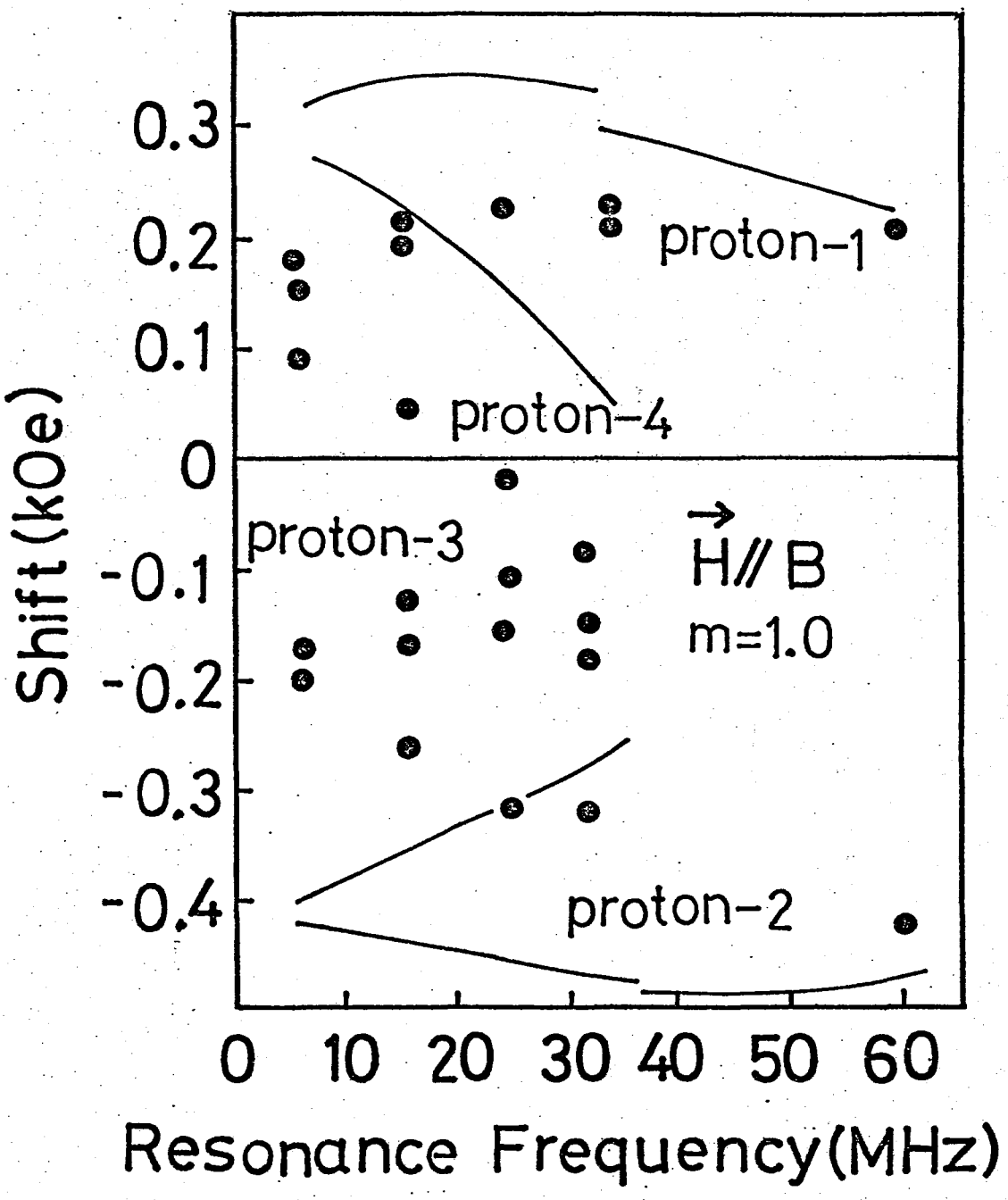
0.3
0.2
0.1
0
-0.1
-0.2
-0.3
-0.4
Shift (kOe)
proton-1
proton-4
proton-3
proton-2
H// B
m=1.0
0 10 20 30 40 50 60
Resonance Frequency (MHz)

6.2 Dipole field

6.2.1 Magnetic unit cell

The angular dependence of the resonance point at 59MHz indicates that the high field state has two internal fields except for small splitting. For this case, the magnetic unit cell is identical with the crystal cell. It is because we have two internal fields if the magnetic cell is the same as the crystal cell*) and have larger number of fields when the magnetic cell is larger than the crystal cell. The magnetization curve shows that the magnetic structure is a 2-sublattice weak ferromagnet in which adjacent spins in the 2d ab-plane are nearly antiparallel and those in neighboring planes are parallel. The result is shown in Fig. 4(b) by taking the spin direction parallel to the b-axis.**)

In the low field phase, the magnetic unit cell consists of two crystal cells adjoining along the c-direction. The reason is as follows. The differential susceptibility in the 2-sublattice state[2] indicates that the spins in the 2d ab-plane are coupled by a strong antiferromagnetic interaction of 10^6 Oe as has been expected from the crystal structure. Therefore, 2-sublattice type arrangement of spins in the ab-plane is stable throughout the present experiment.

---

*) The internal field of protons with a primed number in Fig. 5 is equal to that of the corresponding unprimed ones.

**) In §6.3, one sees that this is the case for $\vec{H}$ in the ac-plane.

Four protons in the unit rectangle of the ab-plane(See Fig. 5.) reduce to two independent protons. In the low field state, the observed number of internal field is four except for small splitting. Therefore, magnetic unit cell of the low field state consists of two crystal cells adjoining along the c-axis. The symmetry of the internal field shows that the magnetic structure at zero external field is a 4-sublattice antiferromagnet in which spins of neighboring planes are antiparallel. The symmetry also shows that the antiferromagnetic axis lies in the ac-plane or parallel to the b-axis. Hidden canting is allowed.

In the following subsections, details of the spin direction are studied for two limiting cases(5.7MHz and 59MHz) and for three typical intermediate frequencies(16.2, 20.5, 22.6MHz) by assuming that the origin of $\vec{H}^i$ is pure dipole field.

6.2.2 Calculation of dipole field

The dipole field is calculated for four types of spin arrangement, AR-1 to 4 given in Table III. Cases of ferromagnetic layers, AR-1 and 2, are examined for estimating contributions of weak ferromagnetism.

At first, g-tensor of two ions is considered. Matrix form of the tensor is

$$\tilde{g}_{1,2} = \begin{pmatrix} g_{xx} & \pm g_{xy} & g_{zx} \\ \pm g_{xy} & g_{yy} & \pm g_{yz} \\ g_{zx} & \pm g_{yz} & g_{zz} \end{pmatrix} . \qquad (6\text{-}3)$$

Table III Four types of spin arrangement, AR-1 to 4. The number of copper ions is taken from Fig. 5. Elements of $\tilde{d}$ are also shown in unit of kOe. The figures in parentheses are for the weak ferromagnetic moment of $2.7 \times 10^{-2}\mu_B$ per ion.

type		AR-1	AR-2	AR-3	AR-4
spin arrangement		1:+ 2:+ 3:+ 4:+	1:+ 2:+ 3:- 4:-	1:+ 2:- 3:+ 4:-	1:+ 2:- 3:- 4:+
elemnts of $\tilde{d}$	d_{xx}	0.35(0.01)	0.54(0.01)	-0.50	-0.51
	d_{yy}	0.32(0.01)	0.51(0.01)	0.51	0.48
	d_{zz}	-0.75(-0.02)	-1.18(-0.03)	0.0	0.05
	d_{xy} d_{yx}	-0.89(-0.02) -0.88(-0.02)	-0.88(-0.02) -0.87(-0.02)	0.02 0.02	0.02 0.02
	d_{yz} d_{zy}	-0.07(0.0) -0.04(0.0)	-0.05(0.0) -0.03(0.0)	-0.21 -0.19	-0.25 -0.22
	d_{zx} d_{xz}	-0.03(0.0) -0.05(0.0)	-0.08(0.0) -0.05(0.0)	0.20 0.19	0.23 0.25

Notations + and - correspond to $\tilde{g}_1$ of corner ions and $\tilde{g}_2$ of base-center ions respectively. The xyz-coordinate system given in Fig. 5 is used. The g-tenser $\tilde{g}_{sym}$ appearing in the paramagnetic resonance is given by the average of $\tilde{g}_1$ and $\tilde{g}_2$. The matrix form of $\tilde{g}_{sym}$ is obtained by taking $g_{xy} = g_{yz} = 0$ in the matrix form of $\tilde{g}_1$ and $\tilde{g}_2$. The elements, g_{xx}=2.078, g_{yy}=2.116, g_{zz}=2.354 and g_{zx}=0.047, are obtained from the experimental result[27] by changing the axes. Calculation of dipole field is done first by using $\tilde{g}_{sym}$ instead of $\tilde{g}_1$ and $\tilde{g}_2$. A correction due to the antisymmetric part(difference between $\tilde{g}_{1,2}$ and $\tilde{g}_{sym}$) is considered later.

The dipole field for proton-1, $\vec{H}^d$ in unit of kOe, is given by

$$\vec{H}^d = \tilde{d}\,\vec{m}\,, \tag{6-4}$$

where $\tilde{d}$ and $\vec{m}$ stand for

$$\tilde{d} = \tilde{D}\,\tilde{g}_{sym}\,S \tag{6-5}$$

and

$$m = <\vec{S}_1>/S \tag{6-6}$$

respectively. The tensor $\tilde{D}$ is $10^{-3}\mu_B$ times of the usual dipole sum tensor. The symbol <> represents thermal average. The calculated elements of $\tilde{d}$ are given in Table III. The dipole field(=internal field) of other protons is obtained by changing the elements of $\tilde{d}$ after Table IV.

Correction due to the antisymmetric part of $\tilde{g}_{1,2}$ is estimated by using the dipole field of AR-1 and 2. As a result, a small correction is made in the high field 2-sublattice state. Effect of spin canting due to the DM-interaction is negligible because the canting is only about 0.6% of the copper moment.

Table Ⅳ Sign of d-elements of four protons. The uv element of proton-n, $d_{uv}(n)$, is obtained by changing the sign of d_{uv} given in Table Ⅲ when $d_{uv}(n)$ in this table is assigned by -.

kind of arrangement	component of $\tilde{d}$	proton-1	proton-2	proton-3	proton-4
AR-1	xx,yy,zz,zx,xz	+	+	+	+
	xy,yx,yz,zy	+	-	+	-
AR-2	xx,yy,zz,zx,xz	+	+	-	-
	xy,yx,yz,zy	+	-	-	+
AR-3	xx,yy,zz,zx,xz	+	-	+	-
	xy,yx,yz,zy	+	+	+	+
AR-4	xx,yy,zz,zx,xz	+	-	-	+
	xy,yx,yz,zy	+	+	-	-

6.3 Interpretation of the results

6.3.1 Low field 4-sublattice state

In the followings, the vector $\vec{m}$ is kept in the ac-plane, because the direction of calculated internal fields for $\vec{m}//b$ is completely different from the experimental result. The conclusion of the magnetization measurement supports the former case.

The direction of $\vec{m}$ is, for the sake of argument, moved in the zx(ac)-plane. The internal fields for proton-1 to 4 are given by $\vec{H}'$, $\vec{H}''$, $-\vec{H}'$, $-\vec{H}''$, respectively. Components of $\vec{H}'$ and $\vec{H}''$ are written, by using Table III and IV, as

$$H'_x \ , \ H''_x = \mp 0.51m_x \pm 0.25m_z \ ,$$

$$H'_y \ , \ H''_y = 0.02m_x - 0.25m_z \ ,$$

$$H'_z \ , \ H''_z = \pm 0.23m_x \pm 0.05m_z \ . \qquad (6\text{-}7)$$

The vector $\vec{m}$ lies close to the x(a)-axis, because the second of the above equations indicates that the observed small y(b) component of the internal field is obtained when $\vec{m}$ lies close to x. Calculated angular dependence of the resonance field for $\vec{H}$ in the zx-plane is shown in Fig. 22(a). Solid lines correspond to $\vec{m}//L_3$ and dotted ones to $\vec{m}//a''(m_x>0,$ *) $m=0.50$ **)). Accurate

---

*) The component m_x can be selected positive with no loss of generality.

**) When m is changed, the amplitude of the calculated curve changes almost proportionally.

determination of the direction of $\vec{m}$ is impossible. Calculated results for $\vec{H}$ in the L_3b(close to xy)-plane are given in Fig. 22(a'). Calculated results for the yz(bc')-plane are shown in Fig. 22(a''). Experiment and calculation both agree with those of Dupas and Renard.[15] In Fig. 22(a''), correspondence between experiment and calculation is not good(Also see §6.3.5.).

A problem of the foregoing argument is that a 2-sublattice magnetic structure with domains gives a similar set of internal field. Dupas and Renard examined the problem by considering protons of water molecules because two magnetic structures may result different sets of internal field for these protons.[15] Agreement between calculation and experiment was poor.*) Consequently, the possibility of 2-sublattice structure has not yet been excluded.[35] However, about 20% of saturation weak ferromagnetic moment should be observed along the b-axis even in very weak external field if the magnetic structure is 2-sublattice type.[16] It is inconsistent with the observation. In conclusion, the 2-sublattice structure is excluded.

---

*) The origin is probably a deficient accuracy of the assumed H_2O proton positions.

6.3.2 High field 2-sublattice state

For $\vec{H}$ in the ac-plane, ΔH is given from Table III and IV by

$$\Delta H = -(\pm 0.20 m_x - 0.19 m_y - 0.02)\cos\theta_H$$
$$-(\mp 0.50 m_x + 0.02 m_y \pm 0.19 m_z)\sin\theta_H \ , \qquad (6\text{-}8)$$

where θ_H is an angle between $\vec{H}$ and c'(See Fig. 24(a).). The upper and the lower of the double sign correspond to proton-1 and 2 respectively. A term independent of $\vec{m}$ comes from the ferromagnetic moment of $2.7\times10^{-2}\mu_B$ parallel to the L_1-axis.

The shift ΔH for $\vec{H}$ in the bc'-plane is given by

$$\Delta H = -(0.01 - 0.03\sin^2\theta_H)$$
$$-(0.02 m_x \pm 0.51 m_y - 0.21 m_z)\cos\theta_H$$
$$-(\pm 0.20 m_x - 0.19 m_y)\sin\theta_H \ , \qquad (6\text{-}9)$$

where θ_H is an angle between $\vec{H}$ and b. For $\vec{H}$ in the L_3b-plane, the shift is given by

$$\Delta H = -(\mp 0.02\sin\theta_H + 0.01\cos\theta_H)$$
$$-(0.02 m_x \pm 0.51 m_y - 0.21 m_z)\cos\theta_H$$
$$-(\mp 0.52 m_x + 0.05 m_y \pm 0.19 m_z)\sin\theta_H \ , \qquad (6\text{-}10)$$

where θ_H is an angle between $\vec{H}$ and b. The direction of weak ferromagnetic moment is taken parallel to the b-axis for $\vec{H}$ in the L_3b-plane and parallel

to the external field for $\vec{H}$ in the bc'-plane.

The experiment in the ac-plane is considered first. Equation (6-8) indicates that the shift corresponding to the center of two lines is approximately given by the term $0.19m_y\cos\theta_H$. The experimental result shows $m_y=-0.95$(independent of θ_H). The observed separation corresponds to $m_x=0.15$, $m_z=0.16$ or $m_x=-0.15$, $m_z=-0.16$. However, non-zero value of m_x and m_z is spurious. It is because the nature of weak ferromagnetism indicates that m_x and m_z are zero for $\vec{H}$ in the ac-plane and because the measurement in the bc'-plane shows that the separation is sensitive to mis-orientation of crystal. In conclusion, one obtains

$$m_x = 0 \ , \quad m_y = \mp(0.95\pm0.05) \ ,$$

$$m_z = 0 \ , \quad m = |m_y| \ , \tag{6-11}$$

where ± in ( ) represents the accuracy of estimation and - and + of m_y correspond to $H_z>0$ and $H_z<0$ respectively. The experimental condition and the observed $\vec{m}$ are shown in Fig. 24(a) and (a') respectively. The calculated result of the resonance field is given in Fig. 22(d)(solid line).

The case of bc'-plane is considered next. Equation (6-9) indicates that ΔH corresponding to the center of two lines is approximately given by $0.21m_z\cos\theta_H+0.19m_y\sin\theta_H$. The experimental result is -0.18(independent of θ_H). Using a condition $m_y=-0.95$, $m_z=0$ for $\theta_H=90°$, one obtains $m_z=-0.86\cos\theta_H$, $m_y=-0.95\sin\theta_H$. The condition for m_y and m_z is introduced so as to ensure the consistency with the result in the ac-plane. The component m_x is

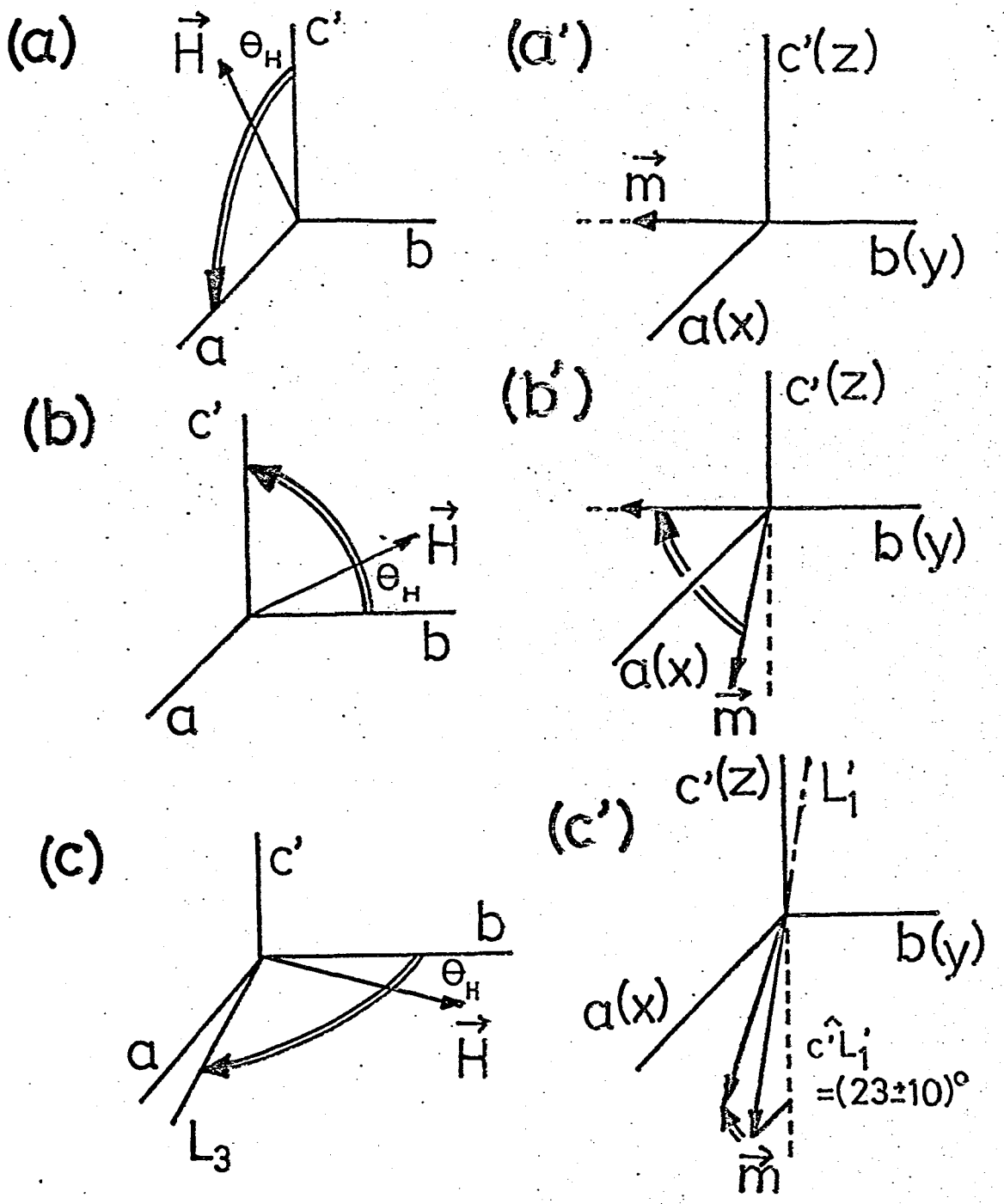

Fig. 24 The relation between the direction of the external field and that of the moment of copper-1($\vec{m}$) for high field 2-sublattice state of $Cu(HCOO)_2 \cdot 4D_2O$ at 4.2K. Figures (a)-(c) show three planes in which the angular dependence of proton nmr is studied. Figures (a')-(c') show the observed motion of the moment $\vec{m}$. Details of the spin direction are given as eqs.(6-11)∿(6-13) of the text.

estimated from the separation of lines. Calculations including smaller terms result in

$$m_x = (0.35\pm0.15)\cos\theta_H ,$$

$$m_y = -(0.89\pm0.05)\sin\theta_H ,$$

$$m_z = -(0.81\pm0.05)\cos\theta_H ,$$

$$m = 0.89\pm0.06 . \qquad (6\text{-}12)$$

The calculated angular dependence of resonance field is shown in Fig. 22(b''). The observed motion of $\vec{m}$ with the field direction(See Fig. 24(b) and (b').) is consistent with a model of tilted g-tensor type weak ferromagnetism. Finite separation between L_1 and the antiferromagnetic axis L_1' for $\vec{H}//b$(See Fig. 24(c').) indicates that the weak ferromagnetism is not entirely tilted g-tensor origin. The magnetization measurement supports the conclusion.

For $\vec{H}$ in the L_3b-plane, components of $\vec{m}$ are estimated as follows. The shift corresponding to the center of lines is approximately given by $0.21m_z\cos\theta_H$. Experimental result is $-0.20\cos\theta_H$. Therefore, we obtain $m_z \simeq -1$. Substituting it into eq.(6-10), one has $-1.0m_y\cos\theta_H+(1.0m_x+0.4)\sin\theta_H$ for the separation of lines. The components m_x and m_y are estimated from the experimental result of separation and the condition that their values for $\theta_H=0°$ must agree with the corresponding values obtained in the bc'-plane. By taking

smaller terms into account, the followings are obtained:

$$m_x = (0.35\pm0.15)\cos\theta_H \ ,$$

$$m_y = -(0.33\pm0.16)\sin\theta_H \ ,$$

$$m_z = -(0.81\pm0.05) \ ,$$

$$m = 0.88\pm0.07 \ . \qquad (6\text{-}13)$$

The calculated result is given in Fig. 22(d')(solid line). Figures 24(c) and (c') represent the relation between $\vec{H}$ and $\vec{m}$.

6.3.3 Intermediate region

(a) ac-plane

The shift of resonance field for proton-1 and 2 is calculated for simplicity by the first term of eq. (6-2). Namely,

$$\Delta H = -(\mp 0.51 m_{1x} + 0.02 m_{1y} \pm 0.25 m_{1z})\sin\theta_H$$
$$-(\pm 0.23 m_{1x} - 0.19 m_{1y} \pm 0.05 m_{1z})\cos\theta_H \ , \qquad (6\text{-}14)^{*)}$$

where θ_H is the angle of $\vec{H}$ from z(See Fig. 25(a).). Vectors $\vec{m}_1 = \langle\vec{S}_1\rangle/S$ and $\vec{m}_3 = \langle\vec{S}_3\rangle/S$ are distinguished because, in the intermediate region, they are neither parallel nor antiparallel. The shifts for proton-3 and 4 are calculated by replacing components of $\vec{m}_1$ in eq. (6-14) by the corresponding components of $\vec{m}_3$.

At first, conclusion of §6.3.1(the low field state) is recollected. They are $m_{1x} = -m_{3x} \simeq 0.5$, $m_{1y} = m_{3y} = 0$, $m_{1z} = -m_{3z} \simeq 0$. For this case, ΔH of proton-4 and 3 are equal to those of 1 and 2 respectively. Neither of separation between 1 and 4 nor between 2 and 3 are observed even in the intermediate region. Therefore, one obtains

$$m_{1x} = -m_{3x} \ , \qquad m_{1y} = m_{3y} \ , \qquad m_{1z} = -m_{3z} \ . \qquad (6\text{-}15)$$

---

*) Elements of $\tilde{d}$ for AR-3 are used for m_{1y} because m_{1y} and m_{3y} are equal as is shown later.

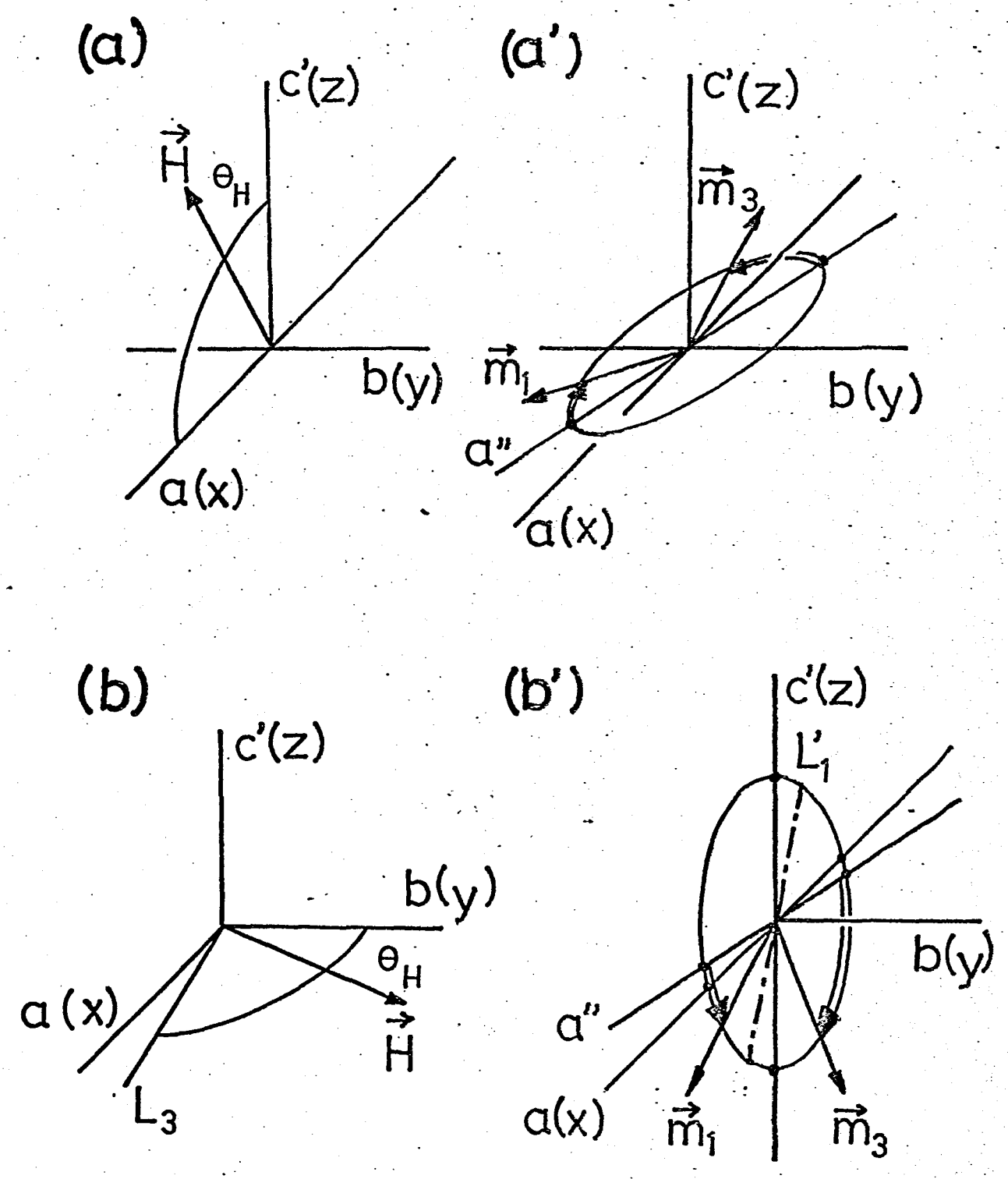

Fig. 25 Relation between the direction of the external field and the spin directions in the intermediate region of $Cu(HCOO)_2 \cdot 4D_2O$ at 4.2K. Figures (a) and (a') correspond to the case where $\vec{H}$ is in the ac-plane. Figures (b) and (b') to the case $\vec{H}$ in the L_3b-plane.

Next, the cross point or zero-separation point of two lines is considered. The condition $\Delta H_{\text{proton-1}} = \Delta H_{\text{proton-2}}$ reduces to the following equation for θ_H:

$$(+0.51m_{1x} - 0.25m_{1z})\sin\theta_H + (-0.23m_{1x} - 0.05m_{1z})\cos\theta_H = 0 \ . \qquad (6\text{-}16)$$

The experimental result shows that the angle of zero separation θ_{H0} (solution of eq. (6-16)) is independent of the resonance field. Accordingly, m_{1z} (and m_{3z}) at θ_{H0} is much smaller than m_{1x} (and m_{3x}) even in the intermediate region. Hereafter, contributions of m_{1z} (and m_{3z}) are neglected for all θ_H. Then, eq. (6-14) reduces to

$$\Delta H = (\pm 0.51m_{1x} - 0.02m_{1y})\sin\theta_H + (\mp 0.23m_{1x} + 0.19m_{1y})\cos\theta_H \ . \qquad (6\text{-}17)$$

The shift corresponding to the center of lines and the separation between them are proportional to m_{1y} and m_{1x}, respectively. For $\vec{H}$ close to c', the center moves to the low field side and the separation decreases. These facts indicate that, by applying the external magnetic field, a negative value of m_{1y} (and m_{3y}) is introduced and m_{1x} decreases from the initial value as is shown schematically in Fig. 25(a'). The spin motion is consistent with the prediction of the theory. The components m_{1x} and m_{1y} are estimated quantitatively in three typical cases. The result is given in Fig. 26. The increase of the y-component and the decrease of the x-component are both attributable to the weak ferromagnetism whose preferred axis of ferromagnetic moment is the L_1-axis.

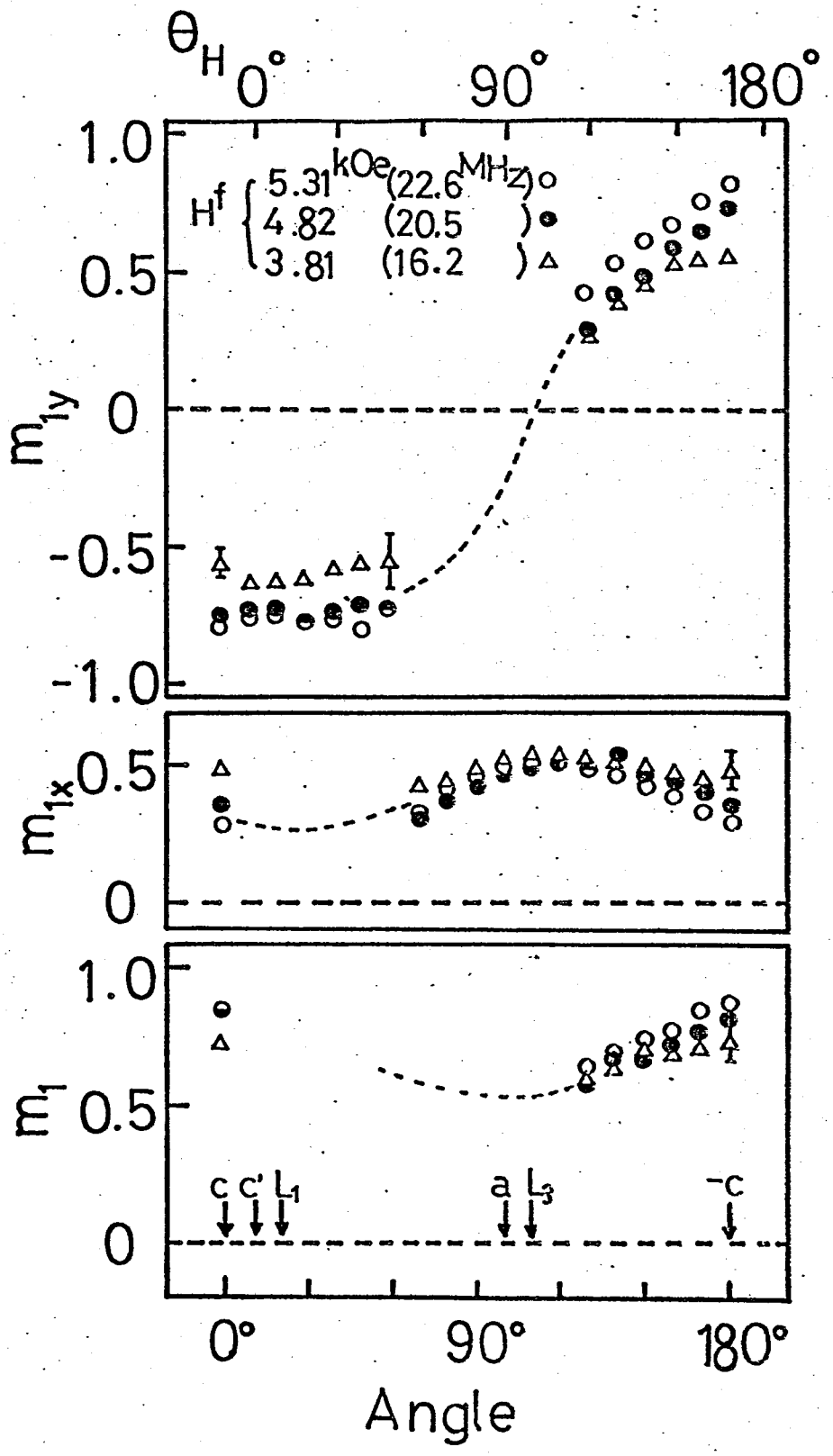

Fig. 26 Dependence of m_{1x}, m_{1y} and m on the field direction and the field intensity for three typical intermediate frequencies in the ac-plane.

(b) L_3b-plane

The shift of proton-1, 2 is given by

$$\Delta H = -(\mp 0.54 m_{1x} + 0.05 m_{1y} \pm 0.19 m_{1z}) \sin\theta_H$$
$$-(0.02 m_{1x} \pm 0.48 m_{1y} - 0.21 m_{1z}) \cos\theta_H \ , \qquad (6\text{-}18)$$

where θ_H is the angle of $\vec{H}$ from b. First, separation of two lines is considered near the b-axis. The separation is given by $2 \times 0.48 m_{1y}$. The experimental result(For example, see the result at 15.8MHz.) indicates that m_{1y} is nearly zero. As it is also zero at zero external field, $m_{1y} = m_{3y} = 0$ is assumed in the followings.

Next, the center of two lines is considered in a region close to b. For this case, the center is given by $0.21 m_{1z}$. The experimental result indicates that both m_{1z} and m_{3z} are negative. On the other hand, considering the factor of $\sin\theta_H$, one sees that a small separation pair($m_x < 0$) corresponds to proton-3, 4. Large separation pair($m_x > 0$) corresponds to proton-1, 2. Symmetry of nmr pattern indicates that the spin motion is caused by the weak ferromagnetism whose preferred axis of ferromagnetic moment is the b-axis. The spin motion is shown schematically in Fig. 25(b').

The components m_{1x}, m_{3x}, m_{1z} and m_{3z} are estimated quantitatively from the shift of the center and the separation. The absolute value m is also calculated. The results are similar to those obtained in the ac-plane.

An interesting phenomenon is observed when the results at 31.5MHz and 59.6MHz are compared. Namely, increasing the magnetic field, we can observe

jump of $\vec{m}_3$ to the position of $\vec{m}_1$. The observation is a little inconsistent with our previous simple theory,[29] because the jumping spin is $\vec{m}_1$ in the theory and $\vec{m}_3$ in the experiment. The disagreement disappears if one introduces small DM-interaction as is shown in §3.*)

---

*) In the previous theory,[29] only the g-tilting is considered as the mechanism of the weak ferromagnetism so that we obtain $g_{XY}^{**} = g_{XY}^{*}$ and $g_{ZX}^{**} = g_{ZX}^{*}$. In this paper, the DM-interaction is also taken into account and we obtain $g_{XY}^{**} \simeq g_{XY}^{*}$ and $g_{ZX}^{**} \simeq -g_{ZX}^{*}$ for CuFTH.

6.3.5 On the assumption of the pure dipole field

Now at the end of this subsection, the assumption of proton position and pure dipole field should be re-examined because the conclusions on the magnitude of $\vec{m}$ seem to be unfamiliar. If one modifies certain elements of $\tilde{d}$ by 30%,*) the calculated magnitude m changes to 0.75S(result of spin wave calculation) independent of the external field. The modification is done so as to keep the conclusions of magnetic cell and spin direction because they are determined mostly from the symmetry of nmr spectra and are consistent with the result of other experiments. Therefore, the value of m depends completely on the assumptions and may be less reliable than the magnetic cell, the spin direction and the phase boundary.

---

*) Also see Appendix G. Tensor elements of the paraelectric and the antiferroelectric states of CuFTH are compared there.

6.4 Comparison with the result of magnetization measurement

In this subsection, the proton nmr results of CuFTD are examined by using the magnetic parameters estimated from the analysis of the magnetization process of CuFTH.

6.4.1 Frequency dependence of the shift

The frequency dependence of the shift given in Fig. 23(a)-(c) is compared with the calculated shift. A small contribution from the weak ferromagnetic component is neglected for simplicity.

(a) $\vec{H}//L_3$

The L_3 direction is characterized by the fact that the weak ferromagnetism does not act along this direction. The angle between L_3 and the easy axis a" is 17.9°. Therefore, the magnetization curve should be a "rounded spin-flop" type curve which is seen in an ordinary antiferromagnet when the external field is applied close but not strictly parallel to the easy axis.[39] The magnetization curve for L_3 indicates that the spin flop starts gradually above about 14kOe so that the nmr shift is calculated by neglecting the spin motion. The result for $m \equiv \langle S \rangle / S = 0.5$ is shown in Fig. 23(b). The correspondence between calculations and experiments is good.

(b) $\vec{H}//L_1$

As the field direction is not strictly perpendicular to the easy axis, the spin motion may be influenced, in principle, by the difference between the parallel and perpendicular susceptibilities. However, this contribution is dropped out in calculating the spin motion, because it is practically negligible as is seen from the good linearlity of the magnetization curve. Then, the spin direction is given by the equation

$$\sin\theta = H/H_{BL1} \quad , \tag{6-19}$$

where θ is an angle between $\vec{m}_1$ and the easy direction a". The effective bending field for L_1, H_{BL1}, is 5.3 kOe. $\vec{m}_1$ rotates to the -b-axis, because g_{XY}** is negative(See foot note.*)). The calculated curves in Fig. 23(a) correspond to m = 0.5(dotted lines) and m = 1.0(solid lines). The experimental results are between them.

(c) $\vec{H}//B$

We consider the spin motion by assuming that the component of $\vec{H}$ along the b-axis determines the spin direction. Negative g_{XY}* and positive g_{ZX}* are used because of the following reasons: (1) If g_{XY}* is positive, the angular dependence in the high field region can not be reproduced(The shift

---

*) If it is positive one obtains $\Delta H > 0$ for the high field region, which conflicts with the experimental results.

along b becomes positive.). (2) If g_{ZX}^* is negative the resonance points arising from proton-1 and 2 disappear and those from 3 and 4 remain, which contradicts the experiments. The resulting shift is shown in Fig. 23(c). The change of m mentioned in the preceding section also appears here. Characteristics of the calculated curve agree with those of the experimental results except for the unnatural change of m.

6.4.2 Angular dependence in the high field region

(a) ac-plane

As the interpretations in the preceding section agree with the theoretical predictions(Put H_X=0 in (3-85a) ∿ (3-85c) and compare them with (6-11).), we would not repeat here.

(b) bc'-plane

The spin motion is given in eqs. (3-89a) ∿ (3-89c). By using the parameters obtained in the analysis of the magnetization curve, the vector components L, M and N are obtained as

$$L = -0.52\sin\omega/G' \qquad (6\text{-}20a)$$

$$M = -0.59\cos\omega/G' \qquad (6\text{-}20b)$$

$$N = 0.12\cos\omega/G' \ , \qquad (6\text{-}20c)$$

where G' is given by the relation:

$$G' = (0.27\sin^2\omega + 0.36\cos^2\omega)^{\frac{1}{2}} . \qquad (6\text{-}21)$$

When m is assumed to be 1.0,*) m_x, m_y and m_z are written as

$$m_x = 0.21\cos\omega/G' , \qquad (6\text{-}22a)$$

$$m_y = -0.52\sin\omega/G' , \qquad (6\text{-}22b)$$

$$m_z = -0.57\cos\omega/G' . \qquad (6\text{-}22c)$$

These results agree well with the spin motion suggested previously(See eq. (6-12).). The calculated resonance points for m = 1.0 is given in Fig. 22(b'') (dotted lines). If one assumes that the weak ferromagnetism is mainly due to the DM-mechanism, the calculated shift is, as is shown in Fig. 22(b'') with broken lines, completely different from the experimental result.

(c) L_3b-plane

For this case the vector (L,M,N) is given by

$$L = 0.0018\tan\omega , \qquad (6\text{-}23a)$$

$$M = -0.98 , \qquad (6\text{-}23b)$$

$$N = 0.20 , \qquad (6\text{-}23c)$$

---

*) The nmr shift is proportional to m practically.

where the contribution of L to G' is neglected so that ω should be limited within 80°. The vector $\vec{m}$ is given, for m = 1.0, by

$$m_x = 0.34$$

$$m_y = 0.0018\tan\omega$$

$$m_z = -0.94 \quad . \tag{6-24}$$

These results are close to the spin motion obtained for CuFTD when the field direction is not far from the b-axis. The calculated resonance points are shown in Fig. 22(d')(dotted lines). The discrepancy near the L_3 axis seems to indicate that the neglection of the anisotropy for obtaining eqs. (3-89a) ∿ (3-89c) are unreasonable when $\vec{H}$ is close to L_3 where the torque due to the weak ferromagnetism becomes ineffective.

§ 7. The case of $Cu(HCOO)_2 \cdot 2(NH_2)_2CO \cdot 2H_2O$[38]

Copper formate bisurea dihydrate(CuFUH or UH) crystal contains Cu^{2+} layers quite similar to the layers appearing in copper formate tetrahydrate (CuFTH or TH) crystal.[18] While the intralayer exchanges of two crystals seem to be equal within the experimental error,[17] the interlayer magnetic coupling of UH is expected to be smaller than that of TH, because the interlayer spacing of UH is larger by about 30% than that of TH(See Fig. 27.) As the interlayer coupling is one of the important parameters of the nearly two-dimensional magnetic system,[1] the relation between the magnetic properties of UH and those of TH is interesting.

Results of the susceptibility and the specific heat measurements for two crystals are quite similar.[7,17] In this case one has two possibilities; (1) The interlayer couplings of these crystals are nearly equal or (2) Néel temperature T_N is not sensitive to the interlayer coupling. In connection with this problem, the jump of the magnetization is studied in UH and the result is compared with that of TH because the jumping field is a good measure of the interlayer coupling.*)

Experiments were made at 4.2K in three crystal planes L_1L_3, L_2L_3 and $L_{1Z}'L_2$. The direction L_{1Z}'(See Fig. 29.) is close to the L_{1Z}-axis which gives the largest g-value for the paramagnetic resonance at room temperature($g(L_{1Z})=2.37$, $g(L_2)=2.11$, $g(L_{3Z})=2.08$, angle$(a,L_{1Z})=4.9°$, angle$(L_{1Z},c)=91.5°$, angle$(a,L_{1Z}')=14°$, angle$(c,L_{1Z}')=82°$). Figure 28

---

*) Throughout the present paper, we assume that the magnetic properties of two kinds of crystals are similar.

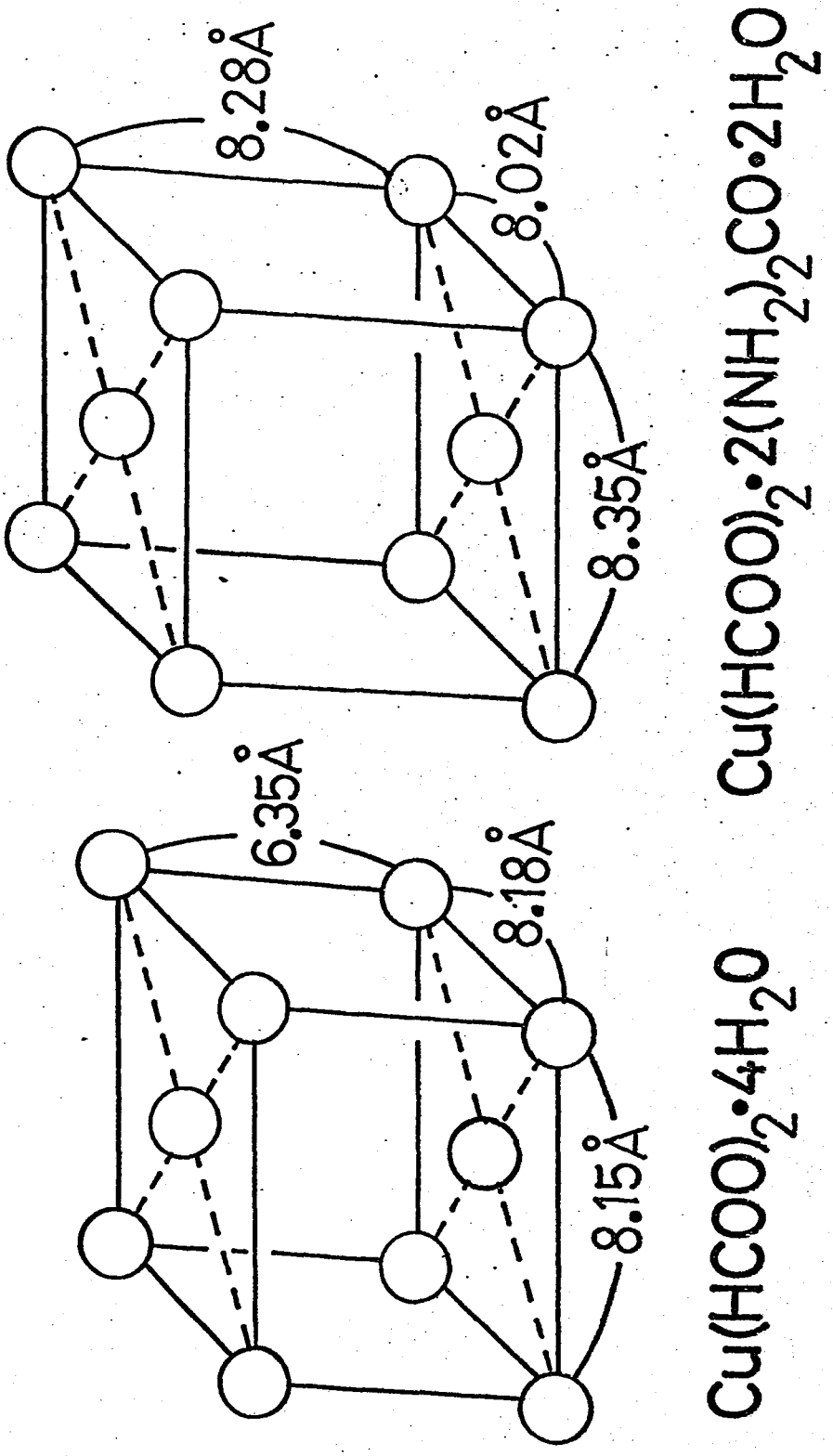

Fig. 27 Cell dimensions of $Cu(HCOO)_2 \cdot 4H_2O$ and $Cu(HCOO)_2 \cdot 2(NH_2)_2CO \cdot 2H_2O$.

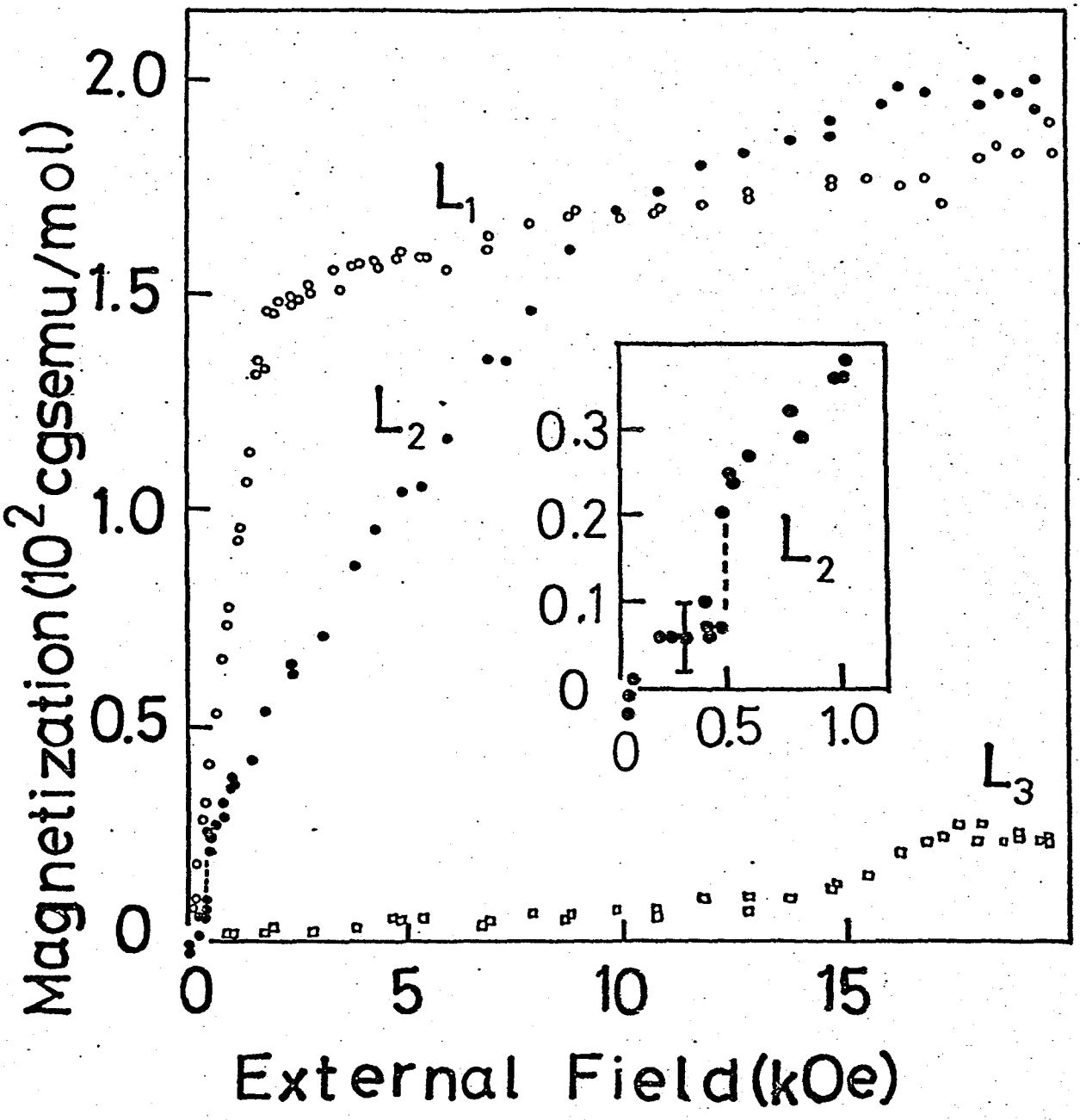

Fig. 28 Magnetization curves for a single crystal of $Cu(HCOO)_2 \cdot 2(NH_2)_2CO \cdot 2H_2O$ at 4.2K. The insert is the magnetization curve around the jump for $\vec{H}//L_2$. The results for other field directions are given in Appendix H.

represents the magnetization curves for three typical directions. Hysteresis is not observed within the experimental error. The anisotropy of g-tensor and the anisotropic intralayer exchanges are not substantially different from those of TH(See foot note.*). On the contrary, the jumping field for $\vec{H}//L_2$ (480 Oe) is much lower than the corresponding field(5.3kOe) of TH. This problem is discussed in the next parapraph. Figure 29 shows the outline of the 4-sublattice 2-sublattice phase boundary determined in L_1L_2, L_2L_3, $L_1'L_2$-planes by using the bend and the jump of the magnetization curve.

A preliminary analysis of the jump is done by starting from eq. (3-80). When $h_{ex} \ll H_{K+}^*$, the jumping field H_J is given by

$$H_J = 2h_{ex}/g_{ZX}^* \ . \tag{7-1}$$

The jump of the magnetization ΔM is given by

$$\Delta M(\text{per ion}) = \mu_B g_{ZX}^*/2 \ , \tag{7-2}$$

where the spin contraction effect is neglected for simplicity. Combining eqs. (7-1) and (7-2), we have

$$h_{ex} = H_J \Delta M/\mu_B \ . \tag{7-3}$$

---

*) In TH, $|g_{XY}^*| = 0.06$, $|g_{ZX}^*/g_{XY}^*| = 0.02$, $H_{K-}^* = 60$ Oe, $H_{K+}^* = 220$ Oe. In UH, they are estimated to be about 0.06, 0.01, 50 Oe and 300 Oe, respectively. Detailed analysis is in progress.

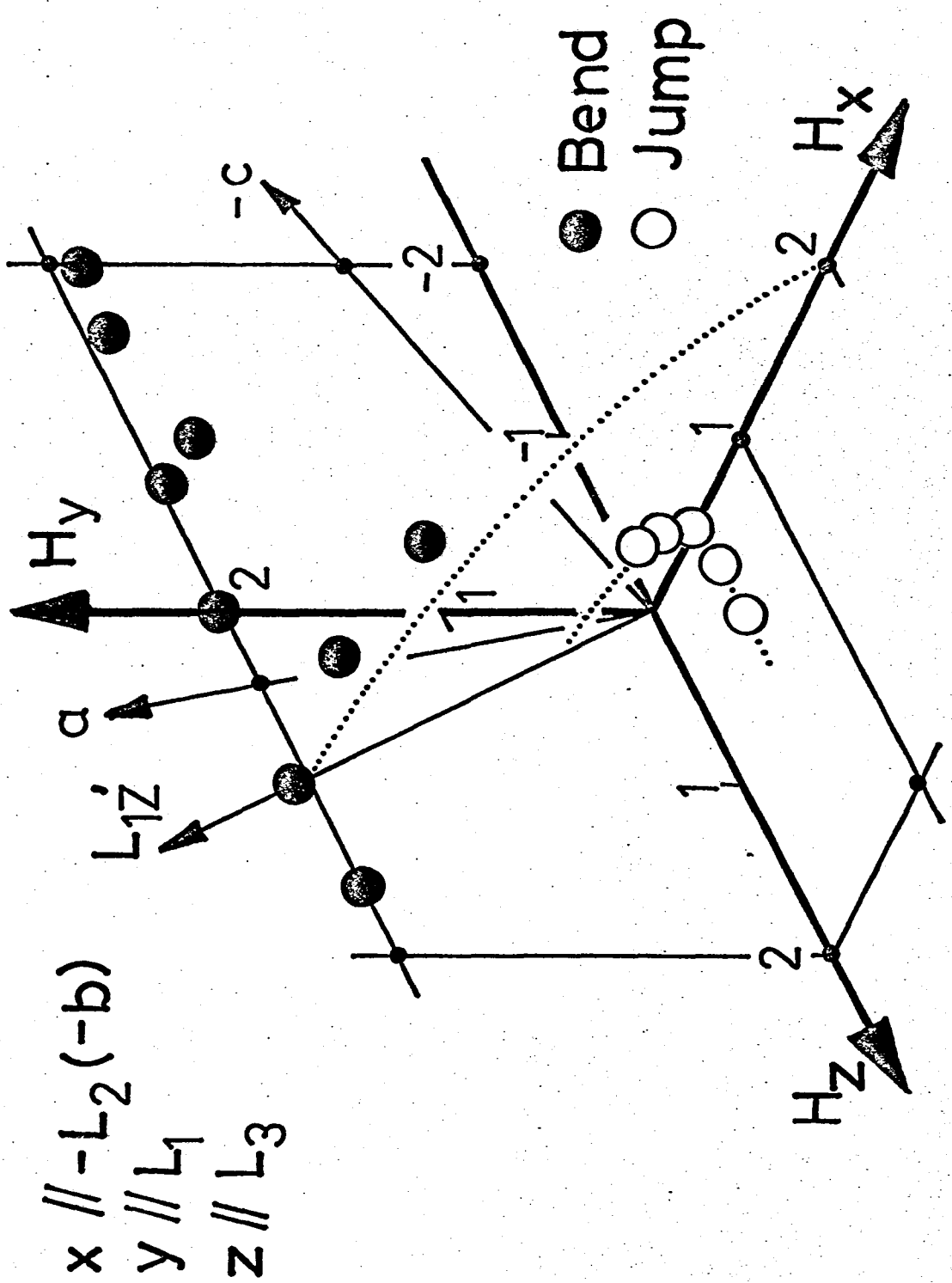

Fig. 29 Phase boundary of $Cu(HCOO)_2 \cdot 2(NH_2)_2CO \cdot 2H_2O$ at 4.2K.

h_{ex} of UH and TH are calculated to be 1.7 Oe and 33 Oe, respectively. These results indicate that the assumption of weak interlayer coupling($h_{ex} \ll H_{K+}^*$) is true for the case of UH but is not for the case of TH($H_{K+}^* = 220$ Oe). The result of the numerical calculation,[29] however, shows that eq. (7-3) works even in the case of TH within 20% error. Therefore, the interlayer coupling of UH is about 1/20 of that in TH. In conclusion, one sees that T_N is not sensitive to the interlayer coupling while the entropy change around T_N seems to be influenced by the coupling.[17] It should be noticed that the ratio of the interlayer coupling to the intralayer exchange is of the order of 10^{-6} in UH.

§ 8. Discussions

8.1 AFMR in the 2-sublattice region

Seehra and Castner(SC)[16] tried to fit their AFMR data(open circles in Fig. 30) on the basis of the 2-sublattice model and estimated some parameters mostly at low field region. However, we conclude in §5 and §6 that the magnetic structure at low field region is not the 2-sublattice type but the structure above about 5kOe for $\vec{H}//X$ and Y is the 2-sublattice type. In this subsection we treat the interpretation of the AFMR results in the 2-sublattice region. The AFMR frequencies are assumed to have the same expressions as those of the pure 2-sublattice case, because AFMR theory applicable to the present 4-sublattice system is not known yet. This assumption may be an over simplification for the present case.

The expressions of the AFMR frequencies for the 2-sublattice case have been obtained by SC. For $\vec{H}//Y(c'')$ the frequencies are given by

$$(\omega_+/\gamma)^2 \simeq H_{//b}{}^2 + H_{Y,red}{}^2 + (H_{Y,red}H_{DM}' - H_{//c}{}^2) , \tag{8-1}$$

$$(\omega_-/\gamma)^2 \simeq H_{Y,red}H_{DM}' - H_{//c}{}^2 , \tag{8-2}$$

where zero-field AFMR frequencies $H_{//b}{}^2$, $H_{//c}{}^2$ and reduced field $H_{Y,red}$ are written as

$$H_{//b}{}^2 \simeq (2H_{ex} + H_{K+})H_{K+} + h_{DM}{}^2 - H_{DM}{}^2 , \tag{8-3}$$

$$H_{//c}{}^2 \simeq (2H_{ex} + H_{K-})H_{K-} - H_{DM}{}^2 , \tag{8-4}$$

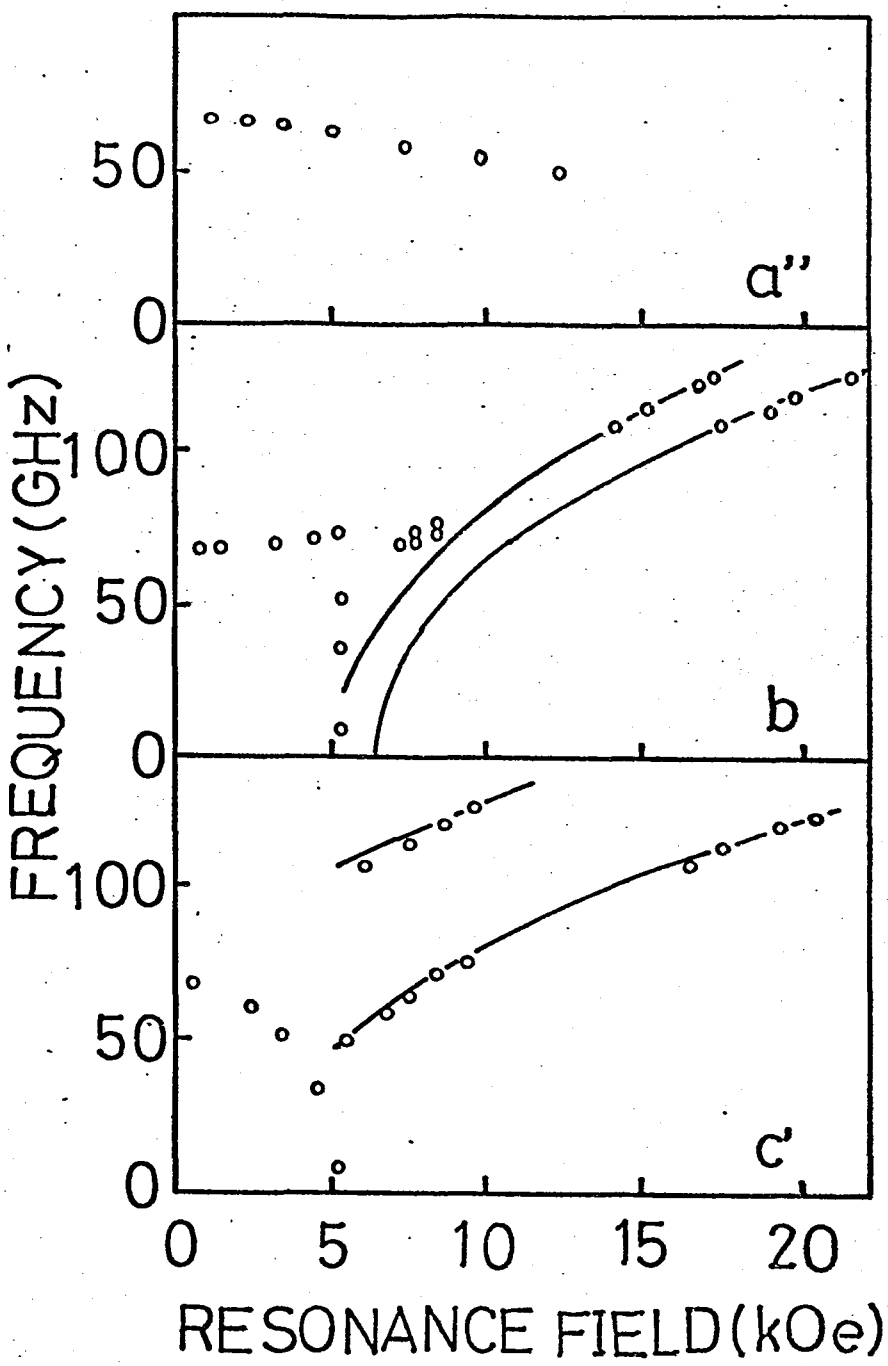

Fig. 30 The experimental AFMR frequency-field diagram by Seehra and Castner and the calculated one based on the 2-sublattice model in the high field region.

$$H_{Y,\,red} = \frac{1}{2} g_{ZZ} H_Y \ . \tag{8-5}$$

New notation $H_{Y,red}$ is used instead of SC's H_Y and, in this paper, H_Y is used for the Y-component of the external field $\vec{H}$. The effective canting field H_{DM}' is written as follows:

$$H_{DM}' \simeq H_{DM} + 2H_{ex}(g_{XY}'/g_{YY}) \ , \tag{8-6}$$

where

$$g_{XY}' = g_{XY}\cos\alpha - g_{YZ}\sin\alpha \tag{8-7}$$

and the initial canting angle α is given by

$$\tan 2\alpha = 2h_{DM}/(2H_{ex} + H_{K+}) \ . \tag{8-8}^{*)}$$

For $\vec{H}//X(b)$ the AFMR frequencies are written as

$$(\omega_+/\gamma)^2 = H_{//c}^{\ 2} - H_{//b}^{\ 2}\sin\theta \ + H_{X,red}H_{DM}^* + H_{X,red}^{\ 2} \ , \tag{8-9}$$

$$(\omega_-/\gamma)^2 = H_{//b}^{\ 2}(1-2\sin^2\theta) + H_{X,red}H_{DM}^* \ . \tag{8-10}$$

The reduced field $H_{X,red}$ and the effective canting field H_{DM}^* are given by

$$H_{X,red} = \frac{1}{2} g_{XX} H \tag{8-11}$$

$$H_{DM}^* = H_{DM}''\sin\theta + h_{DM}'\cos\theta \ , \tag{8-12}$$

where θ, the angle between the antiferromagnetic axis and the a''-axis (See Fig. 31(a).), is a solution of the equation,

---

*) This equation can be simplified as $\alpha = h_{DM}/2H_{ex}$ because h_{DM} and H_{K+} are much smaller than H_{ex}. An equivalent relation can be readily obtained from eq. (3-18a) by making N=1 and $L=M=H_X=H_Y=H_Z=0$.

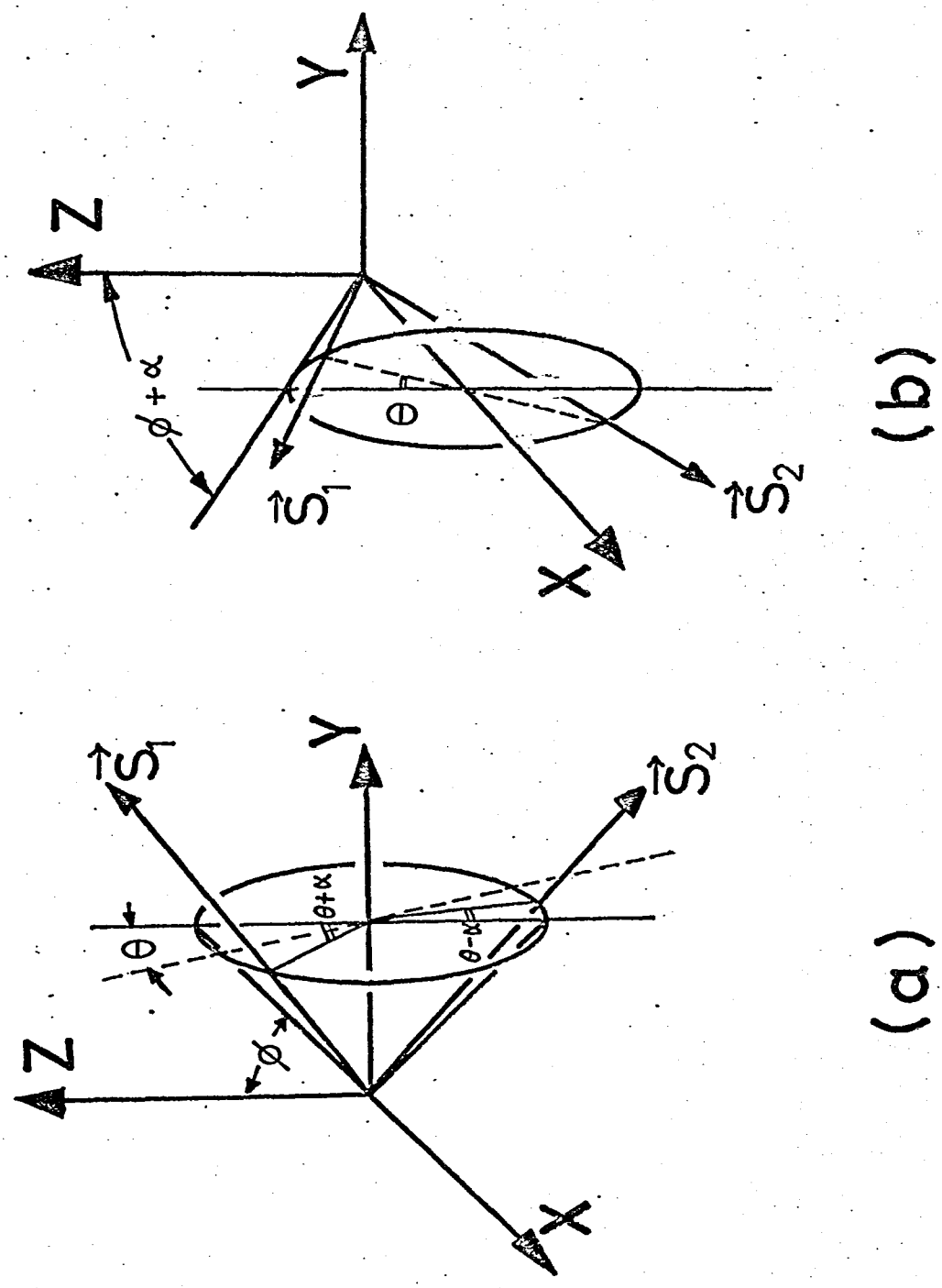

Fig. 31 Definition of the angles appearing in the analysis of the AFMR. (a) Definition for $\vec{H}$//Y. (b) Definition for $\vec{H}$//X. For details see text.

$$\sin\theta + H_{X,red}h_{DM}'\tan\theta/H_{//b}^{2} = H_{X,red}H_{DM}''/H_{//b}^{2} \quad . \tag{8-13}$$

The quantities H_{DM}'' and h_{DM}' are given by the relations:

$$H_{DM}'' = -H_{DM} + 2H_{ex}(g_{XY}/g_{XX}) \quad , \tag{8-14}$$

$$h_{DM}' = h_{DM} + 2H_{ex}(g_{ZX}/g_{XX}) \quad . \tag{8-15}$$

Equations (8-1) and (8-2) are transformed into

$$(\omega_{+}/\gamma)^{2} = H_{//b}^{2} + H_{Y,red}^{2} + \frac{1}{2}g_{YY}(H_{Y} - H_{o})H_{DM}' \quad , \tag{8-16}$$

$$(\omega_{-}/\gamma)^{2} = \frac{1}{2}g_{YY}(H_{Y} - H_{o})H_{DM}' \quad , \tag{8-17}$$

by using H_{o} defined as

$$H_{o} = H_{//c}^{2}/(\tfrac{1}{2}g_{YY}H_{DM}') \quad . \tag{8-18}$$

In addition to the above results obtained by SC, we introduce θ_{o}, the high field limit of θ, given by

$$\tan\theta_{o} = H_{DM}''/h_{DM}' \tag{8-19}$$

and $H_{DM,0}^{*}$ as

$$H_{DM,0}^{*} \equiv (H_{DM}^{*})_{\theta=\theta_{o}} \quad . \tag{8-20}$$

The experimental results for $\vec{H}//Y$ are considered first. Equations (8-16) and (8-17) indicate that ω_{+} corresponds to the observed high frequency branch. By using the experimental data for ω_{-}, H_{DM}' and $H_{//c}^{2}$ are determined

as follows:

$$H_{//c}{}^2 = (3.0 \pm 0.3) \times 10^8 \text{ Oe}^2 , \tag{8-21}$$

$$H_{DM'} = (9.4 \pm 0.3) \times 10^4 \text{ Oe} . \tag{8-22}$$

$H_{//c}$ is given by

$$H_{//c} = (1.73 \pm 0.06) \times 10^4 \text{ Oe} . \tag{8-23}$$

By using the above values of $H_{//c}{}^2$ and $H_{DM'}$, $H_{//b}{}^2$ is estimated from the data of ω_+ as

$$H_{//b}{}^2 = (11.0 \pm 0.4) \times 10^8 \text{ Oe}^2 . \tag{8-24}$$

$H_{//b}$ is given by

$$H_{//b} = (3.32 \pm 0.07) \times 10^4 \text{ Oe} . \tag{8-25}$$

The calculated frequencies and the experimental results are compared in Fig. 30.

The case $\vec{H}//X$ is considered next. The angle θ tends to θ_o of eq. (8-19) as the weak ferromagnetic moment approaches the saturation value. Then, $(\omega_+/\gamma)^2 - H_{X,red}{}^2$ and $(\omega_-/\gamma)^2$ plotted as a function of $H_{X,red}$ should be a pair of parallel lines. By using the experimental data by SC, we obtain the parallel lines above about 14 kOe when the high frequency branch is assigned to the ω_+-mode. Using $H_{//c}{}^2$, $H_{//b}{}^2$ of eqs. (8-21), (8-24) and the experimental result of the present case, we have

$$\sin^2\theta_o = 0.89 \pm 0.02 \ . \tag{8-26a}$$

Namely, θ_o is given by

$$\sin\theta_o = 0.94 \pm 0.01 \quad \text{or} \quad \theta_o = (71 \pm 3)^\circ \ . \tag{8-26b}$$

$H_{DM,0}^*$ is estimated, from the slope of two lines mentioned above, as

$$H_{DM,0}^* = (12.9 \pm 0.5) \times 10^4 \text{ Oe} \ . \tag{8-26c}$$

The calculated and the experimental results are compared in Fig. 30. θ_o is used instead of θ throughout the calculation. The experimental results at about 8.5 kOe can be fitted by taking θ as about 60°.

The angle θ_o satisfies the relation

$$H_{DM}'' = H_{DM,0}^* \sin\theta_o \ . \tag{8-27}$$

By using this relation, H_{DM}'' is estimated as

$$H_{DM}'' \equiv -H_{DM} + 2H_{ex}(g_{XY}/g_{XX}) = (12.1 \pm 0.5) \times 10^4 \text{ Oe} \ . \tag{8-28}$$

We recall that H_{DM}' is obtained as eq. (8-22),

$$H_{DM}' \equiv +H_{DM} + 2H_{ex}(g_{XY}/g_{XX}) = (9.4 \pm 0.3) \times 10^4 \text{ Oe} \ . \tag{8-29}$$

From eq. (8-19), h_{DM}' is determined as

$$h_{DM}' \equiv h_{DM} + 2H_{ex}(g_{ZX}/g_{XX}) = (4.2 \pm 0.2) \times 10^4 \text{ Oe} \ . \tag{8-30}$$

Summary of these results is given in Table V. The quantities $H_{//c}^2$, $H_{//b}^2$, H_{DM}', H_{DM}'' are all larger by 50% than the corresponding values

Table V Magnetic parameters of $Cu(HCOO)_2 \cdot 4H_2O$ determined from the analysis of the antiferromagnetic resonance in the high-field 2-sublattice state.

	Parameters estimated from the AFMR results	Parameters estimated from the magnetization curve and the proton nmr(§)
$H_{//c}^2$	3.0×10^8 Oe^2	1.81×10^8 Oe^2
($H_{//c}$	1.73×10^4 Oe)	(1.35×10^4 Oe)
$H_{//b}^2$	11.0×10^8 Oe^2	6.6×10^8 Oe^2
($H_{//b}$	3.32×10^4 Oe)	(2.57×10^4 Oe)
H_{DM}'	9.4×10^4 Oe	6.5×10^4 Oe
H_{DM}''	12.1×10^4 Oe	8.5×10^4 Oe
h_{DM}'	4.2×10^4 Oe	1.7×10^4 Oe
θ_o	71°	79°, 76°(§)

calculated from the magnetization data. h_{DM}' is larger by 140%.

8.2 Intra- and interlayer dipole-dipole couplings

In the followings, the effect of the intra- and interlayer diploe-dipole couplings which are not included in the hamiltonian is considered qualitatively. The dipole tensor in unit of Oe, μ_B times of the usual dipole tensor, is given for Cu-1 in Table VI. For estimating the dipole field precisely, the product of the tensor and $\frac{1}{2}\tilde{g}$ should be calculated, but, for simplicity, the latter factor is replaced here by unity. The dipole-dipole coupling energy is estimated from the negative of the product of the dipole field and $1\mu_B$ whose direction is parallel to the spin of Cu-1.

First, it is noticed that the dipole-dipole coupling between Cu-1 and 2 is already implicitly included in K-, K'- and A-terms of the hamiltonian. Next, the coupling between a Cu-1 and "other Cu-1" is considered. This causes the one-ion type anisotropy which is not included in the hamiltonian. However, calculations based on an approximate method similar to that in §3 show that the contribution of the one-ion anisotropy fields to the magnetization process can be taken into account merely by modifying the magnitudes of the exchange-type anisotropy fields. The framework of the present paper seems to be kept unchanged by the existence of these two intralayer terms.

In considering the dipole fields arising from "Cu-3" and "Cu-4", we assume that the 3 and 4 moments are antiparallel. This is consistent with the approximations in §3. Then, the interlayer dipole tensor which represents the sum of the dipole fields from antiparallel 3 and 4 spins is given by

$$D_{ij}(\text{interlayer}) = D_{ij}(\text{all Cu-3}) - D_{ij}(\text{all Cu-4}) \ , \qquad (8\text{-}30)$$

Table VI Elements of the dipole tensor $\tilde{D}$ related to the dipole field acting on a Cu-1 ion from other ions. For example, D_{xy} of "all Cu-2" row represents the x-component of the dipole field arising from the moments of $1\mu_B$ parallel to the y-direction placed on all Cu-2 ions. The dipole sum is calculated for a sphere of 100Å in diameter.

$Cu(HCOO)_2 \cdot 4H_2O$						
	D_{xx}	D_{yy}	D_{zz}	D_{xy}, D_{yx}	D_{yz}, D_{zy}	D_{zx}, D_{xz}
other Cu-1	Oe 29.2	Oe 30.5	Oe - 59.7	Oe 0	Oe 0	Oe - 0.3
all Cu-2	94.8	93.0	-187.8	0	0	0.2
all Cu-3	-62.1	-72.1	134.2	0	0	-23.8
all Cu-4	-35.8	-27.4	63.2	0	0	13.1

$Cu(HCOO)_2 \cdot 2(NH_2)_2CO \cdot 2H_2O$						
	D_{xx}	D_{yy}	D_{zz}	D_{xy}, D_{yx}	D_{yz}, D_{zy}	D_{zx}, D_{xz}
other Cu-1	Oe 47.2	Oe 35.6	Oe - 82.8	Oe 0	Oe 0	Oe - 0.2
all Cu-2	95.2	114.3	-209.4	0	0	0.0
all Cu-3	-39.5	-40.9	80.4	0	0	- 3.3
all Cu-4	-32.5	-30.6	63.1	0	0	2.5

where i and j stand for x, y and z.

In the case of CuFTH, the dipole tensor referred to the ZXY(a"bc")-coordinate system is convenient compared with that referred to the xyz(abc') system. By using the angle between two systems, 8.5°, the tensor is transformed into

$$D(\text{interlayer, CuFTH}) = \begin{array}{c} \begin{matrix} Z & X & Y \end{matrix} \\ \begin{pmatrix} -35.0 & 0 & -21.1 \\ 0 & -44.7 & 0 \\ -21.1 & 0 & +79.7 \end{pmatrix} \end{array} . \qquad (8\text{-}31)$$

For $\vec{H}//Y$ and Z, two fictitious spins move in the ZX-plane. Considering the tensor elements($D_{ZZ} \simeq D_{XX}$), we conclude that, for this case, the role of the dipole-dipole coupling is nearly equal to that of the isotropic antiferromagnetic interaction.

For $\vec{H}//X$, the motion of the spins is considered in the YZ-plane. The anisotropy of the dipole-dipole coupling in this plane cannot be reduced to any of the terms treated in §3. However, this term seems to work like the intralayer anisotropy throughout the magnetization process except the magnetization jump which is subtly correlated to the interlayer coupling. Therefore, hereafter, we consider the magnetization jump. The interlayer dipole-dipole coupling can be taken into account by replacing

$$h_{ex}(\mathbb{M}\mathbb{M}' + NN') \equiv E_{inter} \qquad (8\text{-}32a)$$

of eq. (3-80) by

$$h_{ex}(MM' + NN') - D_{YY}MM' - D_{ZZ}NN'$$

$$- D_{YZ}(MN' + M'N) \equiv E'_{inter} \quad . \tag{8-32b}$$

The changes of these interlayer energies at the transition from the 4-sublattice state:

$$N \simeq -N' \equiv N_0 \simeq 1 \quad , \qquad M \simeq M' \equiv M_0 \quad , \tag{8-33a}$$

to the 2-sublattice state:

$$N = N' \simeq N_0 \quad , \qquad M = M' \simeq M_0 \tag{8-33b}$$

are given by

$$\Delta E_{inter} = 2h_{ex} \tag{8-34a}$$

and

$$\Delta E'_{inter} = 2(h_{ex} - D_{ZZ} - D_{YZ}M_0) \quad , \tag{8-34b}$$

respectively. Therefore, h_{ex} obtained in §5 should be interpreted to $h_{ex}-D_{ZZ}-D_{YZ}M_0$. The first two terms, the exchange and the diagonal dipole-dipole terms, constitute the interlayer coupling at zero external field. The last term is estimated to be about -10 Oe, because D_{YZ} and M_0 are -21.1 Oe and about -0.5, respectively. Its absolute value is considerably smaller than the sum of the first two terms estimated to be about 50 Oe. In conclusion, essentials of the mechanism of the magnetization jump are not changed by the existence of the dipole-dipole coupling except for the

interpretation of h_{ex} to $h_{ex}-D_{ZZ}$.

In the case of CuFUH, the last term is estimated as follows: first, D_{YZ} is calculated by

$$D_{YZ} = \frac{1}{2}(-D_{xx} + D_{zz})\sin 2\phi + D_{zx}\cos 2\phi \quad , \tag{8-35}$$

where ϕ(unknown) is an angle between the easy axis in the ac-plane and the a-axis. D_{xx}, D_{zz} and D_{zx} are estimated from Table VI to be -7.0 Oe, +17.3 Oe and -5.8 Oe, respectively. Equation (8-35) indicates that $|D_{YZ}|$ never exceeds

$$[\{\frac{1}{2}(-D_{xx} + D_{zz})\}^2 + D_{zx}{}^2]^{\frac{1}{2}} \simeq 13 \text{ Oe} \quad . \tag{8-36}$$

Next, $|M_0|$ is estimated from the magnetization curve to be about 1/16. Then we have

$$|D_{YZ}M_0| < 0.8 \text{ Oe} \quad . \tag{8-37}$$

In conclusion, the interlayer coupling $h_{ex}-D_{ZZ}$ is estimated to be 1.7 ± 0.8 Oe.

References

1) L. J. de Jongh and A. R. Miedema: Experiments on Simple Magnetic Model Systems(Taylor and Francis Ltd., London, 1974).

2) H. Kobayashi and T. Haseda: J. Phys. Soc. Japan 18(1963) 541.

3) R. Kiriyama, H. Ibamoto and K. Matsuo: Acta cryst. 7(1954) 482.

4) J. Itoh and Y. Kamiya: J. Phys. Soc. Japan 17(1962) Suppl. B-I 512.

5) R. L. Martin and H. Waterman: J. Chem. Soc.(London) 1959(1959) 1359.

6) Y. Yamamoto, M. Matsuura and T. Haseda: J. Phys. Soc. Japan 38(1975) 1776.

7) M. Matsuura, Y. Yamamoto, H. Yamakawa, T. Haseda and Y. Ajiro: Proc. Int. Conf. Magnetism, Amsterdam, 1977, p. 680.

8) Y. Morimoto and M. Date: J. Phys. Soc. Japan 29(1970) 1093.

9) K. Nagata: J. Phys. Soc. Japan 40(1976) 1209.

10) Y. Ajiro and N. Terata: Proc. 12 Intern. Conf. Low Temperature Physics, Kyoto, 1970, p. 813.

11) Y. Ajiro, K. Enomoto, N. Terata and M. Matsuura: Solid State Comm. 20(1976) 1151.

12) M. Matsuura and Y. Ajiro: J. Phys. Soc. Japan 41(1976) 44.

13) Y. Ajiro, Y. Endoh, N. Terata and M. Matsuura: J. Phys. Soc. Japan 45(1978) 695.

14) P. van der Leeden, P. A. van Dalen and W. J. M. de Jonge: Physica 33(1967) 202.

15) A. Dupas and J. -P. Renard: CR. Acad. Sci. 271B(1970) 154.

16) M. S. Seehra and T. G. Castner, Jr.: Phys. Rev. 1B(1970) 2289.

17) Y. Yamamoto, M. Matsuura and T. Haseda: J. Phys. Soc. Japan 40(1976) 1300.

18) H. Kiriyama and K. Kitahama: Acta cryst. B32(1976) 330.

19) K. Okada, M. I. Kay, D. T. Cromer and I. Almodovar: J. chem. Phys. 44(1966) 1648.

20) G. Soda and T. Chiba: J. Phys. Soc. Japan 26(1969) 249.

21) K. C. Turberfield: Solid State Comm. 5(1967) 887.

22) H. Kiriyama: Bull. Chem. Soc. Japan 35(1962) 1200.

23) M. I. Kay and R. Kleinberg: Ferroelectrics 4(1972) 147.

24) M. I. Kay: Ferroelectrics 9(1975) 171.

25) T. Matsuo, Y. Kume, H. Suga and S. Seki: J. Phys. Chem. Solids 37 (1976) 499.

26) J. Shimada, H. Abe and K. Ōno: J. Phys. Soc. Japan 11(1956) 137.

27) M. S. Seehra and T. G. Castner, Jr.: Phys. kond. Materie 7(1968) 185.

28) M. S. Seehra: Phys. Letters 28A(1969) 754.

29) K. Yamagata, Y. Kozuka, E. Masai and M. Hayama: J. Phys. Soc. Japan 40(1976) 1593.

30) R. B. Flippen and S. A. Friedberg: J. chem. Phys. 38(1963) 2652.

31) K. Yamagata, M. Hayama and T. Odaka: J. Phys. Soc. Japan 31(1971) 1279.

32) K. Yamagata, M. Hayama and T. Odaka: J. Phys. Soc. Japan 42(1977) 445.

33) R. J. Joenk: Phys. Rev. 126(1962) 565.

34) O. P. van Wier, T. van Peski-Tinbergen and C. J. Gorter: Physica 25(1959) 116.

35) A. Dupas and J. -P. Renard: Proc. 13 Intern. Conf. Low Temperature Physics, Boulder, 1974, p. 389.

36) Bussei Jōsūhyō(in Japanese), Asakura Shoten, Tokyo, 1969, edited by S. Iida, K. Ōno, H. Kanzaki, H. Kumagai and S. Sawada, p. 158.

37) A. Dupas and J. -P. Renard: Phys. Letters 33A(1970) 480.

38) K. Yamagata, Y. Kozuka, E. Masai, M. Taniguchi, T. Sakai and I. Takata: J. Phys. Soc. Japan 44(1978) 139.

39) J. Poulis and C. J. Gorter: Progress in Low Temperature Physics, Vol. I, Chap. XIII, North-Holland Publishing Company, Amsterdam, 1955, edited by C. J. Gorter.

40) T. Moriya: Magnetism, Vol. 1, Chap. 3, Academic Press, New York and London, 1963, edited by G. T. Rado and H. Suhl.

41) J. Kanamori: Magnetism, Vol. 1, Chap. 4, Academic Press, New York and London, 1963, edited by G. T. Rado and H. Suhl.

Appendices

A. Neglected terms in eqs. (3-14a) and (3-14b)

(a) Order of magnitude of various terms

The order of magnitude of the neglected and unneglected terms in eqs. (3-14a) and (3-14b) is estimated as follows: In §2, we see that J is about 36K. This implies H_{ex} is about 1.1×10^6 Oe when <S> is assumed to be S(=½). h_{ex} is $10^{2\sim3}$ Oe as is presented in §2. The upper limit of H_{DM} and h_{DM} is given[40] by $H_{ex}(\Delta g/g) \simeq 10^5$ Oe. However, in this crystal they are estimated to be 10^4 Oe. It is because that the 3% canting of the induced magnetic moment in the paramagnetic region is almost due to the g-tilting mechanism,[2,7,9,11,12] so that the ratio of H_{DM} and h_{DM} to H_{ex} should be considerably smaller than 3%. We take 1% as the upper limit of this ratio and estimated H_{DM} and h_{DM}. H_K, $H_{K'}$ and H_A are not more than[41] $H_{ex}(\Delta g/g)^2 \simeq 10^4$ Oe. However, they are estimated to be $10^{2\sim3}$ Oe, because in the antiferromagnetic state the direction of spins changes widely under the external field of 10^4 Oe coupled with the ferromagnetic moment of 3%. The external magnetic field up to 10^4 Oe is considered. Elements of g-tensors are estimated as g_{XX}-2, g_{YY}-2, g_{ZZ}-2 $\simeq 10^{-1}$, g_{XY}, $g_{YZ} \simeq 10^{-1}$, $g_{ZX} \simeq 10^{-2}$ from the characters of copper ion and the octahedrons of anions. From these values of magnetic parameters, L, M, N, L', M', N' are considered as about 1 and l, m, n, l', m', n' are estimated to be 10^{-2}. These estimated values of constants are listed in the upper half of Table VII. From these values, magnitude of various terms

Table VII Order of magnitude of constants appearing in the equation of motion and that of terms in eqs. (3-14a) and (3-14b).

constants			
H_{ex}	10^6 Oe	h_{ex}	$10^{2\sim3}$ Oe
H_{DM}, h_{DM}	10^4 Oe	H_K, $H_{K'}$, H_A	$10^{2\sim3}$ Oe
H_X, H_Y, H_Z	$\lesssim 10^4$ Oe		
g_{XX}, g_{YY}, g_{ZZ}	1	g_{XY}, g_{YZ}	10^{-1}
g_{ZX}	10^{-2}		
components of normalized spin vectors			
L, M, N, L', M', N'	1	l, m, n, l', m, n'	10^{-2}
terms in eq. (3-14a)		terms in eq. (3-14b)	
$H_K MN$	$10^{2\sim3}$ Oe	$H_{ex} mN$	10^4 Oe
$h_{ex} MN'$	$10^{2\sim3}$	$h_{DM} LM$	10^4
$H_X g_{XY} N$	$\lesssim 10^3$	$H_Z g_{ZZ} M$	$\lesssim 10^4$
	↑ unneglected ↓ neglected		↑ unneglected ↓ neglected
$h_{DM} lM$	10^2		
$H_X g_{ZX} M$	$\lesssim 10^2$	$H_Y g_{YZ} M$(§)	$\lesssim 10^3$
$H_Z g_{ZZ} m$	$\lesssim 10^2$	$H_X g_{XY} n$	$\lesssim 10$
	↑ unneglected ↓ neglected	$H_K mN$	$10^{0\sim1}$
$H_Y g_{YZ} m$(§)	$\lesssim 10$	$h_{ex} mN'$	$10^{0\sim1}$
$H_K mn$	$10^{-2\sim-1}$	$h_{DM} lm$	1
$h_{ex} mn'$	$10^{-2\sim-1}$	$H_X g_{ZX} m$	$\lesssim 1$

in eqs. (3-14a) and (3-14b) are estimated. The lower half of the table shows them. They are listed following the order of magnitude. For the terms of type-one,*) those equal to or smaller than 10^{-1} Oe in eq. (3-14a) and those equal to or smaller than 10 Oe in (3-14b) are neglected. They are smaller than the leading terms of the corresponding equations by a factor 10^3. This seems to imply that (L,M,N), (L',M',N'), (l,m,n) and (l',m',n') are calculated within the accuracy of 0.1%. In the following subsection (b) of this Appendix, we examine this problem.

---

*) The notation (§) in the Table is used for the terms of type-two. Terms due to the difference between $g_{YY}(g_{ZZ})$ and g are not shown there, but they are of the same order of magnitude to g_{YZ}-terms.

(b) Effect of the type-one terms

Effect of the neglected terms of type-one is considered quantitatively. The order of magnitude of the external magnetic field is limited within 10^4 Oe because (1) the experiment was done below 2×10^4 Oe and (2) the calculation becomes complex above about 10^4 Oe. The outline of the examination is as follows: We consider the difference between the solution of the original equations and that of the simplified ones. Functions appearing in the left hand sides of the original equations as (3-14a,b) are expanded around the solution of the simplified ones as (3-16a,b) up to the first order of the difference. The zeroth order terms satisfy the simplified equations and the difference satisfies a set of linear equations. Then the order of magnitude of the difference can be estimated by using the order of magnitude of the determinant which consists of the coefficients in the linear equations. In principle, the determinant can be always evaluated if we fully use the computer, but, in this paper, the calculation is done only for certain special cases mainly corresponding to $\vec{H}//Y$. The result shows that the difference is not negligible in two cases. The first case arises when an accidental relation such as $H_K^* = H_{K'}^*$ exists between the magnetic parameters. We disregard such a possibility. The second case arises when a special relation corresponding to the bending point of the magnetization exists between the external field and the magnetic parameters. For this case, the original rigorous equations must be used, but this problem is not treated in the present paper. For $\vec{H}//Z$ and X, it is certain by the analogy of the $\vec{H}//Y$ case that the bending point for $\vec{H}//Z$ is the only situation where the simplified equations can not be used.

First, we consider the difference between (l,m,n) calculated from the rigorous equations and that calculated from the simplified ones. The rigorous (3-14b) and similar equations are transformed into

$$l = (BN - CM)/G \ , \tag{A-1a}$$

$$m = (CL - AN)/G \ , \tag{A-1b}$$

$$n = (AM - BL)/G \ . \tag{A-1c}$$

and similar equations for (l',m',n'). Quantities A, B, C and G are given by

$$A = A_1 + A_2 \ , \quad B = B_1 + B_2 \ , \quad C = C_1 + C_2 \ , \tag{A-2}$$

$$G \equiv L^2 + M^2 + N^2 = 1 - (l^2 + m^2 + n^2) \ , \tag{A-3}$$

$$\begin{aligned} A_1 = (1/4H_{ex})\{&-2h_{DM}LM - 2H_{DM}LN \\ &+(H_Y g_{YZ} + H_Z g_{ZZ})M - (H_Y g_{YY} + H_Z g_{YZ})N\} \ , \end{aligned} \tag{A-4a}$$

$$\begin{aligned} A_2 = (1/4H_{ex})\{&-2(H_K - H_{K'})(-mN + Mn) + 2h_{DM}lm + 2H_{DM}ln \\ &+H_X g_{ZX} m - H_X g_{XY} n \\ &-2h_{ex}(mN' + Mn' - nM' - Nm')\} \end{aligned} \tag{A-4b}$$

and similar equations for B_1, B_2, C_1 and C_2. On the other hand, l, m and n are calculated as (3-18a) $\sim$ (3-18c) from the simplified (3-16b) and similar equations. It is readily seen that (3-18a$\sim$c) can be also derived from

(A-1a) ∿ (A-4b) by neglecting A_2, B_2, C_2 and by assuming $G = 1$.*) The order of magnitude of the error due to these simplifications is estimated to be 10^{-5}, namely 1/1000 of the order of 1, m and n.

Next, we compare another rigorous equation (3-14a) and the corresponding simplified equation (3-16a). The type-one neglected terms and the error arising from the substitution of (l,m,n) derived from (3-16b) to (3-16a) are estimated to be both of the order of 10^{-1}. Therefore, difference between solutions of two cases can be estimated by comparing solutions of the followings: (1) (3-23a) ∿ (3-23c) and similar three equations derived from the simplified equations.**) The simplified normalization conditions given by

$$L^2 + M^2 + N^2 = 1 \quad , \qquad L'^2 + M'^2 + N'^2 = 1 \tag{A-5a}$$

are used. (2) Equations obtained by substituting α, β, γ, α', β', γ' of the order of 10^{-1} to the right hand sides of (3-23a) and similar five equations. The normalization conditions are given by

$$L^2 + M^2 + N^2 - 1 = 10^{-3} \cdot 2\delta \quad , \qquad L'^2 + M'^2 + N'^2 - 1 = 10^{-3} \cdot 2\delta' \quad , \tag{A-5b}$$

where δ and δ' are constants of the order of 10^{-1}. The solution of the first and the second groups are written as (L,M,N), (L',M',N') and (L_0,M_0,N_0),

---

*) Strictly speaking, (3-18a) ∿ (3-18c) are obtained by applying the simplification of type-two (neglection of type-two terms), too.

**) Strictly speaking, (3-23a) ∿ (3-23c) are obtained by the additional neglection of the type-two terms and the use of the condition (3-21). In this Appendix we use equations before the neglection.

(L'_0,M'_0,N'_0), respectively. Deviations, ΔL, ΔM, ΔN are introduced by

$$L_0 = L + \Delta L \quad , \qquad M_0 = M + \Delta M \quad , \qquad N_0 = N + \Delta N \quad . \tag{A-6}$$

Similar equations stand for $\Delta L'$, $\Delta M'$ and $\Delta N'$. Substituting them to the second group equations and neglecting products of the deviations, we obtain equations for determining the deviations. The zeroth order terms become zero because (L,M,N) and (L',M',N') satisfy the simplified equations, so that six linear equations are obtained for the deviations. Three of them are given as follows:

$$\{(A-b^2+c^2)N + 2bcM - X_1 + hN'\}\Delta M$$

$$+ \{(A-b^2+c^2)M - 2bcN + X_2 - hM'\}\Delta N - hN\cdot\Delta M' + hM\cdot\Delta N' = \alpha \quad , \tag{A-7a}$$

$$\{(B+a^2-c^2)N - bcM + X_1 - hN'\}\Delta L - bcL\cdot\Delta M$$

$$+ \{(B+a^2-c^2)L - (Y+Z) + hL'\}\Delta N + hN\cdot\Delta L' - hL\cdot\Delta N' = \beta \quad , \tag{A-7b}$$

$$\{(C-a^2+b^2)M + bcN - X_2 + hM'\}\Delta L + \{(C-a^2+b^2)L + (Y+Z) - hL'\}\Delta M$$

$$+ bcL\cdot\Delta N - hM\cdot\Delta L' + hL\cdot\Delta M' = \gamma \quad , \tag{A-7c}$$

where the direction of the external field is limited to one of the three principal axes, XYZ, and the parameter H_A is eliminated by using (3-21).*)

---

*) Much complex equations are obtained without these simplifications and the above equations are sufficient for the present case.

The remaining three equations are obtained by interchanging primed and corresponding unprimed quantities and by changing α, β, γ to the primed ones. Newly defined quantities appearing in the above equations are given by

$$A = -2(H_K^* + H_{K'}^*) \ , \qquad B = 2(H_K^* - H_{K'}^*) \ , \qquad C = 4H_{K'}^* \ , \tag{A-8a}$$

$$a = H_X g_{XX} (4H_{ex})^{-\frac{1}{2}} \ ,$$

$$b = (H_Y g_{YY} + H_Z g_{YZ}) (4H_{ex})^{-\frac{1}{2}} \ ,$$

$$c = (H_Y g_{YZ} + H_Z g_{ZZ}) (4H_{ex})^{-\frac{1}{2}} \ , \tag{A-8b}$$

$$X_1 = g_{ZX}^* H_X \ , \qquad X_2 = g_{XY}^* H_X \ , \tag{A-8c}$$

$$Y = g_{XY}^{**} H_Y \ , \qquad Z = g_{ZX}^{**} H_Z \ , \tag{A-8d}$$

$$h = 2h_{ex} \ . \tag{A-8e}$$

The normalization conditions are transformed into

$$10^3 L \cdot \Delta L + 10^3 M \cdot \Delta M + 10^3 N \cdot \Delta N = \delta \ , \tag{A-9a}$$

$$10^3 L' \cdot \Delta L' + 10^3 M' \cdot \Delta M' + 10^3 N' \cdot \Delta N' = \delta' \ . \tag{A-9b}$$

It should be noticed that only four of (A-7a) $\sim$ (A-7c) and three similar equations are independent and that which of these are independent is determined by the solution (L,M,N), (L',M',N'). We will pass this problem here for simplicity but take it into account in the following discussions. The selected four equations and the two normalization equations can be used for determining the deviations because, as is seen below, they are independent

in general. The independence is readily concluded if a seventh equation which is obtained by requiring the determinant of the coefficients of the equations to be zero is not satisfied automatically by the solutions. We have found a solution which does not satisfy the seventh equation and we reject the automaticity. For this case the deviations are estimated to be of the order of 10^{-3} or less so that are negligible for practical purpose.

The remaining problem is that certain solutions may accidentally satisfy the seventh equation. In principle, this can be fully examined when we use the computer for the direct numerical evaluation of the determinant. In this paper, however, we treat analytically soluble cases only. The result suggests that the numerical computation is not essential. The followings are the results of the analytical treatment.

(i) $H = h = 0$: fictitious one-spin system at zero external field

For this case, the primed system need not be included. When we consider the solution N=1, L=M=0, the determinant is given by

$$\begin{vmatrix} 0 & A & 0 \\ B & 0 & 0 \\ 0 & 0 & 10^3 \end{vmatrix} = -10^3AB. \qquad \text{(A-10)}$$

A is always negative and B is not zero in orthorhombic cases so that the determinant is not zero except for the accidental $H_K^* = H_{K'}^*$ case. We neglect such a possibility.

(ii) $H = 0$, $h \neq 0$: fictitious two-spin system at zero external field

The determinant corresponding to the solution L=L'=M=M'=0, N=-N'=1 is written as

$$\begin{vmatrix} 0 & A-h & 0 & 0 & -h & 0 \\ B+h & 0 & 0 & h & 0 & 0 \\ 0 & 0 & 10^3 & 0 & 0 & 0 \\ 0 & h & 0 & 0 & -(A-h) & 0 \\ -h & 0 & 0 & -(B+h) & 0 & 0 \\ 0 & 0 & 0 & 0 & 0 & -10^3 \end{vmatrix}$$

$$= -10^6\{(A-h)^2 - h^2\}\{-(C+h)^2 + h^2\} \quad . \qquad \text{(A-11)}$$

The right hand side is always positive because $A < 0$, $C > 0$, $h > 0$.

(iii) $h=0$, $\vec{H}//Y$, $g_{YZ}=0$: fictitious one-spin system under the external field parallel to the hard axis (Anisotropy of the g-tensor in the ac-plane is neglected.)

The mathematics for the general $\vec{H}//Y$ case is complex but the calculation becomes simple when we treat a special case satisfying $g_{YZ}=0$. As this term plays no essential roles in the magnetization process, examination of this case gives useful informations for the $\vec{H}//Y$ case. The following solution is considered,

$$L = Y/B \ , \quad M = 0 \ , \quad N = \pm(1 - L^2)^{\frac{1}{2}} \quad . \qquad \text{(A-12a)}$$

The L=Y=0 case should not be included in the followings because we select the independent equations so as to include N=0 case but as to exclude L=0 case. The determinant is written as

$$\begin{vmatrix} BN & 0 & 0 \\ 0 & (C+b^2)L+Y & 0 \\ 10^3L & 0 & 10^3N \end{vmatrix} = 10^3BN^2\{(C+b^2)/B+1\}Y \quad . \qquad \text{(A-12b)}$$

The right hand side is zero when and only when N=0, namely the bending point of the magnetization.

(iv) h=0, $\vec{H}$//X: fictitious one-spin system under the external field parallel to the intermediate axis

The solutions satisfying L=0, N≠0 are considered. The equation determining M(and N) is given by

$$AMN - X_1M + X_2N = 0 \quad . \qquad \text{(A-13a)}$$

This is just the equation (3-48a) and we can rewrite it as

$$(H_K^* + H_{K'}^*)\sin 2\theta + (g_{XY}^{*2} + g_{ZX}^{*2})^{\frac{1}{2}}\sin(\theta - \Delta) = 0 \quad , \qquad \text{(A-13b)}$$

where θ and Δ defined in (3-53b) are used. The 3 × 3 determinant splits into a 1 × 1 and a 2 × 2 determinants for ΔL and for ΔM and ΔN, respectively. ΔL is readily estimated to be negligible and the determinant for ΔM and ΔN are given as

$$\begin{vmatrix} AN-X_1 & AM+X_2 \\ 10^3M & 10^3N \end{vmatrix} \quad . \qquad \text{(A-14a)}$$

Requiring it to be zero we obtain

$$2(H_K^* + H_{K'}^*)\cos 2\theta + (g_{XY}^{*2} + g_{ZX}^{*2})^{\frac{1}{2}}\sin(\theta - \Delta) = 0 \quad . \qquad \text{(A-14b)}$$

Equations (A-13b) and (A-14b) are satisfied simultaneously at the confluence point(See §3.2.2 (c).) only. Therefore, the simplified equations are reliable.

(v) $h \neq 0$, $\vec{H}//Y$, $g_{YZ}=0$: fictitious two-spin system under the external field parallel to the hard axis(g-anisotropy in the ac-plane is neglected.)

Following the treatment in case (iii) we consider the special case satisfying $c=0$. The solution fulfilling $L=L' \neq 0$, $M=M'=0$, $N=-N'$ is considered. The 6×6 determinant splits into a 2×2 and a 4×4 determinants for ΔM, $\Delta M'$ and for ΔL, $\Delta L'$, ΔN, $\Delta N'$, respectively. The former determinant

$$\begin{vmatrix} (C+b^2-h)L+Y & hL \\ hL & (C+b^2-h)L+Y \end{vmatrix}$$

$$= \{(C+b^2-h)L+Y\}^2 - h^2L^2$$

$$= Y^2(B+2h)^{-2}\{(B+C+b^2+h)^2 - h^2\} \qquad \text{(A-15)}$$

is always positive, so that ΔL and $\Delta L'$ are small. The latter determinant is written as

$$\begin{vmatrix} (B+h)N & (B+h)L-Y & hN & -hL \\ 10^3L & 10^3N & 0 & 0 \\ -hN & -hL & -(B+h)N & (B+h)L-Y \\ 0 & 0 & 10^3L & -10^3N \end{vmatrix} , \qquad \text{(A-16a)}$$

where the relations L=L' and N=-N' are used. Requiring this to be zero we obtain

$$10^6N^2(B+2h)h = 0 \quad . \tag{A-16b}$$

As in the case (iii), the simplification is allowable unless N=0.

These examples suggest that the deviations are divergent when and only when the lowest-energy solutions of the simplified equations degenerate in the LMNL'M'N'-space. It is clear that such is a consequence of the mathematics that a small perturbation to an equation causes only a slight change in the solution when it is not degenerate. Therefore, the simplification, a small modification of the equation, is allowable in general and the exceptions for $\vec{H}$//X, Y, Z are only the bending points for $\vec{H}$//Y and Z.

B. Twelve fundamental equations

Twelve equations determining vectors (L,M,N), (L',M',N'), (1,m,n) and (1',m',n') are presented here.

($dR_1/dt+dR_2/dt$ type)

$$-2(H_K+H_{K'})MN - 2H_A(M^2-N^2) - 2h_{DM}(1M-Lm) + 2H_{DM}(nL-N1)$$
$$- (H_X g_{ZX} M + H_Z gm - H_X g_{XY} N - H_Y gn) + 2h_{ex}(MN'-NM') = 0 ,$$

$$2(H_K-H_{K'})NL + 2H_A LM + 2H_{DM}(-mN+Mn)$$
$$-\{-H_X g_{ZX} L - H_Z g1 + H_X gn + (H_Y g_{XY}+H_Z g_{ZX})N\}$$
$$+ 2h_{ex}(NL'-LN') = 0 ,$$

$$4H_{K'}LM - 2H_A NL - 2h_{DM}(-mN+Mn)$$
$$- \{H_X g_{XY} L + H_Y g1 - H_X gm - (H_Y g_{XY}+H_Z g_{ZX})M\}$$
$$+ 2h_{ex}(LM'-ML') = 0 .$$

($dR_3/dt+dR_4/dt$ type)

$$-2(H_K+H_{K'})M'N' - 2H_A(M'^2-N'^2) - 2h_{DM}(1'M'-L'm') + 2H_{DM}(n'L'-N'1')$$
$$- (H_X g_{ZX} M' + H_Z gm' - H_X g_{XY} N' - H_Y gn') + 2h_{ex}(M'N-N'M) = 0 ,$$

$$2(H_K - H_{K'})N'L' + 2H_A L'M' + 2H_{DM}(-m'N' + M'n')$$

$$- \{-H_X g_{ZX} L' - H_Z g l' + H_X g n' + (H_Y g_{XY} + H_Z g_{ZX})N'\}$$

$$+ 2h_{ex}(N'L - L'N) = 0 ,$$

$$4H_{K'} L'M' - 2H_A N'L' - 2h_{DM}(-m'N' + M'n')$$

$$- \{H_X g_{XY} L' + H_Y g l' - H_X g m' - (H_Y g_{XY} + H_Z g_{ZX})M'\}$$

$$+ 2h_{ex}(L'M - M'L) = 0 .$$

($dR_1/dt - dR_2/dt$ type)

$$4H_{ex}(-mN + Mn) + 2h_{DM} LM + 2H_{DM} NL$$

$$- (H_Z g M - H_Y g N) = 0 ,$$

$$4H_{ex}(-nL + Nl) - 2h_{DM}(L^2 + N^2) + 2H_{DM} MN$$

$$- (-H_Z g L + H_X g N) = 0 ,$$

$$4H_{ex}(-lM + Lm) + 2h_{DM} MN - 2H_{DM}(L^2 + M^2)$$

$$- (H_Y g L - H_X g M) = 0 .$$

($dR_3/dt - dR_4/dt$ type)

$$4H_{ex}(-m'N' + M'n') + 2h_{DM} L'M' + 2H_{DM} N'L'$$

$$- (H_Z g M' - H_Y g N') = 0 ,$$

$$4H_{ex}(-n'L'+N'1') - 2h_{DM}(L'^2+N'^2) + 2H_{DM}M'N'$$

$$- (-H_Z gL' + H_X gN') = 0 ,$$

$$4H_{ex}(-1'M'+L'm') + 2h_{DM}M'N' - 2H_{DM}(L'^2+M'^2)$$

$$- (H_Y gL' - H_X gM') = 0 .$$

C. 36 solutions of the H=0 and $h_{ex} > 0$ case

36 solutions of eqs. (3-31a) ∿ (3-31c) and the associated equations are grouped into (i) ∿ (ix) .

(i) $L = \pm 1, \quad M = 0, \quad N = 0,$

$L' = \mp 1, \quad M' = 0, \quad N' = 0.$

(ii) $L = 0, \quad M = 0, \quad N = \pm 1,$

$L' = 0, \quad M' = 0, \quad N' = \pm 1.$

(iii) (a) $L = \mp L_1, \quad M = 0, \quad N = \pm N_1,$

$L' = \pm N_1, \quad M' = 0, \quad N' = \pm L_1,$

where $L_1 = F_1(H_K^* - H_{K'}^*), \quad N_1 = F_2(H_K^* - H_{K'}^*)$

and functions F_1, F_2 are given by

$$F_1(x) \equiv \{\frac{1}{2} - \frac{1}{2}(1 - 4h_{ex}^2 x^{-2})^{\frac{1}{2}}\}^{\frac{1}{2}},$$

$$F_2(x) \equiv \{\frac{1}{2} + \frac{1}{2}(1 - 4h_{ex}^2 x^{-2})^{\frac{1}{2}}\}^{\frac{1}{2}}.$$

(b) $L = \pm N_1, \quad M = 0, \quad N = \pm L_1,$

$L' = \mp L_1, \quad M' = 0, \quad N' = \pm N_1.$

(a') $L = \mp N_1$, $M = 0$, $N = \pm L_1$,

$L' = \pm L_1$, $M' = 0$, $N' = \pm N_1$.

(b') $L = \pm L_1$, $M = 0$, $N = \pm N_1$,

$L' = \mp N_1$, $M' = 0$, $N' = \pm L_1$.

(iv) $L = \pm 1$, $M = 0$, $N = 0$,

$L' = \pm 1$, $M' = 0$, $N' = 0$.

(v) $L = 0$, $M = \pm 1$, $N = 0$,

$L' = 0$, $M' = \mp 1$, $N' = 0$.

(vi) (a) $L = \pm L_2$, $M = \mp M_2$, $N = 0$,

$L' = \pm M_2$, $M' = \pm L_2$, $N' = 0$,

where $L_2 = F_2(2H_{K'}, *)$ and $M_2 = F_1(2H_{K'}, *)$.

(b) $L = \pm M_2$, $M = \pm L_2$, $N = 0$,

$L' = \pm L_2$, $M' = \mp M_2$, $N' = 0$.

(a') $L = \pm M_2$, $M = \mp L_2$, $N = 0$,

$L' = \pm L_2$, $M' = \pm M_2$, $N = 0$.

(b') $L = \pm L_2$, $M = \pm M_2$, $N = 0$,

$L' = \pm M_2$, $M' = \mp L_2$, $N' = 0$.

(vii) $L = 0$, $M = 0$, $N = \pm 1$,

$L' = 0$, $M' = 0$, $N' = \mp 1$.

(viii) $L = 0$, $M = \pm 1$, $N = 0$,

$L' = 0$, $M' = \pm 1$, $N' = 0$.

(ix) (a) $L = 0$, $M = \mp M_3$, $N = \pm N_3$,

$L' = 0$, $M' = \pm N_3$, $N' = \pm M_3$,

where $M_3 = F_1(H_K^* + H_{K'}^*)$ and $N_3 = F_2(H_K^* + H_{K'}^*)$.

(b) $L = 0$, $M = \pm N_3$, $N = \pm M_3$,

$L' = 0$, $M' = \mp M_3$, $N' = \pm N_3$.

(a') $L = 0$, $M = \mp N_3$, $N = \pm M_3$,

$L' = 0$, $M' = \pm M_3$, $N' = \pm N_3$.

(b') $L = 0$, $M = \pm M_3$, $N = \pm N_3$,

$L' = 0$, $M' = \mp N_3$, $N' = \pm M_3$.

D. Free energies in the 2-sublattice $\vec{H}//Z$ case

For the 2-sublattice $\vec{H}//Z$ case, the free energy is written as

$$f = -H_K{}^*N^2 - (H_{K'}{}^* + kH_Z{}^2)L^2 + (H_{K'}{}^* - kH_Z{}^2)M^2 - g_{ZX}{}^{**}H_Z L \ , \qquad \text{(D-1)}$$

where a simplified notation k is used instead of $g^2/8H_{ex}$. The equilibrium condition is given as follows:

$$-2(H_K{}^* + H_{K'}{}^*)MN = 0 \ , \qquad \text{(D-2a)}$$

$$2(H_K{}^* - H_{K'}{}^* - kH_Z{}^2)NL - g_{ZX}{}^{**}H_Z N = 0 \ , \qquad \text{(D-2b)}$$

$$4H_{K'}{}^*ML + g_{ZX}{}^{**}H_Z M = 0 \ . \qquad \text{(D-2c)}$$

Solutions of (D-2a) are considered first. They are

$$M = 0 \qquad \text{(D-3a)}$$

and

$$N = 0 \ . \qquad \text{(D-3b)}$$

We call the former and the latter as Case A and Case B, respectively.

Case A: M=0

Equation (D-2c) is satisfied automatically. Solutions of eq. (D-2b) are

$$N = 0 \qquad \text{(D-4a)}$$

and

$$L = g_{ZX}^{**}H_Z/2(H_K^* - H_{K'}^* - kH_Z^2) \ , \qquad |L| \leqq 1 \ . \tag{D-4b}$$

The former and the latter are called as Case Aa and Case Ab, respectively.

(Case Aa) M=N=0

For this case L and f are obtained as follows:

$$L = \pm 1 \ , \tag{D-5a}$$

$$f = - (H_{K'}^* + kH_Z^2) \mp g_{ZX}^{**}H_Z \ . \tag{D-5b}$$

Of these two solutions, we pick up one which is given by

$$L = \mathrm{sign}(g_{ZX}^{**}) \cdot 1 \ , \tag{D-5a'}$$

$$f = - (H_{K'}^* + kH_Z^2) - |g_{ZX}^{**}|H_Z \equiv f_{Aa}(H_Z) \ , \tag{D-5b'}$$

because the free energy of the other case is always larger than f_{Aa}.

(Case Ab) M=0, $L=g_{ZX}^{**}H_Z/2(H_K^* - H_{K'}^* - kH_Z^2)$

$$N = \pm \{1 - g_{ZX}^{**2}H_Z^2/4(H_K^* - H_{K'}^* - kH_Z^2)^2\} \ , \tag{D-6a}$$

$$f = - H_K^* - g_{ZX}^{**2}H_Z^2/4(H_K^* - H_{K'}^* - kH_Z^2) \equiv f_{Ab}(H_Z) \ . \tag{D-6b}$$

Case B: N=0

Equation (D-2b) is satisfied automatically. Solutions of eq. (D-2c) are

$$M = 0 \tag{D-7a}$$

and

$$L = - g_{ZX}^{**} H_Z / 4 H_{K'}^{*} , \qquad |L| \leqq 1 . \tag{D-7b}$$

(Case Ba) M=N=0

This case has been treated as the Case Aa.

(Case Bb) N=0, $L=-g_{ZX}^{**} H_Z / 4 H_{K'}^{*}$

For this case M and f are calculated as

$$M = \pm \{ 1 - g_{ZX}^{**2} H_Z^2 / 16 H_{K'}^{*2} \} , \tag{D-8a}$$

$$f = H_{K'}^{*} - k H_Z^2 + g_{ZX}^{**2} H_Z^2 / 8 H_{K'}^{*} \equiv f_{Bb}(H_Z) . \tag{D-8b}$$

We readily see

$$f_{Aa}(H_Z) < f_{Bb}(H_Z) . \tag{D-9}$$

Therefore, the problem is reduced to the examination of f_{Aa} and f_{Ab}.

First, $F(H_Z)$ is defined as

$$F(H_Z) \equiv f_{Aa}(H_Z) - f_{Ab}(H_Z) . \tag{D-10}$$

A simple calculation gives

$$F(H_Z) = (H_{K-}^{*} - k H_Z^2)(1 - 2h + h^2) , \tag{D-11a}$$

where

$$h = |g_{ZX}^{**}| H_Z / 2 (H_{K-}^{*} - k H_Z^2) . \tag{D-11b}$$

The first factor of eq. (D-11a) can not be zero because, if it is zero, L given by eq. (D-4b) diverges. Therefore,

$$F(H_Z) \geqq 0 \qquad \text{for} \quad 0 < H_Z < H_{div}$$

and

$$F(H_Z) \leqq 0 \qquad \text{for} \quad H_{div} < H_Z \tag{D-12a}$$

where the equality stands for h=1, in other words(See (D-11b).),

$$|g_{ZX}^{**}|H_Z/2(H_{K-}^{*} - kH_Z^2) = 1 \tag{D-12b}$$ *)

and H_{div} is given by

$$H_{div} = (H_{K-}^{*}/k)^{\frac{1}{2}} . \tag{D-12c}$$

Summing up these results, Case Ab is the lowest state when $H_Z < H_{div}$ and $|L| \leqq 1$, otherwise Case Aa is the lowest state. When the positive solution H_{BZ} of eq. (D-12b) satisfies $H_{BZ} < H_{div}$, the transition occurs smoothly.

The inequality $|L| \leqq 1$, in other words(See (D-4b).),

$$-1 \leqq g_{ZX}^{**}H_Z/2(H_{K-}^{*} - kH_Z^2) \leqq 1 \tag{D-13}$$

is considered next. This inequality has solutions:

$$H_Z \leqq (1/4k)\{-|g_{ZX}^{**}| + (|g_{ZX}^{**}|^2 + 16kH_{K-}^{*})^{\frac{1}{2}}\} < H_{div} \tag{D-14a}$$

and

$$H_Z \geqq (1/4k)\{|g_{ZX}^{**}| + (|g_{ZX}^{**}|^2 + 16kH_{K-}^{*})^{\frac{1}{2}}\} > H_{div} . \tag{D-14b}$$

---

*) When h=1, L for Case Ab is ±1 depending on the sign of $g_{ZX}^{**}(\gtrless 0)$.

The former is consistent with the required condition and the latter is not. In conclusion, by increasing H_Z, a smooth transition from the Ab-state to the Aa-state occurs at H_{BZ} defined by a selfconsistent equation:

$$H_{BZ} = 2(H_{K-}{}^{*} - kH_{BZ}{}^{2})/|g_{ZX}{}^{**}| \ . \qquad \text{(D-15)}$$

E. Solution of eq. (3-65)

Equation (3-65) is solved following the method by Gorter and coworkers.[34] The minimum of the free energy

$$f^* = -(N^2 + N'^2) - x(L + L') + h(LL' + NN') \tag{E-1}$$

is considered under the following conditions for the variable x corresponding to the external field and the constant h corresponding to the interlayer exchange:

$$x(\text{variable}) \geqq 0 , \qquad h(\text{constant}) > 0 . \tag{E-2}$$

By writing

$$N = \cos\theta, \qquad L = \sin\theta \qquad (0 \leqq \theta \leqq 2\pi) , \tag{E-3a}$$

$$N' = \cos\theta', \qquad L' = \sin\theta' \qquad (0 \leqq \theta' \leqq 2\pi) , \tag{E-3b}$$

f^* is transformed into

$$f^* = -(\cos^2\theta + \cos^2\theta') - x(\sin\theta + \sin\theta') + h(\sin\theta\sin\theta' + \cos\theta\cos\theta') . \tag{E-4}$$

Next, by introducing new angles α and β defined as

$$\alpha \equiv \frac{1}{2}(\theta + \theta') \qquad (0 \leqq \alpha \leqq 2\pi) , \tag{E-5a}$$

$$\beta \equiv \frac{1}{2}(\theta - \theta') \qquad (-\pi \leqq \beta \leqq \pi) , \tag{E-5b}$$

f^* is further converted into

$$f^* = -2(\cos^2\alpha\cos^2\beta + \sin^2\alpha\sin^2\beta) - 2x\sin\alpha\cos\beta + h\cos2\beta \ . \qquad \text{(E-6)}$$

The energy minimum conditions $\partial f^*/\partial\alpha = 0$ and $\partial f^*/\partial\beta = 0$ yield

$$2\cos\alpha(2\sin\alpha\cos^2\beta - 2\sin\alpha\sin^2\beta - x\cos\beta) = 0 \ , \qquad \text{(E-7a)}$$

$$2\sin\beta(2\cos^2\alpha\cos\beta - 2\sin^2\alpha\cos\beta + x\sin\alpha - 2h\cos\beta) = 0 \ . \qquad \text{(E-7b)}$$

Equations (E-7a) and (E-7b) have four solutions. They are as follows:

Case I $\quad \cos\alpha = 0, \ \sin\beta = 0 \ .$

By using $\sin\alpha = \pm1$ and $\cos\beta = \pm1$, the free energy are calculated as

$$f^* = -2x(\underset{\uparrow}{\pm1})(\underset{\uparrow}{\pm1}) + h \ . \qquad \text{(E-8)}$$
$$\qquad\quad \sin\alpha \ \cos\beta$$

To minimize the free energy, $\sin\alpha$ and $\cos\beta$ should have the same sign. The ++ selection or $\alpha = \pi/2, \ \beta = 0$ results in $\theta=\theta'=\pi/2$. The -- selection similarly results in $\theta = 5\pi/2, \ \theta' = \pi/2$ and $\theta = \pi/2, \ \theta' = 5\pi/2$. However, the -- solutions violate the limit for θ and θ' so that we neglect them hereafter. The result $\theta=\theta'=\pi/2$ satisfies the required condition L=L', N=-N'. Of course, eq. (E-8) can be simplified to

$$f^* = -2x + h \equiv f^*_I(x) \ . \qquad \text{(E-9)}$$

Case II $\quad \cos\alpha = 0, \ 2\cos^2\alpha\cos\beta - 2\sin^2\alpha\cos\beta + x\sin\alpha - 2h\cos\beta = 0 \ .$

By using $\sin\alpha = \pm1$, $\cos\beta$ is calculated as

$$\cos\beta = \pm x/2(1+h) \ , \qquad x \leqq 2(1+h) \ . \tag{E-10}$$

Just as for Case I, the ++ selection is the only case to be considered further. For this case, θ and θ' are given by

$$\theta = \frac{1}{2}\pi \pm \beta_0 \ , \qquad \theta' = \frac{1}{2}\pi \mp \beta_0 \ , \tag{E-11}$$

where β_0 is a positive acute angle defined by

$$\cos\beta_0 = x/2(1+h) \ . \tag{E-12}$$

These θ and θ' satisfy the condition L=L', N=-N'. The free energy is written as

$$f^* = -2 - h - x^2/2(1+h) \equiv f^*_{\text{II}}(x) \ . \tag{E-13}$$

Case III $\quad 2\sin\alpha\cos^2\beta - 2\sin\alpha\sin^2\beta - x\cos\beta = 0 \ , \ \sin\beta = 0 \ .$

By using $\cos\beta = \pm 1$, $\sin\alpha$ is obtained as

$$\sin\alpha = \pm x/2 \ , \qquad x \leqq 2 \ . \tag{E-14}$$

The ++ case is selected as before. The angles θ and θ' are given by

$$\theta = \theta' = \alpha_0 \ , \ \pi - \alpha_0 \ , \tag{E-15}$$

where α_0 is a positive acute angle defined as follows:

$$\sin\alpha_0 = x/2 \ . \tag{E-16}$$

The expression of the free energy is simplified to

$$f^* = -2 + h - x^2/2 = f^*_{III}(x) \ . \qquad \text{(E-17)}$$

Case IV

$$2\sin\alpha\cos^2\beta - 2\sin\alpha\sin^2\beta - x\cos\beta = 0 \ , \qquad \text{(E-18)}$$

$$2\cos^2\alpha\cos\beta - 2\sin^2\alpha\cos\beta + x\sin\alpha - 2h\cos\beta = 0 \ . \qquad \text{(E-19)}$$

By adding (E-18)×sinα and (E-19)×cosβ, the following equation is derived:

$$2\cos^2\beta - 2\sin^2\alpha - 2h\cos^2\beta = 0 \ . \qquad \text{(E-20)}$$

Then a useful relation between sinα and cosβ is obtained as

$$\cos\beta = \pm\sin\alpha(1-h)^{-\frac{1}{2}} \ . \qquad \text{(E-21)}$$

By inserting this relation, eq. (E-18) is transformed into

$$2\sin^3\alpha/(1-h) - 2\sin\alpha\{1 - \sin^2\alpha/(1-h)\} \mp x\sin\alpha/(1-h)^{\frac{1}{2}} = 0 \ . \qquad \text{(E-22)}$$

Equation (E-22) has two solutions:

$$\sin\alpha = 0 \qquad \text{(E-23)}$$

and

$$\sin^2\alpha = \frac{1}{2}(1-h) \pm \frac{1}{4}x(1-h)^{\frac{1}{2}} \ . \qquad \text{(E-24)}$$

The former solution yields $\cos\beta = 0$ so that f* is calculated as

$$f^* = -h \ . \tag{E-25}$$

As this value -h is always larger than f^*_{II}(See (E-13).), we disregard it hereafter. The latter solution results in

$$\cos 2\alpha = h \mp \frac{1}{2}x(1-h)^{\frac{1}{2}} \ , \tag{E-26}$$

$$\cos 2\beta = \pm\frac{1}{2}x(1-h)^{-\frac{1}{2}} \ , \tag{E-27}$$

$$f^* = \frac{1}{4}x^2 \mp (1-h)^{\frac{1}{2}}x - 1 \ . \tag{E-28}$$

Of course, the upper of the double sign leads to lower energy, so that the lower of the double sign can be neglected. The free energy $f^*_{IV}(x)$ is defined as

$$f^*_{IV}(x) \equiv \frac{1}{4}x^2 - (1-h)^{\frac{1}{2}}x - 1 \ . \tag{E-29}$$

By employing the expressions for cos2α and cos2β, namely eqs. (E-26) and (E-27), the domain of the variable x is taken as

$$x \leqq 2(1-h)^{\frac{1}{2}} \ . \tag{E-30}$$

Next, f^*_{III} and f^*_{IV} are compared with f^*_{II}.

Case A f^*_{III} versus f^*_{II}

The following definitions of the free energies are reminded:

$$f^*_{II} = -2 - h - x^2/2(1+h) \qquad x \leqq 2(1+h) \ ,$$

$$f^*_{III} = -2 + h - x^2/2 \qquad x \leqq 2 \ .$$

At $x=0$ f^*_{II} is smaller than f^*_{III} so that, if the positive solution of the equation $f^*_{II}=f^*_{III}$ is larger than 2, we can conclude $f^*_{II} < f^*_{III}$. The equality can be simplified to

$$x^2\{\frac{1}{2}-\frac{1}{2}/(1+h)\} = 2h \ . \qquad \text{(E-31)}$$

The positive solution

$$x = 2(1+h)^{\frac{1}{2}} \qquad \text{(E-32)}$$

is larger than 2.

Case B f^*_{IV} versus f^*_{II}

We consider the cross point of two curves. The equation $f^*_{II} - f^*_{IV}=0$ is simplified to

$$-\frac{1}{4}x^2(3+h)/(1+h) + (1-h)^{\frac{1}{2}}x - (1+h) = 0 \ . \qquad \text{(E-33)}$$

The discriminant of this equation is obtained as

$$(1-h) - (3+h) = -2-2h \ . \qquad \text{(E-34)}$$

As this quantity is negative, two curves do not cross. At $x=0$ f^*_{II} is smaller than f^*_{IV}, so that always $f^*_{II} < f^*_{IV}$.

F. Magnetization jump and the jumping field

Two parameters, $|g_{ZX}^*/g_{XY}^*|$ and $2h_{ex}/H_{K+}^*$, are determined by comparing details of the calculated and experimental magnetization curves. The calculation was done for 30 combinations of the parameters shown in Table VIII. Examples of the calculated curves are given in Fig. 32(a) and (b). It is noticed that the jump of the magnetization remains constant when the second parameter, $2h_{ex}/H_{K+}^*$, is changed. Two quantities A and B which charaterize the shape of the curves are considered. A, the reduced jump in %, is 100(jump per ion)/μ_B<S> $\{(g_{XY}^*)^2 + (g_{ZX}^*)^2\}^{\frac{1}{2}}$ and B, the reduced jumping field in %, is 100(H_X of the jump)/H_{IBX}, where H_{IBX} is the imaginary bending field for $\vec{H}$//X given by eq. (5-11). Table VIII shows the calculated values of A and B corresponding to the 30 cases. The experimental result for CuFTH indicates that A and B are 21 and 53% respectively. Rounding them to 20 and 55% respectively, we obtain $|g_{ZX}^*/g_{XY}^*| = 0.20$ and $2h_{ex}/H_{K+}^* = 0.35$.

Table VII Dependence of the magnetization jump and the jumping field on two parameters $|g_{ZX}^*/g_{XY}^*|$ and $2h_{ex}/H_{K+}^*$. In the expression A/B, A represents the reduced jump in %, namely 100(jump per ion)/$\mu_B\langle S\rangle\times[(g_{XY}^*)^2+(g_{ZX}^*)^2]^{\frac{1}{2}}$, and B represents the reduced jumping field in %, 100(H_X of the jump)/H_{IBX}, respectively.

$2h_{ex}/H_{K+}^*$ \ $\lvert g_{ZX}^*/g_{XY}^*\rvert$	0.10	0.15	0.20	0.25	0.30
0.20	10/64	15/49	21/39	26/33	29/26
0.25	11/71	16/55	20/45	25/37	29/31
0.30	11/76	15/61	20/51	26/42	29/38
0.35	9/81	15/66	20/55	26/46	29/40
0.40	7/83	15/69	19/58	25/49	29/44
0.45	5/86	13/73	20/61	23/53	29/41

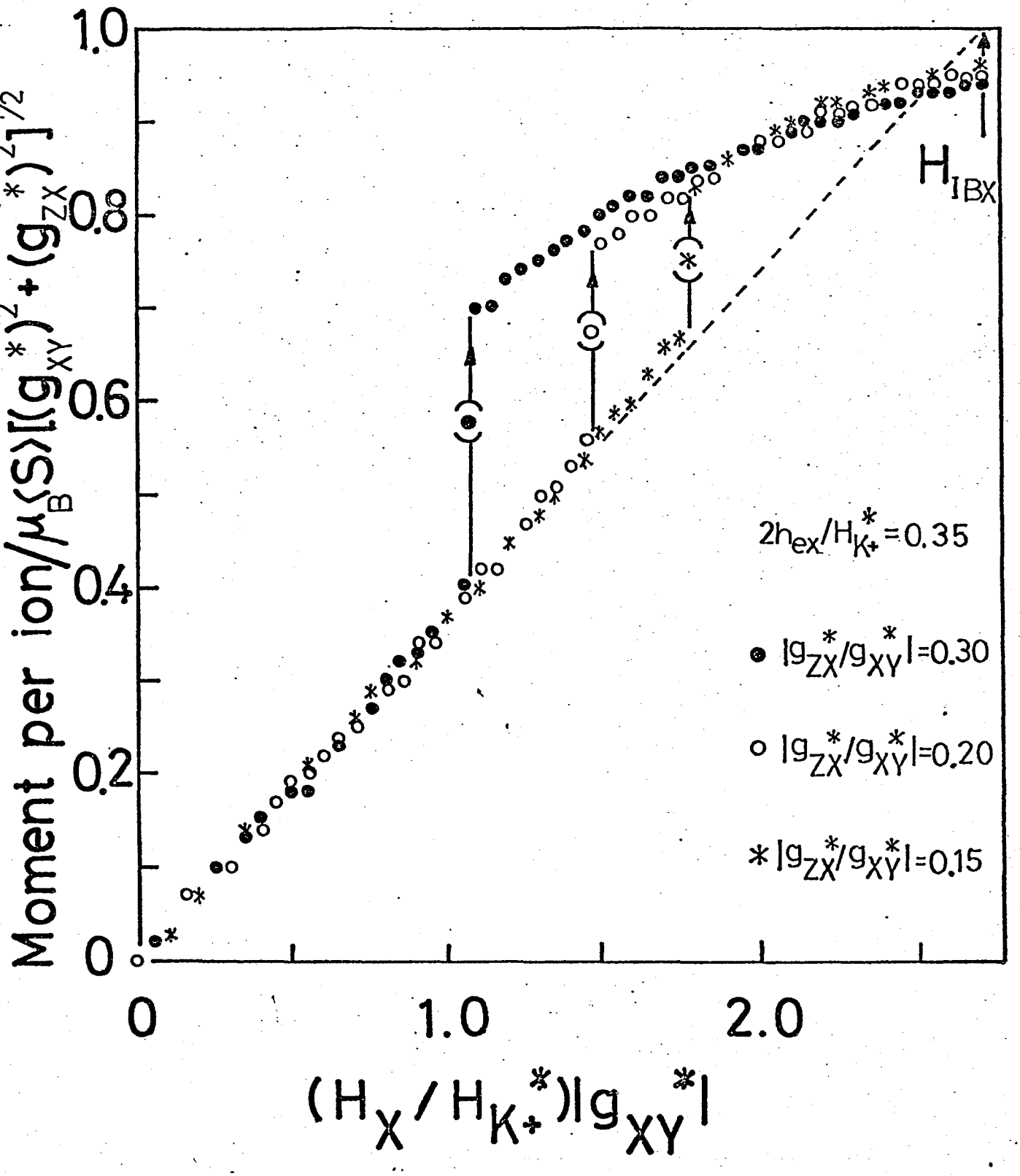

Fig. 32(a) Theoretical magnetization curves around the jump for three $|g_{ZX}^*/g_{XY}^*|$'s.

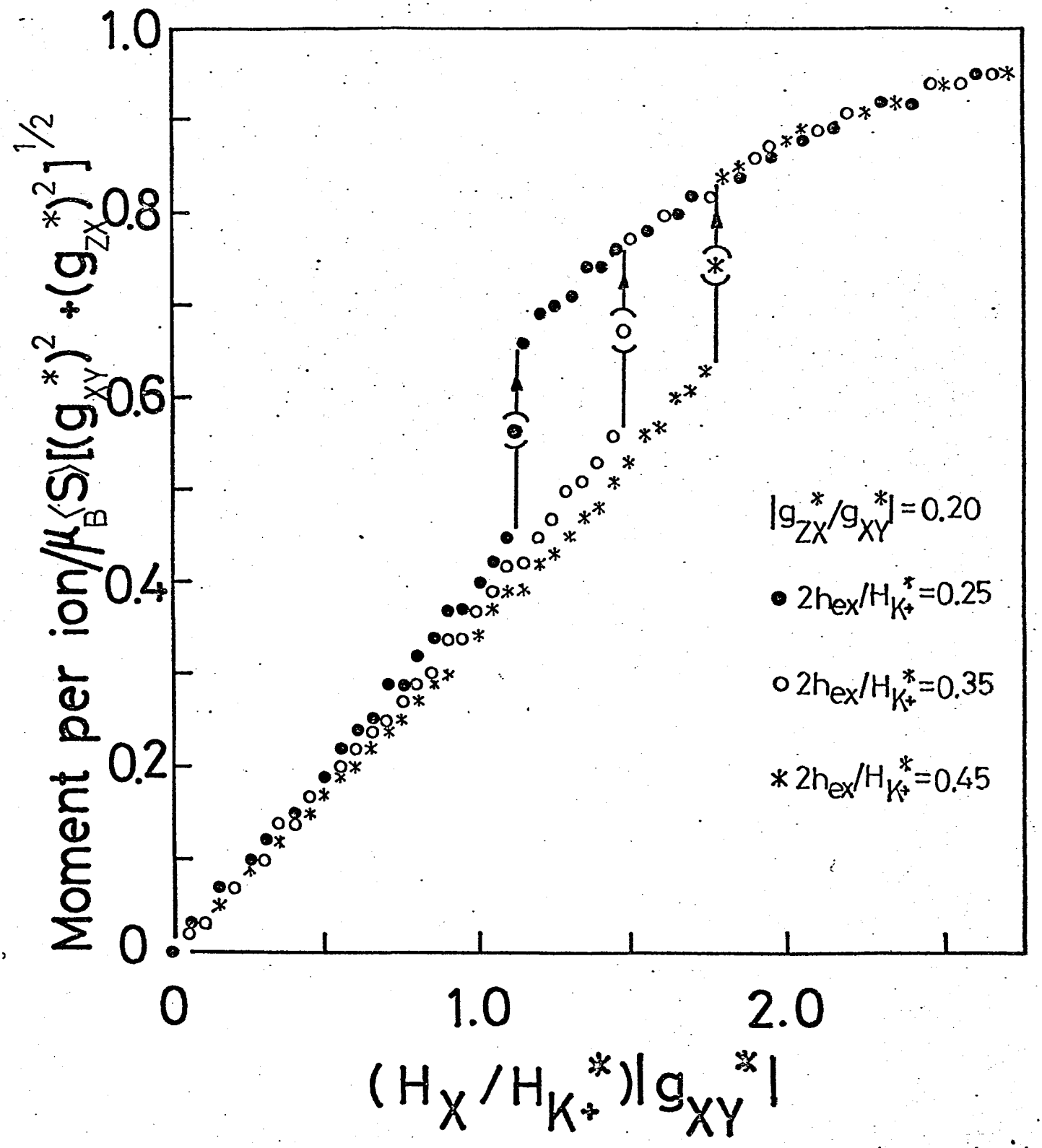

Fig. 32(b) Theoretical magnetization curves around the jump for three $2h_{ex}/H_{K+}^*$'s.

G. Antiferroelectric state of $Cu(HCOO)_2 \cdot 4H_2O$

Lattice and positional parameters have recently been reported by Kay and Kleinberg[23] for the antiferroelectric state of CuFTH. Table IX shows (1) the lattice parameter, the positional parameter of $HCOO^-$-proton and the dipole tensor $\tilde{D}$ corresponding to the paraelectric state studied by Okada et al.[19] and (2) those corresponding to the antiferroelectric state mentioned above. As is presented in §2, the former is used for CuFTD throughout the present paper. Here we examine qualitatively how the conclusions of §6 are modified when the dipole tensor of the latter case is used, because the crystal structure of the antiferroelectric state of CuFTD may be closer to the latter than to the former. The essence of the difference between two cases is the change of z/c positional parameter, which results in different D_{yz} and D_{zx}. In the low field 4-sublattice state, the spins are nearly parallel to the x-axis so that the internal field is mostly determined by D_{xx}. Therefore, the internal fields for two cases are similar and the conclusions of §6 remain unchanged. In the high field 2-sublattice state, the spins rotate in the L_1'b-plane when the external field is in the bc'-plane. About one half of the shift is determined by D_{yz} so that the shift for the latter case is calculated larger than that for the former by $15 \sim 30\%$. Therefore, we see that $m \equiv \langle S \rangle / S$ in the 2-sublattice state may not be 0.9 but $0.7 \sim 0.8$.

Table IX Dipole sum tensors for the paraelectric[19] and antiferroelectric[23] states of $Cu(HCOO)_2 \cdot 4H_2O$.

		paraelectric state		antiferroelectric state	
lattice parameters	a	8.18 Å	a	8.00 Å	
	b	8.15	b	8.18	
	c	6.35	c	6.205	
	β	101.1°	β	101.1°	
positional parameters of $HCOO^-$ proton	x/a	0.207	x/a	0.2052	
	y/b	0.692	y/b	0.6959	
	z/c	0.071	z/c	0.0904	
			kOe		kOe
AR-3 (2-sublattice)	D_{xx}		-0.48		-0.47
	D_{yy}		0.49		0.50
	D_{zz}		-0.01		-0.03
	D_{xy}, D_{yx}		0.02		0.0
	D_{yz}, D_{zy}		-0.18		-0.23
	D_{zx}, D_{xz}		0.18		0.22
AR-4 (4-sublattice)	D_{xx}		-0.49		-0.48
	D_{yy}		0.46		0.46
	D_{zz}		0.03		0.02
	D_{xy}, D_{yx}		0.02		0.0
	D_{yz}, D_{zy}		-0.21		-0.27
	D_{zx}, D_{xz}		0.22		0.27

H. Magnetization curves for $Cu(HCOO)_2 \cdot 2(NH_2)_2CO \cdot 2H_2O$

The magnetization curves for CuFUH are fully presented here. Figures 33(a), (b) and (c) represent the angular dependence of the magnetization curve in the L_1L_3-, $L_{1Z}'L_2$- and L_2L_3-planes, respectively. In Fig. (b) and (c) the inserts are details of the curves around the jump. Figure 34 indicates the lack of hysteresis for $\vec{H}//L_1$ and L_2. Figures 35(a), (b) and (c) show the angular dependence of the magnetization in constant external fields. Figures (a), (b) and (c) correspond to the measurements in the L_1L_3-, $L_{1Z}'L_2$- and L_2L_3-planes, respectively.

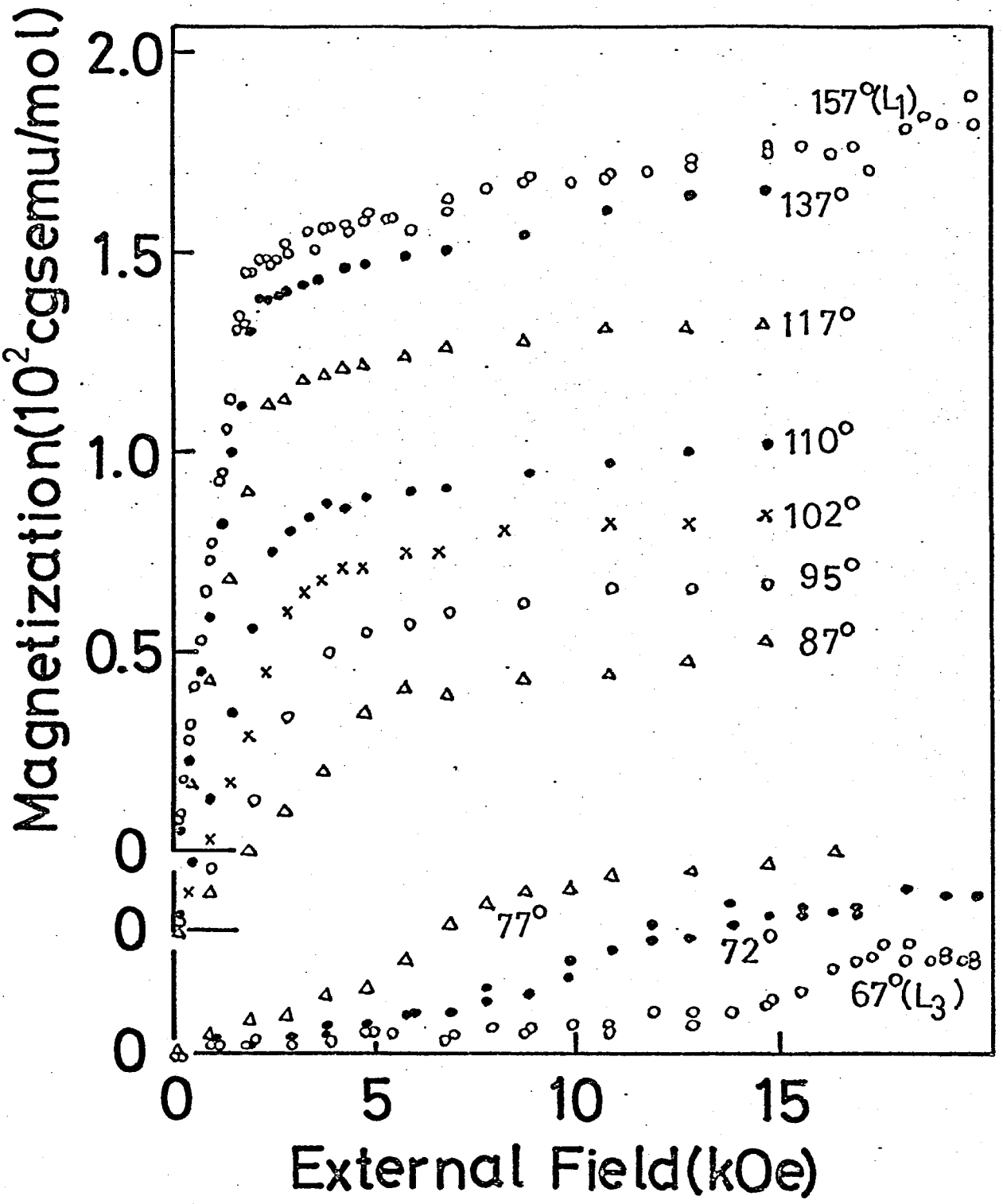

Fig. 33(a) Magnetization curves in the L_1L_3-plane for a single crystal of $Cu(HCOO)_2 \cdot 2(NH_2)_2CO \cdot 2H_2O$ at 4.2K.

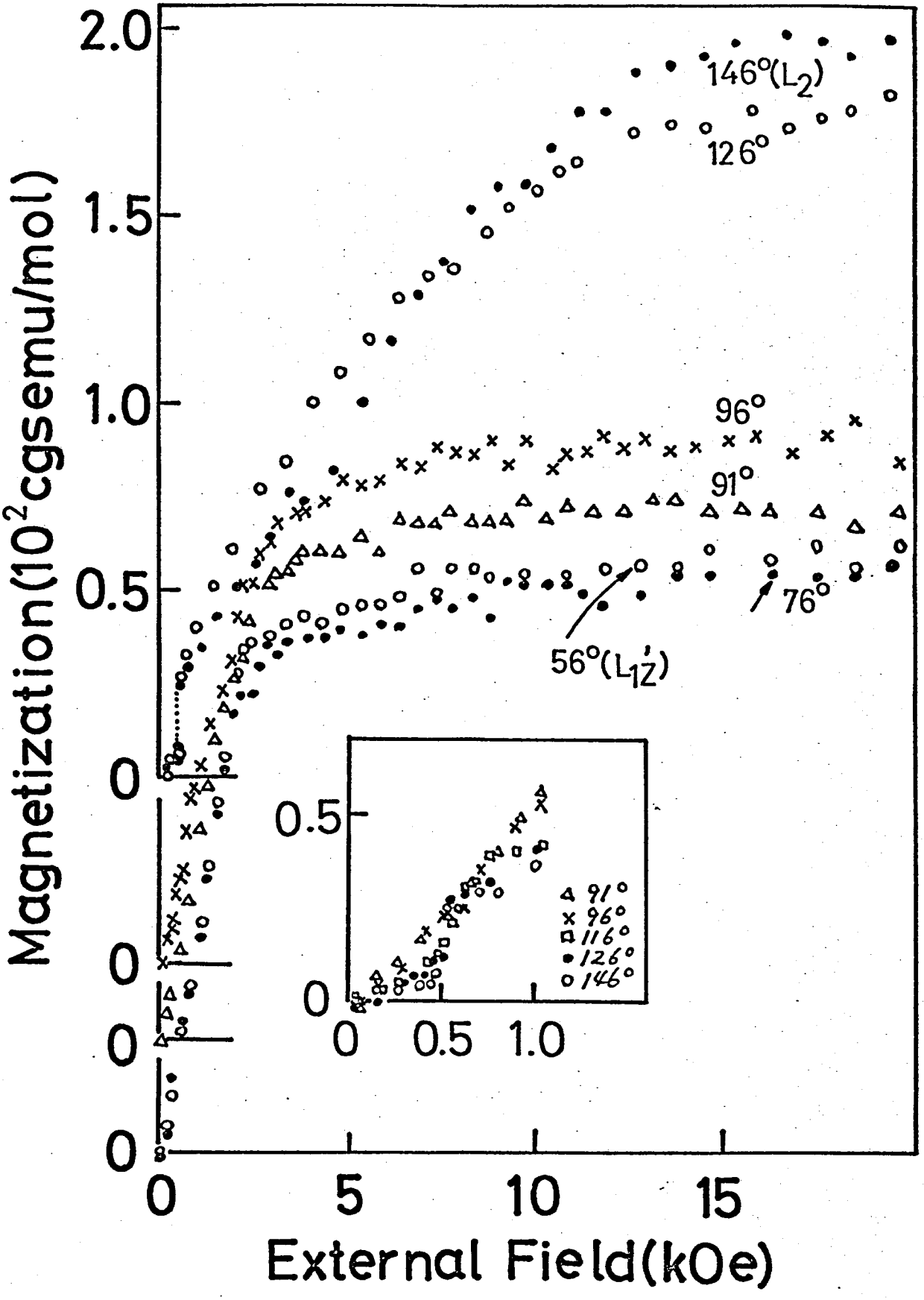

Fig. 33(b) Magnetization curves in the $L_{1Z}'L_2$-plane.

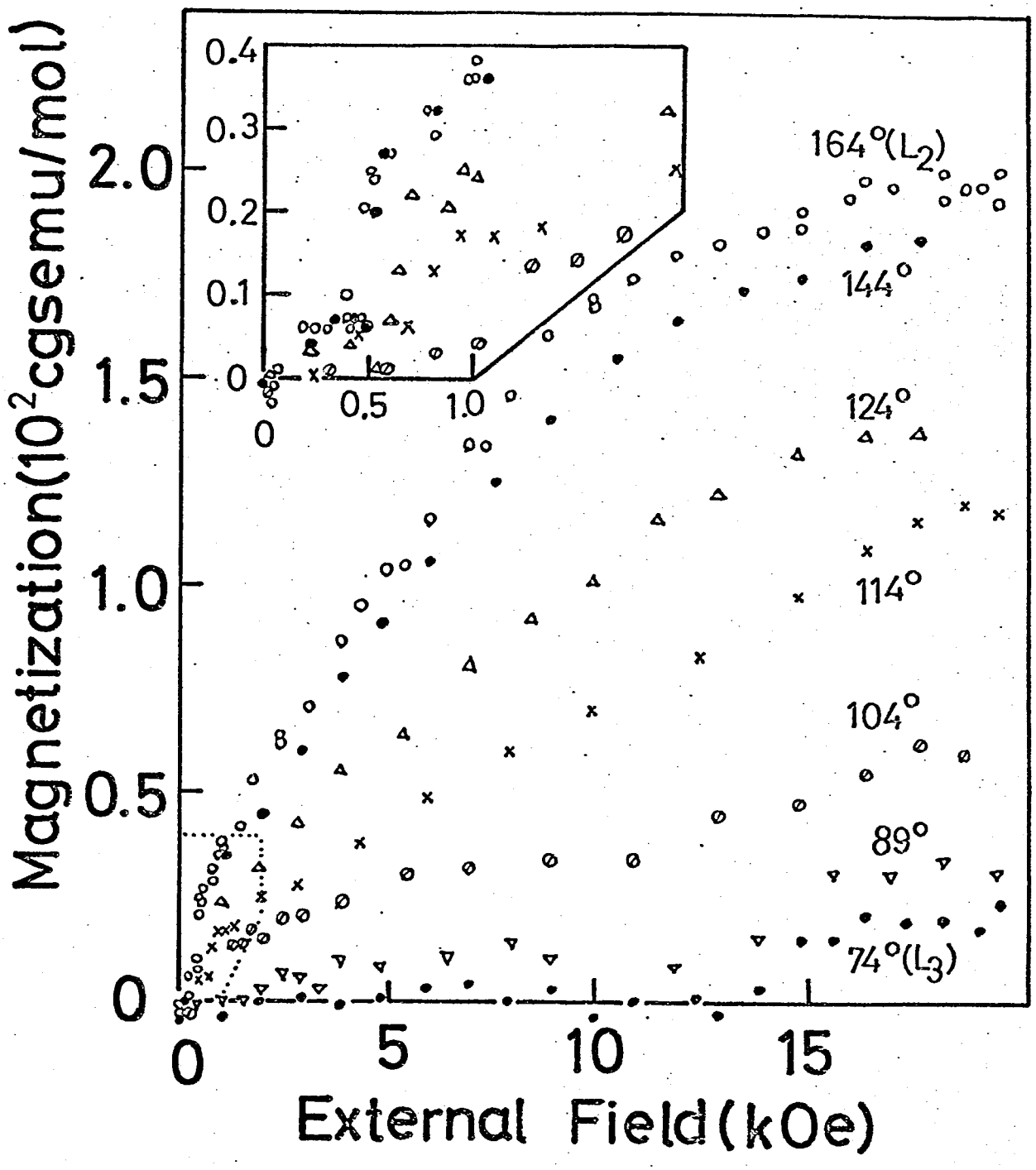

Fig. 33(c) Magnetization curves in the L_2L_3-plane.

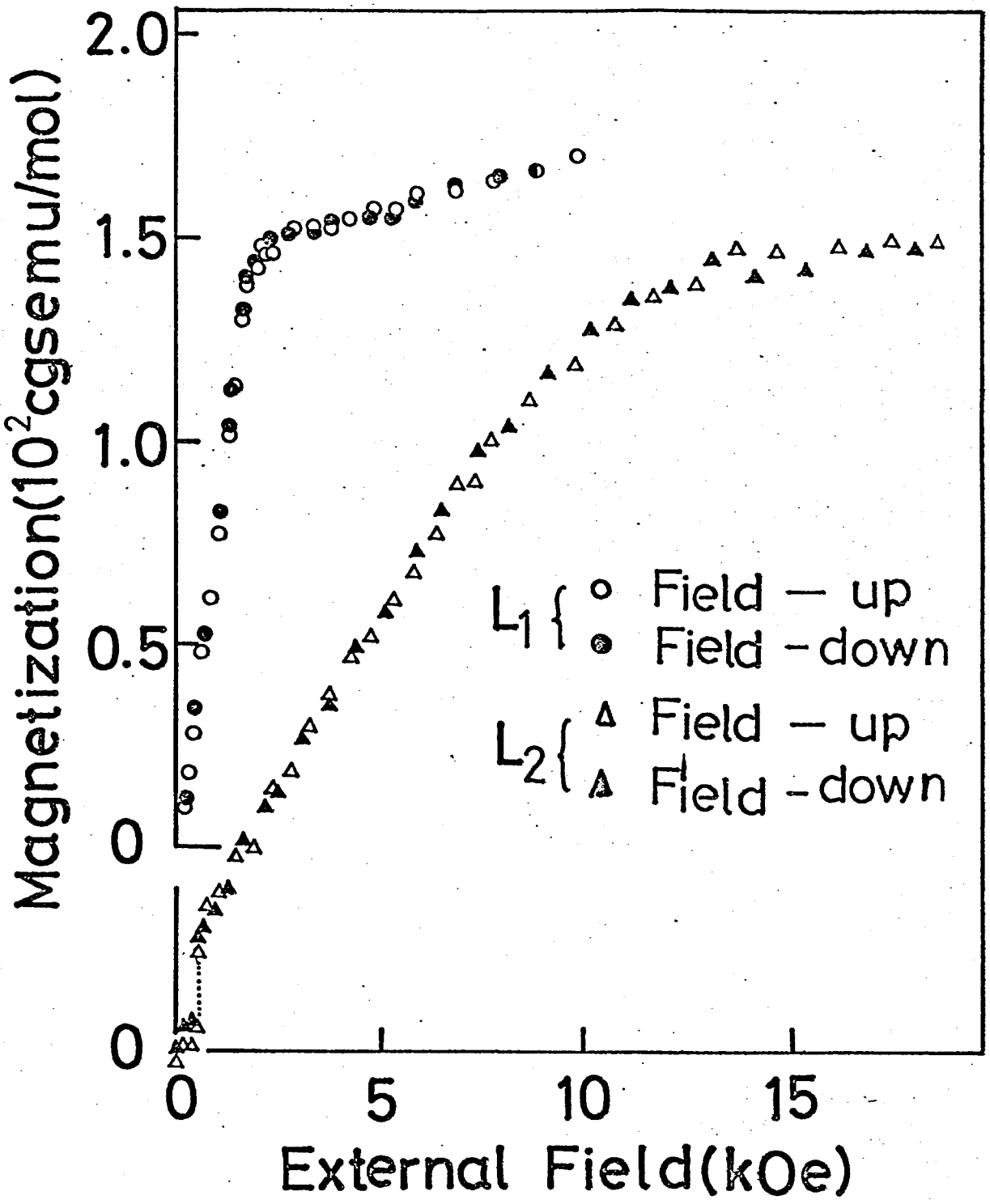

Fig. 34 Magnetization curves obtained by increasing and decreasing the external field for $\vec{H}//L_1$ and L_2 at 4.2K.

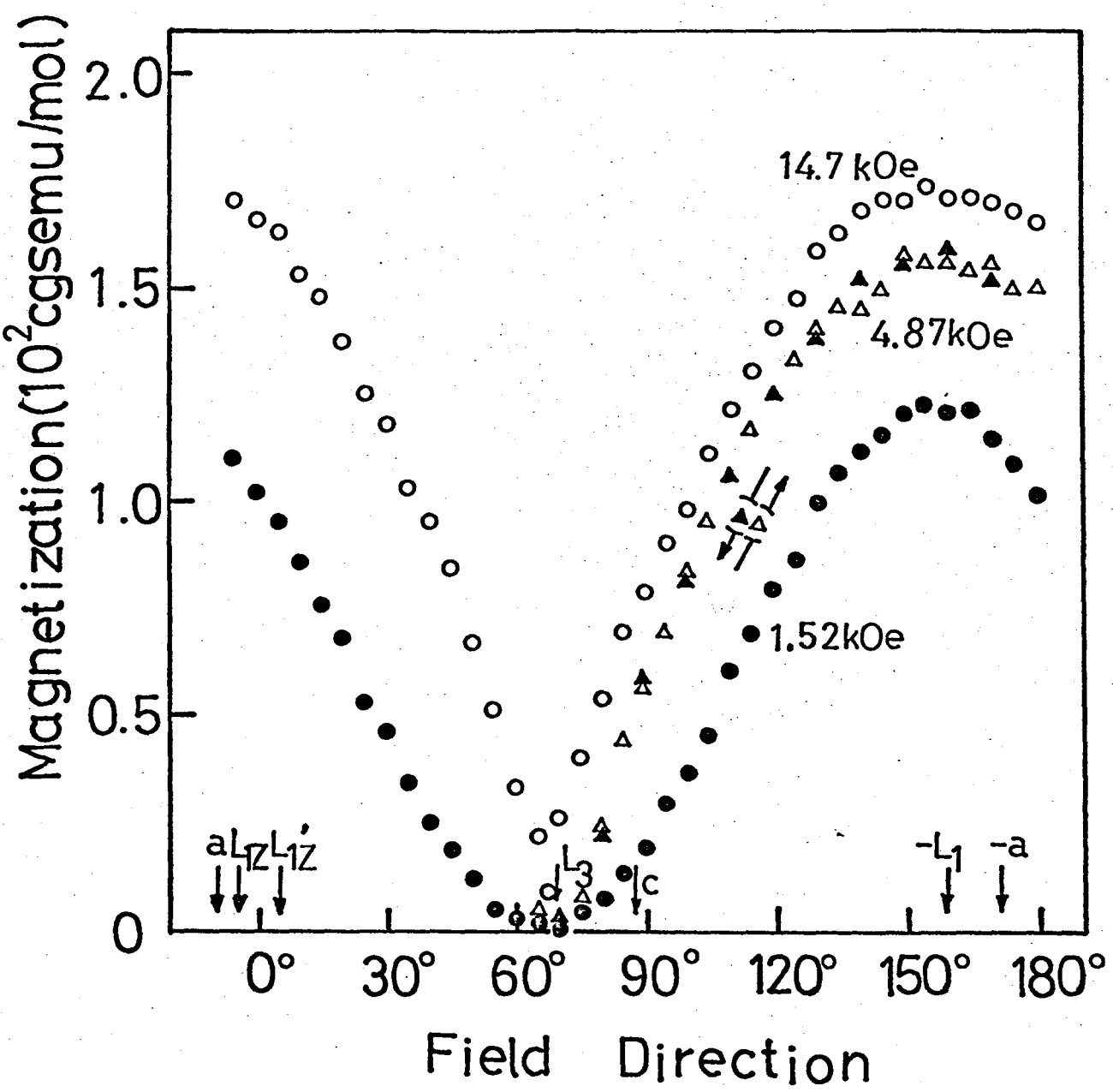

Fig. 35 Angular dependence of magnetization in $Cu(HCOO)_2 \cdot 2(NH_2)_2CO \cdot 2H_2O$ single crystals at 4.2K. (a) Results in the L_1L_3-plane.

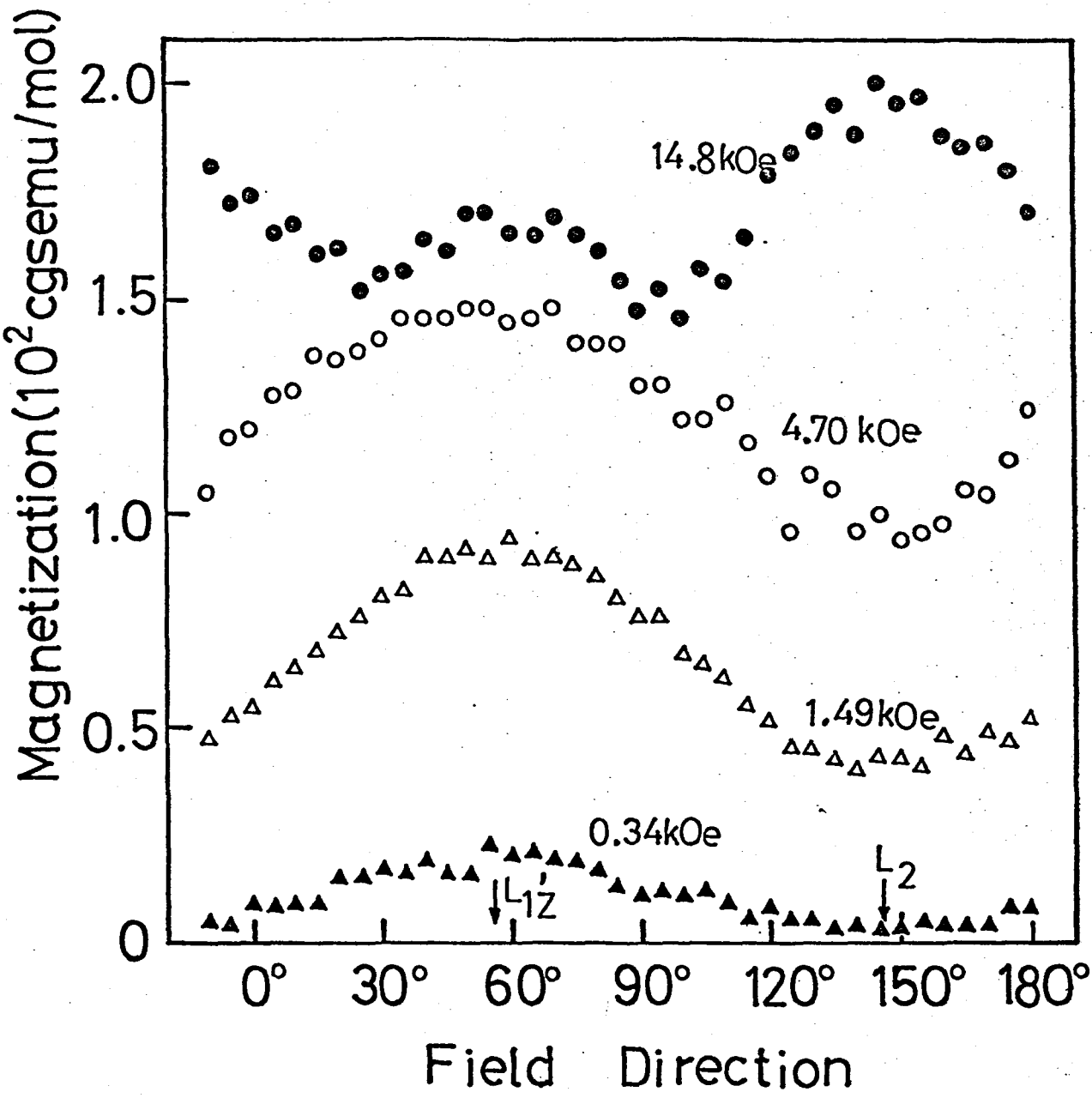

Fig. 35(b) Results in the $L_{1Z}'L_2$-plane.

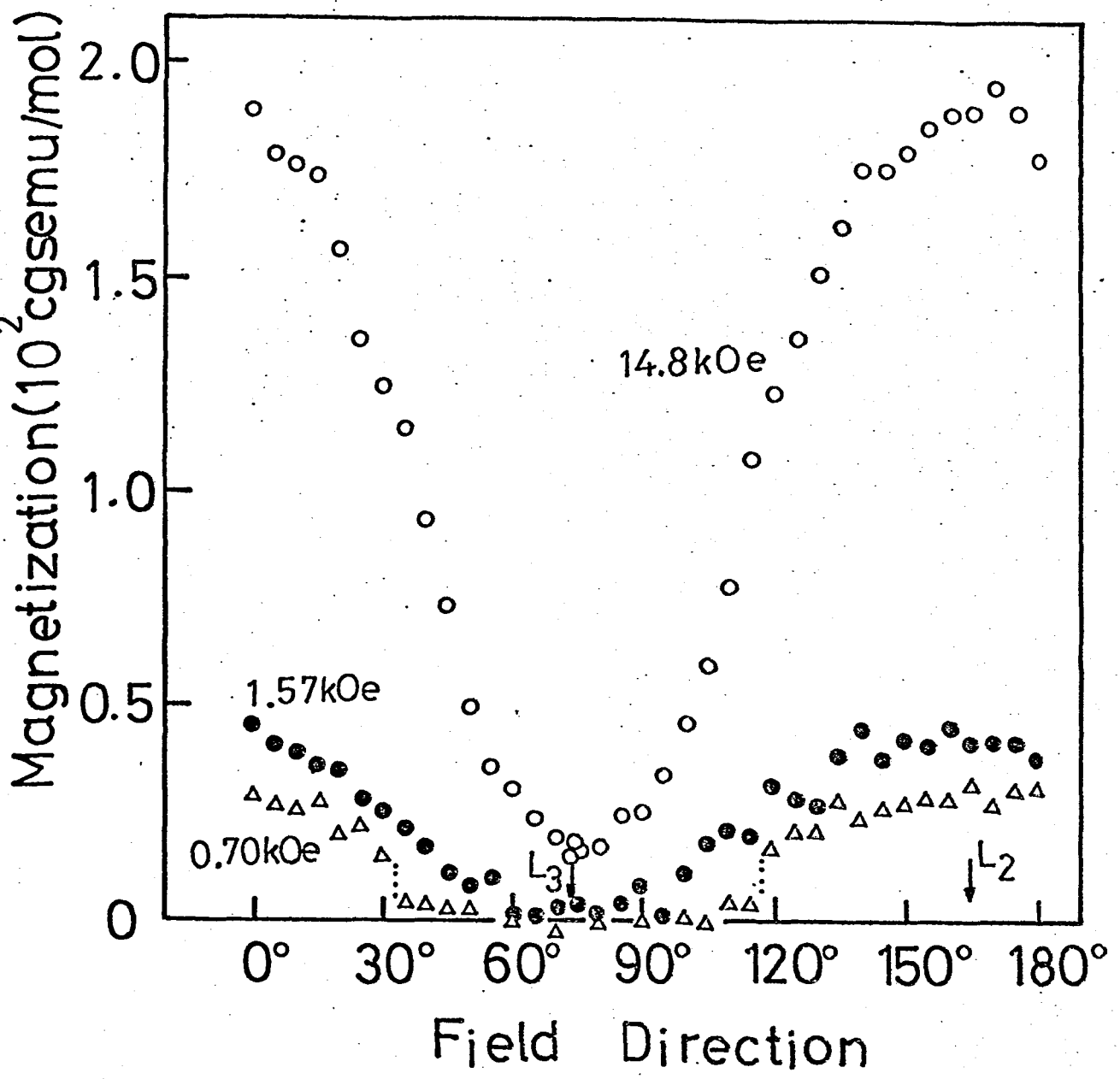

Fig. 35(c) Results in the L_2L_3-plane.

I. Abstract in German

Auszug

Die magnetischen Eigenschaften eines zweidimensionalen Antiferromagnetes, $Cu(HCOO)_2 \cdot 4H_2O$, wurden beide experimental und theoretisch mit besonderen Interessen an den Magnetisierungsprozeß gestudiert. Die Messung der Magnetisierung bis zu 20 kOe wurde bei 4.2K auf Einkristalle von $Cu(HCOO)_2 \cdot 4H_2O$ gemacht und auch die Protonenresonanz des deuterierten Salzes, $Cu(HCOO)_2 \cdot 4D_2O$, wurde bei 4.2K gestudiert. Es wurde gefunden, daß einige experimentelle Ergebnisse z. B. ein Magnetisierungssprung gebeobachtet bei 5.3 kOe, wenn ein äußeres Feld zur b-Achse parallel ist, nach dem zweiuntergitteren Modell gebraucht von Seehra und Castner nicht geerklärt werden können. Die vieruntergittere Theorie, in der die inter- und intra-schichten Austausch-wechselwirkungen, die symmetrischen und antisymmetrischen Anisotropien und die Zeeman-Energien in Betracht gezogen wurden, wurde zu dieser Verbindung angewandt und die experimentellen Ergebnisse würden genug geerklärt.

Die inter- und intra-schichten Austauschfelder, H_{ex} und h_{ex}, wurden wie 1.5×10^6 Oe und 4.0×10 Oe beziehungsweise geerlangt. Das kleine Verhältnis von h_{ex}/H_{ex}, 2.7×10^{-5}, bestätigt der Zweidimensionalität dieses Kristalls.

Die Magnetisierungskurve einer ähnlichen Verbindung, $Cu(HCOO)_2 \cdot 2(NH_2)_2CO \cdot 2H_2O$, wurde bei 4.2K gestudiert. Die Ergebnisse zeigen an, daß die inter-schichte Kuppelung dieses Kristalls ist um 1/20 von der in $Cu(HCOO)_2 \cdot 4H_2O$, während der intra-schichte Austausch beider Kristalle ist in der gleichen Größenordnung.